11

Variational Formulation of Bar Element

TABLE OF CONTENTS

§11.1. A New Beginning

This Chapter begins Part II of the course. This Part focuses on the construction of structural and continuum finite elements using a *variational formulation* based on the Total Potential Energy. Why only elements? Because the other synthesis steps of the DSM: globalization, merge, BC application and solution, remain the same as in Part I. Those operations are not element dependent.

Individual elements are constructed in this Part beginning with the simplest ones and progressing to more complicated ones. The formulation of 2D finite elements from a variational standpoint is discussed in Chapters 14 and following. Although the scope of that formulation is broad, exceeding structural mechanics, it is better understood by going through specific elements first.

From a geometrical standpoint the simplest finite elements are one-dimensional or *line elements*. This means that the *intrinsic dimensionality* is one, although these elements may be used in one, two or three space dimensions upon transformation to global coordinates as appropriate. The simplest one-dimensional structural element is the *two-node bar element*, which we have already encountered in Chapters 2, 3 and 5 as the truss member.

In this Chapter the bar stiffness equations are rederived using the variational formulation. For uniform properties the resulting equations are the same as those found previously using the physical or Mechanics of Materials approach. The variational method has the advantage of being readily extendible to more complicated situations, such as variable cross section or more than two nodes.

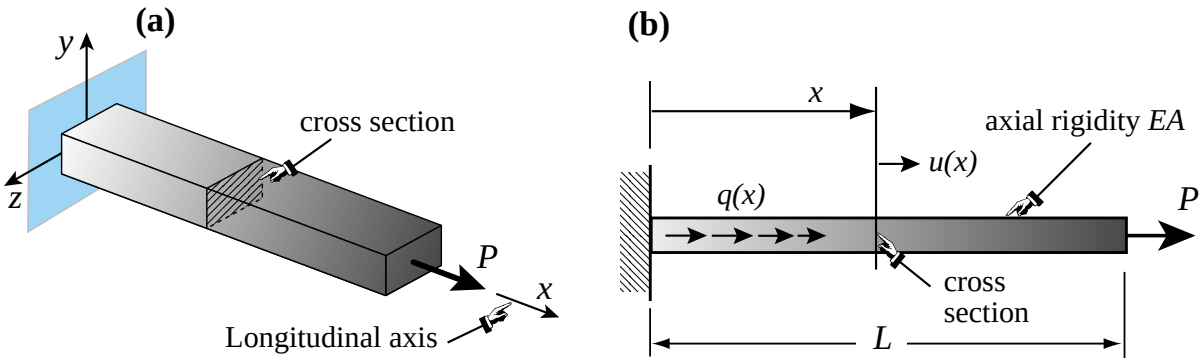

FIGURE 11.1. A fixed-free bar member: (a) 3D view showing reference frame; (b) 2D view on $\{x, y\}$ plane highlighting some quantities that are important in bar analysis.

§11.2. Definition of Bar Member

In structural mechanics a *bar* is a structural component characterized by two properties:

(1) One preferred dimension: the *longitudinal dimension* or *axial dimension* is much larger that the other two dimensions, which are collectively known as *transverse dimensions*. The intersection of a plane normal to the longitudinal dimension and the bar defines the *cross sections*. The longitudinal dimension defines the *longitudinal axis*. See Figure 11.1(a).

(2) The bar resists an internal axial force along its longitudinal dimension.

Table 11.1 Nomenclature for Mathematical Model of Axially Loaded Bar

Quantity	*Meaning*
x	Longitudinal bar axis*
$(.)'$	$d(.)/dx$
$u(x)$	Axial displacement
$q(x)$	Distributed axial force, given per unit of bar length
L	Total bar length
E	Elastic modulus
A	Cross section area; may vary with x
EA	Axial rigidity
$e = du/dx = u'$	Infinitesimal axial strain
$\sigma = Ee = Eu'$	Axial stress
$F = A\sigma = EAe = EAu'$	Internal axial force
P	Prescribed end load

* x is used in this Chapter instead of $\bar{x}$ (as in Chapters 2–3) to simplify the notation.

In addition to trusses, bar elements are used to model cables, chains and ropes. They are also used as fictitious elements in penalty function methods, as discussed in Chapter 9.

We will consider here only *straight bars*, although their cross section may vary. Our one-dimensional mathematical model assumes that the bar material is linearly elastic obeying Hooke's law, and that displacements and strains are infinitesimal. Figure 11.1(b) pictures some relevant quantities for a fixed-free bar. Table 11.1 collects the necessary terminology for the governing equations.

Figure 11.2 displays the governing equations of the bar in a graphic format called a *Tonti diagram*. The formal similarity with the diagrams used in Chapter 5 to explain MoM elements should be noted, although the diagram of Figure 11.2 pertains to the continuum bar model rather than to the discrete one. (The qualifier "strong form" is explained in the next Chapter.)

§11.3. Variational Formulation

To illustrate the variational formulation, the finite element equations of the bar will be derived from the Minimum Potential Energy principle.

§11.3.1. The Total Potential Energy Functional

In Mechanics of Materials it is shown that the *internal energy density* at a point of a linear-elastic material subjected to a one-dimensional state of stress σ and strain e is $\mathcal{U} = \frac{1}{2}\sigma(x)e(x)$, where σ is to be regarded as linked to the displacement u through Hooke's law $\sigma = Ee$ and the strain-displacement relation $e = u' = du/dx$. This $\mathcal{U}$ is also called the *strain energy density*. Integration over the volume of the bar gives the total internal energy

$$U = \tfrac{1}{2}\int_V \sigma\, e\, dV = \tfrac{1}{2}\int_0^L Fe\, dx = \tfrac{1}{2}\int_0^L (EAu')u'\, dx = \tfrac{1}{2}\int_0^L u'EAu'\, dx. \qquad (11.1)$$

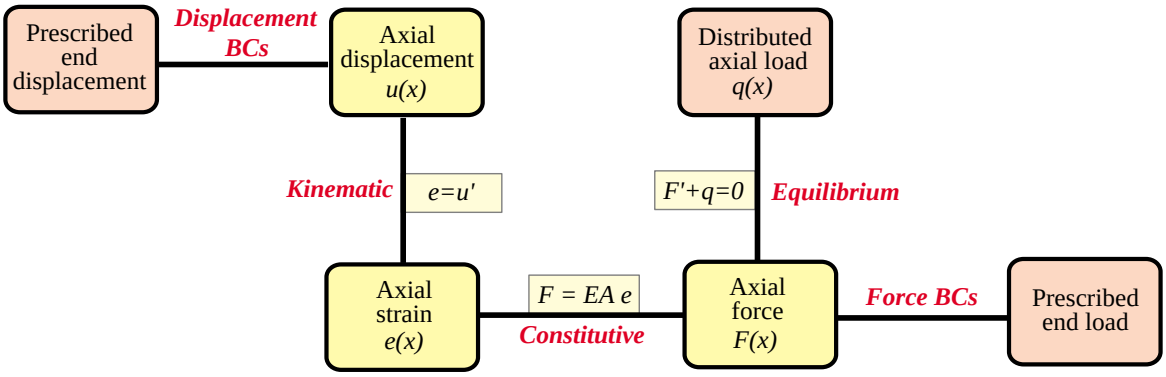

FIGURE 11.2. Strong-form Tonti diagram for the continuum model of a bar member. Field equations and BCs are represented as lines connecting the boxes. Yellow (brown) boxes contain unknown (given) quantities.

All integrand quantities in (11.1) may depend on x.

The *external work potential* is the work performed by applied mechanical loads working on the bar displacements. This potential is denoted by W. (The *external energy* V is the negative of the work potential: $V = -W$. In the ensuing derivations W will be used instead of V.) It collects contributions from two sources:

1. The distributed load $q(x)$. This contributes a cross-section density of $q(x)u(x)$ because q is assumed to be already integrated over the section.
2. Any specified axial point load(s). For the fixed-free example of Figure 11.1 the end load P would contribute $P\,u(L)$.

The second source may be folded into the first by conventionally writing any point load P acting at a cross section $x = a$ as a contribution $P\,\delta(a)$ to $q(x)$, in which $\delta(a)$ denotes the one-dimensional Dirac delta function at $x = a$. If this is done the external energy can be concisely expressed as

$$W = \int_0^L q\,u\,dx. \tag{11.2}$$

The total potential energy of the bar is given by

$$\boxed{\Pi = U - W} \tag{11.3}$$

Mathematically Π is a *functional*, called the *Total Potential Energy* functional or TPE. It depends only on the axial displacement $u(x)$. In Variational Calculus $u(x)$ is called the *primary variable* of the functional. When the dependence of Π on u needs to be emphasized we shall write $\Pi[u] = U[u]-W[u]$, with brackets enclosing the primary variable. To display both primary and independent variables we write, for example, $\Pi[u(x)] = U[u(x)] - W[u(x)]$.

Remark 11.1. According to the rules of Variational Calculus, the Euler-Lagrange equation for Π is

$$\mathcal{E} = \frac{\partial \Pi}{\partial u} - \frac{d}{dx}\frac{\partial \Pi}{\partial u'} = -q - (E\,A\,u')' \tag{11.4}$$

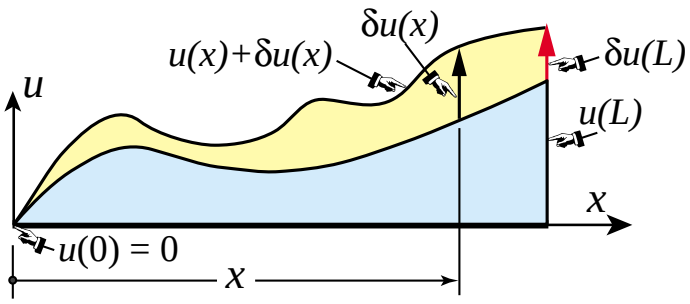

FIGURE 11.3. Concept of admissible variation of the axial displacement function $u(x)$. For convenience $u(x)$ is plotted normal to the longitudinal axis. Both $u(x)$ and $u(x)+\delta u(x)$ shown above are kinematically admissible, and so is the variation $\delta u(x)$. Note that the variation $\delta u(L)$ is not zero because the BC at $x = L$ is natural.

The stationary condition for Π is $\mathcal{E} = 0$, or

$$(E A u')' + q = 0 \tag{11.5}$$

This is the strong (pointwise) equation of equilibrium in terms of the axial displacement, which reduces to $E A u'' + q = 0$ if $E A$ is constant. This equation is not explicitly used in the FEM development. It is instead replaced by $\delta\Pi = 0$, with the variation restricted over the class of finite element interpolation functions.

§11.3.2. Admissible Variations

The concept of *admissible variation* is fundamental in both variational calculus and the variationally formulated FEM. *Only the primary variable(s) of a functional may be varied.* For the TPE functional (11.3) this is the axial displacement $u(x)$. Suppose that $u(x)$ is changed to $u(x) + \delta u(x)$.[1] This is illustrated in Figure 11.3, where for convenience $u(x)$ is plotted normal to x. The TPE functional changes accordingly as

$$\Pi = \Pi[u] \;\Rightarrow\; \Pi + \delta\Pi = \Pi[u + \delta u]. \tag{11.6}$$

The function $\delta u(x)$ and the scalar $\delta\Pi$ are called the *variations* of $u(x)$ and Π, respectively. The variation $\delta u(x)$ should not be confused with the ordinary differential $du(x) = u'(x)\,dx$ since on taking the variation the independent variable x is *frozen*; that is, $\delta x = 0$.

A displacement variation $\delta u(x)$ is said to be *admissible* when both $u(x)$ and $u(x) + \delta u(x)$ are *kinematically admissible* in the sense of the Principle of Virtual Work (PVW). This agrees with the conditions of classical variational calculus, and are restated next.

A *kinematically admissible* axial displacement $u(x)$ obeys two conditions:

(i) It is continuous over the bar length, that is, $u(x) \in \mathcal{C}^0$ in $x \in [0, L]$.

(ii) It satisfies exactly any displacement boundary condition, such as the fixed-end specification $u(0) = 0$ of Figure 11.1. See of Figure 11.3.

The variation $\delta u(x)$ pictured in Figure 11.3 is kinematically admissible because both $u(x)$ and $u(x) + \delta u(x)$ satisfy the foregoing conditions. Note that the variation $\delta u(L)$ at the free end $x = L$ is not necessarily zero because that boundary condition is natural; that is, not specified directly in terms of the displacement $u(L)$. On the other hand, $\delta(0) = 0$.

The physical meaning of conditions (i)–(ii) is the subject of Exercise 11.1.

[1] The symbol δ not immediately followed by a parenthesis is not a delta function but instead denotes variation with respect to the variable that follows.

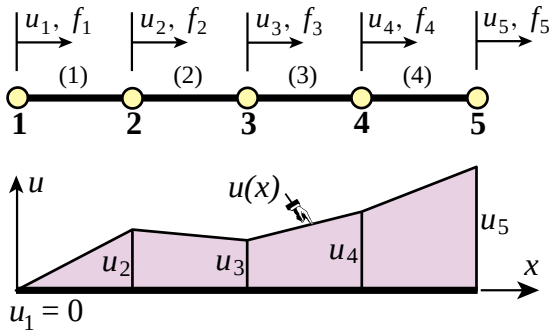

FIGURE 11.4. FEM discretization of bar member. A piecewise- linear admissible displacement trial function $u(x)$ is drawn underneath the mesh. It is assumed that the left end is fixed; thus $u_1 = 0$.

§11.3.3. The Minimum Total Potential Energy Principle

The Minimum Total Potential Energy (MTPE) principle states that the actual displacement solution $u^*(x)$ that satisfies the governing equations is that which renders Π stationary:[2]

$$\boxed{\delta\Pi = \delta U - \delta W = 0 \quad \text{iff} \quad u = u^*} \tag{11.7}$$

with respect to *admissible* variations $u = u^* + \delta u$ of the exact displacement field $u^*(x)$.

Remark 11.2. Using standard techniques of variational calculus[3] it can be shown that if $EA > 0$ and kinematic boundary conditions weed out any rigid motions, the solution $u^*(x)$ of (11.7) exists, is unique, and renders $\Pi[u]$ a minimum over the class of kinematically admissible displacements. The last attribute explains the "minimum" in the name of the principle.

§11.3.4. TPE Discretization

To apply the TPE functional (11.3) to the derivation of FEM equations we replace the continuum mathematical model by a discrete one consisting of a union of bar elements. For example, Figure 11.4 illustrates the subdivision of a fixed-free bar member into four two-node elements.

Functionals are scalars. Therefore, for a discretization such as that shown in Figure 11.4, the TPE functional (11.3) may be decomposed into a sum of contributions of individual elements:

$$\boxed{\Pi = \Pi^{(1)} + \Pi^{(2)} + \ldots + \Pi^{(N_e)}} \tag{11.8}$$

in which N_e denotes the number of elements. The same decomposition applies to both its internal energy and external work potential components:

$$\boxed{\delta U = \delta U^{(1)} + \ldots + \delta U^{(N_e)} = 0, \qquad \delta W = \delta W^{(1)} + \ldots + \delta W^{(N_e)} = 0,} \tag{11.9}$$

as well as to the stationarity condition (11.7):

$$\boxed{\delta\Pi = \delta\Pi^{(1)} + \delta\Pi^{(2)} + \ldots + \delta\Pi^{(N_e)} = 0.} \tag{11.10}$$

[2] The symbol "iff" in (11.7) is an abbreviation for "if and only if".

[3] See references in **Notes and Bibliography** at the end of Chapter.

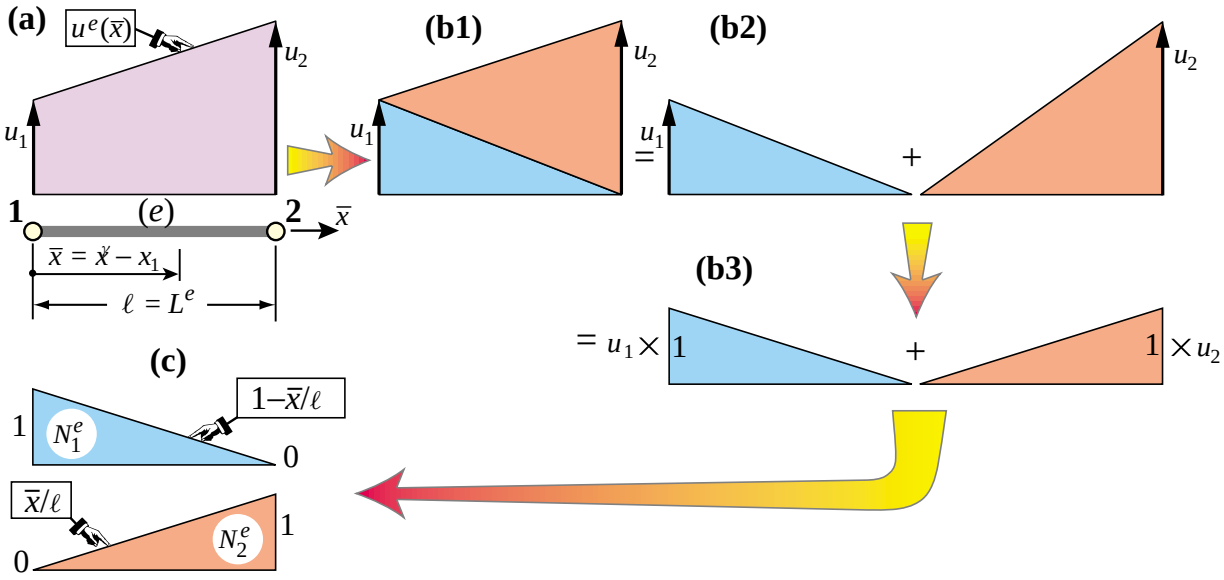

FIGURE 11.5. A two-node, TPE-based bar element: (a) element configuration and axial displacement variation (plotted normal to element axis for better visibility); (b1,b2,b3) displacement interpolation expressed in terms of linear shape functions; (c) element shape functions.

Using the fundamental lemma of variational calculus,[4] it can be shown that (11.10) implies that for a generic element e we may write

$$\boxed{\delta\Pi^e = \delta U^e - \delta W^e = 0.} \tag{11.11}$$

This *variational equation* is the basis for the derivation of element stiffness equations once the displacement field has been discretized over the element, as described next.

Remark 11.3. In mathematics (11.11) is called a *first variation form*. It is a special case of a more general expression called a *weak form*, which is covered in more detail later. In mechanics it states the *Principle of Virtual Work* or PVW for each element: $\delta U^e = \delta W^e$, which says that the virtual work of internal and external forces on admissible displacement variations is equal if the element is in equilibrium [588].

§11.3.5. Bar Element Discretization

Figure 11.5(a) depicts a generic bar element e. It has two nodes, which are labeled 1 and 2. These are called the *local node numbers*.[5] The element is referred to its local axis $\bar{x} = x - x_1$, which measures the distance from its left end. The two degrees of freedom are u_1^e and u_2^e. (Bars are not necessary since the directions of $\bar{x}$ and x are the same.) The element length is $\ell = L^e$.

The mathematical concept of bar finite elements is based on *approximating* axial displacement $u(x)$ over the element. The exact displacement u^* is replaced by an approximate displacement

$$u^*(x) \approx u^e(x) \tag{11.12}$$

[4] See, e.g., Chapter II of Gelfand and Fomin [297].

[5] Note the notational change from the labels i and j of Part I. This will facilitate transition to multidimensional elements in Chapters 14ff.

over the finite element mesh. This approximate displacement, $u^e(x)$, taken over all elements $e = 1, 2, \ldots N^e$, is called the *finite element trial expansion* or simply *trial expansion*. See Figure 11.4. This FE trial expansion must belong to the class of kinematically admissible displacements defined in **?**. Consequently, it must be C^0 continuous over and between elements. The most common choices fpr u^e are polynomials in x, as in the development that follows.

§11.3.6. Interpolation by Shape Functions

In a two-node bar element the only possible polynomial choice of the displacement u^e that satisfies the interelement continuity requirement is *linear*. It can be expressed by the following interpolation formula, which is graphically developed in Figure 11.5(b1,b2,b3):

$$\boxed{u^e(x) = N_1^e\, u_1^e + N_2^e\, u_2^e = [\, N_1^e \quad N_2^e \,] \begin{bmatrix} u_1^e \\ u_2^e \end{bmatrix} = \mathbf{N}^e\, \mathbf{u}^e.} \tag{11.13}$$

The functions N_1^e and N_2^e that multiply the node displacements u_1 and u_2 are called *shape functions*, while $\mathbf{N}$ is called the *shape function matrix*. In this case $\mathbf{N}^e$ reduces to a row vector.

The shape functions *interpolate* the internal displacement u^e directly from the node values. They are pictured in Figure 11.5(c). For this element, with $\bar{x} = x - x_1$ measuring the axial distance from the left node i, the shape functions are

$$N_1^e = 1 - \frac{\bar{x}}{\ell} = 1 - \zeta, \qquad N_2^e = \frac{\bar{x}}{\ell} = \zeta. \tag{11.14}$$

Here

$$\zeta = \frac{x - x_1}{\ell} = \frac{\bar{x}}{\ell}, \tag{11.15}$$

is a dimensionless coordinate, also known as a *natural coordinate*, that varies from 0 through 1 over the element. Note that $dx = \ell\, d\zeta$ and $d\zeta = dx/\ell$. The shape function N_1^e has the value 1 at node 1 and 0 at node 2. Conversely, shape function N_2^e has the value 0 at node 1 and 1 at node 2. This is a general property of shape functions. It follows from the fact that element displacement interpolations such as (11.13) are based on physical node values.

§11.3.7. The Strain-Displacement Matrix

The axial strain associated with the trial function u^e is

$$e = \frac{du^e}{dx} = (u^e)' = \left[\, \frac{dN_1^e}{dx} \quad \frac{dN_2^e}{dx} \,\right] \begin{bmatrix} u_1^e \\ u_2^e \end{bmatrix} = \frac{1}{\ell}\, [\, -1 \quad 1 \,] \begin{bmatrix} u_1^e \\ u_2^e \end{bmatrix} = \mathbf{B}\, \mathbf{u}^e, \tag{11.16}$$

in which

$$\mathbf{B} = \frac{1}{\ell}\, [\, -1 \quad 1 \,], \tag{11.17}$$

is called the *strain-displacement* matrix. Note that $\mathbf{B}$ is constant over the element.

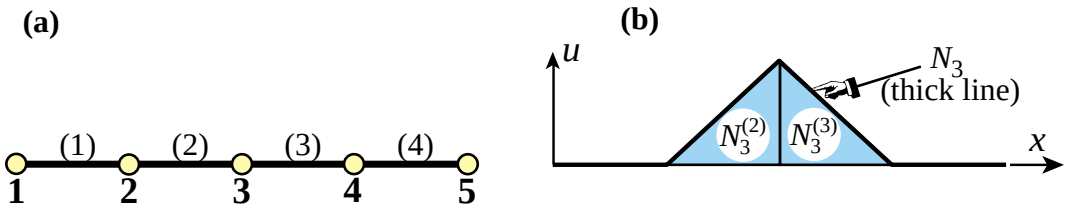

FIGURE 11.6. Trial basis function (a.k.a. hat function) for node 3 of a four-element bar discretization.

§11.3.8. *Trial Basis Functions

Shape functions are associated with elements. A *trial basis function*, or simply *basis function*, is associated with a node. Suppose node i of a bar discretization connects elements $(e1)$ and $(e2)$. The trial basis function N_i is defined as

$$N_i(x) = \begin{cases} N_i^{(e1)} & \text{if } x \in \text{element } (e1) \\ N_i^{(e2)} & \text{if } x \in \text{element } (e2) \\ 0 & \text{otherwise} \end{cases} \tag{11.18}$$

For a piecewise linear discretization, such as that used in the two-node bar, this function has the shape of a hat. Thus it is also called a *hat function* or *chapeau function*. See Figure 11.6, in which $i = 3$, $e1 = 2$, and $e2 = 3$. The concept is important in the variational interpretation of FEM as a Rayleigh-Ritz method.

Remark 11.4. In addition to continuity, shape and trial functions must satisfy a *completeness* requirement with respect to the governing variational principle. This condition is stated and discussed in later Chapters. Suffices for now to say that the shape functions (11.14), as well as the associated trial functions, do satisfy this requirement.

§11.4. The Finite Element Equations

In linear FEM the discretization process based on the TPE functional leads to the following algebraic form in the node displacements

$$\Pi^e = U^e - W^e, \quad \text{in which} \quad U^e \stackrel{\text{def}}{=} \tfrac{1}{2}(\mathbf{u}^e)^T\,\mathbf{K}^e\,\mathbf{u}^e \quad \text{and} \quad W^e \stackrel{\text{def}}{=} (\mathbf{u}^e)^T\,\mathbf{f}^e. \tag{11.19}$$

Here $\mathbf{K}^e$ and $\mathbf{f}^e$ are called the *element stiffness matrix* and the *element consistent nodal force vector*, respectively. The three scalars Π^e, U^e and W^e are only function of the node displacements $\mathbf{u}^e$. (This is a consequence of displacements being the only primary variable of the TPE functional.) Note that U^e and W^e depend *quadratically* and *linearly*, respectively, on those displacements. Taking the variation of Π^e with respect to the node displacements gives[6]

$$\delta\Pi^e = \left(\delta\mathbf{u}^e\right)^T \frac{\partial \Pi^e}{\partial \mathbf{u}^e} = \left(\delta\mathbf{u}^e\right)^T \left[\mathbf{K}^e\,\mathbf{u}^e - \mathbf{f}^e\right] = 0. \tag{11.20}$$

Because the variations $\delta\mathbf{u}^e$ can be arbitrary, the bracketed expression must vanish, which yields

$$\boxed{\mathbf{K}^e\,\mathbf{u}^e = \mathbf{f}^e.} \tag{11.21}$$

These are the familiar element stiffness equations. Hence the foregoing names given to $\mathbf{K}^e$ and $\mathbf{f}^e$ are justified *a posteriori*.

[6] The $\frac{1}{2}$ factor disappears on taking the variation because U^e is quadratic in the node displacements. For a review on the calculus of discrete quadratic forms, see Appendix D.

§11.4.1. The Stiffness Matrix

We now apply the foregoing expressions to the two-node bar element. Its internal energy U^e is

$$U^e = \tfrac{1}{2}\int_{x_1}^{x_2} e\,EA\,e\,dx = \tfrac{1}{2}\int_0^1 e\,EA\,e\,\ell\,d\zeta. \tag{11.22}$$

Note that the integration variable x has been changed to the natural coordinate ζ defined in (11.15) that varies from 0 through 1, whence $dx = \ell\,d\zeta$. This form is symmetrically expanded using the strain-displacement matrix relation (11.16), by inserting $e = e^T = (\mathbf{u}^e)^T\mathbf{B}^T$ and $e = \mathbf{B}\,\mathbf{u}^e$ into the first and second e of (11.22), respectively, to get

$$U^e = \tfrac{1}{2}\int_0^1 (\mathbf{u}^e)^T\mathbf{B}^T EA\,\mathbf{B}\,\mathbf{u}^e\,\ell\,d\zeta = \tfrac{1}{2}\int_0^1 [\,u_1^e \quad u_2^e\,]\,\frac{1}{\ell}\begin{bmatrix}-1\\1\end{bmatrix} EA\,\frac{1}{\ell}[\,-1 \quad 1\,]\begin{bmatrix}u_1^e\\u_2^e\end{bmatrix}\ell\,d\zeta. \tag{11.23}$$

The nodal displacements do not depend on position and can be moved out of the integral. Also $\mathbf{B}^T EA\,\mathbf{B} = EA\,\mathbf{B}^T\mathbf{B}$ since EA is a scalar:

$$U^e = \tfrac{1}{2}(\mathbf{u}^e)^T\int_0^1 EA\,\mathbf{B}^T\mathbf{B}\,\ell\,d\zeta\,\mathbf{u}^e = \tfrac{1}{2}[\,u_1^e \quad u_2^e\,]\int_0^1 \frac{EA}{\ell^2}\begin{bmatrix}1 & -1\\-1 & 1\end{bmatrix}\ell\,d\zeta\,\begin{bmatrix}u_1^e\\u_2^e\end{bmatrix}. \tag{11.24}$$

By (11.19) this is expressible as $\frac{1}{2}\left(\mathbf{u}^e\right)^T\mathbf{K}^e\,\mathbf{u}^e$. Since $\mathbf{u}^e$ is arbitrary, $\mathbf{K}^e$ is extracted as

$$\boxed{\mathbf{K}^e = \int_0^1 EA\,\mathbf{B}^T\mathbf{B}\,\ell\,d\zeta = \int_0^1 \frac{EA}{\ell^2}\begin{bmatrix}1 & -1\\-1 & 1\end{bmatrix}\ell\,d\zeta = \frac{1}{\ell}\begin{bmatrix}1 & -1\\-1 & 1\end{bmatrix}\int_0^1 EA\,d\zeta.} \tag{11.25}$$

This is the bar element stiffness matrix. For a homogeneous and prismatic bar of constant rigidity, EA can be moved outside the integral, $\int_0^1 d\zeta = 1$ and (11.25) collapses to

$$\boxed{\mathbf{K}^e = \frac{EA}{\ell}\begin{bmatrix}1 & -1\\-1 & 1\end{bmatrix}.} \tag{11.26}$$

This is the same element stiffness matrix of the prismatic truss member derived in Chapters 2 and 5 by a Mechanics of Materials approach, but now obtained through a variational argument.

§11.4.2. The Consistent Node Force Vector

The *consistent node force vector* $\mathbf{f}^e$ defined in (11.19) comes from the element contribution to the external work potential W:

$$W^e = \int_{x_1}^{x_2} q\,u\,dx = \int_0^1 q\,\mathbf{N}^T\mathbf{u}^e\,\ell\,d\zeta = \left(\mathbf{u}^e\right)^T\int_0^1 q\begin{bmatrix}1-\zeta\\ \zeta\end{bmatrix}\ell\,d\zeta \;\stackrel{\text{def}}{=}\; \left(\mathbf{u}^e\right)^T\mathbf{f}^e, \tag{11.27}$$

Since $\mathbf{u}^e$ is arbitrary,

$$\boxed{\mathbf{f}^e = \int_{x_1}^{x_2} q\begin{bmatrix}1-\zeta\\ \zeta\end{bmatrix}dx = \int_0^1 q\begin{bmatrix}1-\zeta\\ \zeta\end{bmatrix}\ell\,d\zeta.} \tag{11.28}$$

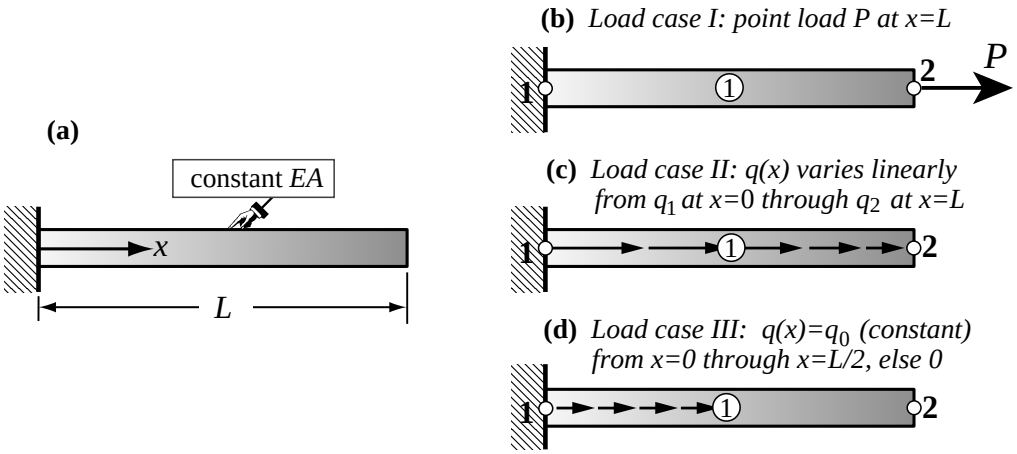

FIGURE 11.7. Fixed-free, prismatic bar example: (a) configuration; (b,c,d) FEM discretization and load cases.

in which ζ is defined by (11.15). If q is constant over the element, it may be taken out of the integral:

$$\boxed{\mathbf{f}^e = q \int_0^1 \begin{bmatrix} 1-\zeta \\ \zeta \end{bmatrix} \ell \, d\zeta.} \tag{11.29}$$

This gives the same results as with the EbE lumping method of Chapter 7. See Exercise 11.3.

Example 11.1. The two-node bar element is tested on the benchmark problem defined in Figure 11.7. A fixed-free, homogeneous, prismatic bar of length L, elastic modulus E and cross section area A has the configuration illustrated in Figure 11.7(a). It is discretized with a *single* element as shown in Figure 11.7(b,c,d), and subjected to the three load cases pictured there. Case I involves a point load P at the free end, which may be formally represented as

$$q^I(x) = P \ \delta(L) \tag{11.30}$$

where $\delta()$ denotes the delta function with argument x.

Case II involves a distributed axial load that varies linearly from $q_1 = q(0)$ at the fixed end through $q_2 = q(L)$ at the free end:

$$q^{II}(x) = q_1(1-\zeta) + q_2\zeta, \tag{11.31}$$

in which $\zeta = 1 - x/L$. Case III involves a "box" distributed load $q(x)$ that is constant and equal to q_0 from the fixed end $x = 0$ through midspan $x = L/2$, and zero otherwise:

$$q^{III}(x) = q_0 \left(H(x) - H(x - \tfrac{1}{2}L)\right), \tag{11.32}$$

in which $H()$ denotes the Heaviside unit step function with argument x. The master stiffness equations constructed using the prismatic stiffness matrix (11.26) with $\ell = L$ and $\bar{x} \to x$ are

$$\frac{EA}{L}\begin{bmatrix} 1 & -1 \\ -1 & 1 \end{bmatrix}\begin{bmatrix} u_1^m \\ u_2^m \end{bmatrix} = \begin{bmatrix} f_1^m \\ f_2^m \end{bmatrix} = \mathbf{f}^m. \tag{11.33}$$

Here supercript m identifies the load case. The consistent node forces computed from (11.28) with $\ell = L$ and $\bar{x} \to x$ are

$$\mathbf{f}^I = \begin{bmatrix} 0 \\ P \end{bmatrix}, \qquad \mathbf{f}^{II} = \frac{L}{6}\begin{bmatrix} 2q_1 + q_2 \\ q_1 + 2q_2 \end{bmatrix}, \qquad \mathbf{f}^{III} = \frac{q_0 L}{8}\begin{bmatrix} 3 \\ 1 \end{bmatrix}. \tag{11.34}$$

On applying the fixed end support condition $u_1^m = 0$ and solving for u_2^m, the free end deflections are

$$u_2^I = \frac{PL}{EA}, \qquad u_2^{II} = \frac{(q_1 + 2q_2)L^2}{6EA}, \qquad u_2^{III} = \frac{q_0 L^2}{8EA}. \tag{11.35}$$

The analytical solutions for $u(x)$, obtained on integrating the ODE $EAu'' + q = 0$ with boundary conditions $u(0) = 0$, $F(L) = EA\,u'(L) = P$ for case I and $F(L) = EA\,u'(L) = 0$ for cases II and III, are

$$u^I(x) = \frac{Px}{EA}, \quad u^{II}(x) = \frac{x\,[3(q_1+q_2)L^2 - 3q_1Lx + (q_1-q_2)x^2]}{6EA}, \quad u^{III}(x) = \frac{q_0}{2EA}\big(Lx - x^2 + \langle x - \tfrac{1}{2}L\rangle^2\big). \tag{11.36}$$

In the expression of $u^{III}(x)$, $\langle x - \frac{1}{2}L\rangle^2$ means $(x - \frac{1}{2}L)^2$ if $x \ge \frac{1}{2}L$, else zero (Macauley's bracket notation for discontinuity functions). Evaluating (11.36) at $x = L$ and comparing to (11.35), one finds that the three computed end deflections are *exact*.

For case I this agreement is no surprise: the exact $u^I(x)$ is linear in x, which is contained in the span of the linear shape functions. But for II and III this is far from obvious since the exact solutions are cubic and piecewise quadratic, respectively, in x. The fact that the exact solution is verified at the free end node is an instance of the *nodal exactness* property discussed in §11.6.1.

Note that in cases II and III the FEM displacement solutions *inside* the element, which vary linearly, will not agree pointwise with the exact solutions, which do not. For example the exact midspan displacement is $u^{III}(\frac{1}{2}L) = q_0L^2/(8EA) = u^{III}(L)$, whereas the FEM interpolation would give $q_0L^2/(16EA)$ there, in error by 100%. To reduce such internal discrepancies the member may be divided into more elements.

§11.5. Weak Forms

Weak forms are expressions notoriously difficult to explain to newcomers. They occupy an intermediate position between differential equations and functionals. There are so many variants and procedural kinks, however, that their position in the mathematical food chain is fuzzy. Confusion is compounded by the use of disparate terminology, some generic, some application oriented. To shed some sunlight into this murky swamp, we go through a specific example: the bar member.

§11.5.1. From Strong to Weak

The governing differential equation for a bar member in terms of axial displacements is $\big(EA\,u'(x)\big)' + q(x) = 0$, or $EA\,u''(x) + q(x) = 0$ if the rigidity EA is constant. Replace the zero by $r(x)$, which stands for *residual*, and move it to the left-hand side:

$$r(x) = \big(EA\,u'(x)\big)' + q(x), \quad \text{or if } EA \text{ is constant:} \quad r(x) = EA\,u''(x) + q. \tag{11.37}$$

The governing ODE may be compactly stated as $r(x) = 0$. This must hold *at each point* over the member span, say $x \in [0, L]$. Hence the term *strong form* (SF) used for this kind of mathematical model. No ambiguity so far. But suppose that insisting on $r(x) = 0$ everywhere is too demanding. We would like to relax that condition so it is satisfied only in an *average sense*. To accomplish that, multiply the residual by a function $v(x)$, integrate over the problem domain, and set the result to zero:

$$J = \int_0^L r(x)\,v(x)\,dx = 0. \tag{11.38}$$

Here $v(x)$ is supposed to be sufficiently well behaved for the integral to exist. Ignoring boundary conditions for now, (11.38) is called a *weak form*, which is often abbreviated to WF in the sequel.

Function $v(x)$ receives two names in the literature: *test function* in a general mathematical context, and *weight function* (also *weighting function*) in the context of approximation methods based on weak forms. In what follows both terms will be used within the appropriate context.

§11.5.2. Weak Form Based Approximation Example

To show how weak forms can be used to generate approximate solutions, consider again a fixed-free, prismatic, homogeneous bar member (that is, EA is constant), under uniform load $q(x) = q_0$ along its length and zero load at the free end. The WF (11.38) becomes

$$J = \int_0^L \big(EA\,u''(x) + q_0\big)\,v(x)\,dx = 0. \tag{11.39}$$

subject to the end conditions

$$u(0) = 0, \quad F(L) = EA\,u'(L) = 0. \tag{11.40}$$

We will restrict both $u(x)$ and $v(x)$ to be *quadratic* polynomials:

$$u(x) = a_0 + a_1\,x + a_2\,x^2, \quad v(x) = b_0 + b_1\,x + b_2\,x^2. \tag{11.41}$$

in which a_i and b_i are numerical coefficients, real in this case. Once assumptions such as those in (11.41) are made, more terminology kicks in. The assumed $u(x)$ is now called a *trial function*, which is spanned by the linear-space basis $\{1, x, x^2\}$ of dimension 3. The assumed $v(x)$ is called a *weight function*, which is spanned by exactly the same basis. There is a special name for the scenario when the trial and weight function bases coalesce: the *Galerkin method*.[7]. We will call the end result a *Galerkin solution*. Replacing (11.41) into (11.39) we get

$$J = \frac{L}{6}(6b_0 + 3b_1\,L + 2b_2\,L^2)\,(2EA\,a_2 + q_0). \tag{11.42}$$

Now J must vanish for any arbitrary value of $\{b_0, b_1, b_2\}$. On extracting the expressions that multiply those coefficients we obtain the same equation thrice: $2EA\,a_2 + q_0 = 0$. Thus $a_2 = -q_0/(2EA)$, whereas a_0 and a_1 remain arbitrary. Consequently the Galerkin solution *before* BC is

$$u(x) = a_0 + a_1\,x - \frac{q_0}{2EA}x^2. \tag{11.43}$$

ODE aficionados would recognize this as the general solution of $EAu'' + q_0 = 0$ so Uncle Boris has done the job. Applying the end conditions (11.40) gives $a_0 = 0$ and $a_1 = q_0/(EA)$ whence the final solution is

$$u(x) = \frac{q_0}{2EA}\,x(2L - x). \tag{11.44}$$

Replacing into (11.37) and (11.40) it may be verified that this is the exact analytical solution.

Instead of applying the end conditions *a posteriori* we may try to incorporate them *a priori* into the trial function assumption. On enforcing (11.40) into the assumed $u(x)$ of (11.41) we find that $a_0 = 0$ and $a_1 = -2a_2\,L$. The trial function becomes

$$u(x) = a_2\,x\,(x - 2L), \tag{11.45}$$

[7] Introduced by Boris Galerkin in 1912. For a brief account of the general methodology, see **Notes and Bibliography**

and only one free coefficient remains. Accordingly only one weight basis function is needed: either 1, x or x^2 does the job, and the exact solution (11.44) is obtained again.[8]

What happens if the load $q(x)$ varies, say, linearly and the same quadratic polynomial assumptions (11.41) are used? Then Galerkin goes gaga. See Exercise 11.8.

Even for this trivial example, several procedural choices are apparent. If we allow the trial and weight function spaces to differ, volatility zooms up. Furthermore, we can apply transformations to the residual integral as done in the next subsection. Compared to the well ordered world of variational-based FEM, confusion reigns supreme.

§11.5.3. Balanced Weak Forms

Some method in the madness can be injected by balancing. A look at (11.39) reveals an unpleasant asymmetry. Second derivatives of $u(x)$ appear, but none of $v(x)$. This places unequal restrictions on smoothness of the trial and test function spaces. Integration by parts restores derivative order balance. Replacing $\int_0^L E\,A\,u''\,v\,dx = -\int_0^L E\,A\,u'\,v'\,dx + (E\,A u')v\big|_0^L$ and rearranging terms yields

$$J = \int_0^L E\,A\,u'(x)\,v'(x)\,dx - \int_0^L q(x)\,v(x)\,dx - \big(E\,A\,u'(x)\big)\,v(x)\big|_0^L\,. \tag{11.46}$$

This will be called a *balanced-derivative weak form*, or simply a *balanced weak form* (BWF). It displays obvious advantages: (i) same smoothness requirements for assumed u and v, and (ii) end BC appear explicitly in the non-integral term, neatly factored into essential and natural. A minor flaw is that the original residual is no longer clearly visible.

For a bar with variable axial rigidity replace $E\,A\,u''$ by $(E\,A\,u')'$ in the first integrand.

On repeating the Galerkin procedure of the previous subsection with the assumptions (11.41) one finds an identical J, as may be expected, and the same final solution. Again one has the choice of pre- or post-imposing the end conditions (11.40). Generally the latter choice is far more convenient in a computer implementation.

§11.5.4. Principle of Virtual Work as Balanced Weak Form

There is a close relationship between the BWF (11.46) and one of the fundamental tools of Analytical Mechanics: the Principle of Virtual Work (PVW). To exhibit it, set the test function to be an admissible variation of $u(x)$: $v(x) = \delta\,u(x)$, in which $\delta u(x)$ strongly satisfies all essential BC. Then assume that J is the first variation of a functional Π:

$$J = \int_0^L E\,A\,u'(x)\,\delta u'(x)\,dx - \int_0^L q(x)\,\delta u(x)\,dx - \big(E\,A\,u'(x)\big)\,\delta u(x)\big|_0^L \stackrel{\text{def}}{=} \delta\Pi. \tag{11.47}$$

Indeed this is the first variation of the TPE functional:

$$\Pi = U - W = \tfrac{1}{2}\int_0^L u'(x)\,E\,A\,u'(x)\,dx - \int_0^L q(x)\,u(x)\,dx \tag{11.48}$$

[8] Some early works covering weighted residual methods, for example Crandall [159], proclaim that the trial function must satisfy *all* BC *ab initio*. Later ones, e.g., [260,261], relax that rule to BC of essential type (in Galerkin methods, this rule applies to both trial and test functions since the spaces coalesce). In practice this rule can be often relaxed further, as in the example of §11.5.2, applying essential BCs at the last moment.

Hence $J = 0$ is the same as $\delta\Pi = 0$ or $\delta U = \delta W$, which is the PVW for an elastic bar member. This relationship can be used to prove an important property: *Galerkin method is equivalent to a variational formulation* if the residual is the Euler-Lagrange equation of a functional.

Remark 11.5. Where does the boundary term $\big(EA\,u'(x)\big)\,\delta u(x)\big|_0^L$ in (11.47) go? Actually, into δW. This immersion is a bit tricky, and depends on redefining $q(x)$ to include prescribed end point forces such as $N(L) = EA\,u'(L) = P$ through delta functions. This is the subject of Exercise 11.9.

§11.5.5. *Weighted Residual Methods

Galerkin method is widely used in computational mechanics, but does not exhaust all possibilities of using a weak form as source for obtaining numerical solutions. The main generalization consist of allowing trial and test (weight) functions to be different. This leads to a rich class of approximation methods unified under the name *Method of Weighted Residuals* or MWR.

The key idea is as follows. Both $u(x)$ and $v(x)$ are restricted to belong to linear function spaces of *finite dimension* N_u and N_v. These are the *trial function space* and the *test function space*, respectively. which are spanned by basis functions $\phi_i(x)$ and $\psi(x)$, respectively:

$$u(x) = \text{span}\big\{\phi_i(x), 1 \le i \le N_u\big\}, \qquad v(x) = \text{span}\big\{\psi_i(x), 1 \le i \le N_v\big\} \tag{11.49}$$

in which usually $N_u = N_v$. Since the spaces are linear, any $u(x)$ and $v(x)$ can be represented as linear combination of the basis functions:

$$u(x) = \sum_{i=1}^{N_u} a_i\,\phi_i(x), \qquad v(x) = \sum_{i=1}^{N_v} b_i\,\psi_i(x). \tag{11.50}$$

Here a_i and b_i are scalar coefficients, which may be real or complex depending on the nature of the problem. Insert these into the weak form, perform the necessary integrations, and extract the N_v expressions that are coefficients of the b_i. Solve these equations for the coefficients a_i, and replace in the first of (11.50) to get the approximate solution $u(x)$.

The MWR methodology is of course not restricted to one space dimension. It also extends to time-dependent problems. It can be merged smoothly with the FEM concept of piecewise approximation using shape functions. Some references are provided under **Notes and Bibliography**.

§11.6. *Accuracy Analysis

Low order 1D elements may give surprisingly high accuracy. In particular the lowly two-node bar element can display infinite accuracy under some conditions. This phenomenon is studied in this advanced section as it provides an introduction to modified equation methods and Fourier analysis along the way.

§11.6.1. *Nodal Exactness and Superconvergence

Suppose that the following two conditions are satisfied:

1. The bar properties are constant along the length (prismatic member).
2. The distributed load $q(x)$ is zero between nodes. The only applied loads are point forces at the nodes.

If so, a linear axial displacement $u(x)$ as defined by (11.13) and (11.14) is the exact solution over each element since constant strain and stress satisfy, element by element, all of the governing equations listed in Figure 11.2.[9]

[9] The internal equilibrium equation $p' + q = EA\,u'' + q = 0$ is trivially verified because $q = 0$ from the second assumption, and $u'' = 0$ because of shape function linearity.

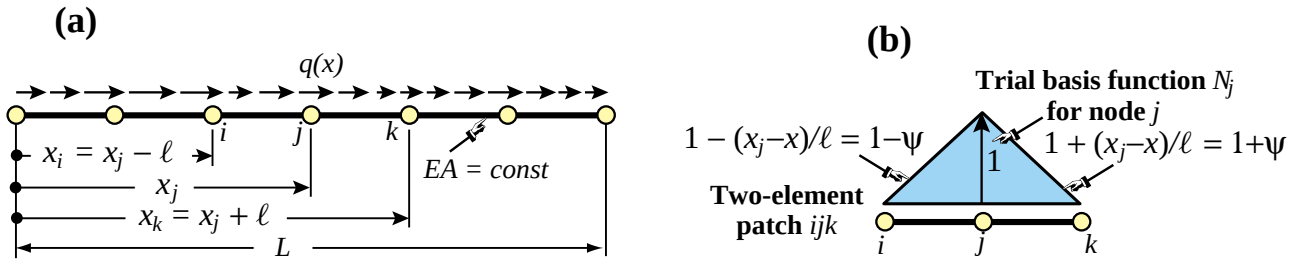

FIGURE 11.8. Superconvergence patch analysis: (a) lattice of bar elements; (b) two element patch.

It follows that if the foregoing conditions are verified the FEM solution is *exact*; that is, it agrees with the analytical solution of the mathematical model.[10] Adding extra elements and nodes would not change the solution. That is the reason behind the truss discretizations used in Chapters 2–3: *one element per member is enough* if they are prismatic and loads are applied to joints. Such models are called *nodally exact*.

What happens if the foregoing assumptions are not met? Exactness is then generally lost, and several elements per member may be beneficial if spurious mechanisms are avoided.[11] For a 1D lattice of equal-length, prismatic two-node bar elements, an interesting and more difficult result is: *the solution is nodally exact for any loading if consistent node forces are used.* This is proven in the subsection below. This result underlies the importance of computing node forces correctly.

If conditions such as equal-length are relaxed, the solution is no longer nodally exact but convergence at the nodes is extremely rapid (faster than could be expected by standard error analysis) as long as consistent node forces are used. This phenomenon is called *superconvergence* in the FEM literature.

§11.6.2. *Fourier Patch Analysis

The following analysis is based on the modified differential equation (MoDE) method of Warming and Hyett [**?**] combined with the Fourier patch analysis approach of Park and Flaggs [553,554]. Consider a lattice of two-node prismatic bar elements of constant rigidity EA and equal length ℓ, as illustrated in Figure 11.8. The total length of the lattice is L. The system is subject to an arbitrary axial load $q(x)$. The only requirement on $q(x)$ is that it has a convergent Fourier series in the space direction.

From the lattice extract a patch[12] of two elements connecting nodes x_i, x_j and x_k as shown in Figure 11.8. The FEM patch equations at node j are

$$\frac{EA}{\ell}\begin{bmatrix} -1 & 2 & -1 \end{bmatrix}\begin{bmatrix} u_i \\ u_j \\ u_k \end{bmatrix} = f_j, \tag{11.51}$$

in which the node force f_j is obtained by consistent lumping:

$$f_j = \int_{x_i}^{x_k} q(x) N_j(x)\, dx = \int_{-1}^{0} q(x_j + \psi\ell)(1+\psi)\,\ell\, d\psi + \int_{0}^{1} q(x_j + \psi\ell)(1-\psi)\,\ell\, d\psi. \tag{11.52}$$

Here $N_j(x)$ is the "hat" trial basis function for node j, depicted in Figure 11.8, and $\psi = (x - x_j)/\ell$ is a dimensionless coordinate that takes the values -1, 0 and 1 at nodes i, j and k, respectively. If $q(x)$ is expanded

[10] In variational language: the Green function of the $u'' = 0$ problem is included in the FEM trial space.

[11] These can happen when transforming such elements for 2D and 3D trusses. See Exercise E11.7.

[12] A patch is the set of all elements connected to a node; in this case j.

in Fourier series

$$q(x) = \sum_{m=1}^{M} q_m e^{i\beta_m x}, \quad \beta_m = m\pi/L, \tag{11.53}$$

(the term $m = 0$ requires special handling) the exact solution of the continuum equation $EA\,u'' + q = 0$ is

$$u^*(x) = \sum_{m=1}^{M} u_m^* e^{i\beta_m x}, \quad u_m^* = \frac{q_m e^{i\beta_m x}}{EA\beta_m^2}. \tag{11.54}$$

Evaluation of the consistent force using (11.52) gives

$$f_j = \sum_{m=1}^{M} f_{jm}, \quad f_{jm} = q_m \ell \frac{\sin^2(\frac{1}{2}\beta_m \ell)}{\frac{1}{4}\beta_m^2 \ell^2} e^{i\beta_m x_2}. \tag{11.55}$$

To construct a modified differential equation (MoDE), expand the displacement by Taylor series centered at node j. Evaluate at i and k: $u_i = u_j - \ell u_j' + \ell^2 u_j''/2! - \ell^3 u_j'''/3! + \ell^4 u_j^{iv}/4! + \ldots$ and $u_k = u_j + \ell u_j' + \ell^2 u_j''/2 + \ell^3 u_j'''/3! + \ell^4 u_j^{iv}/4! + \ldots$. Replace these series into (11.51) to get

$$-2EA\ell \left(\frac{1}{2!} u_j'' + \frac{\ell^2}{4!} u_j^{iv} + \frac{\ell^4}{6!} u_j^{vi} + \ldots \right) = f_j. \tag{11.56}$$

This is an ODE of infinite order. It can be reduced to an algebraic equation by assuming that the response of (11.56) to $q_m\, e^{i\beta_m x}$ is harmonic: $u_{jm} e^{i\beta_m x}$. If so $u_{jm}'' = -\beta_m^2 u_{jm}$, $u_{jm}^{iv} = \beta_m^4 u_{jm}$, etc, and the MoDE becomes

$$2EA\ell\beta_m^2 \left(\frac{1}{2!} - \frac{\beta_m^2 \ell^2}{4!} + \frac{\beta_m^4 \ell^4}{6!} - \ldots \right) u_{jm} = 4EA\ell \sin^2(\tfrac{1}{2}\beta_m \ell)\, u_{jm} = f_{jm} = q_m \ell \frac{\sin^2(\frac{1}{2}\beta_m \ell)}{\frac{1}{4}\beta_m^2 \ell^2} e^{i\beta_m x_j}. \tag{11.57}$$

Solving gives $u_{jm} = q_m e^{i\beta_m x_j}/(EA\beta_m^2)$, which compared with (11.54) shows that $u_{jm} = u_m^*$ for any $m > 0$. Consequently $u_j = u_j^*$. In other words, the MoDE (11.56) and the original ODE: $EAu'' + q = 0$ have the same value at $x = x_j$ for any load $q(x)$ developable as (11.53). This proves nodal exactness. In between nodes the two solutions will not agree.[13]

The case $m = 0$ has to be treated separately since the foregoing expressions become $0/0$. The response to a uniform $q = q_0$ is a quadratic in x, and it is not difficult to prove nodal exactness.

§11.6.3. *Robin Boundary Conditions

Suppose that for a bar of length L one has the following end conditions: $u'(0) = au(0) + b$ at $x = 0$ and $u'(L) = au(L) + b$ at $x = L$, in which a and b are given coefficients. Those are called Robin BCs in the literature. Adjoining them as Courant penalty terms gives the functional

$$F(u) = \int_0^L [\tfrac{1}{2} EA\,(u')^2 - q\,u]\,dx + \tfrac{1}{2}[u'(0) - au(0) - b]^2 + \tfrac{1}{2}[u'(L) + au(L) + b]^2. \tag{11.58}$$

Divide [0,L] into N_e elements and $N = N_e + 1$ nodes. Do C^0 linear interpolation over each element, insert into $F(u)$ to get $F_d(u) = \frac{1}{2}\mathbf{u}^T\mathbf{K}\mathbf{u} - \mathbf{f}^T\mathbf{v}$, in which $\mathbf{u}$ is the vector of node values, $\mathbf{K}$ the master stiffness matrix and $\mathbf{f}$ the master force vector. Coefficients a and b will affect both $\mathbf{K}$ and $\mathbf{f}$.

[13] The FEM solution varies linearly between nodes whereas the exact one is generally trigonometric.

Vanishing of the first variation: $\delta F_d = 0$ yields the FEM equations $\mathbf{Ku} = \mathbf{f}$ to be solved for $\mathbf{u}$. The Robin BCs at $x = 0$ and $x = L$ will affect the stiffness and force contributions of the first and last elements, but not those of interior elements.

This kind of boundary value problem (i.e., with Robin BCs) is common in heat conduction and heat transfer with convection given over cooling surfaces. In that case the heat flux is proportional to the difference of the (unknown) surface temperature and that of the cooling fluid. Elements that "touch" the convention boundary are affected.

Notes and Bibliography

The foregoing account pertains to the simplest structural finite element: the two-node bar element. For bar members these developments may be generalized in several directions, three of which are mentioned next.

Refined bar models. Adding internal nodes we can pass from linear to quadratic and cubic shape functions. These elements are rarely useful on their own right, but as accessories to 2D and 3D high order continuum elements (for example, to model edge reinforcements.) For that reason they are not considered here. The 3-node bar element is developed in exercises assigned in Chapter 16.

Use in 2D and 3D truss structures. The only additional ingredients are the local-to-global transformations discussed in Chapters 3 and 6.

Curved bar elements. These can be derived using isoparametric mapping, a device introduced later.

Matrices for straight bar elements are available in any finite element book; for example Przemieniecki [596].

Tonti diagrams were introduced in the 1970s in papers now difficult to access, for example [749]. Scanned images are available, howewer, from `http://www.dic.units.it/perspage/discretephysics`

The fundamentals of Variational Calculus may be studied in the excellent textbook [297], which is now available in an inexpensive Dover edition. The proof of the MPE principle can be found in texts on variational methods in mechanics. For example: Langhaar [435], which is the most readable "old fashioned" treatment of the energy principles of structural mechanics, with a clear treatment of virtual work. (Out of print but used copies may be found via the web engines cited in §1.5.2.) The elegant treatment by Lanczos [434] is recommended as reading material although it is more oriented to physics than structural mechanics.

It was noted that weak forms occupy an intermediate position between two older classical areas: differential equations (introduced in the XVII Century by the Calculus founders) and variational forms (introduced by Euler in the XVIII Century). Some weak forms in disguise are also ancient; e.g., the PVW was placed on firm mathematical grounds by Lagrange in the late XVIII Century [430]. But their rapid development as tools for producing approximate solutions of ODEs and PDEs took place in the early XIX Century. Five important variants are: Galerkin (1915), subdomain (1923), least squares (1928), moments (1932), and collocation (1937). These, as well as a few others of less importance, were unified in 1956 under the label Method of Weighted Residuals or MWR, by Crandall [159]. Other attempts at unification during this period may be found in [19,147]. The use of MWR methods, especially Galerkin's, as enabling devices to generate finite element equations developed rapidly following the pioneer paper [820]. The chief motivation was to accommodate application problems where a classical variational formulation does not exist, or is inconvenient to use.

The first accuracy study of FEM discretizations using modified equation methods is by Waltz et. al. [780]; however their procedures were faulty, which led to incorrect conclusions. The first correct derivation of modified equations appeared in [783]. The topic has recently attracted interest from applied mathematicians because modified equations provide a systematic tool for *backward error analysis* of differential equations: the discrete solution is the exact solution of the modified problem. This is particularly important for the study of long term behavior of discrete dynamical systems, whether deterministic or chaotic. Recommended references along these lines are [318,327,709].

Nodal exactness of bar models for point node loads is a particular case of a theorem by Tong [746]. For arbitrary loads it was proven by Park and Flaggs [553,554], who followed a variant of the scheme of §11.6.2.

A different technique is used in Exercise 11.10. The budding concept of superconvergence, which emerged in the late 1960s, is outlined in the book of Strang and Fix [698]. There is a monograph [781] devoted to the subject; it covers only Poisson problems but provides a comprehensive reference list until 1995.

References

Referenced items moved to Appendix R.

Homework Exercises for Chapter 11
Variational Formulation of Bar Element

EXERCISE 11.1 [D:10] Explain the kinematic admissibility requirements stated in **?** in terms of physics, namely ruling out the possibility of gaps or interpenetration as the bar material deforms.

EXERCISE 11.2 [A/C:15] Using (11.25), derive the stiffness matrix for a *tapered* bar element in which the cross section area varies linearly along the element length:

$$A = A_i(1-\zeta) + A_j\,\zeta, \tag{E11.1}$$

where A_i and A_j are the areas at the end nodes, and $\zeta = x^e/\ell$ is the dimensionless coordinate defined in §11.3.6. Show that this yields the same answer as that of a stiffness of a constant-area bar with cross section $\frac{1}{2}(A_i + A_j)$. Note: the following *Mathematica* script may be used to solve this exercise:[14]

```
ClearAll[Le,x,Em,A,Ai,Aj];
Be={{-1,1}}/Le; ζ=x/Le; A=Ai*(1-ζ)+Aj*ζ;
Ke=Integrate[Em*A*Transpose[Be].Be,{x,0,Le}];
Ke=Simplify[Ke];
Print["Ke for varying cross section bar: ",Ke//MatrixForm];
```

In this and following scripts `Le` stands for ℓ.

EXERCISE 11.3 [A:10] Find the consistent load vector $\mathbf{f}^e$ for a bar of *constant* area A subject to a *uniform* axial force $q = \rho g A$ per unit length along the element. Show that this vector is the same as that obtained with the element-by-element (EbE) "lumping" method of §8.4, which simply assigns half of the total load: $\frac{1}{2}\rho g A\ell$, to each node. Hint: use (11.29) and $\int_0^1 \zeta\, d\zeta = 1/2$.

EXERCISE 11.4 [A/C:15] Repeat the previous calculation for the tapered bar element subject to a force $q = \rho g A$ per unit length, in which A varies according to (E11.1) whereas ρ and g are constant. Check that if $A_i = A_j$ one recovers $f_i = f_j = \frac{1}{2}\rho g A\ell$. Note: the following *Mathematica* script may be used to solve this exercise:[15]

```
ClearAll[q,A,Ai,Aj,ρ,g,Le,x];
ζ=x/Le; Ne={{1-ζ,ζ}}; A=Ai*(1-ζ)+Aj*ζ; q=ρ*g*A;
fe=Integrate[q*Ne,{x,0,Le}];
fe=Simplify[fe];
Print["fe for uniform load q: ",fe//MatrixForm];
ClearAll[A];
Print["fe check: ",Simplify[fe/.{Ai->A,Aj->A}]//MatrixForm];
```

EXERCISE 11.5 [A/C:20] A tapered bar element of length ℓ, end areas A_i and A_j with A interpolated as per (E11.1), and constant density ρ, rotates on a plane at uniform angular velocity ω (rad/sec) about node i. Taking axis x along the rotating bar with origin at node i, the centrifugal axial force is $q(x) = \rho A\omega^2 x$ along the length, in which $x \equiv x^e$. Find the consistent node forces as functions of ρ, A_i, A_j, ω and ℓ, and specialize the result to the prismatic bar $A = A_i = A_j$. Partial result check: $f_j = \frac{1}{3}\rho\omega^2 A\ell^2$ for $A = A_i = A_j$.

---

[14] The `ClearAll[...]` at the start of the script is recommended programming practice to initialize variables and avoid "cell crosstalk." In a `Module` this is done by listing the local variables after the `Module` keyword.

[15] The `ClearAll[A]` before the last statement is essential; else `A` would retain the previous assignation.

EXERCISE 11.6 [A:15] (Requires knowledge of Dirac's delta function properties.) Find the consistent load vector $\mathbf{f}^e$ if the bar is subjected to a concentrated axial force Q at a distance $x = a$ from its left end. Use (11.28), with $q(x) = Q\,\delta(a)$, in which $\delta(a)$ is the one-dimensional Dirac's delta function at $x = a$. Note: the following script does it by *Mathematica*, but it is overkill:

```
ClearAll[Le,q,Q,a,x];
ζ=x/Le; Ne={{1-ζ,ζ}}; q=Q*DiracDelta[x-a];
fe=Simplify[ Integrate[q*Ne,{x,-Infinity,Infinity}] ];
Print["fe for point load Q at x=a: ",fe//MatrixForm];
```

EXERCISE 11.7 [C+D:20] In a learned paper, Dr. I. M. Clueless proposes "improving" the result for the example truss by putting three extra nodes, 4, 5 and 6, at the midpoint of members 1–2, 2–3 and 1–3, respectively. His "reasoning" is that more is better. Try Dr. C.'s suggestion using the *Mathematica* implementation of Chapter 4 and verify that the solution "blows up" because the modified master stiffness is singular. Explain physically what happens.

EXERCISE 11.8 [C+D:15] This exercise illustrates "Galerkin surprises." Take up again the example of §11.5.2, but suppose now that the axial load varies linearly, as in (11.31). The trial and weight function assumptions are the quadratic polynomials (11.41). Show that the integral (11.39) is given by

$$12\,J/L = b_0\left(24EA\,a_2 + 6(q_1{+}q_2)\right) + b_1\left(12EA\,a_2 + 2(q_1{+}2q_2)\right) + b_2\left(8EA\,a_2 + (q_1{+}3q_2)\right), \quad \text{(E11.2)}$$

and that the resulting 3 equations for a_2 are *inconsistent* unless $q_1 = q_2$. Only one weight function gives the correct solution at $x = L$; which one? Note that the Galerkin method is generally viewed as the "most reliable" member of the MWR tribe. But unforeseen surprises have a silver lining: more papers can be written to explain them. Here is a partial fix: make the test function satisfy the essential BC *a priori*.

EXERCISE 11.9 [A:20]. Prove that (11.47) is the first variation of (11.48), thus linking the PVW with the TPE functional. See Remark 11.5 for a hint on how to treat the boundary term in (11.47).

EXERCISE 11.10 [A:35, close to research paper level]. Prove nodal exactness of the two-node bar element for arbitrary but Taylor expandable loading without using the Fourier series approach. Hints: expand $q(x) = q(x_j) + (\ell\psi)q'(x_j) + (\ell\psi)^2 q''(x_j)/2! + \ldots$, where $\ell\psi = x - x_j$ is the distance to node j, compute the consistent force $f_j(x)$ from (11.52), and differentiate the MoDE (11.56) repeatedly in x while truncating all derivatives to a maximum order $n \geq 2$. Show that the original ODE: $EAu'' + q = 0$, emerges as an identity regardless of how many derivatives are kept.

12

Variational Formulation of Plane Beam Element

TABLE OF CONTENTS

§12.1. Introduction

The previous Chapter introduced the TPE-based variational formulation of finite elements, which was illustrated for the bar element. This Chapter applies that technique to a more complicated one-dimensional element: the plane beam described by engineering beam theory.

Mathematically, the main difference of beams with respect to bars is the increased order of continuity required for the assumed transverse-displacement functions to be admissible. Not only must these functions be continuous but they must possess continuous x first derivatives. To meet this requirement both deflections *and* slopes are matched at nodal points. Slopes may be viewed as *rotational* degrees of freedom in the small-displacement assumptions used here.

§12.2. What is a Beam?

Beams are the most common type of structural component, particularly in Civil and Mechanical Engineering. A *beam* is a bar-like structural member whose primary function is to support *transverse loading* and carry it to the supports. See Figure 12.1.

By "bar-like" it is meant that one of the dimensions is considerably larger than the other two. This dimension is called the *longitudinal dimension* or *beam axis*. The intersection of planes normal to the longitudinal dimension with the beam member are called *cross sections*. A *longitudinal plane* is one that passes through the beam axis.

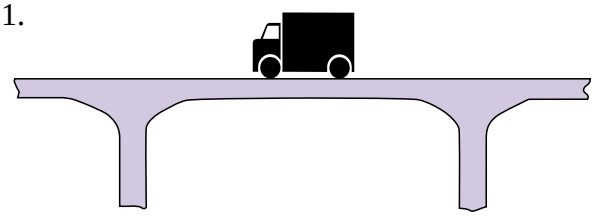

FIGURE 12.1. A beam is a structural member designed to resist transverse loads.

A beam resists transverse loads mainly through *bending action*, Bending produces compressive longitudinal stresses in one side of the beam and tensile stresses in the other.

The two regions are separated by a *neutral surface* of zero stress. The combination of tensile and compressive stresses produces an internal *bending moment*. This moment is the primary mechanism that transports loads to the supports. The mechanism is illustrated in Figure 12.2.

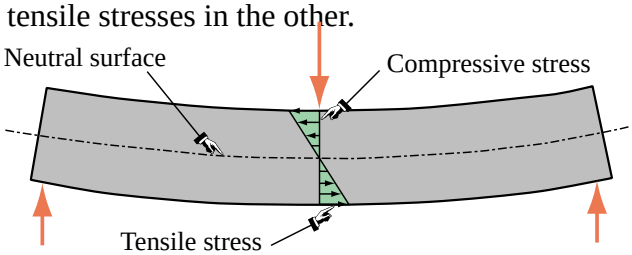

FIGURE 12.2. Beam transverse loads are primarily resisted by bending action.

§12.2.1. Terminology

A *general beam* is a bar-like member designed to resist a combination of loading actions such as biaxial bending, transverse shears, axial stretching or compression, and possibly torsion. If the internal axial force is compressive, the beam has also to be designed to resist buckling. If the beam is subject primarily to bending and axial forces, it is called a *beam-column*. If it is subjected primarily to bending forces, it is called simply a beam. A beam is *straight* if its longitudinal axis is straight. It is *prismatic* if its cross section is constant.

A *spatial beam* supports transverse loads that can act on arbitrary directions along the cross section. A *plane beam* resists primarily transverse loading on a preferred longitudinal plane. This Chapter considers only plane beams.

§12.2.2. Mathematical Models

One-dimensional mathematical models of structural beams are constructed on the basis of *beam theories*. Because beams are actually three-dimensional bodies, all models necessarily involve some form of approximation to the underlying physics. The simplest and best known models for straight, prismatic beams are based on the *Bernoulli-Euler beam theory* (also called *classical beam theory* and *engineering beam theory*), and the *Timoshenko beam theory*. The Bernoulli-Euler theory is that taught in introductory Mechanics of Materials courses, and is the one emphasized in this Chapter. The Timoshenko beam model is presented in Chapter 13, which collects advanced material.

Both models can be used to formulate beam finite elements. The Bernoulli-Euler beam theory leads to the so-called *Hermitian* beam elements.[1] These are also known as C^1 elements for the reason explained in §12.5.1. This model neglects the effect of transverse shear deformations on the internal energy. Elements based on Timoshenko beam theory, also known as C^0 elements, incorporate a first order correction for transverse shear effects. This model assumes additional importance in dynamics and vibration.

§12.2.3. Assumptions of Classical Beam Theory

The Bernoulli-Euler or classical beam theory for *plane beams* rests on the following assumptions:

1. *Planar symmetry*. The longitudinal axis is straight and the cross section of the beam has a longitudinal plane of symmetry. The resultant of the transverse loads acting on each section lies on that plane. The support conditions are also symmetric about this plane.
2. *Cross section variation*. The cross section is either constant or varies smoothly.
3. *Normality*. Plane sections originally normal to the longitudinal axis of the beam remain plane and normal to the deformed longitudinal axis upon bending.
4. *Strain energy*. The internal strain energy of the member accounts only for bending moment deformations. All other contributions, notably transverse shear and axial force, are ignored.
5. *Linearization*. Transverse deflections, rotations and deformations are considered so small that the assumptions of infinitesimal deformations apply.
6. *Material model*. The material is assumed to be elastic and isotropic. Heterogeneous beams fabricated with several isotropic materials, such as reinforced concrete, are not excluded.

§12.3. The Bernoulli-Euler Beam Theory

§12.3.1. Element Coordinate Systems

Under transverse loading one of the top surfaces shortens while the other elongates; see Figure 12.2. Therefore a *neutral surface* that undergoes no axial strain exists between the top and the bottom. The intersection of this surface with each cross section defines the *neutral axis* of that cross section.[2]

[1] The qualifier "Hermitian" relates to the use of a transverse-displacement interpolation formula studied by the French mathematician Hermite. The term has nothing to do with the mathematical model used.

[2] If the beam is homogenous, the neutral axis passes through the centroid of the cross section. If the beam is fabricated of different materials — for example, a reinforced concrete beam — the neutral axes passes through the centroid of an "equivalent" cross section. This topic is covered in Mechanics of Materials textbooks; for example Popov [595].

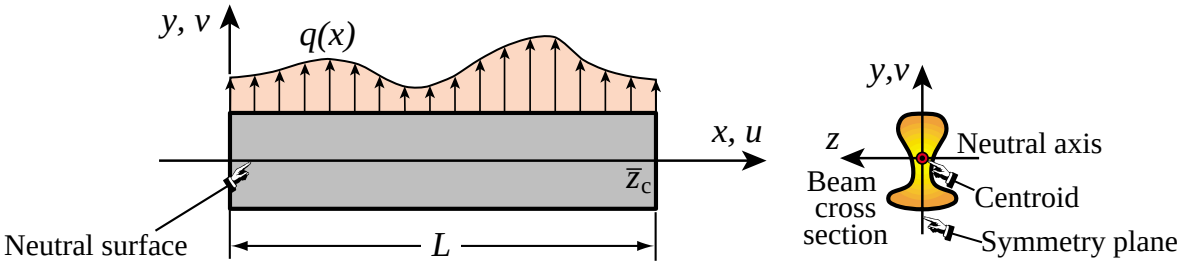

FIGURE 12.3. Terminology and choice of axes for Bernoulli-Euler model of plane beam.

The Cartesian axes for plane beam analysis are chosen as shown in Figure 12.3. Axis x lies along the longitudinal beam axis, at neutral axis height. Axis y lies in the symmetry plane and points upwards. Axis z is directed along the neutral axis, forming a RHS system with x and y. The origin is placed at the leftmost section. The total length (or span) of the beam member is called L.

§12.3.2. Kinematics

The *motion* under loading of a plane beam member in the x, y plane is described by the two dimensional displacement field

$$\begin{bmatrix} u(x,y) \\ v(x,y) \end{bmatrix}, \tag{12.1}$$

where u and v are the axial and transverse displacement components, respectively, of an arbitrary beam material point. The motion in the z direction, which is primarity due to Poisson's ratio effects, is of no interest. The normality assumption of the Bernoulli-Euler model can be represented mathematically as

$$u(x,y) = -y\frac{\partial v(x)}{\partial x} = -yv' = -y\theta, \qquad v(x,y) = v(x). \tag{12.2}$$

Note that the slope $v' = \partial v/\partial x = dv/dx$ of the deflection curve has been identified with the *rotation* symbol θ. This is permissible because θ represents to first order, according to the kinematic assumptions of this model, the rotation of a cross section about z positive CCW.

§12.3.3. Loading

The transverse force *per unit length* that acts on the beam in the $+y$ direction is denoted by $q(x)$, as illustrated in Figure 12.3. Concentrated loads and moments acting on isolated beam sections can be represented by the delta function and its derivative. For example, if a transverse point load F acts at $x = a$, it contributes $F\delta(a)$ to $q(x)$. If the concentrated moment C acts at $x = b$, positive CCW, it contributes $C\delta'(b)$ to $q(x)$, where δ' denotes a doublet acting at $x = b$.

§12.3.4. Support Conditions

Support conditions for beams exhibit far more variety than for bar members. Two canonical cases are often encountered in engineering practice: simple support and cantilever support. These are illustrated in Figures 12.4 and 12.5, respectively. Beams often appear as components of skeletal structures called frameworks, in which case the support conditions are of more complex type.

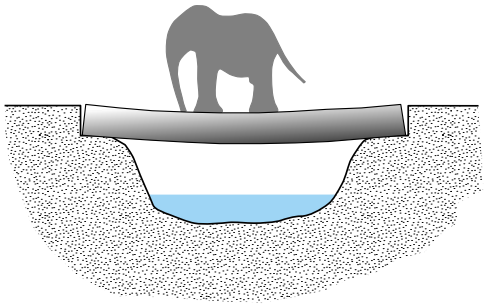

FIGURE 12.4. A simply supported beam has end supports that preclude transverse displacements but permit end rotations.

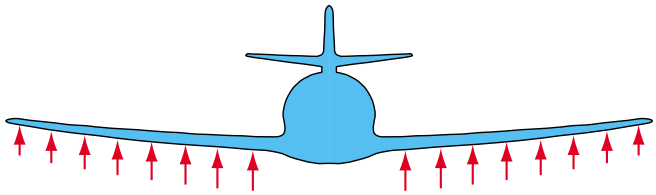

FIGURE 12.5. A cantilever beam is clamped at one end and free at the other. Airplane wings and stabilizers are examples of this configuration.

§12.3.5. Strains, Stresses and Bending Moments

The Bernoulli-Euler or classical model assumes that the internal energy of beam member is entirely due to bending strains and stresses. Bending produces axial stresses σ_{xx}, which will be abbreviated to σ, and axial strains e_{xx}, which will be abbreviated to e. The strains can be linked to the displacements by differentiating the axial displacement $u(x)$ of (12.2):

$$e = \frac{\partial u}{\partial x} = -y\frac{\partial^2 v}{\partial x^2} = -y\frac{d^2 v}{dx^2} = -yv'' = -y\kappa. \tag{12.3}$$

Here κ denotes the deformed beam axis curvature, which to first order is $\kappa \approx d^2v/dx^2 = v''$. The bending stress $\sigma = \sigma_{xx}$ is linked to e through the one-dimensional Hooke's law

$$\sigma = Ee = -Ey\frac{d^2 v}{dx^2} = -Ey\kappa, \tag{12.4}$$

where E is the longitudinal elastic modulus. The most important stress resultant in classical beam theory is the *bending moment* M, which is defined as the cross section integral

$$M = \int_A -y\sigma \, dA = E\frac{d^2 v}{dx^2}\int_A y^2 \, dA = EI\,\kappa. \tag{12.5}$$

Here $I \equiv I_{zz}$ denotes the moment of inertia $\int_A y^2\, dA$ of the cross section with respect to the z (neutral) axis. The bending moment M is considered positive if it compresses the upper portion: $y > 0$, of the beam cross section, as illustrated in Figure 12.6. This convention explains the negative sign of y in the integral (12.5). The product EI is called the *bending rigidity* of the beam with respect to flexure about the z axis.

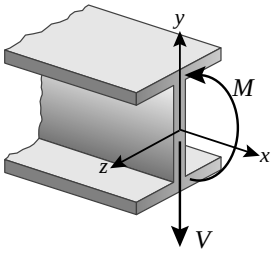

FIGURE 12.6. Positive sign convention for M and V.

The governing equations of the Bernoulli-Euler beam model are summarized in the Tonti diagram of Figure 12.7.

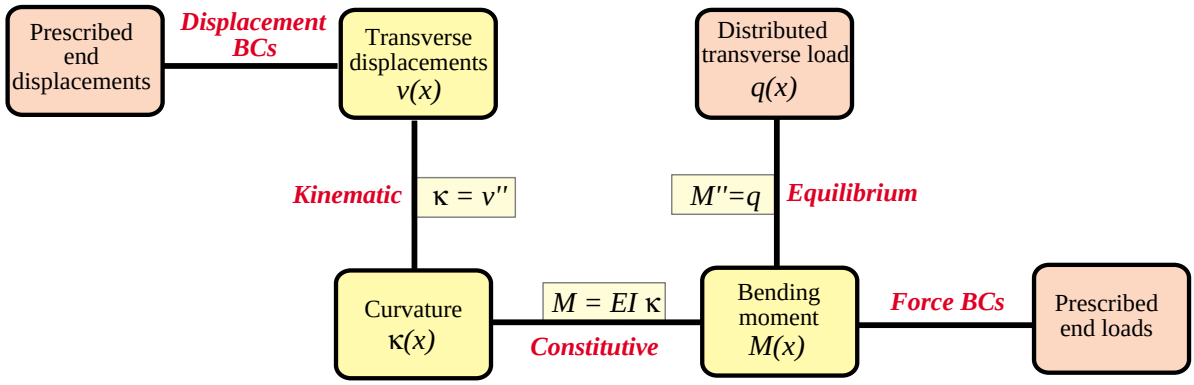

FIGURE 12.7. The Tonti diagram for the governing equations of the Bernoulli-Euler beam model.

§12.4. Total Potential Energy Functional

The total potential energy of the beam is

$$\boxed{\Pi = U - W} \tag{12.6}$$

where as usual U and W denote the internal and external energies, respectively. As previously explained, in the Bernoulli-Euler model U includes only the bending energy:

$$\boxed{U = \tfrac{1}{2}\int_V \sigma e\, dV = \tfrac{1}{2}\int_0^L M\kappa\, dx = \tfrac{1}{2}\int_0^L EI\kappa^2\, dx = \tfrac{1}{2}\int_0^L EI\left(v''\right)^2\, dx = \tfrac{1}{2}\int_0^L v''EIv''\, dx.} \tag{12.7}$$

The external work W accounts for the applied transverse force:

$$\boxed{W = \int_0^L qv\, dx.} \tag{12.8}$$

The three functionals Π, U and W must be regarded as depending on the transverse displacement $v(x)$. When this dependence needs to be emphasized we write $\Pi[v]$, $U[v]$ and $W[v]$.

Note that $\Pi[v]$ includes up to second derivatives in v, because $v'' = \kappa$ appears in U. This number is called the *variational index*. Variational calculus tells us that since the index is 2, admissible displacements $v(x)$ must be continuous, have continuous first derivatives (slopes or rotations), and satisfy the displacement BCs exactly. This continuity requirement can be succintly stated by saying that admissible displacements must be C^1 continuous. This condition guides the construction of beam finite elements described below.

Remark 12.1. If there is an applied distributed moment $m(x)$ per unit of beam length, the external energy (12.8) must be augmented with a $\int_0^L m(x)\theta(x)\, dx$ term. This is further elaborated in Exercises 12.4 and 12.5. Such kind of distributed loading is uncommon in practice although in framework analysis occasionally the need arises for treating a concentrated moment between nodes.

§12.5. Beam Finite Elements

Beam finite elements are obtained by subdividing beam members longitudinally. The simplest Bernoulli-Euler plane beam element has two end nodes: 1 and 2, and four degrees of freedom (DOF). These are collected in the node displacement vector

$$\mathbf{u}^e = [\, v_1 \;\; \theta_1 \;\; v_2 \;\; \theta_2 \,]^T \,. \tag{12.9}$$

The element is shown in Figure 12.8, which pictures the undeformed and deformed configurations.

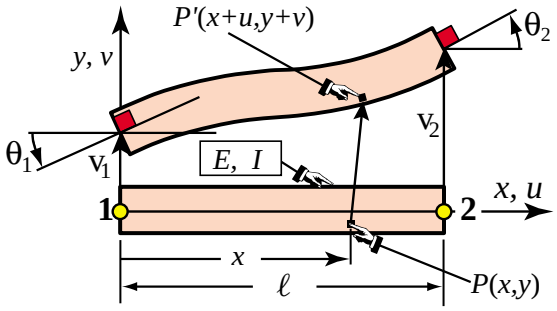

FIGURE 12.8. The two-node Bernoulli-Euler plane beam element with four DOFs.

§12.5.1. Finite Element Trial Functions

The freedoms (12.9) are used to define uniquely the variation of the transverse displacement $v^e(x)$ over the element. The C^1 continuity requirement says that both $v(x)$ and the slope $\theta = v'(x) = dv(x)/dx$ must be continuous over the entire member, and in particular between beam elements.

C^1 continuity can be trivially met *within each element* by choosing polynomial interpolation shape functions as shown below, because polynomials are C^∞ continuous. Matching nodal displacements and rotations with *adjacent elements* enforces the necessary interelement continuity.

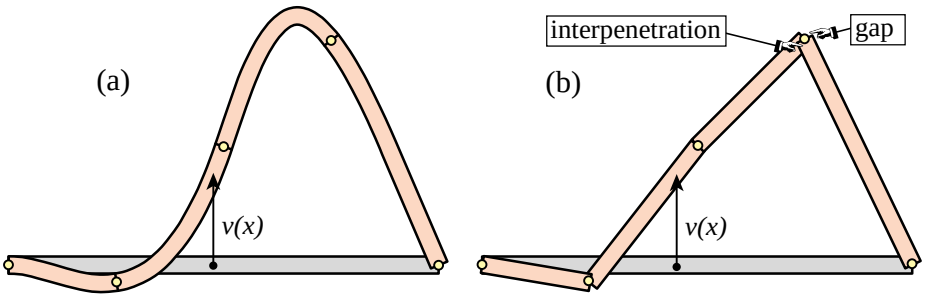

FIGURE 12.9. Deflection of a clamped-SS beam discretized with four elements, grossly exaggerated for visibility. (a) Cubic deflection elements; (b) linear deflection elements. The latter maintains only C^0 continuity, leading to unacceptable material gap and interpenetration at nodes.

Remark 12.2. The physical reason for C^1 continuity is illustrated in Figure 12.9, in which the lateral deflection curve $v(x)$ is grossly exaggerated for visibility. The left figure shows the approximation of $v(x)$ by four cubic functions, which maintain the required continuity. The right figure shows an attempt to approximate $v(x)$ by four piecewise linear functions that maintain only C^0 continuity. In this case material gap and interpenetration occur at the nodes, as well as at the clamped left end, because section rotations jump between elements.

§12.5.2. Shape Functions

The simplest shape functions that meet the C^1 continuity requirement for the nodal DOF configuration (12.9) are called the *Hermitian cubic* shape functions. The interpolation formula based on these functions is

$$v^e = [\, N^e_{v1} \;\; N^e_{\theta 1} \;\; N^e_{v2} \;\; N^e_{\theta 2} \,] \begin{bmatrix} v_1 \\ \theta_1 \\ v_2 \\ \theta_2 \end{bmatrix} = \mathbf{N}^e\, \mathbf{u}^e. \tag{12.10}$$

These shape functions are conveniently expressed in terms of the dimensionless "natural" coordinate

$$\xi = \frac{2x}{\ell} - 1, \tag{12.11}$$

where ℓ is the element length. Coordinate ξ varies from $\xi = -1$ at node 1 ($x = 0$) to $\xi = +1$ at node 2 ($x = \ell$). Note that $dx/d\xi = \frac{1}{2}\ell$ and $d\xi/dx = 2/\ell$. The shape functions in terms of ξ are

$$\boxed{\begin{aligned} N^e_{v1} &= \tfrac{1}{4}(1-\xi)^2(2+\xi), \\ N^e_{\theta 1} &= \tfrac{1}{8}\ell(1-\xi)^2(1+\xi), \\ N^e_{v2} &= \tfrac{1}{4}(1+\xi)^2(2-\xi), \\ N^e_{\theta 2} &= -\tfrac{1}{8}\ell(1+\xi)^2(1-\xi). \end{aligned}} \tag{12.12}$$

These four functions are depicted in Figure 12.10.

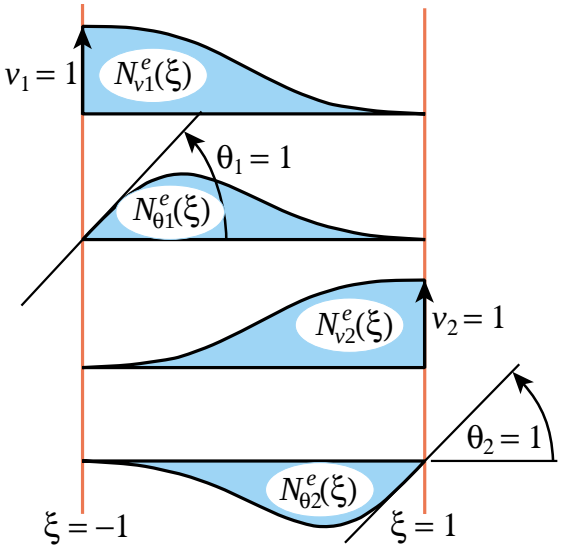

FIGURE 12.10. Cubic shape functions of plane beam element.

The curvature κ that appears in U can be expressed in terms of the nodal displacements by differentiating twice with respect to x:

$$\kappa = \frac{d^2 v^e(x)}{dx^2} = \frac{4}{\ell^2}\frac{d^2 v^e(\xi)}{d\xi^2} = \frac{4}{\ell^2}\frac{d\mathbf{N}^e}{d\xi^2}\mathbf{u}^e = \mathbf{B}\,\mathbf{u}^e = \mathbf{N}''\,\mathbf{u}^e. \tag{12.13}$$

Here $\mathbf{B} = \mathbf{N}''$ is the 1×4 curvature-displacement matrix

$$\boxed{\mathbf{B} = \frac{1}{\ell}\left[\, 6\frac{\xi}{\ell} \quad 3\xi - 1 \quad -6\frac{\xi}{\ell} \quad 3\xi + 1 \,\right].} \tag{12.14}$$

Remark 12.3. The $4/\ell^2$ factor in (12.13) comes from the differentiation chain rule. If $f(x)$ is a function of x, and $\xi = 2x/\ell - 1$, noting that $d(2/\ell)/dx = 0$ one gets

$$\frac{df(x)}{dx} = \frac{df(\xi)}{d\xi}\frac{d\xi}{dx} = \frac{2}{\ell}\frac{df(\xi)}{d\xi}, \qquad \frac{d^2 f(x)}{dx^2} = \cancelto{0}{\frac{d(2/\ell)}{dx}}\frac{df(\xi)}{d\xi} + \frac{2}{\ell}\frac{d}{dx}\left(\frac{df(\xi)}{d\xi}\right) = \frac{4}{\ell^2}\frac{d^2 f(\xi)}{d\xi^2}. \tag{12.15}$$

```
ClearAll[EI,l,ξ];
Be={{6*ξ,(3*ξ-1)*l,-6*ξ,(3*ξ+1)*l}}/l^2;
Ke=(EI*l/2)*Integrate[Transpose[Be].Be,{ξ,-1,1}];
Ke=Simplify[Ke]; Print["Ke for prismatic beam:"];
Print[Ke//MatrixForm];
Print[Simplify[Ke*l^2/EI]//MatrixForm];
```

Ke for prismatic beam:

$$\begin{pmatrix} \frac{12\,EI}{l^3} & \frac{6\,EI}{l} & -\frac{12\,EI}{l^3} & \frac{6\,EI}{l^2} \\ \frac{6\,EI}{l^2} & \frac{4\,EI}{l} & -\frac{6\,EI}{l^2} & \frac{2\,EI}{l} \\ -\frac{12\,EI}{l^3} & -\frac{6\,EI}{l^2} & \frac{12\,EI}{l^3} & -\frac{6\,EI}{l^2} \\ \frac{6\,EI}{l^2} & \frac{2\,EI}{l} & -\frac{6\,EI}{l^2} & \frac{4\,EI}{l} \end{pmatrix}$$

FIGURE 12.11. Using *Mathematica* to form $\mathbf{K}^e$ for a prismatic beam element.

```
ClearAll[q,l,ξ];
Ne={{2*(1-ξ)^2*(2+ξ), (1-ξ)^2*(1+ξ)*l,
     2*(1+ξ)^2*(2-ξ),-(1+ξ)^2*(1-ξ)*l}}/8;
fe=(q*l/2)*Integrate[Ne,{ξ,-1,1}]; fe=Simplify[fe];
Print["fe^T for uniform load q:\n",fe//MatrixForm];
```

fe^T for uniform load q:

$$\begin{pmatrix} \frac{l\,q}{2} & \frac{l^2 q}{12} & \frac{l\,q}{2} & -\frac{l^2 q}{12} \end{pmatrix}$$

FIGURE 12.12. Using *Mathematica* to form $\mathbf{f}^e$ for uniform transverse load q.

§12.6. The Finite Element Equations

Insertion of (12.12) and (12.14) into the TPE functional specialized to this element, yields the quadratic form in the nodal displacements

$$\Pi^e = \tfrac{1}{2}(\mathbf{u}^e)^T\mathbf{K}^e\mathbf{u}^e - (\mathbf{u}^e)^T\mathbf{f}^e, \tag{12.16}$$

where

$$\boxed{\mathbf{K}^e = \int_0^\ell EI\ \mathbf{B}^T\mathbf{B}\,dx = \int_{-1}^1 EI\ \mathbf{B}^T\mathbf{B}\ \tfrac{1}{2}\ell\,d\xi,} \tag{12.17}$$

is the element stiffness matrix and

$$\boxed{\mathbf{f}^e = \int_0^\ell \mathbf{N}^T q\,dx = \int_{-1}^1 \mathbf{N}^T q\ \tfrac{1}{2}\ell\,d\xi,} \tag{12.18}$$

is the consistent element node force vector. The calculation of the entries of $\mathbf{K}^e$ and $\mathbf{f}^e$ for prismatic beams and uniform load q is studied next. More complex cases are treated in the Exercises.

§12.6.1. The Stiffness Matrix of a Prismatic Beam

If the bending rigidity EI is constant over the element it can be moved out of the ξ-integral in (12.17):

$$\mathbf{K}^e = \tfrac{1}{2}EI\,\ell\int_{-1}^1 \mathbf{B}^T\mathbf{B}\,d\xi = \frac{EI}{2\ell}\int_{-1}^1 \begin{bmatrix} \frac{6\xi}{\ell} \\ 3\xi-1 \\ \frac{-6\xi}{\ell} \\ 3\xi+1 \end{bmatrix}\begin{bmatrix} \frac{6\xi}{\ell} & 3\xi-1 & \frac{-6\xi}{\ell} & 3\xi+1 \end{bmatrix} d\xi. \tag{12.19}$$

Expanding and integrating over the element yields

$$\mathbf{K}^e = \frac{EI}{2\ell^3}\int_{-1}^1 \begin{bmatrix} 36\xi^2 & 6\xi(3\xi-1)\ell & -36\xi^2 & 6\xi(3\xi+1)\ell \\ & (3\xi-1)^2\ell^2 & -6\xi(3\xi-1)\ell & (9\xi^2-1)\ell^2 \\ & & 36\xi^2 & -6\xi(3\xi+1)\ell \\ \textit{symm} & & & (3\xi+1)^2\ell^2 \end{bmatrix} d\xi = \frac{EI}{\ell^3}\begin{bmatrix} 12 & 6\ell & -12 & 6\ell \\ & 4\ell^2 & -6\ell & 2\ell^2 \\ & & 12 & -6\ell \\ \textit{symm} & & & 4\ell^2 \end{bmatrix} \tag{12.20}$$

Although the foregoing integrals can be easily carried out by hand, it is equally expedient to use a CAS such as *Mathematica* or *Maple*. For example the *Mathematica* script listed in the top box of Figure 12.11 processes (12.20) using the `Integrate` function. The output, shown in the bottom box, corroborates the hand integration result.

§12.6.2. Consistent Nodal Force Vector for Uniform Load

If q does not depend on x it can be moved out of (12.18), giving

$$\mathbf{f}^e = \tfrac{1}{2}q\ell\int_{-1}^{1}\mathbf{N}^T\,d\xi = \tfrac{1}{2}q\ell\int_{-1}^{1}\begin{bmatrix}\frac{1}{4}(1-\xi)^2(2+\xi)\\ \frac{1}{8}\ell(1-\xi)^2(1+\xi)\\ \frac{1}{4}(1+\xi)^2(2-\xi)\\ -\frac{1}{8}\ell(1+\xi)^2(1-\xi)\end{bmatrix}d\xi = \tfrac{1}{2}\,q\,\ell\begin{bmatrix}1\\ \frac{1}{6}\ell\\ 1\\ -\frac{1}{6}\ell\end{bmatrix}. \qquad (12.21)$$

This shows that a uniform load q over the beam element maps to two transverse node loads $q\ell/2$, as may be expected, plus two nodal moments $\pm q\ell^2/12$. The latter are called the *fixed-end moments* in the structural mechanics literature.[3] The hand result (12.21) can be verified with the *Mathematica* script of Figure 12.12, in which $\mathbf{f}^e$ is printed as a row vector to save space.

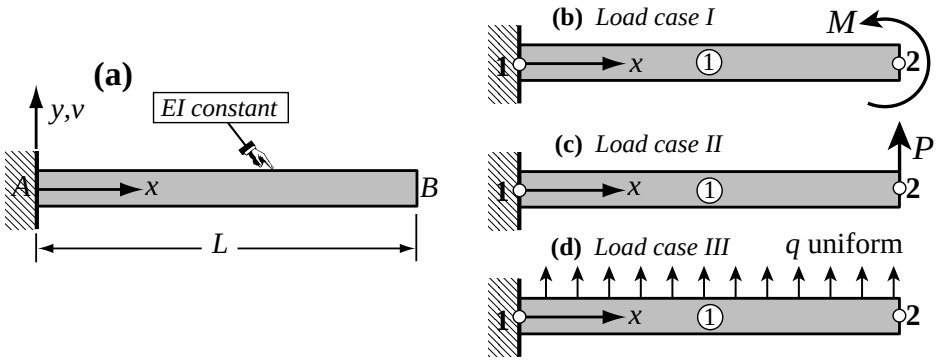

FIGURE 12.13. Cantilever beam problem for Example 12.1: (a) structure, (b-c): one-element FEM idealizations for three load cases.

Example 12.1. To see the beam element in action consider the cantilever illustrated in Figure 12.13(a). The beam is prismatic with constant rigidity EI and span L. It is discretized with a single element as shown in Figure 12.13(b,c,d), and subjected to the three load cases pictured there. Case I involves an applied end moment M, case II a transverse end force P, and case III a uniformly distributed load q over the entire beam. The FEM equations are constructed using the stiffness matrix (12.20) with $\ell = L$.

For the first two load cases, forces at end node 2 are directly set up from the given loads since no lumping is needed. Applying the support conditions $v_1 = \theta_1 = 0$ gives the reduced stiffness equations

$$\frac{EI}{L^3}\begin{bmatrix}12 & -6L\\ -6L & 4L^2\end{bmatrix}\begin{bmatrix}v_2^I\\ \theta_2^I\end{bmatrix} = \begin{bmatrix}0\\ M\end{bmatrix}, \quad \frac{EI}{L^3}\begin{bmatrix}12 & -6L\\ -6L & 4L^2\end{bmatrix}\begin{bmatrix}v_2^{II}\\ \theta_2^{II}\end{bmatrix} = \begin{bmatrix}P\\ 0\end{bmatrix}, \qquad (12.22)$$

[3] Introduced by Hardy Cross in 1930 (long before FEM) as a key ingredient for his moment distribution method. Indeed the title of his famous paper [174] is "Analysis of continuous frames by distributing fixed-end moments."

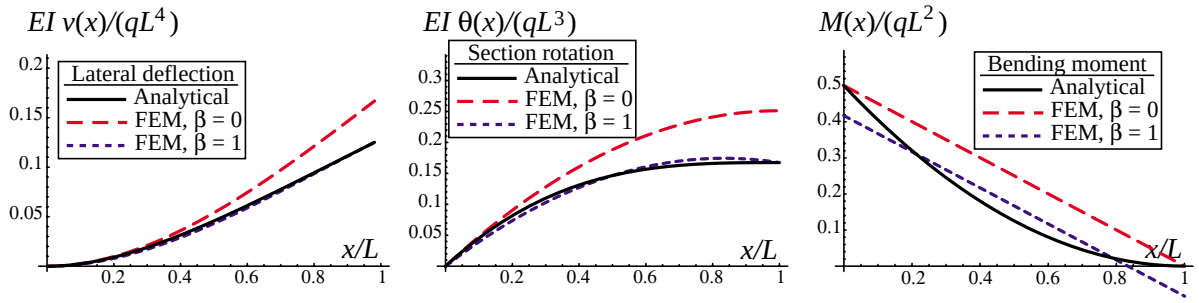

FIGURE 12.14. FEM versus analytical solutions for load case III of Example 12.1.

for load cases I and II, respectively. Solving gives the tip deflections $v_2^I = ML^2/(2EI)$ and $v_2^{II} = PL^3/(3EI)$, and the tip rotations $\theta_2^I = ML/EI$ and $\theta_2^{II} = PL^2/(2EI)$. These agree with the analytical values provided by Bernoulli-Euler beam theory. Thus a one-element idealization is sufficient for exactness. The reason is that the analytical deflection profiles $v(x)$ are quadratic and cubic polynomials in x for cases I and II, respectively. Both are included in the span of the element shape functions. Displacements $v(x)$, rotations $\theta(x)$ and moments $M(x)$ expressed as functions of x also agree with the analytical solution, as may be expected.

The results for load case III are more interesting since now the exact deflection is a quartic polynomial, which lies beyond the span of the FEM shape functions. A dimensionless parameter $0 \le \beta \le 1$ is introduced in the reduced stiffness equations to study the effect of load lumping method on the solution:

$$\frac{EI}{L^3}\begin{bmatrix} 12 & -6L \\ -6L & 4L^2 \end{bmatrix}\begin{bmatrix} v_2^{III} \\ \theta_2^{III} \end{bmatrix} = \tfrac{1}{2}\,q\,L\begin{bmatrix} 1 \\ -\frac{1}{6}\beta\,L \end{bmatrix}. \tag{12.23}$$

Setting $\beta = 1$ gives the energy consistent load lumping (12.21) whereas $\beta = 0$ gives the EbE (here same as NbN) load lumping $f_2^{III} = \frac{1}{2}\,q\,L$ with zero fixed-end moments. The solution of (12.23) is $v_2^{III} = q\,L^4(4-\beta)/(24\,EI)$ and $\theta_2^{III} = q\,L^3(3-\beta)/(12\,EI)$. From this one recovers the displacement, rotation and bending moment over the beam as

$$v^{III}(x) = q\,L^2\,x^2\,\frac{L(6{-}\beta) - 2x}{24\,EI}, \quad \theta^{III}(x) = q\,L\,x\,\frac{L(6{-}\beta) - 3x}{12\,EI}, \quad M^{III}(x) = \frac{q\,L}{12}\big(L(6{-}\beta) - 6x\big). \tag{12.24}$$

The analytical (exact) solution is

$$v_{ex}^{III}(x) = \frac{q\,x^2(3L^2{-}3Lx{+}x^2)}{24\,EI}, \quad \theta_{ex}^{III}(x) = \frac{q\,x\,(6L^2{-}4Lx{+}x^2)}{6\,EI}, \quad M_{ex}^{III}(x) = \tfrac{1}{2}\,q(L-x)^2. \tag{12.25}$$

The FEM and analytical solutions (12.24)-(12.25) are graphically compared in Figure 12.14. Deflections and rotations obtained with the consistent load lumping $\beta = 1$ agree better with the analytical solution. In addition the nodal values are exact (a superconvergence result further commented upon in the next Example). For the bending moment the values provided by the EbE lumping $\beta = 0$ are nodally exact but over the entire beam the $\beta = 1$ solution gives a better linear fit to the parabolic function $M_{ex}^{III}(x)$.

Example 12.2. The second example involves a simply supported beam under uniform line load q, depicted in Figure 12.15(a). It is prismatic with constant rigidity EI, span L, and discretized with two elements of length $L_1 = L(1/2 + \alpha)$ and $L_2 = L - L_1 = L(1/2 - \alpha)$, respectively. (Ordinarily two elements of the same length $1/2L$ would be used; the scalar $\alpha \in (-1/2, 1/2)$ is introduced to study the effect of unequal element sizes.)

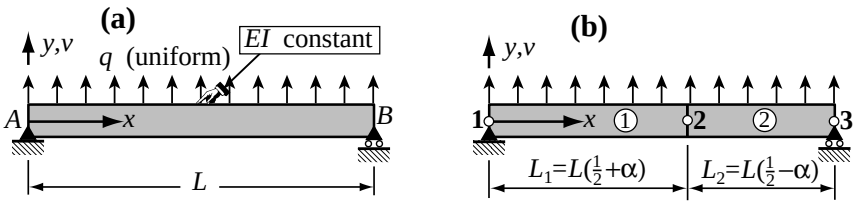

FIGURE 12.15. SS beam problem for Example 12.2: (a) structure, (b) two-element FEM idealization.

Using (12.20) and (12.21) to form the stiffness and consistent forces for both elements, assembling and applying the support conditions $v_1 = v_3 = 0$, provides the reduced stiffness equations

$$\frac{EI}{L^3}\begin{bmatrix} \frac{8L^2}{1+2\alpha} & \frac{-24L}{(1+2\alpha)^2} & \frac{4L^2}{1+2\alpha} & 0 \\ \frac{-24L}{(1+2\alpha)^2} & \frac{192(1+12\alpha^2)}{(1-4\alpha^2)^3} & \frac{192L\alpha}{(1-4\alpha^2)^2} & \frac{24L}{(1-2\alpha)^2} \\ \frac{4L^2}{1+2\alpha} & \frac{192L\alpha}{(1-4\alpha^2)^2} & \frac{16L^2}{1-4\alpha^2} & \frac{4L^2}{1-2\alpha} \\ 0 & \frac{24L}{(1-2\alpha)^2} & \frac{4L^2}{1-2\alpha} & \frac{8L^2}{1-2\alpha} \end{bmatrix} \begin{bmatrix} \theta_1 \\ v_2 \\ \theta_2 \\ \theta_3 \end{bmatrix} = \frac{qL}{2}\begin{bmatrix} \frac{L(1+2\alpha)^2}{24} \\ 1 \\ -\frac{L\alpha}{3} \\ -\frac{L(1-2\alpha)^2}{24} \end{bmatrix}. \qquad (12.26)$$

Solving for the lateral displacement of node 2 gives $v_2 = qL^4(5 - 24\alpha^2 + 16\alpha^4)/(384EI)$. The exact deflection is $v(x) = qL^4(\zeta - 2\zeta^3 + \zeta^4)/(24EI)$ with $\zeta = x/L$. Replacing $x = L_1 = L(1/2 + \alpha)$ yields $v_2^{exact} = qL^4(5 - 24\alpha^2 + 16\alpha^4)/(384EI)$, which is the same as the FEM result. Likewise θ_2 is exact.

The result seems *prima facie* surprising. First, since the analytical solution is a quartic polynomial in x we have no reason to think that a cubic element will be exact. Second, one would expect accuracy deterioration as the element sizes differ more and more with increasing α. The fact that the solution at nodes is exact for any combination of element lengths is an illustration of *superconvergence*, a phenomenon already discussed in §11.5. A general proof of nodal exactness is given in §13.7, but it does require advanced mathematical tools. Note that displacements and rotations *inside* elements will not agree with the exact one; this can be observed in Figure 12.14(a,b) for load case III of the previous example.

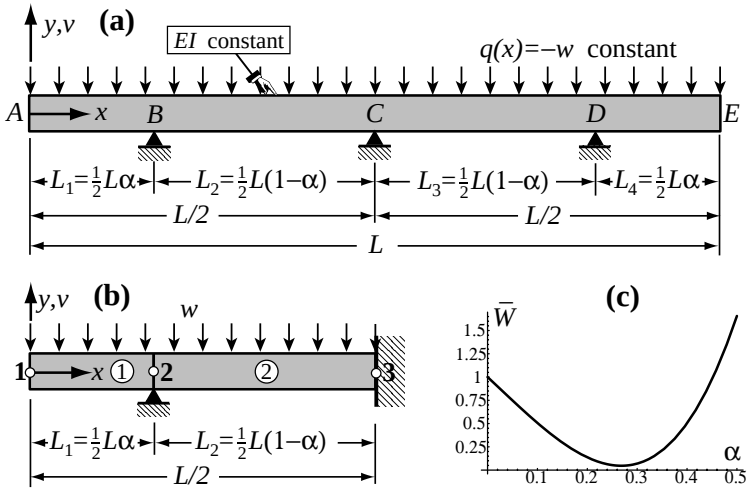

FIGURE 12.16. Continuum beam problem for Example 12.3, (a): structure, (b) two-element FEM model of half beam, (c) scaled external energy of FEM model as function of α.

Example 12.3. (Adapted from a driven-tank experiment by Patrick Weidman). This example displays the advantages of symbolic computation for solving a problem in geometric design: optimal location of supports. The prismatic continuous beam shown in Figure 12.16(a) is free at ends A and E, and simply supported at B, C and D. The beam has total span L and constant bending rigidity EI. It is loaded by a uniform distributed load $q(x) = -w$. Support C is at midspan whereas B and D are at distances $L_1 = L_4 = \frac{1}{2}L\alpha$ from the left and right free ends, respectively. Here $0 \le \alpha < 1$ is a design parameter to be determined as discussed later.

Since the problem is symmetric about midspan C only one half of the structure, say AC, need to be discretized. The finite element model of this portion is shown in Figure 12.16(b). It has two beam elements and three nodes placed at A, B and C, respectively. Element lengths depend on the design parameter α, which is carried along as a variable. The six degrees of freedom are collected in $\mathbf{u} = [\, v_1 \;\; \theta_1 \;\; v_2 \;\; \theta_2 \;\; v_3 \;\; \theta_3 \,]^T$. The master stiffness equations are

$$\frac{4EI}{L^3}\begin{bmatrix} \frac{24}{\alpha^3} & \frac{6L}{\alpha^2} & -\frac{24}{\alpha^3} & \frac{6L}{\alpha^2} & 0 & 0 \\ \frac{6L}{\alpha^2} & \frac{2L^2}{\alpha} & -\frac{6L}{\alpha^2} & \frac{L^2}{\alpha} & 0 & 0 \\ -\frac{24}{\alpha^3} & -\frac{6L}{\alpha^2} & \frac{24\left(1-3\alpha\hat{\alpha}\right)}{\alpha^3\hat{\alpha}^3} & -\frac{6L(1-2\alpha)}{\alpha^2\hat{\alpha}^2} & -\frac{24}{\hat{\alpha}^3} & \frac{6L}{\hat{\alpha}^2} \\ \frac{6L}{\alpha^2} & \frac{L^2}{\alpha} & -\frac{6L(1-2\alpha)}{\alpha^2\hat{\alpha}^2} & \frac{2L^2}{\alpha\hat{\alpha}} & -\frac{6L}{\hat{\alpha}^2} & \frac{L^2}{\hat{\alpha}} \\ 0 & 0 & -\frac{24}{\hat{\alpha}^3} & -\frac{6L}{\hat{\alpha}^2} & \frac{24}{\hat{\alpha}^3} & -\frac{6L}{\hat{\alpha}^2} \\ 0 & 0 & \frac{6L}{\hat{\alpha}^2} & \frac{L^2}{\hat{\alpha}} & -\frac{6L}{\hat{\alpha}^2} & \frac{2L^2}{\hat{\alpha}} \end{bmatrix} \begin{bmatrix} v_1 \\ \theta_1 \\ v_2 \\ \theta_2 \\ v_3 \\ \theta_3 \end{bmatrix} = \frac{wL}{4}\begin{bmatrix} -\alpha \\ \frac{-L\alpha^2}{12} \\ -1 \\ \frac{L(2\alpha-1)}{12} \\ -\hat{\alpha} \\ \frac{L\hat{\alpha}^2}{12} \end{bmatrix} + \begin{bmatrix} 0 \\ 0 \\ f_2^r \\ 0 \\ f_3^r \\ m_3^r \end{bmatrix} \tag{12.27}$$

in which $\hat{\alpha} = 1 - \alpha$. Note that reaction forces are carefully segregated in (12.27) to simplify application of the general recovery technique discussed in §3.4.3. The support BCs are $v_2 = v_3 = \theta_3 = 0$, where the latter comes from the symmetry condition at C. Removing those freedoms provides the reduced stiffness equations

$$\frac{4EI}{L^3}\begin{bmatrix} \frac{24}{\alpha^3} & \frac{6L}{\alpha^2} & \frac{6L}{\alpha^2} \\ \frac{6L}{\alpha^2} & \frac{2L^2}{\alpha} & \frac{L^2}{\alpha} \\ \frac{6L}{\alpha^2} & \frac{L^2}{\alpha} & \frac{2L^2}{\alpha\hat{\alpha}} \end{bmatrix} \begin{bmatrix} v_1 \\ \theta_1 \\ \theta_2 \end{bmatrix} = \frac{wL}{4}\begin{bmatrix} -\alpha \\ \frac{-L\alpha^2}{12} \\ \frac{L(2\alpha-1)}{12} \end{bmatrix}. \tag{12.28}$$

Solving yields

$$v_1 = -\frac{wL^4}{768\,EI}\,\alpha\left((1+\alpha)^3-2\right), \quad \theta_1 = \frac{wL^3}{384\,EI}\left((1+\alpha)^3-2\right), \quad \theta_2 = \frac{wL^3}{384\,EI}\,\hat{\alpha}\,(1-2\alpha-5\alpha^2). \tag{12.29}$$

The complete solution is $\mathbf{u} = [\, v_1 \;\; \theta_1 \;\; 0 \;\; \theta_2 \;\; 0 \;\; 0 \,]^T$. Inserting into (12.27) and solving for reactions gives

$$f_{r2} = \frac{wL}{16}\,\frac{3+2\alpha+\alpha^2}{\hat{\alpha}}, \quad f_{r3} = \frac{wL}{16}\,\frac{5-10\alpha-\alpha^2}{\hat{\alpha}}, \quad m_{r3} = -\frac{wL^2}{32}(1-2\alpha-\alpha^2). \tag{12.30}$$

whence the support reactions follow as $R_B = f_{r2}$ and $R_C = 2\,f_{r3}$. It remains to find the best α. Of course "best" depends on the optimality criterion. Four choices are examined below.

Minimum External Energy. The external energy at equilibrium is $W(\alpha) = \mathbf{f}^T\,\mathbf{u} = w^2L^5\,\bar{W}(\alpha)/(18432\,EI)$, in which $\bar{W}(\alpha) = 1 - 5\alpha - 2\alpha^2 + 26\alpha^3 + 5\alpha^4 + 3\alpha^5$. Minimizing W with respect to α may be interpreted as finding the stiffest structure (in the energy sense) under the given load vector $\mathbf{f}$. A plot of $\bar{W}(\alpha)$ over $0 \le \alpha \le \frac{1}{2}$ clearly displays a minimum at $\alpha \approx 0.27$ as shown in Figure 12.16(c). Solving the quartic equation $d\bar{W}/d\alpha = 0$ gives one positive real root in the range $\alpha \in [0, 1)$, which to 5 places is $\alpha_{best} = 0.26817$.

Equal Reactions. A second choice is to require that supports at B and C take the same load: $R_B = R_C$ (note that, because of symmetry, $R_D = R_B$). Setting $f_{r2} = 2\,f_{r3}$ with their expressions taken from (12.30), yields $3 + 2\alpha + \alpha^2 = 10 - 20\alpha - 2\alpha^2$, or $7 - 22\alpha - 3\alpha^2 = 0$. This quadratic has the roots $\alpha = \frac{1}{3}(-11 \pm \sqrt{142})$. The positive real root $\alpha_{best} = 0.30546$ makes $R_B = R_C = R_D = wL/3$, as may be expected.

Minimum Relative Deflection. Consider two sections located at x_i and x_j, in which $\{x_i, x_j\} \in [0, \frac{1}{2}L]$, with lateral displacements $v_i = v(x_i)$ and $v_j = v(x_j)$, respectively. The maximum relative deflection is defined as $v_{ji}^{max}(\alpha) = \max|v_j - v_i|$ for a fixed α. We seek the $\alpha \in [0, 1)$ that minimizes $v_{ji}^{max}(\alpha)$. The computations are far more complex than for the previous two criteria and are the subject of Exercise 12.11. Result: the best α is the positive real root of $4 + 11\alpha - 81\alpha^2 - 49\alpha^3 - 47\alpha^4 = 0$, which to 5 places is $\alpha_{best} = 0.26681$. If this value is adopted, the relative deflection does not exceed $v_{ij}^{max} < wL^4/(67674EI)$.

Minimum Absolute Moment. Let $M(x, \alpha)$ denote the bending moment function recovered from the FEM solution for a fixed α. The maximum absolute moment is $M^{max}(\alpha) = \max|M(x, \alpha)|$ for $x \in [0, \frac{1}{2}L]$. We seek an $\alpha \in [0, 1)$ that minimizes it. This is the topic of Exercise 12.12. This problem is less well posed than the previous one because $M(x, \alpha)$ varies linearly over each element, is nonzero at node 1 and discontinous at node 2. On the other hand, the exact bending moment varies parabolically, is zero at node 1 and continuous at node 2. Result: using the FEM-recovered $M(x, \alpha)$ and taking the average M at node 2, one finds that the best α is the positive root of $2 - 4\alpha - 15\alpha^2 = 0$, or $\alpha_{best} = 0.25540$, for which $M^{max} < wL^2/589$. The optimal solution using the exact moment distribution, however, is quite different. This is an intrinsic weakness of displacement-based FEM since internal forces are obtained by differentiation, which boosts errors. To get a better result a finer mesh would be needed.

In summary, the optimal α from the foregoing criteria varies between 0.255 to 0.306. As a reasonable compromise an engineer could pick $\alpha_{best} \approx 0.28$.

Notes and Bibliography

The Bernoulli-Euler (BE) beam model synthesizes pioneer work by Jacob and Daniel Bernoulli as well as that of Leonhard Euler in the XVIII Century. Although the model was first enunciated by 1750, it was not applied in structural design and analysis until the second half of the XIX Century. While Galileo Galilei is credited with first attempts at a theory, recent studies [43] argue that Leonardo da Vinci made crucial observations a century before Galileo. However, da Vinci lacked Hooke's law and calculus to complete the theory.

A comprehensive source of stiffness and mass matrices of plane and spatial beams is the book by Przemieniecki [603]. The derivation of stiffness matrices is carried out there using differential equilibrium equations rather than energy methods. This was in fact the common practice before 1962, as influenced by the use of transfer matrix methods [578] on the limited memory computers of the time. Results for prismatic elements, however, are identical.

Energy derivations were popularized by Archer [35,36], Martin [473] and Melosh [490,491].

References

Referenced items have been moved to Appendix R.

Homework Exercises for Chapter 12
Variational Formulation of Plane Beam Element

EXERCISE 12.1 [A/C:20] Use (12.17) to derive the element stiffness matrix $\mathbf{K}^e$ of a Hermitian beam element of variable bending rigidity given by the inertia law

$$I(x) = I_1(1 - \frac{x}{\ell}) + I_2\frac{x}{\ell} = I_1\,\tfrac{1}{2}(1-\xi) + I_2\,\tfrac{1}{2}(1+\xi). \tag{E12.1}$$

Use of *Mathematica* or similar CAS tool is recommended since the integrals are time consuming and error prone. *Mathematica* hint: write

```
EI = EI1*(1-ξ)/2 + EI2*(1+ξ)/2;
```
(E12.2)

and keep `EI` inside the argument of `Integrate`. Check whether you get back (12.20) if `EI=EI1=EI2`. If you use *Mathematica*, this check can be simply done after you got and printed the tapered beam `Ke`, by writing `ClearAll[EI]; Ke=Simplify[ Ke/.{EI1->EI,EI2->EI}];` and printing this matrix.[4]

EXERCISE 12.2 [A/C:20] Use (12.18) to derive the consistent node force vector $\mathbf{f}^e$ for a Hermitian beam element under linearly varying transverse load q defined by

$$q(x) = q_1(1 - \frac{x}{\ell}) + q_2\frac{x}{\ell} = q_1\,\tfrac{1}{2}(1-\xi) + q_2\,\tfrac{1}{2}(1+\xi). \tag{E12.3}$$

Again use of a CAS is recommended, particularly since the polynomials to be integrated are quartic in ξ, and hand computations are error prone. *Mathematica* hint: write

```
q = q1*(1-ξ)/2 + q2*(1+ξ)/2;
```
(E12.4)

and keep `q` inside the argument of `Integrate`. Check whether you get back (12.21) if $q_1 = q_2 = q$ (See previous Exercise for *Mathematica* procedural hints).

EXERCISE 12.3 [A:20] Obtain the consistent node force vector $\mathbf{f}^e$ of a Hermitian beam element subject to a transverse point load P at abscissa $x = a$ where $0 \le a \le \ell$. Use the Dirac's delta function expression $q(x) = P\,\delta(a)$ and the fact that for any continuous function $f(x)$, $\int_0^\ell f(x)\,\delta(a)\,dx = f(a)$ if $0 \le a \le \ell$. Check the special cases $a = 0$ and $a = \ell$.

EXERCISE 12.4 [A:25] Derive the consistent node force vector $\mathbf{f}^e$ of a Hermitian beam element subject to a linearly varying z-moment m per unit length, positive CCW, defined by the law $m(x) = m_1(1-\xi)/2 + m_2(1+\xi)/2$. Use the fact that the external work per unit length is $m(x)\theta(x) = m(x)\,v'(x) = (\mathbf{u}^e)^T(d\mathbf{N}/dx)^T\,m(x)$. For arbitrary $m(x)$ show that this gives

$$\mathbf{f}^e = \int_0^\ell \frac{\partial \mathbf{N}^T}{\partial x} m\,dx = \int_{-1}^1 \frac{\partial \mathbf{N}^T}{\partial \xi}\frac{2}{\ell} m\,\tfrac{1}{2}\ell\,d\xi = \int_{-1}^1 \mathbf{N}_\xi^T m\,d\xi, \tag{E12.5}$$

where $\mathbf{N}_\xi^T$ denote the column vectors of beam shape function derivatives with respect to ξ. Can you see a shortcut that avoids the integral altogether if m is constant?

EXERCISE 12.5 [A:20] Obtain the consistent node force vector $\mathbf{f}^e$ of a Hermitian beam element subject to a concentrated moment ("point moment", positive CCW) C applied at $x = a$. Use the Concentrated moment load on beam element expression (E12.5) in which $m(x) = C\,\delta(a)$, where $\delta(a)$ denotes the Dirac's delta function at $x = a$. Check the special cases $a = 0$, $a = \ell$ and $a = \ell/2$.

[4] `ClearAll[EI]` discards the previous definition (E12.2) of `EI`; the same effect can be achieved by writing `EI=.` (dot).

EXERCISE 12.6 [A/C:25] Consider the one-dimensional Gauss integration rules.[5]

$$\text{One point :} \qquad \int_{-1}^{1} f(\xi)\, d\xi \doteq 2 f(0). \tag{E12.6}$$

$$\text{Two points:} \qquad \int_{-1}^{1} f(\xi)\, d\xi \doteq f(-1/\sqrt{3}) + f(1/\sqrt{3}). \tag{E12.7}$$

$$\text{Three points:} \qquad \int_{-1}^{1} f(\xi)\, d\xi \doteq \frac{5}{9} f(-\sqrt{3/5}) + \frac{8}{9} f(0) + \frac{5}{9} f(\sqrt{3/5}). \tag{E12.8}$$

Try each rule on the monomial integrals

$$\int_{-1}^{1} d\xi, \qquad \int_{-1}^{1} \xi\, d\xi, \qquad \int_{-1}^{1} \xi^2\, d\xi, \quad \ldots \tag{E12.9}$$

until the rule fails. In this way verify that rules (E12.6), (E12.7) and (E12.8) are exact for polynomials of degree up to 1, 3 and 5, respectively. (*Labor-saving hint*: for odd monomial degree no computations need to be done; why?).

EXERCISE 12.7 [A/C:25] Repeat the derivation of Exercise 12.1 using the two-point Gauss rule (E12.7) to evaluate integrals in ξ. A CAS is recommended. If using *Mathematica* you may use a function definition to save typing. For example to evaluate $\int_{-1}^{1} f(\xi)\, d\xi$ in which $f(\xi) = 6\xi^4 - 3\xi^2 + 7$, by the 3-point Gauss rule (E12.8), say

```
f[ξ_]:=6ξ^4-3ξ^2+7; int=Simplify[(5/9)*(f[-Sqrt[3/5]]+f[Sqrt[3/5]])+(8/9)*f[0]];
```

and print `int`. To form an element by Gauss integration define matrix functions in terms of ξ, for example `Be[ξ_]`, or use the substitution operator `/.`, whatever you prefer. Check whether one obtains the same answers as with analytical integration, and explain why there is agreement or disagreement. Hint for the explanation: consider the order of the ξ polynomials you are integrating over the element.

EXERCISE 12.8 [A/C:25] As above but for Exercise 12.2.

EXERCISE 12.9 [A/C:30] Derive the Bernoulli-Euler beam stiffness matrix (12.20) using the method of differential equations. To do this integrate the homogeneous differential equation $EIv'''' = 0$ four times over a cantilever beam clamped at node 1 over $x \in [0, \ell]$ to get $v(x)$. The process yields four constants of integration C_1 through C_4, which are determined by matching the two zero-displacement BCs at node 1 and the two force BCs at node 2. This provides a 2×2 flexibility matrix relating forces and displacements at node j. Invert to get a deformational stiffness, and expand to 4×4 by letting node 1 translate and rotate.

EXERCISE 12.10 [C:20] Using *Mathematica*, repeat Example 12.2 but using EbE lumping of the distributed force q. (It is sufficient to set the nodal moments on the RHS of (12.26) to zero.) Is v_2 the same as the exact analytical solution? If not, study the ratio v_2/v_2^{exact} as function of α, and draw conclusions.

EXERCISE 12.11 [C:25] For the continuous beam of Example 12.3, verify the results given there for the optimal α that minimizes the maximum relative deflection. Plot the deflection profile when $\alpha = \alpha_{best}$.

EXERCISE 12.12 [C:25] For the continuous beam of Example 12.3, verify the results given there for the optimal α that minimizes the absolute bending moment. Plot the moment diagram when $\alpha = \alpha_{best}$.

[5] Gauss integration is studied further in Chapter 17.

14

The Plane Stress Problem

TABLE OF CONTENTS

§14.1. Introduction

We now pass to the variational formulation of two-dimensional *continuum* finite elements. The problem of *plane stress* will serve as the vehicle for illustrating such formulations. As narrated in Appendix O, continuum-based structural finite elements were invented in the aircraft industry (at Boeing during the early 1950s) to solve this kind of problem when it arose in the design and analysis of delta wing panels [765].

The problem is presented here within the framework of the linear theory of elasticity.

§14.2. Plate in Plane Stress

In structural mechanics, a flat thin sheet of material is called a *plate*.[1] The distance between the plate faces is the *thickness*, denoted by h. The *midplane* lies halfway between the two faces.

The direction normal to the midplane is the *transverse* direction. Directions parallel to the midplane are called *in-plane* directions. The global axis z is oriented along the transverse direction. Axes x and y are placed in the midplane, forming a right-handed Rectangular Cartesian Coordinate (RCC) system. Thus the equation of the midplane is $z = 0$. The $+z$ axis conventionally defines the *top surface* of the plate as the one that it intersects, whereas the opposite surface is called the *bottom surface*. See Figure 14.1(a).

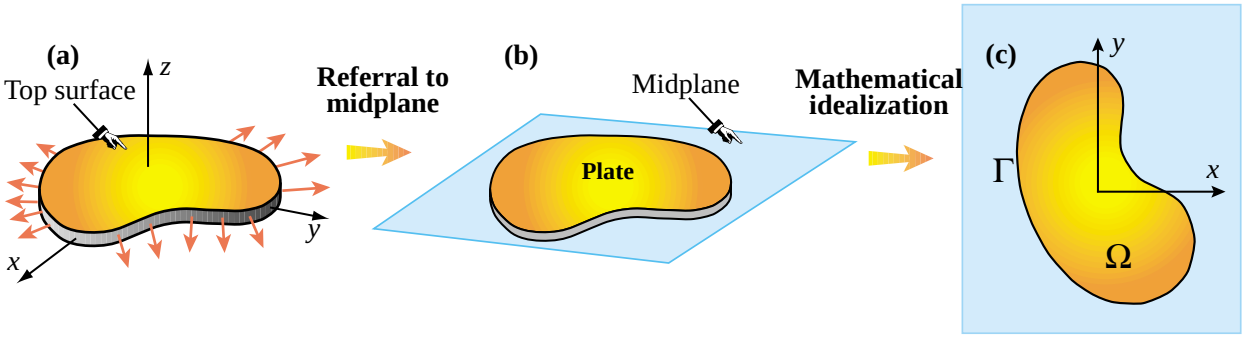

FIGURE 14.1. A plate structure in plane stress: (a) configuration; (b) referral to its midplane; (c) 2D mathematical idealization as boundary value problem.

§14.2.1. Behavioral Assumptions

A plate loaded in its midplane is said to be in a state of *plane stress*, or a *membrane state*, if the following assumptions hold:

1. All loads applied to the plate act in the midplane direction, and are symmetric with respect to the midplane.
2. All support conditions are symmetric about the midplane.
3. In-plane displacements, strains and stresses can be taken to be uniform through the thickness.
4. The normal and shear stress components in the z direction are zero or negligible.

[1] If it is relatively thick, as in concrete pavements or Argentinian beefsteaks, the term *slab* is also used but not usually for plane stress conditions.

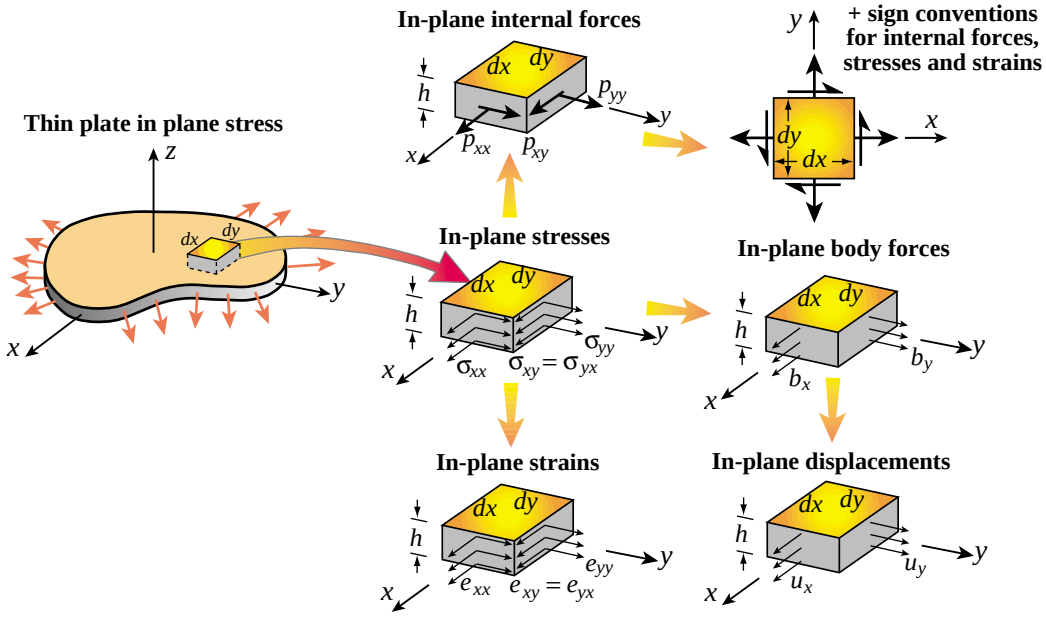

FIGURE 14.2. Notational conventions for in-plane stresses, strains, displacements and internal forces of a thin plate in plane stress.

The last two assumptions are not necessarily consequences of the first two. For the latter to hold, the thickness h should be small, typically 10% or less, than the shortest in-plane dimension. If the plate thickness varies it should do so gradually. Finally, the plate fabrication must exhibit symmetry with respect to the midplane.

To these four assumptions we add the following restriction:

5. The plate is fabricated of the same material through the thickness. Such plates are called *transversely homogeneous* or (in aerospace) *monocoque* plates.

The last assumption excludes wall constructions of importance in aerospace, in particular composite and honeycomb sandwich plates. The development of mathematical models for such configurations requires a more complicated integration over the thickness as well as the ability to handle coupled bending and stretching effects, and will not be considered here.

Remark 14.1. Selective relaxation from assumption 4 leads to the so-called *generalized plane stress state*, in which z stresses are accepted. The *plane strain state* is obtained if strains in the z direction are precluded. Although the construction of finite element models for those states has many common points with plane stress, we shall not consider those models here. For isotropic materials the plane stress and plane strain problems can be mapped into each other through a fictitious-property technique; see Exercise 14.1.

Remark 14.2. Transverse loading on a plate produces *plate bending*, which is associated with a more complex configuration of internal forces and deformations. This subject is studied in [255].

§14.2.2. Mathematical Model

The mathematical model of the plate in plane stress is set up as a two-dimensional boundary value problem (BVP), in which the plate is projected onto its midplane; see Figure 14.1(b). This allows to formulate the BVP over a plane domain Ω with a boundary Γ, as illustrated in Figure 14.1(c).

In this idealization the third dimension is represented as functions of x and y that are *integrated through the plate thickness*. Engineers often work with internal plate forces, which result from integrating the in-plane stresses through the thickness. See Figure 14.2.

§14.2.3. Problem Data

The following summarizes the givens in the plate stress problem.

Domain geometry. This is defined by the boundary Γ illustrated in Figure 14.1(c).

Thickness. Most plates used as structural components have constant thickness. If the thickness does vary, in which case $h = h(x, y)$, it should do so gradually to maintain the plane stress state. Sudden changes in thickness may lead to stress concentrations.

Material data. This is defined by the constitutive equations. Here we shall assume that the plate material is linearly elastic but not necessarily isotropic.

Specified Interior Forces. These are known forces that act in the interior Ω of the plate. There are of two types. *Body forces* or *volume forces* are forces specified per unit of plate volume; for example the plate weight. *Face forces* act tangentially to the plate faces and are transported to the midplane. For example, the friction or drag force on an airplane skin is of this type if the skin is modeled to be in plane stress.

Specified Surface Forces. These are known forces that act on the boundary Γ of the plate. In elasticity they are called *surface tractions*. In actual applications it is important to know whether these forces are specified per unit of surface area or per unit length. The former may be converted to the latter by multiplying through the appropriate thickness value.

Displacement Boundary Conditions. These specify how the plate is supported. Points subject to support conditions may be fixed, allowed to move in one direction, or subject to multipoint constraints. Also symmetry and antisymmetry lines may be identified as discussed in Chapter 8 of IFEM [257].

If no displacement boundary conditions are imposed, the plate is said to be *free-free* or *floating*.

§14.2.4. Problem Unknowns

The unknown fields are displacements, strains and stresses. Because of the assumed wall fabrication homogeneity the in-plane components are assumed to be *uniform through the plate thickness*. Thus the dependence on z disappears and all such components become functions of x and y only.

Displacements. The in-plane displacement field is defined by two components:

$$\mathbf{u}(x, y) = \begin{bmatrix} u_x(x, y) \\ u_y(x, y) \end{bmatrix} \tag{14.1}$$

The transverse displacement component $u_z(x, y, z)$ component is generally nonzero because of Poisson's ratio effects, and depends on z. However, this displacement does not appear in the governing equations.

Strains. The in-plane strain field forms a tensor defined by three independent components: e_{xx}, e_{yy} and e_{xy}. To allow stating the FE equations in matrix form, these components are cast to form a

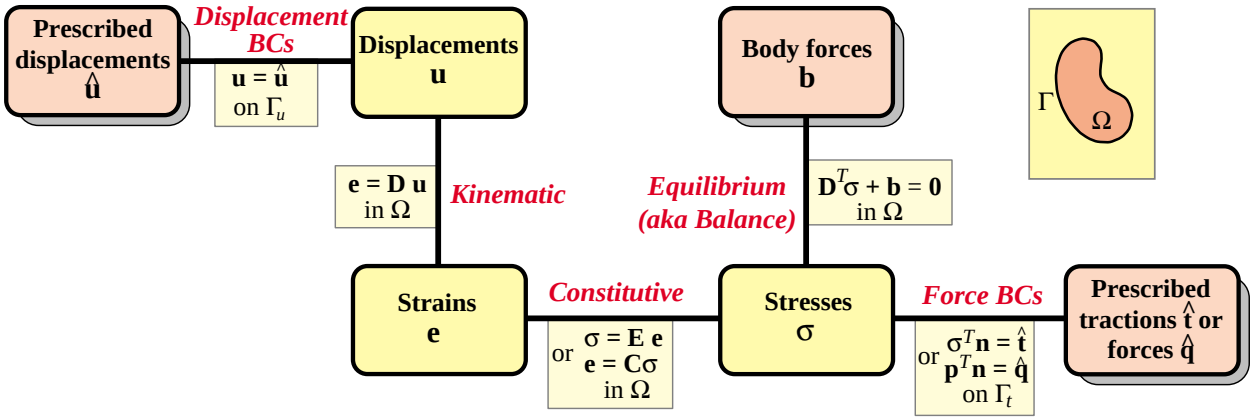

FIGURE 14.3. The Strong Form of the plane stress equations of linear elastostatics displayed as a Tonti diagram. Yellow boxes identify prescribed fields whereas orange boxes denote unknown fields. The distinction between Strong and Weak Forms is explained in §14.3.3.

3-component "strain vector"

$$\mathbf{e}(x,y) = \begin{bmatrix} e_{xx}(x,y) \\ e_{yy}(x,y) \\ 2e_{xy}(x,y) \end{bmatrix} \tag{14.2}$$

The factor of 2 in e_{xy} shortens strain energy expressions. The shear strain components e_{xz} and e_{yz} vanish. The transverse normal strain e_{zz} is generally nonzero because of Poisson's ratio effects. This strain does not enter the governing equations as unknown, however, because the associated stress σ_{zz} is zero. This eliminates the contribution of $\sigma_{zz}e_{zz}$ to the internal energy.

Stresses. The in-plane stress field forms a tensor defined by three independent components: σ_{xx}, σ_{yy} and σ_{xy}. As in the case of strains, to allow stating the FE equations in matrix form, these components are cast to form a 3-component "stress vector"

$$\boldsymbol{\sigma}(x,y) = \begin{bmatrix} \sigma_{xx}(x,y) \\ \sigma_{yy}(x,y) \\ \sigma_{xy}(x,y) \end{bmatrix} \tag{14.3}$$

The remaining three stress components: σ_{zz}, σ_{xz} and σ_{yz}, are assumed to vanish.

The *plate internal forces* are obtained on integrating the stresses through the thickness. Under the assumption of uniform stress distribution,

$$p_{xx} = \sigma_{xx}h, \quad p_{yy} = \sigma_{yy}h, \quad p_{xy} = \sigma_{xy}h. \tag{14.4}$$

These p's also form a tensor. They are called *membrane forces* in the literature. See Figure 14.2.

§14.3. Plane Stress Governing Equations

We shall develop plane stress finite elements in the framework of classical linear elasticity. The necessary governing equations are presented below. They are graphically represented in the Strong Form Tonti diagram of Figure 14.3.

§14.3.1. Governing Equations

The three internal fields: displacements, strains and stresses (14.1)–(14.3) are connected by three field equations: kinematic, constitutive and internal-equilibrium equations. If initial strain effects are ignored, these equations read

$$\begin{bmatrix} e_{xx} \\ e_{yy} \\ 2e_{xy} \end{bmatrix} = \begin{bmatrix} \partial/\partial x & 0 \\ 0 & \partial/\partial y \\ \partial/\partial y & \partial/\partial x \end{bmatrix} \begin{bmatrix} u_x \\ u_y \end{bmatrix},$$
$$\begin{bmatrix} \sigma_{xx} \\ \sigma_{yy} \\ \sigma_{xy} \end{bmatrix} = \begin{bmatrix} E_{11} & E_{12} & E_{13} \\ E_{12} & E_{22} & E_{23} \\ E_{13} & E_{23} & E_{33} \end{bmatrix} \begin{bmatrix} e_{xx} \\ e_{yy} \\ 2e_{xy} \end{bmatrix}, \tag{14.5}$$
$$\begin{bmatrix} \partial/\partial x & 0 & \partial/\partial y \\ 0 & \partial/\partial y & \partial/\partial x \end{bmatrix} \begin{bmatrix} \sigma_{xx} \\ \sigma_{yy} \\ \sigma_{xy} \end{bmatrix} + \begin{bmatrix} b_x \\ b_y \end{bmatrix} = \begin{bmatrix} 0 \\ 0 \end{bmatrix}.$$

The compact matrix version of (14.5) is

$$\boxed{\mathbf{e} = \mathbf{D}\,\mathbf{u}, \qquad \boldsymbol{\sigma} = \mathbf{E}\,\mathbf{e}, \qquad \mathbf{D}^T\boldsymbol{\sigma} + \mathbf{b} = \mathbf{0},} \tag{14.6}$$

Here $\mathbf{E} = \mathbf{E}^T$ is the 3×3 stress-strain matrix of plane stress elastic moduli, $\mathbf{D}$ is the 3×2 symmetric-gradient operator and its transpose the 2×3 tensor-divergence operator.[2]

If the plate material is isotropic with elastic modulus E and Poisson's ratio ν, the moduli in the constitutive matrix $\mathbf{E}$ reduce to $E_{11} = E_{22} = E/(1-\nu^2)$, $E_{33} = \frac{1}{2}E/(1+\nu) = G$, $E_{12} = \nu E_{11}$ and $E_{13} = E_{23} = 0$. See also Exercise 14.1.

§14.3.2. Boundary Conditions

Boundary conditions prescribed on Γ may be of two types: displacement BC or force BC (the latter is also called stress BC or traction BC). To write down those conditions it is conceptually convenient to break up Γ into two subsets: Γ_u and Γ_t, over which displacements and force or stresses, respectively, are specified. See Figure 14.4.

Displacement boundary conditions are prescribed on Γ_u in the form

$$\boxed{\mathbf{u} = \hat{\mathbf{u}}.} \tag{14.7}$$

Here $\hat{\mathbf{u}}$ are prescribed displacements. Often $\hat{\mathbf{u}} = \mathbf{0}$. This happens in fixed portions of the boundary, as the ones illustrated in Figure 14.4.

Force boundary conditions (also called stress BCs and traction BCs in the literature) are specified on Γ_t. They take the form

$$\boxed{\boldsymbol{\sigma}_n = \hat{\mathbf{t}}.} \tag{14.8}$$

Here $\hat{\mathbf{t}}$ are prescribed surface tractions specified as a force per unit area (that is, not integrated through the thickness), and $\boldsymbol{\sigma}_n$ is the stress vector shown in Figure 14.4.

[2] The dependence on (x, y) has been omitted to reduce clutter.

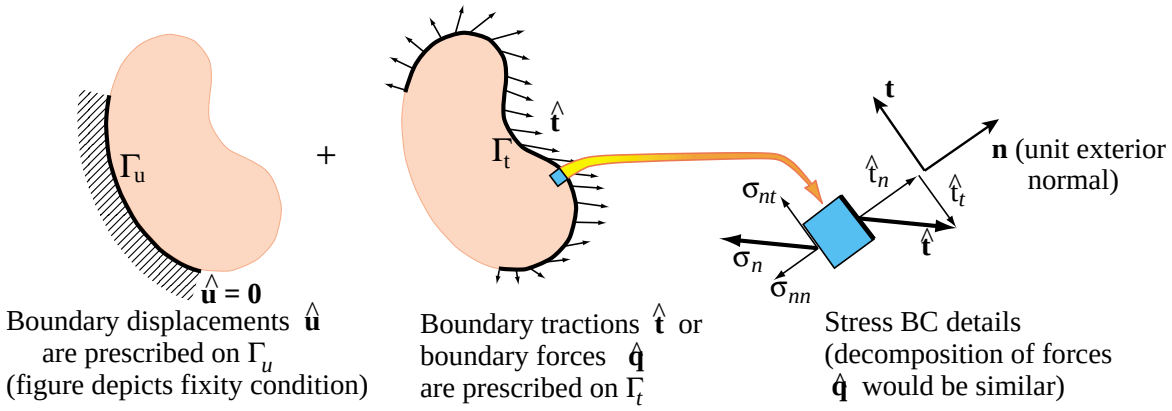

FIGURE 14.4. Displacement and force (stress, traction) boundary conditions for the plane stress problem.

An alternative form of (14.8) uses the internal plate forces:

$$\boxed{\mathbf{p}_n = \hat{\mathbf{q}}.} \tag{14.9}$$

Here $\mathbf{p}_n = \boldsymbol{\sigma}_n h$ and $\hat{\mathbf{q}} = \hat{\mathbf{t}}\, h$. This form is used more often than (14.8) in structural design, particularly when the plate wall construction is inhomogeneous.

The components of $\boldsymbol{\sigma}_n$ in Cartesian coordinates follow from Cauchy's stress transformation formula

$$\boldsymbol{\sigma}_n = \begin{bmatrix} \sigma_{xx} n_x + \sigma_{xy} n_y \\ \sigma_{xy} n_x + \sigma_{yy} n_y \end{bmatrix} = \begin{bmatrix} n_x & 0 & n_y \\ 0 & n_y & n_x \end{bmatrix} \begin{bmatrix} \sigma_{xx} \\ \sigma_{yy} \\ \sigma_{xy} \end{bmatrix}, \tag{14.10}$$

in which n_x and n_y denote the Cartesian components of the unit normal vector $\mathbf{n}^e$ (also called the direction cosines of the normal). Thus (14.8) splits into two scalar conditions: $\hat{t}_x = \sigma_{nx}$ and $\hat{t}_y = \sigma_{ny}$. The derivation of (14.10) is the subject of Exercise 14.4.

It is sometimes convenient to write the condition (14.8) in terms of normal n and tangential t directions:

$$\sigma_{nn} = \hat{t}_n, \qquad \sigma_{nt} = \hat{t}_t \tag{14.11}$$

in which $\sigma_{nn} = \sigma_{nx} n_x + \sigma_{ny} n_y$ and $\sigma_{nt} = -\sigma_{nx} n_y + \sigma_{ny} n_x$. See Figure 14.4.

Remark 14.3. The separation of Γ into Γ_u and Γ_t is useful for conciseness in the mathematical formulation, such as the energy integrals presented below. It does not exhaust, however, all BC possibilities. Frequently at points of Γ one specifies a displacement in one direction and a force (or stress) in the other. An example of these are roller and sliding conditions as well as lines of symmetry and antisymmetry. These are called *mixed displaceent-traction* BC. To cover these situations one needs either a generalization of the boundary split, in which Γ_u and Γ_t are permitted to overlap, or to define another portion Γ_m for'mixed conditions. Such generalizations will not be presented here, as they become unimportant once the FE discretization is done.

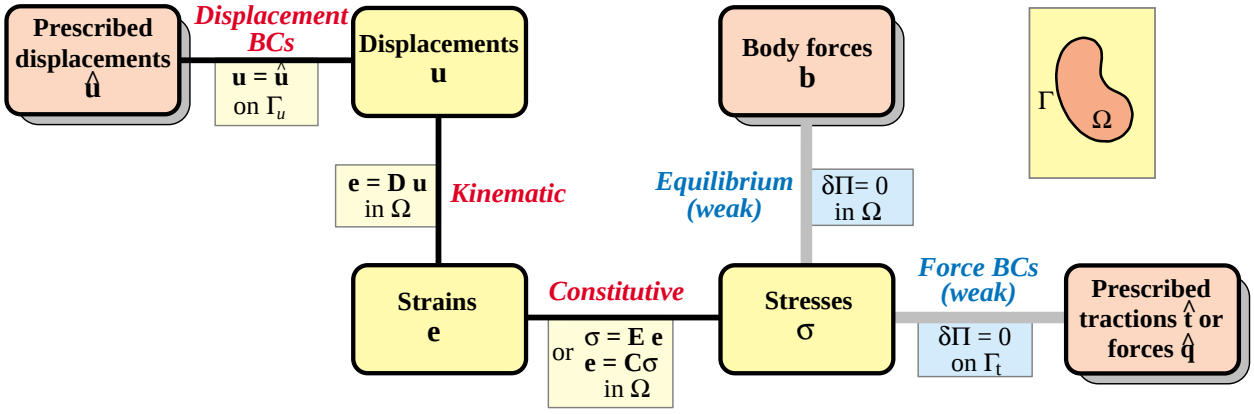

FIGURE 14.5. The TPE-based Weak Form of the plane stress equations of linear elastostatics. Weak links are marked with grey lines.

§14.3.3. Weak versus Strong Form

We introduce now some further terminology from variational calculus. The Tonti diagram of Figure 14.3 is said to display the *Strong Form* of the governing equations because all relations are verified point by point. These relations, called *strong links*, are shown in the diagram with black lines.

A Weak Form is obtained by *relaxing* one or more strong links, as brifley described in Chapter 11. Those are replaced by *weak links*, which enforce relations in an average or integral sense rather than point by point. The weak links are then provided by the variational formulation chosen for the problem. Because in general many variational forms of the same problem are possible, there are many possible Weak Forms. On the other hand the Strong Form is unique.

The Weak Form associated with the Total Potential Energy (TPE) variational form is illustrated in Figure 14.5. The internal equilibrium equations and stress BC become weak links, which are drawn by gray lines. These equations are given by the variational statement $\delta\Pi = 0$, where the TPE functional Π is given in the next subsection. The FEM displacement formulation discussed below is based on this particular Weak Form.

§14.3.4. Total Potential Energy

The Total Potential Energy functional for the plane stress problem is given by

$$\boxed{\Pi = U - W.} \tag{14.12}$$

The internal energy can be expressed in terms of the strains only as

$$\boxed{U = \tfrac{1}{2}\int_\Omega h\,\boldsymbol{\sigma}^T\,\mathbf{e}\,d\Omega = \tfrac{1}{2}\int_\Omega h\,\mathbf{e}^T\,\mathbf{E}\,\mathbf{e}\,d\Omega.} \tag{14.13}$$

in which $\frac{1}{2}\mathbf{e}^T\mathbf{E}\mathbf{e}$ is the *strain energy density*. The derivation details are relegated to Exercise 14.5, The external energy (potential of the applied forces) is the sum of contributions from the given

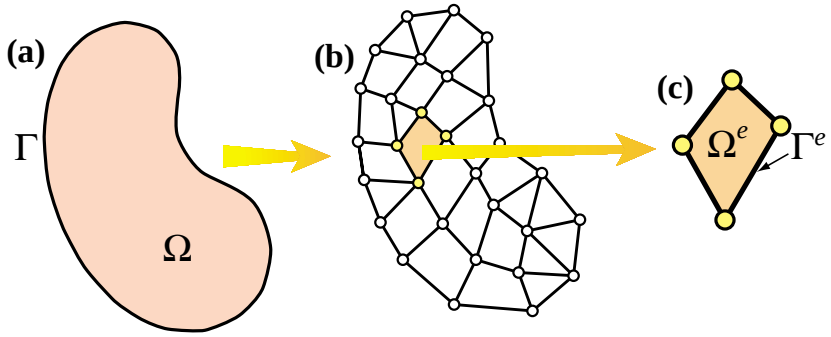

FIGURE 14.6. Finite element discretization and extraction of generic element.

interior (body) and exterior (boundary) forces:

$$\boxed{W = \int_{\Omega} h\,\mathbf{u}^T\,\mathbf{b}\;d\Omega + \int_{\Gamma_t} h\,\mathbf{u}^T\,\hat{\mathbf{t}}\,d\Gamma.} \tag{14.14}$$

Note that the boundary integral over Γ is taken only over Γ_t. That is, the portion of the boundary over which tractions or forces are specified.

§14.4. Finite Element Equations

The necessary equations to apply the finite element method to the plane stress problem are collected here and expressed in matrix form. The domain of Figure 14.6(a) is discretized by a finite element mesh as illustrated in Figure 14.6(b). From this mesh we extract a generic element labeled e with $n \geq 3$ node points. In subsequent derivations the number n is kept *arbitrary*. Therefore, the formulation is applicable to arbitrary two-dimensional elements, for example those sketched in Figure 14.7.

To comfortably accommodate general element types, the node points will be labeled 1 through n. These are called *local node numbers*. Numbering will always start with corners.

The element domain and boundary are denoted by Ω^e and Γ^e, respectively. The element has $2n$ degrees of freedom. These are collected in the element node displacement vector in a node by node arrangement:

$$\mathbf{u}^e = [\,u_{x1} \quad u_{y1} \quad u_{x2} \quad \ldots \quad u_{xn} \quad u_{yn}\,]^T\,. \tag{14.15}$$

§14.4.1. Displacement Interpolation

The displacement field $\mathbf{u}^e(x, y)$ over the element is interpolated from the node displacements. We shall assume that the same interpolation functions are used for both displacement components.[3] Thus

$$u_x(x, y) = \sum_{i=1}^{n} N_i^e(x, y)\,u_{xi}, \qquad u_y(x, y) = \sum_{i=1}^{n} N_i^e(x, y)\,u_{yi}, \tag{14.16}$$

[3] This is the so called *element isotropy* condition, which is studied and justified in advanced FEM courses.

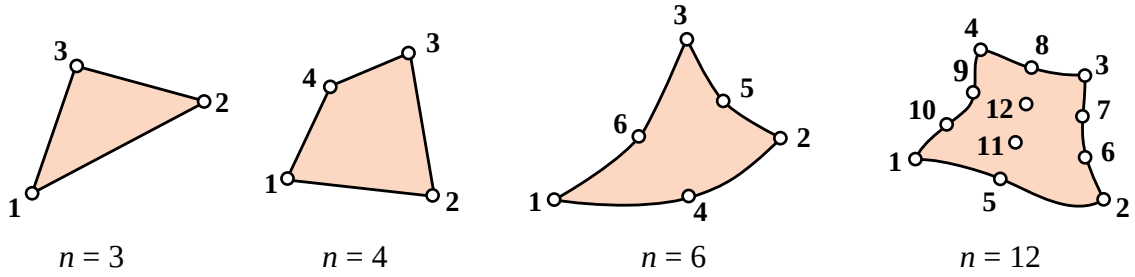

FIGURE 14.7. Example plane stress finite elements, characterized by their number of nodes n.

in which $N_i^e(x, y)$ are the element shape functions. In matrix form:

$$\boxed{\mathbf{u}(x,y) = \begin{bmatrix} u_x(x,y) \\ u_y(x,y) \end{bmatrix} = \begin{bmatrix} N_1^e & 0 & N_2^e & 0 & \dots & N_n^e & 0 \\ 0 & N_1^e & 0 & N_2^e & \dots & 0 & N_n^e \end{bmatrix} \mathbf{u}^e = \mathbf{N}\,\mathbf{u}^e.} \tag{14.17}$$

This **N** (with superscript e omitted to reduce clutter) is called the *shape function matrix*. It has dimensions $2 \times 2n$. For example, if the element has 4 nodes, **N** is 2×8.

The *interpolation condition* on the element shape function $N_i^e(x, y)$ states that it must take the value one at the i^{th} node and zero at all others. This ensures that the interpolation (14.17) is correct at the nodes. Additional requirements on the shape functions are stated in later Chapters.

Differentiating the finite element displacement field yields the strain-displacement relations:

$$\mathbf{e}(x,y) = \begin{bmatrix} \frac{\partial N_1^e}{\partial x} & 0 & \frac{\partial N_2^e}{\partial x} & 0 & \dots & \frac{\partial N_n^e}{\partial x} & 0 \\ 0 & \frac{\partial N_1^e}{\partial y} & 0 & \frac{\partial N_2^e}{\partial y} & \dots & 0 & \frac{\partial N_n^e}{\partial y} \\ \frac{\partial N_1^e}{\partial y} & \frac{\partial N_1^e}{\partial x} & \frac{\partial N_2^e}{\partial y} & \frac{\partial N_2^e}{\partial x} & \dots & \frac{\partial N_n^e}{\partial y} & \frac{\partial N_n^e}{\partial x} \end{bmatrix} \mathbf{u}^e = \mathbf{B}\,\mathbf{u}^e. \tag{14.18}$$

This $\mathbf{B} = \mathbf{D}\,\mathbf{N}$ is called the *strain-displacement matrix*. It is dimensioned $3 \times 2n$. For example, if the element has 6 nodes, **B** is 3×12. The stresses are given in terms of strains and displacements by $\boldsymbol{\sigma} = \mathbf{E}\,\mathbf{e} = \mathbf{E}\mathbf{B}\mathbf{u}^e$, which is assumed to hold at all points of the element.

§14.4.2. Element Energy

To obtain finite element stiffness equations, the variation of the TPE functional is decomposed into contributions from individual elements:

$$\boxed{\delta\Pi^e = \delta U^e - \delta W^e = 0.} \tag{14.19}$$

in which

$$\boxed{U^e = \tfrac{1}{2}\int_{\Omega^e} h\,\boldsymbol{\sigma}^T\mathbf{e}\,d\Omega^e = \tfrac{1}{2}\int_{\Omega^e} h\,\mathbf{e}^T\mathbf{E}\mathbf{e}\,d\Omega^e} \tag{14.20}$$

and

$$\boxed{W^e = \int_{\Omega^e} h\,\mathbf{u}^T\mathbf{b}\,d\Omega^e + \int_{\Gamma^e} h\,\mathbf{u}^T\,\hat{\mathbf{t}}\,d\Gamma^e} \tag{14.21}$$

Note that in (14.21) Γ_t^e has been taken equal to the *complete boundary* Γ^e of the element. This is a consequence of the fact that displacement boundary conditions are applied *after* assembly, to a free-free structure. Consequently it does not harm to assume that all boundary conditions are of stress type insofar as forming the element equations.

§14.4.3. Element Stiffness Equations

Inserting the relations $\mathbf{u} = \mathbf{N}\mathbf{u}^e$, $\mathbf{e} = \mathbf{B}\mathbf{u}^e$ and $\boldsymbol{\sigma} = \mathbf{E}\mathbf{e}$ into Π^e yields the quadratic form in the nodal displacements

$$\Pi^e = \tfrac{1}{2}\mathbf{u}^{eT}\mathbf{K}^e\mathbf{u}^e - \mathbf{u}^{eT}\mathbf{f}^e. \tag{14.22}$$

Here the element stiffness matrix is

$$\boxed{\mathbf{K}^e = \int_{\Omega^e} h\,\mathbf{B}^T\mathbf{E}\mathbf{B}\,d\Omega^e,} \tag{14.23}$$

and the consistent element nodal force vector is

$$\boxed{\mathbf{f}^e = \int_{\Omega^e} h\,\mathbf{N}^T\mathbf{b}\,d\Omega^e + \int_{\Gamma^e} h\,\mathbf{N}^T\hat{\mathbf{t}}\,d\Gamma^e.} \tag{14.24}$$

In the second integral of (14.24) the matrix $\mathbf{N}$ is evaluated on the element boundary only.

The calculation of the entries of $\mathbf{K}^e$ and $\mathbf{f}^e$ for several elements of historical or practical interest is described in subsequent Chapters.

Notes and Bibliography

The plane stress problem is well suited for introducing continuum finite elements, from both historical and technical standpoints. Some books use the Poisson equation for this purpose, but problems such as heat conduction cannot illustrate features such as vector-mixed boundary conditions and shear effects.

The first continuum structural finite elements were developed at Boeing in the early 1950s to model delta-wing skin panels [146,765]. A plane stress model was naturally chosen for the panels. The paper that gave the method its name [137] used the plane stress problem as application driver.

The technical aspects of plane stress can be found in any book on elasticity. A particularly readable one is the excellent textbook by Fung [289], which is unfortunately out of print.

References

Referenced items have been moved to Appendix R.

Homework Exercises for Chapter 14
The Plane Stress Problem

EXERCISE 14.1 [A+C:15] Suppose that the structural material is isotropic, with elastic modulus E and Poisson's ratio ν. The in-plane stress-strain relations for plane stress ($\sigma_{zz} = \sigma_{xz} = \sigma_{yz} = 0$) and plane strain ($e_{zz} = e_{xz} = e_{yz} = 0$) as given in any textbook on elasticity, are

$$\begin{aligned}
\text{plane stress:}\quad & \begin{bmatrix} \sigma_{xx} \\ \sigma_{yy} \\ \sigma_{xy} \end{bmatrix} = \frac{E}{1-\nu^2} \begin{bmatrix} 1 & \nu & 0 \\ \nu & 1 & 0 \\ 0 & 0 & \frac{1-\nu}{2} \end{bmatrix} \begin{bmatrix} e_{xx} \\ e_{yy} \\ 2e_{xy} \end{bmatrix}, \\
\text{plane strain:}\quad & \begin{bmatrix} \sigma_{xx} \\ \sigma_{yy} \\ \sigma_{xy} \end{bmatrix} = \frac{E}{(1+\nu)(1-2\nu)} \begin{bmatrix} 1-\nu & \nu & 0 \\ \nu & 1-\nu & 0 \\ 0 & 0 & \frac{1}{2}(1-2\nu) \end{bmatrix} \begin{bmatrix} e_{xx} \\ e_{yy} \\ 2e_{xy} \end{bmatrix}.
\end{aligned} \tag{E14.1}$$

Show that the constitutive matrix of plane strain can be formally obtained by replacing E by a fictitious modulus E^* and ν by a fictitious Poisson's ratio ν^* in the plane stress constitutive matrix. Find the expression of E^* and ν^* in terms of E and ν.

You may also chose to answer this exercise by doing the inverse process: go from plane strain to plain stress by replacing a fictitious modulus and Poisson's ratio in the plane strain constitutive matrix.

This device permits "reusing" a plane stress FEM program to do plane strain, or vice-versa, as long as the material is isotropic.

Partial answer to go from plane stress to plane strain: $\nu^* = \nu/(1-\nu)$.

EXERCISE 14.2 [A:25] In the finite element formulation of near incompressible isotropic materials (as well as plasticity and viscoelasticity) it is convenient to use the so-called *Lamé constants* λ and μ instead of E and ν in the constitutive equations. Both λ and μ have the physical dimension of stress and are related to E and ν by

$$\lambda = \frac{\nu E}{(1+\nu)(1-2\nu)}, \quad \mu = G = \frac{E}{2(1+\nu)}. \tag{E14.2}$$

Conversely

$$E = \frac{\mu(3\lambda+2\mu)}{\lambda+\mu}, \quad \nu = \frac{\lambda}{2(\lambda+\mu)}. \tag{E14.3}$$

Substitute (E14.3) into both of (E14.1) to express the two stress-strain matrices in terms of λ and μ. Then split the stress-strain matrix $\mathbf{E}$ of plane strain as

$$\mathbf{E} = \mathbf{E}_\mu + \mathbf{E}_\lambda \tag{E14.4}$$

in which $\mathbf{E}_\mu$ and $\mathbf{E}_\lambda$ contain only μ and λ, respectively, with $\mathbf{E}_\mu$ diagonal and $E_{\lambda 33} = 0$. This is the Lamé or $\{\lambda, \mu\}$ splitting of the plane strain constitutive equations, which leads to the so-called **B**-bar formulation of near-incompressible finite elements.[4] Express $\mathbf{E}_\mu$ and $\mathbf{E}_\lambda$ also in terms of E and ν.

For the plane stress case perform a similar splitting in which where $\mathbf{E}_\lambda$ contains only $\bar{\lambda} = 2\lambda\mu/(\lambda+2\mu)$ with $E_{\lambda 33} = 0$, and $\mathbf{E}_\mu$ is a diagonal matrix function of μ and $\bar{\lambda}$.[5] Express $\mathbf{E}_\mu$ and $\mathbf{E}_\lambda$ also in terms of E and ν.

---

[4] Equation (E14.4) is sometimes referred to as the deviatoric+volumetric splitting of the stress-strain law, on account of its physical meaning in plane strain. That interpretation is not fully accurate, however, for plane stress.

[5] For the physical significance of $\bar{\lambda}$ see [688, pp. 254ff].

EXERCISE 14.3 [A:20] Include thermoelastic effects in the plane stress constitutive field equations, assuming a thermally isotropic material with coefficient of linear expansion α. Hint: start from the two-dimensional Hooke's law including temperature:

$$e_{xx} = \frac{1}{E}(\sigma_{xx} - \nu\sigma_{yy}) + \alpha\,\Delta T, \quad e_{yy} = \frac{1}{E}(\sigma_{yy} - \nu\sigma_{xx}) + \alpha\,\Delta T, \quad 2e_{xy} = \sigma_{xy}/G, \tag{E14.5}$$

in which $\Delta T = \Delta T(x, y)$ and $G = \frac{1}{2}E/(1+\nu)$. Solve for stresses and collect effects of ΔT in one vector of "thermal stresses."

EXERCISE 14.4 [A:15] Derive the Cauchy stress-to-traction equations (14.10) using force equilibrium along x and y and the geometric relations shown in Figure E14.1. (This is the "wedge method" in Mechanics of Materials.)

Hint: $t_x\,ds = \sigma_{xx}\,dy + \sigma_{xy}\,dx$, etc.

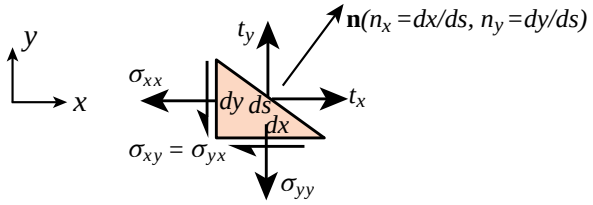

FIGURE E14.1. Geometry for deriving (**?**).

EXERCISE 14.5 [A:25=5+5+15] A linearly elastic plate is in plane stress. It is shown in courses in elasticity that the internal strain energy density stored per unit volume of the plate expressed in terms of stresses and strains is the bilinear form

$$\mathcal{U} = \tfrac{1}{2}(\sigma_{xx}e_{xx} + \sigma_{yy}e_{yy} + \sigma_{xy}e_{xy} + \sigma_{yx}e_{yx}) = \tfrac{1}{2}(\sigma_{xx}e_{xx} + \sigma_{yy}e_{yy} + 2\sigma_{xy}e_{xy}) = \tfrac{1}{2}\,\boldsymbol{\sigma}^T\,\mathbf{e}. \tag{E14.6}$$

(a) Show that (E14.6) can be written in terms of strains only as

$$\mathcal{U} = \tfrac{1}{2}\,\mathbf{e}^T\,\mathbf{E}\,\mathbf{e}, \tag{E14.7}$$

thus justifying the strain energy density expression given in (14.13) for the plane stress problem.

(b) Show that (E14.6) can be written in terms of stresses only as

$$\mathcal{U} = \tfrac{1}{2}\,\boldsymbol{\sigma}^T\,\mathbf{C}\,\boldsymbol{\sigma}, \tag{E14.8}$$

in which $\mathbf{C} = \mathbf{E}^{-1}$ is the elastic compliance (strain-stress) matrix.

(c) Suppose you want to write (E14.6) in terms of the extensional strains $\{e_{xx}, e_{yy}\}$ and of the shear stress $\sigma_{xy} = \sigma_{yx}$. This is known as a *mixed* representation, which is used in finite elements formulated with mixed variational principles. Show that

$$\mathcal{U} = \tfrac{1}{2}\begin{bmatrix} e_{xx} \\ e_{yy} \\ \sigma_{xy} \end{bmatrix}^T \begin{bmatrix} A_{11} & A_{12} & A_{13} \\ A_{12} & A_{22} & A_{23} \\ A_{13} & A_{23} & A_{33} \end{bmatrix} \begin{bmatrix} e_{xx} \\ e_{yy} \\ \sigma_{xy} \end{bmatrix}, \tag{E14.9}$$

and explain how the entries A_{ij} of the kernel matrix $\mathbf{A}$ that appears in (E14.9) can be calculated[6] in terms of the elastic moduli E_{ij}.

Hint. Parts (a,b) are easy. Part (c) is more difficult. It can be symbolically done by the *Mathematica* script

[6] The process of computing $\mathbf{A}$ is an instance of "partial inversion" of the elasticity matrix $\mathbf{E}$. It is closely related to the *Schur complement* concept covered in Appendix P.

```
ClearAll[exx,eyy,gxy,sxx,syy,sxy,E11,E22,E33,E12,E13,E23];
Emat={{E11,E12,E13},{E12,E22,E23},{E13,E23,E33}};
s={sxx,syy,sxy}; e={exx,eyy,gxy}; m={exx,eyy,sxy};
eqs={sxx==E11*exx+E12*eyy+E13*gxy,syy==E12*exx+E22*eyy+E23*gxy,
     sxy==E13*exx+E23*eyy+E33*gxy};
sol=Simplify[Simplify[Solve[eqs,{sxx,syy,gxy}]]];
Print[sol]; U=Simplify[(e.Emat.e/2)/.sol[[1]]];
fac[i_,j_]:=If[i==j,1,1/2];
A=Table[fac[i,j]*Coefficient[U,m[[i]]*m[[j]]],{i,1,3},{j,1,3}];
Print["A=",A//MatrixForm];
```

If you use this solution, make sure to explain what is going on.

Note: the following Table list relations between commonly used moduli for isotropic linear elastic material. Here K is the bulk modulus whereas M is the P-wave modulus used in seismology. Tha table is useful for Exercise 14.2.

	(λ,μ)	(E,μ)	(K,λ)	(K,μ)	(λ,ν)	(μ,ν)	(E,ν)	(K,ν)	(K,E)
$K=$	$\lambda+\frac{2\mu}{3}$	$\frac{E\mu}{3(3\mu-E)}$			$\lambda\frac{1+\nu}{3\nu}$	$\frac{2\mu(1+\nu)}{3(1-2\nu)}$	$\frac{E}{3(1-2\nu)}$		
$E=$	$\mu\frac{3\lambda+2\mu}{\lambda+\nu}$		$9K\frac{K-\lambda}{3K-\lambda}$	$\frac{9K\mu}{3K+\mu}$		$\frac{\lambda(1+\nu)(1-2\nu)}{\nu}$	$2\mu(1+\nu)$		$3K(1-2\nu)$
$\lambda=$		$\mu\frac{E-2\mu}{3\mu-E}$		$K-\frac{2\mu}{3}$		$\frac{2\mu\nu}{1-2\nu}$	$\frac{E\nu}{(1+\nu)(1-2\nu)}$	$\frac{3K}{1+\nu}$	$\frac{3K(3K-E)}{9K-E}$
$\mu=G=$			$\mu\frac{K-\lambda}{2}$		$\lambda\frac{K-\lambda}{3K-\lambda}$	$\frac{9K\mu}{3K+\mu}$	$\frac{\lambda(1-2\nu)}{2\nu}$	$\frac{E}{2(1+\nu)}$	$3K\frac{(1-2\nu)}{2(1+\nu)}$
$\nu=$		$\frac{\lambda}{2(\lambda+\mu)}$	$\frac{E}{2\mu}-1$	$\frac{\lambda}{3K-\lambda}$	$\frac{3K-2\mu}{2(3K+\mu)}$				$\frac{3K-E}{6K}$
$M=$	$\lambda+2\mu$	$\mu\frac{4\mu-E}{3\mu-E}$	$3K-2\lambda$	$K+\frac{4\mu}{3}$	$\lambda\frac{1-\nu}{\nu}$	$\mu\frac{2-2\nu}{1-2\nu}$	$\frac{E(1-\nu)}{(1+\nu)(1-2\nu)}$	$3K\frac{1-\nu}{1+\nu}$	$3K\frac{3K+E}{9K-E}$

(E14.10)

15

Three-Node Plane Stress Triangles

TABLE OF CONTENTS

§15.1. Introduction

This Chapter derives element stiffness equations of three-node triangles constructed with linear displacements for the plane stress problem formulated in Chapter 14. These elements have six displacement degrees of freedom, which are placed at the *connection nodes*. There are two main versions that differ on where the connection nodes are located:

1. The *Turner triangle* has connection nodes located at the corners.
2. The *Veubeke equilibrium triangle* has connection nodes located at the side midpoints.

The triangle geometry is defined by the corner locations or *geometric nodes* in both cases. Of the two versions, the Turner triangle is by far the most practically important one in solid and structural mechanics.[1] Thus most of the material in this Chapter is devoted to it. It enjoys several important properties:

(i) It belongs to both the isoparametric and subparametric element families, which are introduced in the next Chapter.

(ii) It allows closed form derivations for the stiffness matrix and consistent force vector without need for numerical integration.

(iii) It cannot be improved by the addition of internal degrees of freedom.

Properties (ii) and (iii) are shared by the Veubeke equilibrium triangle. Since this model is rarely used in structural applications it is covered only as advanced material in §15.5.

The Turner triangle is not a good performer for structural stress analysis. It is still used in problems that do not require high accuracy, as well as in non-structural applications such as thermal and electromagnetic analysis. One reason is that triangular meshes are easily generated over arbitrary two-dimensional domains using techniques such as Delaunay triangulation.

§15.2. Background

§15.2.1. Parametric Representation of Functions

The concept of *parametric representation* of functions is crucial in modern FEM. Together with multidimensional numerical integration, it is a key enabling tool for developing elements in two and three space dimensions.[2] Without these tools the developer would become lost in an algebraic maze as element geometry and shape functions get more complicated. The essentials of parametric representation can be illustrated through a simple example. Consider the following alternative representations of the unit-circle function, $x^2 + y^2 = 1$:

$$\text{(I)}\;\; y = \sqrt{1 - x^2}, \qquad \text{(II)}\;\; x = \cos\theta \;\; \text{and}\; y = \sin\theta. \tag{15.1}$$

The direct representation (I) fits the conventional function notation, i.e., $y = f(x)$. Given a value of x, it returns one or more y. On the other hand, the parametric representation (II) is indirect: both x

[1] The triangle was one of the two plane-stress continuum elements presented by Turner, Clough, Martin and Topp in their 1956 paper [786]. This publication is widely regarded as the start of the present FEM. The derivation was not done, however, with assumed displacements. See **Notes and Bibliography** at the end of this Chapter.

[2] Numerical integration is not useful for the triangular elements covered here, but essential in the more complicated iso-P models covered in Chapters 16ff.

and y are given in terms of one parameter, the angle θ. Elimination of θ through the trigonometric identity $\cos^2\theta + \sin^2\theta = 1$ recovers $x^2 + y^2 = 1$. But there are situations in which working with the parametric form throughout the development is more convenient. Continuum finite elements provide a striking illustration of this point.

§15.2.2. Geometry

The geometry of the 3-node triangle shown in Figure 15.1(a) is specified by the location of its three corner nodes on the $\{x, y\}$ plane. Nodes are labelled 1, 2, 3 while traversing the sides in *counterclockwise* fashion. Their location is defined by their Cartesian coordinates: $\{x_i,\ y_i\}$ for $i = 1, 2, 3$.

The Turner triangle has six degrees of freedom, defined by the six corner displacement components $\{u_{xi}, u_{yi}\}$, for $i = 1, 2, 3$. The interpolation of the internal displacements $\{u_x, u_y\}$ from these six values is studied in §15.3, after triangular coordinates are introduced. The triangle area can be obtained as

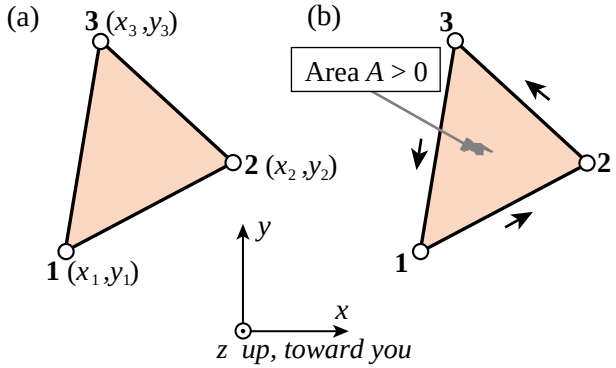

FIGURE 15.1. The three-node, linear-displacement plane stress triangular element: (a) geometry; (b) area and positive boundary traversal.

$$2A = \det \begin{bmatrix} 1 & 1 & 1 \\ x_1 & x_2 & x_3 \\ y_1 & y_2 & y_3 \end{bmatrix} = (x_2y_3 - x_3y_2) + (x_3y_1 - x_1y_3) + (x_1y_2 - x_2y_1). \tag{15.2}$$

The area given by (15.2) is a *signed* quantity. It is positive if the corners are numbered in cyclic counterclockwise order (when looking down from the $+z$ axis), as illustrated in Figure 15.1(b). This convention is followed in the sequel.

§15.2.3. Triangular Coordinates

Points of the triangle may also be located in terms of a *parametric* coordinate system:

$$\zeta_1,\ \zeta_2,\ \zeta_3. \tag{15.3}$$

In the literature these 3 parameters receive an astonishing number of names, as the list collected in Table 15.1 shows. In the sequel the name *triangular coordinates* will be used to emphasize the close association with this particular geometry.

Equations

$$\zeta_i = constant \tag{15.4}$$

represent a set of straight lines parallel to the side opposite to the i^{th} corner, as depicted in Figure 15.2. The equations of sides 2–3, 3–1 and 1–2 are $\zeta_1 = 0$, $\zeta_2 = 0$ and $\zeta_3 = 0$, respectively. The three corners have coordinates (1,0,0), (0,1,0) and (0,0,1). The three midpoints of the sides have coordinates $(\frac{1}{2}, \frac{1}{2}, 0)$, $(0, \frac{1}{2}, \frac{1}{2})$ and $(\frac{1}{2}, 0, \frac{1}{2})$, the centroid has coordinates $(\frac{1}{3}, \frac{1}{3}, \frac{1}{3})$, and so on. The coordinates are not independent because their sum is unity:

$$\zeta_1 + \zeta_2 + \zeta_3 = 1. \tag{15.5}$$

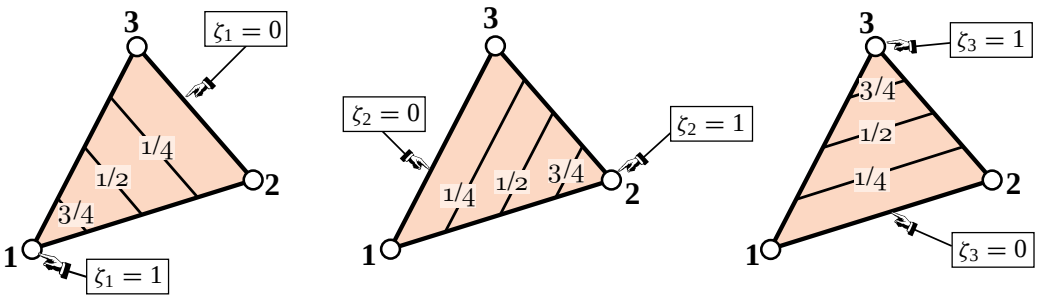

FIGURE 15.2. Triangular coordinates ζ_1, ζ_2, ζ_3.

Table 15.1 Names of element parametric coordinates

Name	*Applicable to*
natural coordinates	all elements
isoparametric coordinates	isoparametric elements
shape function coordinates	isoparametric elements
barycentric coordinates	simplices (triangles, tetrahedra, ...)
Möbius coordinates	triangles
triangular coordinates	all triangles
area (also written "areal") coordinates	straight-sided triangles

Triangular coordinates normalized as per $\zeta_1 + \zeta_2 + \zeta_3 = 1$ are often qualified as "homogeneous" in the mathematical literature.

Remark 15.1. In pre-1970 FEM publications, triangular coordinates were often called *area coordinates*, and occasionally *areal coordinates*. This comes from the following interpretation: $\zeta_i = A_{jk}/A$, where A_{jk} is the area subtended by the subtriangle formed by the point P and corners j and k, in which j and k are 3-cyclic permutations of i. Historically this was the way coordinates were defined in 1960s papers. However this relation does not carry over to general isoparametric triangles with curved sides and thus it is not used here.

§15.2.4. Linear Interpolation

Consider a function $f(x, y)$ that varies *linearly* over the triangle domain. In terms of Cartesian coordinates it may be expressed as

$$f(x, y) = a_0 + a_1 x + a_2 y, \tag{15.6}$$

where a_0, a_1 and a_2 are coefficients to be determined from three conditions. In finite element work such conditions are often the *nodal values* taken by f at the corners:

$$f_1, \quad f_2, \quad f_3. \tag{15.7}$$

The expression in triangular coordinates makes direct use of those three values:

$$f(\zeta_1, \zeta_2, \zeta_3) = f_1\zeta_1 + f_2\zeta_2 + f_3\zeta_3 = \begin{bmatrix} f_1 & f_2 & f_3 \end{bmatrix} \begin{bmatrix} \zeta_1 \\ \zeta_2 \\ \zeta_3 \end{bmatrix} = \begin{bmatrix} \zeta_1 & \zeta_2 & \zeta_3 \end{bmatrix} \begin{bmatrix} f_1 \\ f_2 \\ f_3 \end{bmatrix}. \tag{15.8}$$

Formula (15.8) is called a *linear interpolant* for f.

§15.2.5. Coordinate Transformations

Quantities that are closely linked with the element geometry are best expressed in triangular coordinates. On the other hand, quantities such as displacements, strains and stresses are usually expressed in the Cartesian system $\{x, y\}$. Thus we need transformation equations through which it is possible to pass from one coordinate system to the other.

Cartesian and triangular coordinates are linked by the relation

$$\boxed{\begin{bmatrix} 1 \\ x \\ y \end{bmatrix} = \begin{bmatrix} 1 & 1 & 1 \\ x_1 & x_2 & x_3 \\ y_1 & y_2 & y_3 \end{bmatrix} \begin{bmatrix} \zeta_1 \\ \zeta_2 \\ \zeta_3 \end{bmatrix}.} \tag{15.9}$$

The first equation says that the sum of the three coordinates is one. The next two express x and y linearly as homogeneous forms in the triangular coordinates. These are obtained by applying the linear interpolant (15.8) to the Cartesian coordinates: $x = x_1\zeta_1 + x_2\zeta_2 + x_3\zeta_3$ and $y = y_1\zeta_1 + y_2\zeta_2 + y_3\zeta_3$. Assuming $A \neq 0$, inversion of (15.9) yields

$$\begin{bmatrix} \zeta_1 \\ \zeta_2 \\ \zeta_3 \end{bmatrix} = \frac{1}{2A} \begin{bmatrix} x_2y_3 - x_3y_2 & y_2 - y_3 & x_3 - x_2 \\ x_3y_1 - x_1y_3 & y_3 - y_1 & x_1 - x_3 \\ x_1y_2 - x_2y_1 & y_1 - y_2 & x_2 - x_1 \end{bmatrix} \begin{bmatrix} 1 \\ x \\ y \end{bmatrix} = \frac{1}{2A} \begin{bmatrix} 2A_{23} & y_{23} & x_{32} \\ 2A_{31} & y_{31} & x_{13} \\ 2A_{12} & y_{12} & x_{21} \end{bmatrix} \begin{bmatrix} 1 \\ x \\ y \end{bmatrix}. \tag{15.10}$$

Here $x_{jk} = x_j - x_k$, $y_{jk} = y_j - y_k$, A is the triangle area given by (15.2) and A_{jk} denotes the area subtended by corners j, k and the origin of the x–y system. If this origin is taken at the centroid of the triangle, $A_{23} = A_{31} = A_{12} = A/3$.

§15.2.6. Partial Derivatives

From equations (15.9) and (15.10) we immediately obtain the following relations between partial derivatives:

$$\frac{\partial x}{\partial \zeta_i} = x_i, \qquad \frac{\partial y}{\partial \zeta_i} = y_i, \tag{15.11}$$

$$2A\frac{\partial \zeta_i}{\partial x} = y_{jk}, \qquad 2A\frac{\partial \zeta_i}{\partial y} = x_{kj}. \tag{15.12}$$

In (15.12) j and k denote the *3-cyclic permutations* of i. For example, if $i = 2$, then $j = 3$ and $k = 1$. The derivatives of a function $f(\zeta_1, \zeta_2, \zeta_3)$ with respect to x or y follow immediately from (15.12) and application of the chain rule:

$$\boxed{\begin{aligned} \frac{\partial f}{\partial x} &= \frac{1}{2A}\left(\frac{\partial f}{\partial \zeta_1}y_{23} + \frac{\partial f}{\partial \zeta_2}y_{31} + \frac{\partial f}{\partial \zeta_3}y_{12}\right) \\ \frac{\partial f}{\partial y} &= \frac{1}{2A}\left(\frac{\partial f}{\partial \zeta_1}x_{32} + \frac{\partial f}{\partial \zeta_2}x_{13} + \frac{\partial f}{\partial \zeta_3}x_{21}\right) \end{aligned}} \tag{15.13}$$

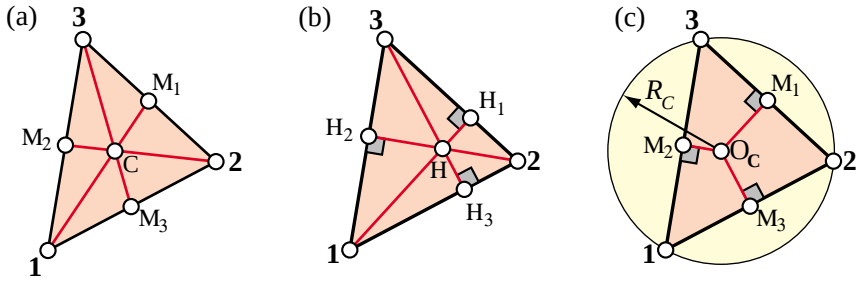

FIGURE 15.3. Interesting points and lines of a triangle.

which in matrix form is

$$\begin{bmatrix} \dfrac{\partial f}{\partial x} \\ \dfrac{\partial f}{\partial y} \end{bmatrix} = \frac{1}{2A} \begin{bmatrix} y_{23} & y_{31} & y_{12} \\ x_{32} & x_{13} & x_{21} \end{bmatrix} \begin{bmatrix} \dfrac{\partial f}{\partial \zeta_1} \\ \dfrac{\partial f}{\partial \zeta_2} \\ \dfrac{\partial f}{\partial \zeta_3} \end{bmatrix}. \tag{15.14}$$

With these mathematical ingredients in place we are now in a position to handle the derivation of straight-sided triangular elements, and in particular the Turner and Veubeke triangles.

§15.2.7. *Homogeneous Polynomials in Triangular Coordinates

Because ζ_1, ζ_2 and ζ_3 are not independent, polynomial functions in those variables are not unique. For example $3-2\zeta_1+\zeta_2-3\zeta_3$ and $\zeta_1+4\zeta_2$ are identical, since they differ by $3-3(\zeta_1+\zeta_2+\zeta_3)$=0. To achieve uniqueness it is necessary to write the function as a *homogeneous* polynomial, as in the second form of this example.

To reduce the general linear polynomial $c_{000}+c_{100}\zeta_1+c_{010}\zeta_2+c_{001}\zeta_3$ to homogeneous form, subtract $c_{000}(1-\zeta_1-\zeta_2-\zeta_3)$, which is zero, to get $P_1=(c_{100}-c_{000})\zeta_1+(c_{010}-c_{000})\zeta_2+(c_{001}-c_{000})\zeta_3$.

To reduce the general quadratic polynomial $c_{000}+c_{100}\zeta_1+c_{010}\zeta_2+c_{001}\zeta_3+c_{200}\zeta_1^2+c_{020}\zeta_2^2+c_{002}\zeta_3^2+c_{110}\zeta_1\zeta_2+c_{011}\zeta_2\zeta_3+c_{101}\zeta_3\zeta_1$ to homogeneous form, subtract $(c_{000}+c_{100}\zeta_1+c_{010}\zeta_2+c_{001}\zeta_3)(1-\zeta_1-\zeta_2-\zeta_3)$.

And so on. All polynomial expressions used in this book for triangles are expressed in homogeneous form.

§15.2.8. *Interesting Points and Lines

Some distinguished lines and points of a straight-sided triangle are briefly described here for use in other developments as well as in Exercises. The *triangle medians* are three lines that join the corners to the midpoints of the opposite sides, as pictured in Figure 15.3(a). The midpoint opposite corner i is labeled M_i.

The medians 1–M_1, 2–M_2 and 3–M_3 have equations $\zeta_2=\zeta_3$, $\zeta_3=\zeta_1$ and $\zeta_1=\zeta_2$, respectively, in triangular coordinates. They intersect at the centroid C of coordinates $\{\frac{1}{3},\frac{1}{3},\frac{1}{3}\}$. Other names for the centroid are *barycenter* and *center of gravity*. If you make a real triangle out of cardboard, you can balance the triangle at this point. It can be shown that the centroid trisects the medians, that is to say, the distance from a corner to the centroid is twice the distance from the centroid to the opposite side of the triangle.

The *altitudes* are three lines that connect each corner with their projections onto the opposing sides, as depicted in Figure 15.3(b). The projection of corner i is identified H_i, so the altitudes are 1–H_1, 2–H_2 and 3–H_3. Locations H_i are called *altitude feets*. The altitudes intersect at the triangle *orthocenter* H. The lengths of those segments are the *triangle heights*. The triangular coordinates of H_i and H, as well as the altitude equations, are worked out in an Exercise.

Another interesting point is the center O_C of the circumscribed circle, or circumcircle. This is the unique circle that passes through the three corners, as shown in Figure 15.3(c). It can be geometrically constructed by drawing the normal to each side at the midpoints. Those three lines, called the perpendicular side bisectors, intersect at O_C. A famous theorem by Euler asserts that the centroid, the orthocenter and the circumcircle center fall on a straight line, called the Euler line. Furthermore, C lies between O_C and H, and the distance O_C–H is three times the distance H–C.

§15.3. The Turner Triangle

The simplest triangular element for plane stress (and in general, for 2D problems of variational index $m = 1$) is the three-node triangle with *linear shape functions*, with degrees of freedom located at the corners. The shape functions are simply the triangular coordinates. That is, $N_i^e = \zeta_i$ for $i = 1, 2, 3$. When applied to the plane stress problem, this element is called the Turner triangle.

For the plane stress problem we select the linear interpolation (15.8) for the displacement components u_x and u_y at an arbitrary point $P(\zeta_1, \zeta_2, \zeta_3)$:

$$\boxed{u_x = u_{x1}\zeta_1 + u_{x2}\zeta_2 + u_{x3}\zeta_3, \qquad u_y = u_{y1}\zeta_1 + u_{y2}\zeta_2 + u_{y3}\zeta_3.} \tag{15.15}$$

The interpolation is illustrated in Figure 15.4. The two expressions in (15.15) can be combined in a matrix form that befits the expression (14.17) for an arbitrary plane stress element:

$$\begin{bmatrix} u_x \\ u_y \end{bmatrix} = \begin{bmatrix} \zeta_1 & 0 & \zeta_2 & 0 & \zeta_3 & 0 \\ 0 & \zeta_1 & 0 & \zeta_2 & 0 & \zeta_3 \end{bmatrix} \begin{bmatrix} u_{x1} \\ u_{y1} \\ u_{x2} \\ u_{y2} \\ u_{x3} \\ u_{y3} \end{bmatrix} = \mathbf{N}\,\mathbf{u}^e, \tag{15.16}$$

where $\mathbf{N}$ is the matrix of shape functions.

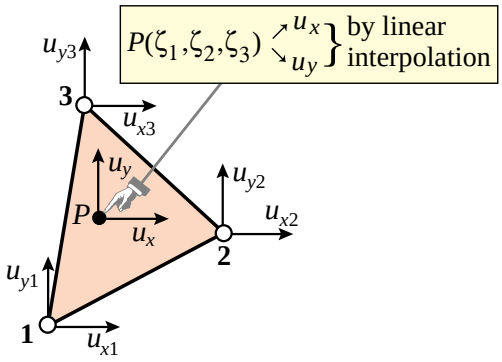

FIGURE 15.4. Displacement interpolation over triangle.

§15.3.1. Strain-Displacement Equations

The strains within the elements are obtained by differentiating the shape functions with respect to x and y. Using (15.14), (15.16) and the general form (14.18) we get

$$\mathbf{e} = \mathbf{D}\,\mathbf{N}\,\mathbf{u}^e = \frac{1}{2A}\begin{bmatrix} y_{23} & 0 & y_{31} & 0 & y_{12} & 0 \\ 0 & x_{32} & 0 & x_{13} & 0 & x_{21} \\ x_{32} & y_{23} & x_{13} & y_{31} & x_{21} & y_{12} \end{bmatrix} \begin{bmatrix} u_{x1} \\ u_{y1} \\ u_{x2} \\ u_{y2} \\ u_{x3} \\ u_{y3} \end{bmatrix} = \mathbf{B}\,\mathbf{u}^e, \tag{15.17}$$

in which $\mathbf{D}$ denotes the symbolic strain-to-displacement differentiation operator given in (14.6), and $\mathbf{B}$ is the strain-displacement matrix. Note that the strains are *constant* over the element. This is the origin of the name *constant strain triangle* (CST) given it in many finite element publications.

§15.3.2. Stress-Strain Equations

The stress field $\boldsymbol{\sigma}$ is related to the strain field by the elastic constitutive equation in (14.5), which is repeated here for convenience:

$$\boldsymbol{\sigma} = \begin{bmatrix} \sigma_{xx} \\ \sigma_{yy} \\ \sigma_{xy} \end{bmatrix} = \begin{bmatrix} E_{11} & E_{12} & E_{13} \\ E_{12} & E_{22} & E_{23} \\ E_{13} & E_{23} & E_{33} \end{bmatrix} \begin{bmatrix} e_{xx} \\ e_{yy} \\ 2e_{xy} \end{bmatrix} = \mathbf{E}\,\mathbf{e}, \tag{15.18}$$

where E_{ij} are plane stress elastic moduli. The constitutive matrix $\mathbf{E}$ will be assumed to be constant over the element. Because the strains are constant, so are the stresses.

§15.3.3. The Stiffness Matrix

The element stiffness matrix is given by the general formula (14.23), which is repeated here

$$\mathbf{K}^e = \int_{\Omega^e} h\,\mathbf{B}^T\mathbf{E}\mathbf{B}\; d\Omega, \tag{15.19}$$

where Ω^e is the triangle domain, and h the plate thickness that appears in the plane stress problem. Since $\mathbf{B}$ and $\mathbf{E}$ are constant, they can be taken out of the integral:

$$\mathbf{K}^e = \mathbf{B}^T\mathbf{E}\mathbf{B}\int_{\Omega^e} h\, d\Omega \tag{15.20}$$

If h is uniform over the element the remaining integral in (15.20) is simply hA, and we obtain the closed form

$$\boxed{\mathbf{K}^e = A\,h\,\mathbf{B}^T\,\mathbf{E}\,\mathbf{B} = \frac{h}{4A}\begin{bmatrix} y_{23} & 0 & x_{32} \\ 0 & x_{32} & y_{23} \\ y_{31} & 0 & x_{13} \\ 0 & x_{13} & y_{31} \\ y_{12} & 0 & x_{21} \\ 0 & x_{21} & y_{12} \end{bmatrix} \begin{bmatrix} E_{11} & E_{12} & E_{13} \\ E_{12} & E_{22} & E_{23} \\ E_{13} & E_{23} & E_{33} \end{bmatrix} \begin{bmatrix} y_{23} & 0 & y_{31} & 0 & y_{12} & 0 \\ 0 & x_{32} & 0 & x_{13} & 0 & x_{21} \\ x_{32} & y_{23} & x_{13} & y_{31} & x_{21} & y_{12} \end{bmatrix}.} \tag{15.21}$$

Exercise 15.1 deals with the case of a linearly varying plate thickness.

§15.3.4. The Consistent Nodal Force Vector

For simplicity we consider here only internal body forces[3] defined by the vector field

$$\mathbf{b} = \begin{bmatrix} b_x \\ b_y \end{bmatrix} \tag{15.22}$$

which is specified per unit of volume. The consistent nodal force vector $\mathbf{f}^e$ is given by the general formula (14.23) of the previous Chapter:

$$\mathbf{f}^e = \int_{\Omega^e} h\,\mathbf{N}^T\,\mathbf{b}\; d\Omega = \int_{\Omega^e} h \begin{bmatrix} \zeta_1 & 0 \\ 0 & \zeta_1 \\ \zeta_2 & 0 \\ 0 & \zeta_2 \\ \zeta_3 & 0 \\ 0 & \zeta_3 \end{bmatrix} \mathbf{b}\; d\Omega. \tag{15.23}$$

[3] For consistent force computations corresponding to distributed boundary loads over a side, see Exercise 15.4.

```
Trig3TurnerMembraneStiffness[ncoor_,Emat_,h_,numer_]:=Module[{
  x1,x2,x3,y1,y2,y3,x21,x32,x13,y12,y23,y31,A,Be,Ke},
  {{x1,y1},{x2,y2},{x3,y3}}=ncoor;
  A=Simplify[(x2*y3-x3*y2+(x3*y1-x1*y3)+(x1*y2-x2*y1))/2];
  {x21,x32,x13,y12,y23,y31}={x2-x1,x3-x2,x1-x3,y1-y2,y2-y3,y3-y1};
  Be={{y23,0,y31,0,y12,0},{0,x32,0,x13,0,x21},
      {x32,y23,x13,y31,x21,y12}}/(2*A);
  If [numer, Be=N[Be]]; Ke=A*h*Transpose[Be].Emat.Be;
  Return[Ke]];
```

FIGURE 15.5. Implementation of Turner triangle stiffness matrix calculation as a *Mathematica* module.

The simplest case is when the body force components (15.22) as well as the thickness h are constant over the element. Then we need the integrals

$$\int_{\Omega^e} \zeta_1 \, d\Omega = \int_{\Omega^e} \zeta_2 \, d\Omega = \int_{\Omega^e} \zeta_3 \, d\Omega = \tfrac{1}{3} A \tag{15.24}$$

which replaced into (15.23) gives

$$\boxed{\mathbf{f}^e = \frac{Ah}{3} [\, b_x \quad b_y \quad b_x \quad b_y \quad b_x \quad b_y \,]^T .} \tag{15.25}$$

This agrees with the simple element-by-element force-lumping procedure, which assigns one third of the total force along the $\{x, y\}$ directions: Ahb_x and Ahb_y, to each corner.

Remark 15.2. The integrals (15.24) are particular cases of the general integration formula of monomials in triangular coordinates:

$$\frac{1}{2A} \int_{\Omega^e} \zeta_1^i \, \zeta_2^j \, \zeta_3^k \, d\Omega = \frac{i!\, j!\, k!}{(i + j + k + 2)!}, \quad i \ge 0, \; j \ge 0, \; k \ge 0. \tag{15.26}$$

which can be derived through the Beta function. Here i, j, k are integer exponents. This formula *only holds for triangles with straight sides*, and thus does not apply for higher order elements with curved sides. Formulas (15.24) are obtained by setting exponents $i = 1$, $j = k = 0$ in (15.26), and permuting $\{i, j, k\}$ cyclically.

§15.3.5. Implementation

The implementation of the Turner triangle in any programming language is very simple. A *Mathematica* module that returns $\mathbf{K}^e$ is shown in Figure 15.5. The module needs only 8 lines of code. It is invoked as

```
Ke=Trig3TurnerMembraneStiffness[ncoor,Emat,h,numer];
```  (15.27)

The arguments are

`ncoor`	Element node coordinates, arranged as a list: `{{x1,y1},{x2,y2},{x3,y3}}`.
`Emat`	A two-dimensional list storing the 3×3 plane stress matrix of elastic moduli as `{{E11,E12,E13},{E12,E22,E23},{E13,E23,E33}}`.
`h`	Plate thickness, assumed uniform over the triangle.

```
ncoor={{0,0},{3,1},{2,2}}; Emat=8*{{8,2,0},{2,8,0},{0,0,3}};
Ke=Trig3TurnerMembraneStiffness[ncoor,Emat,1,False];
Print["Ke=",Ke//MatrixForm];
Print["eigs of Ke=",Chop[Eigenvalues[N[Ke]]]];
Show[Graphics[RGBColor[1,0,0]],Graphics[AbsoluteThickness[2]],
     Graphics[Polygon[ncoor]],Axes->True];
```

$$\text{Ke} = \begin{pmatrix} 11 & 5 & -10 & -2 & -1 & -3 \\ 5 & 11 & 2 & 10 & -7 & -21 \\ -10 & 2 & 44 & -20 & -34 & 18 \\ -2 & 10 & -20 & 44 & 22 & -54 \\ -1 & -7 & -34 & 22 & 35 & -15 \\ -3 & -21 & 18 & -54 & -15 & 75 \end{pmatrix}$$

eigs of Ke = {139.33, 60., 20.6704, 0, 0, 0}

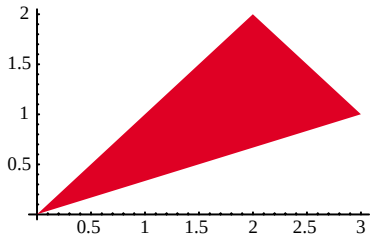

FIGURE 15.6. Test statements to exercise the module of Figure 15.5, and outputs.

`numer` A logical flag: `True` to request floating-point computation, else `False`.

This module is exercised by the statements listed at the top of Figure 15.6, which form a triangle with corner coordinates {{0,0},{3,1},{2,2}}, isotropic material matrix with $E_{11} = E_{22} = 64$, $E_{12} = 16$, $E_{33} = 24$, others zero, (that is, $E = 60$ and $\nu = \frac{1}{4}$) and unit thickness. The results are shown at the bottom of Figure 15.6. The computation of stiffness matrix eigenvalues is always a good programming test, since 3 eigenvalues must be exactly zero and the other 3 real and positive, as explained in Chapter 19. The last test statement draws the triangle (this plot was moved to the right of the numeric output to save space.)

§15.3.6. *Consistency Verification

It remains to check whether the interpolation (15.15) for element displacements meets the completeness and continuity criteria studied in Chapter 19 for finite element trial functions. Such *consistency* conditions are sufficient to insure convergence toward the exact solution of the mathematical model as the mesh is refined.

The variational index for the plane stress problem is $m = 1$. According to the rules stated in §19.3, the trial functions should be 1-complete, C^0 continuous, and C^1 piecewise differentiable.

§15.3.7. *Checking Continuity

Along any triangle side, the variation of u_x and u_y is *linear and uniquely determined by the value at the nodes on that side*. For example, over side 1–2 of an individual triangle, which has equation $\zeta_3 = 0$:

$$\begin{aligned} u_x &= u_{x1}\zeta_1 + u_{x2}\zeta_2 + u_{x3}\zeta_3 = u_{x1}\zeta_1 + u_{x2}\zeta_2, \\ u_y &= u_{y1}\zeta_1 + u_{y2}\zeta_2 + u_{y3}\zeta_3 = u_{y1}\zeta_1 + u_{y2}\zeta_2. \end{aligned} \tag{15.28}$$

The variation of u_x and u_y over side 1-2 depends only on the nodal values u_{x1}, u_{x2}, u_{y1} and u_{y2}.

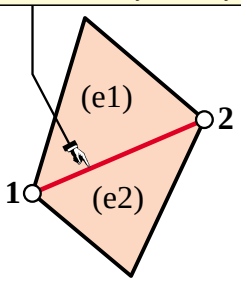

An identical argument holds for that side when it belongs to an adjacent triangle, such as elements (*e*1) and (*e*2) shown in Figure 15.7. Since the node values on all elements that meet at a node are the same, u_x and u_y match along the side, and the trial function is C^0 interelement continuous. Because the functions are continuous inside the elements, it follows that the continuity requirement is met.

FIGURE 15.7. Interelement continuity check.

§15.3.8. *Checking Completeness

The completeness condition for variational order $m = 1$ requires that the shape functions $N_i = \zeta_i$ be able to represent exactly any linear displacement field:

$$u_x = \alpha_0 + \alpha_1 x + \alpha_2 y, \qquad u_y = \beta_0 + \beta_1 x + \beta_1 y. \tag{15.29}$$

To check this we obtain the nodal values associated with the motion (15.29): $u_{xi} = \alpha_0 + \alpha_1 x_i + \alpha_2 y_i$ and $u_{yi} = \beta_0 + \beta_1 x_i + \beta_2 y_i$ for $i = 1, 2, 3$. Replace these in (15.16) and see if (15.29) is recovered. Here are the detailed calculations for component u_x:

$$\begin{aligned} u_x &= \sum_i u_{xi}\zeta_i = \sum_i (\alpha_0 + \alpha_1 x_i + \alpha_2 y_i)\zeta_i = \sum_i (\alpha_0\zeta_i + \alpha_1 x_i\zeta_i + \alpha_2 y_i\zeta_i) \\ &= \alpha_0 \sum_i \zeta_i + \alpha_1 \sum_i (x_i\zeta_i) + \alpha_2 \sum_i (y_i\zeta_i) = \alpha_0 + \alpha_1 x + \alpha_2 y. \end{aligned} \tag{15.30}$$

Component u_y can be similarly verified. Consequently (15.16) satisfies the completeness requirement for the plane stress problem — and in general, for any problem of variational index 1. Finally, a piecewise linear trial function is obviously C^1 piecewise differentiable and consequently has finite energy. Thus the two completeness requirements are satisfied.

§15.3.9. *Tonti Matrix Diagram

For further developments covered in more advanced courses, it is convenient to split the governing equations of the element. In the case of the Turner triangle they are, omitting element superscripts:

$$\mathbf{e} = \mathbf{B}\mathbf{u}, \quad \boldsymbol{\sigma} = \mathbf{E}\mathbf{e}, \quad \mathbf{f} = \mathbf{A}^T\boldsymbol{\sigma} = V\mathbf{B}^T\boldsymbol{\sigma}. \tag{15.31}$$

Here $V = h_m A$ is the volume of the element, h_m being the mean thickness. The equations (15.31) may be graphically represented with the diagram shown in Figure 15.8. This is a discrete Tonti diagram similar to those of Chapter 6.

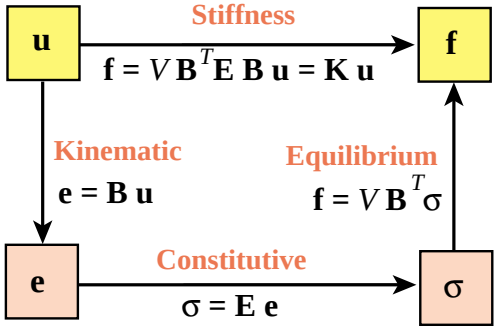

FIGURE 15.8. Tonti matrix diagram for Turner triangle.

§15.4. *Derivation Using Natural Strains and Stresses

The foregoing derivation of the Turner triangle uses Cartesian strains and stresses, as well as $\{x, y\}$ displacements. The only intrinsic quantities are the triangle coordinates. This advanced section examines the derivation of the element stiffness matrix through natural strains, natural stresses and covariant displacements.

Although the procedure does not offer obvious shortcuts over the previous derivation, it becomes important in the construction of more complicated high performance elements. It also helps reading recent literature in assumed strain elements.

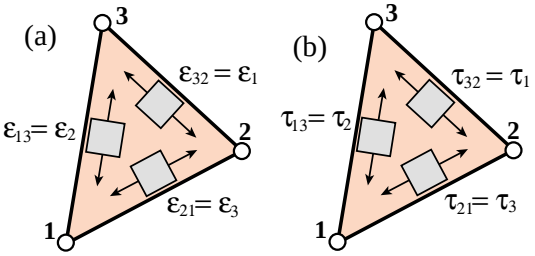

FIGURE 15.9. Geometry-intrinsic fields for the Turner triangle: (a) natural strains ϵ_i, (b) natural stresses τ_i.

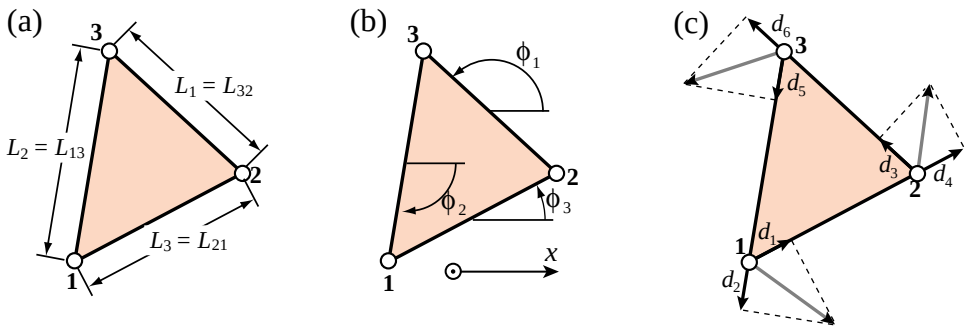

FIGURE 15.10. Additional quantities appearing in natural strain and stress calculations: (a) side lengths, (b) side directions, (c) covariant node displacements.

§15.4.1. *Natural Strains and Stresses

Natural strains are extensional strains directed parallel to the triangle sides, as shown in Figure 15.10(a). Natural strains are denoted by $\epsilon_{21} \equiv \epsilon_3$, $\epsilon_{32} \equiv \epsilon_1$, and $\epsilon_{13} \equiv \epsilon_2$.

Similarly, *natural stresses* are normal stresses directed parallel to the triangle sides, as shown in Figure 15.10(b). Natural stresses are denoted by $\tau_{21} \equiv \tau_3$, $\tau_{32} \equiv \tau_1$, and $\tau_{13} \equiv \tau_2$.

Because both natural stresses and strains are constant over the triangle, no node value association is needed.

The natural strains can be related to Cartesian strains by the following tensor transformation[4]

$$\boldsymbol{\epsilon} = \begin{bmatrix} \epsilon_1 \\ \epsilon_2 \\ \epsilon_3 \end{bmatrix} = \begin{bmatrix} c_1^2 & s_1^2 & s_1 c_1 \\ c_2^2 & s_2^2 & s_2 c_2 \\ c_3^2 & s_3^2 & s_3 c_3 \end{bmatrix} \begin{bmatrix} e_{xx} \\ e_{yy} \\ 2e_{xy} \end{bmatrix} = \mathbf{T}_e^{-1}\mathbf{e}. \tag{15.32}$$

Here $c_1 = x_{32}/L_1$, $s_1 = y_{32}/L_1$, $c_2 = x_{13}/L_2$, $s_2 = y_{13}/L_2$, $c_3 = x_{21}/L_3$, and $s_3 = y_{21}/L_3$, are sines and cosines of the side directions with respect to $\{x, y\}$, as illustrated in Figure **?**(a,b). The inverse of this relation is

$$\mathbf{e} = \begin{bmatrix} e_{xx} \\ e_{yy} \\ 2e_{xy} \end{bmatrix} = \frac{1}{4A^2} \begin{bmatrix} y_{31}y_{21}L_1^2 & y_{12}y_{32}L_2^2 & y_{23}y_{13}L_3^2 \\ x_{31}x_{21}L_1^2 & x_{12}x_{32}L_2^2 & x_{23}x_{13}L_3^2 \\ (y_{31}x_{12}+x_{13}y_{21})L_1^2 & (y_{12}x_{23}+x_{21}y_{32})L_2^2 & (y_{23}x_{31}+x_{32}y_{13})L_3^2 \end{bmatrix} \begin{bmatrix} \epsilon_1 \\ \epsilon_2 \\ \epsilon_3 \end{bmatrix} = \mathbf{T}_e\boldsymbol{\epsilon}. \tag{15.33}$$

Note that $\mathbf{T}_e$ is constant over the triangle. From the invariance of the strain energy density $\boldsymbol{\sigma}^T\mathbf{e} = \boldsymbol{\tau}^T\boldsymbol{\epsilon}$ it follows that the stresses transform as $\boldsymbol{\tau} = \mathbf{T}_e\boldsymbol{\sigma}$ and $\boldsymbol{\sigma} = \mathbf{T}_e^{-1}\boldsymbol{\tau}$. That strain energy density may be expressed as

$$\mathcal{U} = \tfrac{1}{2}\mathbf{e}^T\mathbf{E}\mathbf{e} = \tfrac{1}{2}\boldsymbol{\epsilon}^T\mathbf{E}_n\boldsymbol{\epsilon}, \qquad \mathbf{E}_n = \mathbf{T}_e^T\mathbf{E}\mathbf{T}_e. \tag{15.34}$$

Here $\mathbf{E}_n$ is a stress-strain matrix that relates natural stresses to natural strains as $\boldsymbol{\tau} = \mathbf{E}_n\boldsymbol{\epsilon}$. It may be therefore called the natural constitutive matrix.

§15.4.2. *Covariant Node Displacements

Covariant node displacements d_i are directed along the side directions, as shown in Figure **?**(c), which defines

[4] This is the "straingage rosette" transformation studied in Mechanics of Materials books.

the notation used for them. They are related to the Cartesian node displacements by

$$\mathbf{d} = \begin{bmatrix} d_1 \\ d_2 \\ d_3 \\ d_4 \\ d_5 \\ d_6 \end{bmatrix} = \begin{bmatrix} c_3 & s_3 & 0 & 0 & 0 & 0 \\ c_2 & s_2 & 0 & 0 & 0 & 0 \\ 0 & 0 & c_1 & s_1 & 0 & 0 \\ 0 & 0 & c_3 & s_3 & 0 & 0 \\ 0 & 0 & 0 & 0 & c_2 & s_2 \\ 0 & 0 & 0 & 0 & c_1 & s_1 \end{bmatrix} \begin{bmatrix} u_{x1} \\ u_{y1} \\ u_{x2} \\ u_{y2} \\ u_{x3} \\ u_{y3} \end{bmatrix} = \mathbf{T}_d \mathbf{u}. \tag{15.35}$$

The inverse relation is

$$\mathbf{u} = \begin{bmatrix} u_{x1} \\ u_{y1} \\ u_{x2} \\ u_{y2} \\ u_{x3} \\ u_{y3} \end{bmatrix} = \frac{1}{2A} \begin{bmatrix} L_3 y_{31} & L_2 y_{21} & 0 & 0 & 0 & 0 \\ L_3 x_{13} & L_2 x_{12} & 0 & 0 & 0 & 0 \\ 0 & 0 & L_1 y_{12} & L_3 y_{32} & 0 & 0 \\ 0 & 0 & L_1 x_{21} & L_3 x_{23} & 0 & 0 \\ 0 & 0 & 0 & 0 & L_2 y_{23} & L_1 y_{13} \\ 0 & 0 & 0 & 0 & L_2 x_{32} & L_1 x_{31} \end{bmatrix} \begin{bmatrix} d_1 \\ d_2 \\ d_3 \\ d_4 \\ d_5 \\ d_6 \end{bmatrix} = \mathbf{T}_d^{-1} \mathbf{d}. \tag{15.36}$$

The natural strains are evidently given by the relations $\epsilon_1 = (d_6 - d_3)/L_1$, $\epsilon_2 = (d_2 - d_5)/L_2$ and $\epsilon_3 = (d_4 - d_1)/L_3$. Collecting these in matrix form:

$$\boldsymbol{\epsilon} = \begin{bmatrix} \epsilon_1 \\ \epsilon_2 \\ \epsilon_3 \end{bmatrix} = \begin{bmatrix} 0 & 0 & -1/L_1 & 0 & 0 & 1/L_1 \\ 0 & 1/L_2 & 0 & 0 & -1/L_2 & 0 \\ -1/L_3 & 0 & 0 & 1/L_3 & 0 & 0 \end{bmatrix} \begin{bmatrix} d_1 \\ d_2 \\ d_3 \\ d_4 \\ d_5 \\ d_6 \end{bmatrix} = \mathbf{B}_\epsilon \mathbf{d}. \tag{15.37}$$

§15.4.3. *The Natural Stiffness Matrix

The natural stiffness matrix for constant thickness h is

$$\mathbf{K}_n^e = (Ah)\, \mathbf{B}_\epsilon^T \mathbf{E}_n \mathbf{B}_\epsilon, \quad \mathbf{E}_n = \mathbf{T}_e^T\, \mathbf{E}\, \mathbf{T}_e. \tag{15.38}$$

The Cartesian stiffness matrix is

$$\mathbf{K}^e = \mathbf{T}_d^T\, \mathbf{K}_n\, \mathbf{T}_d. \tag{15.39}$$

Comparing with $\mathbf{K}^e = (Ah)\, \mathbf{B}^T\, \mathbf{E}\, \mathbf{B}$ we see that

$$\mathbf{B} = \mathbf{T}_e \mathbf{B}_\epsilon \mathbf{T}_d, \qquad \mathbf{B}_\epsilon = \mathbf{T}_e^{-1} \mathbf{B} \mathbf{T}_d^{-1}. \tag{15.40}$$

§15.5. *The Veubeke Equilibrium Triangle

The Veubeke equilibrium triangle[5] differs from the Turner triangle in the degree-of-freedom configuration. As illustrated in Figure 15.11, those are moved to the midpoints {4, 5, 6} while the corner nodes {1, 2, 3} still define the geometry of the element. In the FEM terminology introduced in Chapter 6, the geometric nodes {1, 2, 3} and the connection nodes {4, 5, 6} no longer coincide. The node displacement vector collects the freedoms shown in Figure 15.11(b):

$$\mathbf{u}^e = [\, u_{x4} \quad u_{y4} \quad u_{x5} \quad u_{y5} \quad u_{x6} \quad u_{y6} \,]^T. \tag{15.41}$$

The quickest way to formulate the stiffness matrix of this element is to relate 15.41 to the node displacements of the Turner triangle, renamed for convenience as

$$\mathbf{u}_T^e = [\, u_{x1} \quad u_{y1} \quad u_{x2} \quad u_{y2} \quad u_{x3} \quad u_{y3} \,]^T. \tag{15.42}$$

[5] The qualifier *equilibrium* distinguishes this element from others created by Fraeijs de Veubeke, including the 6-node plane stress comforming triangle. See **Notes and Bibliography** for the original derivation from an equilibrium field.

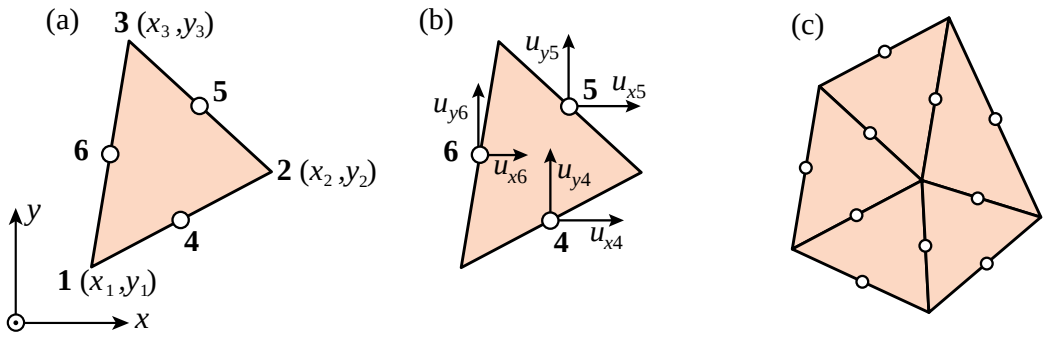

FIGURE 15.11. The Veubeke equilibrium triangle: (a) geometric definition; (b) degree-of-freedom configuration; (c) element patch showing how triangles are connected at the midpoints.

§15.5.1. *Kinematic Relations

The node freedom vectors 15.41 and 15.42 are easily related since by linear interpolation along the sides one obviously has $u_{x4} = \frac{1}{2}(u_{x1} + u_{x2})$, $u_{y4} = \frac{1}{2}(u_{y1} + u_{y2})$, etc. Expressing those links in matrix form gives

$$\begin{bmatrix} u_{x4} \\ u_{y4} \\ u_{x5} \\ u_{y5} \\ u_{x6} \\ u_{y6} \end{bmatrix} = \tfrac{1}{2}\begin{bmatrix} 1 & 0 & 1 & 0 & 0 & 0 \\ 0 & 1 & 0 & 1 & 0 & 0 \\ 0 & 0 & 1 & 0 & 1 & 0 \\ 0 & 0 & 0 & 1 & 0 & 1 \\ 1 & 0 & 0 & 0 & 1 & 0 \\ 0 & 1 & 0 & 0 & 0 & 1 \end{bmatrix}\begin{bmatrix} u_{x1} \\ u_{y1} \\ u_{x2} \\ u_{y2} \\ u_{x3} \\ u_{y3} \end{bmatrix}, \qquad \begin{bmatrix} u_{x1} \\ u_{y1} \\ u_{x2} \\ u_{y2} \\ u_{x3} \\ u_{y3} \end{bmatrix} = \begin{bmatrix} 1 & 0 & -1 & 0 & 1 & 0 \\ 0 & 1 & 0 & -1 & 0 & 1 \\ 1 & 0 & 1 & 0 & -1 & 0 \\ 0 & 1 & 0 & 1 & 0 & -1 \\ -1 & 0 & 1 & 0 & 1 & 0 \\ 0 & -1 & 0 & 1 & 0 & 1 \end{bmatrix}\begin{bmatrix} u_{x4} \\ u_{y4} \\ u_{x5} \\ u_{y5} \\ u_{x6} \\ u_{y6} \end{bmatrix}. \tag{15.43}$$

In compact form: $\mathbf{u}^e = \mathbf{T}_{VT}\,\mathbf{u}^e_T$ and $\mathbf{u}^e_T = \mathbf{T}_{TV}\,\mathbf{u}^e$, with $\mathbf{T}_{VT} = \mathbf{T}^{-1}_{TV}$. The shape functions are

$$N_4 = \zeta_1 + \zeta_2 - \zeta_3, \quad N_5 = -\zeta_1 + \zeta_2 + \zeta_3, \quad N_6 = \zeta_1 - \zeta_2 + \zeta_3. \tag{15.44}$$

Renaming the Turner triangle strain-displacement matrix of (15.17) as $\mathbf{B}_T$, the corresponding matrix that relates $\mathbf{e} = \mathbf{B}\,\mathbf{u}^e$ in the Veubeke equilibrium triangle becomes

$$\mathbf{B} = \mathbf{B}_T\,\mathbf{T}_{TV} = \frac{1}{A}\begin{bmatrix} y_{21} & 0 & y_{32} & 0 & y_{13} & 0 \\ 0 & x_{12} & 0 & x_{23} & 0 & x_{31} \\ x_{12} & y_{21} & x_{23} & y_{32} & x_{31} & y_{13} \end{bmatrix} \tag{15.45}$$

§15.5.2. *Stiffness Matrix

The element stiffness matrix is given by the general formula (14.23). For constant plate thickness h one obtains the closed form

$$\mathbf{K}^e = A\,h\,\mathbf{B}^T\,\mathbf{E}\,\mathbf{B} = \frac{h}{A}\begin{bmatrix} y_{21} & 0 & x_{12} \\ 0 & x_{12} & y_{21} \\ y_{32} & 0 & x_{23} \\ 0 & x_{23} & y_{32} \\ y_{13} & 0 & x_{31} \\ 0 & x_{31} & y_{13} \end{bmatrix}\begin{bmatrix} E_{11} & E_{12} & E_{13} \\ E_{12} & E_{22} & E_{23} \\ E_{13} & E_{23} & E_{33} \end{bmatrix}\begin{bmatrix} y_{21} & 0 & y_{32} & 0 & y_{13} & 0 \\ 0 & x_{12} & 0 & x_{23} & 0 & x_{31} \\ x_{12} & y_{21} & x_{23} & y_{32} & x_{31} & y_{13} \end{bmatrix}. \tag{15.46}$$

The computation of consistent body forces is left as an Exercise.

```
Trig3VeubekeMembraneStiffness[ncoor_,Emat_,h_,numer_]:=Module[{
  x1,x2,x3,y1,y2,y3,x12,x23,x31,y21,y32,y13,A,Be,Te,Ke},
  {{x1,y1},{x2,y2},{x3,y3}}=ncoor;
  A=Simplify[(x2*y3-x3*y2+(x3*y1-x1*y3)+(x1*y2-x2*y1))/2];
  {x12,x23,x31,y21,y32,y13}={x1-x2,x2-x3,x3-x1,y2-y1,y3-y2,y1-y3};
  Be={{y21,0,y32,0,y13,0}, {0,x12,0,x23,0,x31},
      {x12,y21,x23,y32,x31,y13}}/A;
  If [numer,Be=N[Be]]; Ke=A*h*Transpose[Be].Emat.Be;
  Return[Ke]];
```

FIGURE 15.12. Implementation of Veubeke equilibrium triangle stiffness matrix as a *Mathematica* module.

§15.5.3. *Implementation

The implementation of the Veubeke equilibrium triangle as a *Mathematica* module that returns $\mathbf{K}^e$ is shown in Figure 15.12. It needs only 8 lines of code. It is invoked as

```
Ke=Trig3VeubekeMembraneStiffness[ncoor,Emat,h,numer];
```
(15.47)

The arguments have the same meaning as those of the module `Trig3TurnerMembraneStiffness` described in §15.3.6.

```
ncoor={{0,0},{3,1},{2,2}}; Emat=8*{{8,2,0},{2,8,0},{0,0,3}};
Ke=Trig3VeubekeMembraneStiffness[ncoor,Emat,1,False];
Print["Ke=",Ke//MatrixForm];
Print["eigs of Ke=",Chop[Eigenvalues[N[Ke]]]];
```

$$\texttt{Ke=}\begin{pmatrix} 140 & -60 & -4 & -28 & -136 & 88 \\ -60 & 300 & -12 & -84 & 72 & -216 \\ -4 & -12 & 44 & 20 & -40 & -8 \\ -28 & -84 & 20 & 44 & 8 & 40 \\ -136 & 72 & -40 & 8 & 176 & -80 \\ 88 & -216 & -8 & 40 & -80 & 176 \end{pmatrix}$$

```
eigs of Ke={557.318, 240., 82.6816, 0, 0, 0}
```

FIGURE 15.13. Test statements to exercise the module of Figure 15.12, and outputs.

This module is exercised by the statements listed at the top of Figure 15.13, which form a triangle with corner coordinates `{{0,0},{3,1},{2,2}}`, isotropic material matrix with $E_{11} = E_{22} = 64$, $E_{12} = 16$, $E_{33} = 24$, others zero, and unit thickness. The results are shown at the bottom of Figure 15.13. This is the same triangle used to test module `Trig3TurnerMembraneStiffness` in §15.3.6. Note that the element is rank sufficient.

§15.5.4. *Spurious Kinematic Modes

Although an individual Veubeke equilibrium triangle is rank sufficient, assemblies are prone to the appearance of spurious mechanisms. That is, kinematic modes that produce no strain energy although they are not rigid body modes. These will be illustrated by studying the three macroelements pictured in Figure 15.14. For simplicity the macroelements are of rectangular shape, but the conclusions apply to more general geometries.

Type I macroelement is built with two triangles. It has four geometric nodes: 1–4, five connection nodes: 5–9, and 10 degrees of freedom. The eigenvalue analysis of the assembled stiffness **K** is given as an Exercise. It shows that **K** has 4 zero eigenvalues. Since there are 3 rigid body modes in 2D, one is spurious. It is easily

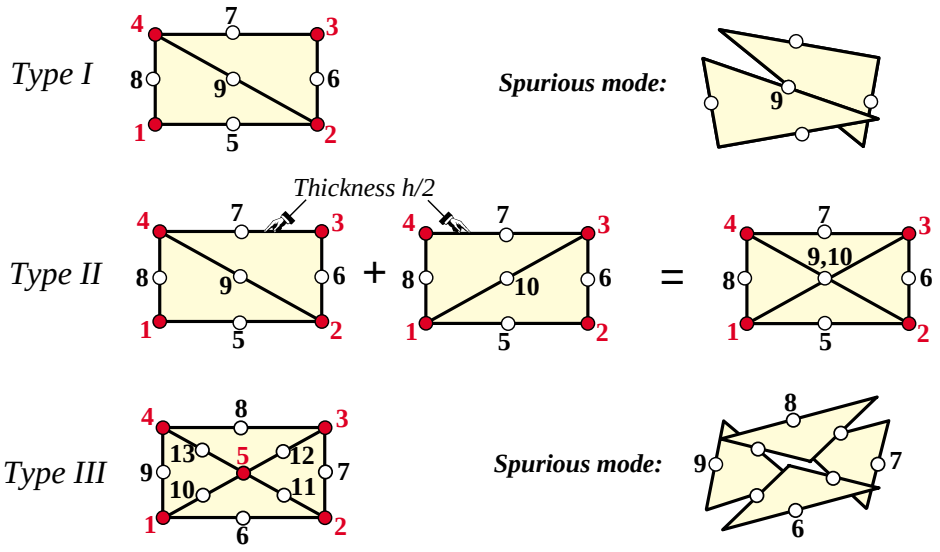

FIGURE 15.14. Three macroelement assemblies fabricated with Veubeke equilibrium triangles to investigate spurious kinematic modes. Red-filled and white-filled circles mark geometric and connection nodes, respectively.

shown that the spurious mode corresponds to the relative rotation of the two triangles with center node 9 as pivot, as pictured to the right of the macroelement.

Type II macroelement is built with four crisscrossed triangles of thickness $h/2$ as illustrated in the Figure. It has four geometric nodes: 1–4, six connection nodes: 5–10, and 12 degrees of freedom. (Note that although 9 and 10 occupy the same location for this geometry, they should be considered as two separate nodes.) The eigenvalue analysis of the assembled stiffness **K** is given as an Exercise. It shows that **K** has 3 zero eigenvalues and therefore this macroelement has no spurious modes.

Type III macroelement is of Union-Jack type and is built with 4 triangles. It has five geometric nodes: 1–5, eight connection nodes: 6–13, and 16 degrees of freedom. The eigenvalue analysis of the assembled stiffness **K** is given as an Exercise. It shows that **K** has 4 zero eigenvalues and consequently one spurious mode. This correspond to the triangles rotating about the midpoints 6–9 as pivots, as pictured to the right of the macroelement.

These examples show that this element, when used in a stiffness code, is prone to *spurious pivot modes* where sides of adjacent triangles rotate relatively from each other about the midpoint connector. This is a consequence of the element being nonconforming: full determination of linearly varying side displacements requires two nodes over that side, and there is only one. Even if a rank sufficiently macroelement mesh unit such as Type II of Figure 15.14 can be constructed, there is no guarantee that spurious pivot modes will not occur when those mesh units are connected. For this reason this element is rarely used in DSM-based structural programs, but acquires importance in applications where flux conservation is important.

§15.6. *Shear Locking in Turner Triangles

A well known deficiency of the 3-node Turner triangle is inability to follow rapidly varying stress fields. This is understandable since stresses within the element, for uniform material properties, are constant. But its 1D counterpart: the 2-node bar element, is nodally exact for displacements under some mild assumptions stated in Chapter 11, and correctly solves loaded-at-joints trusses with one element per member. On the other hand, the triangle can be *arbitrarily way off* under unhappy combinations of loads, geometry and meshing.

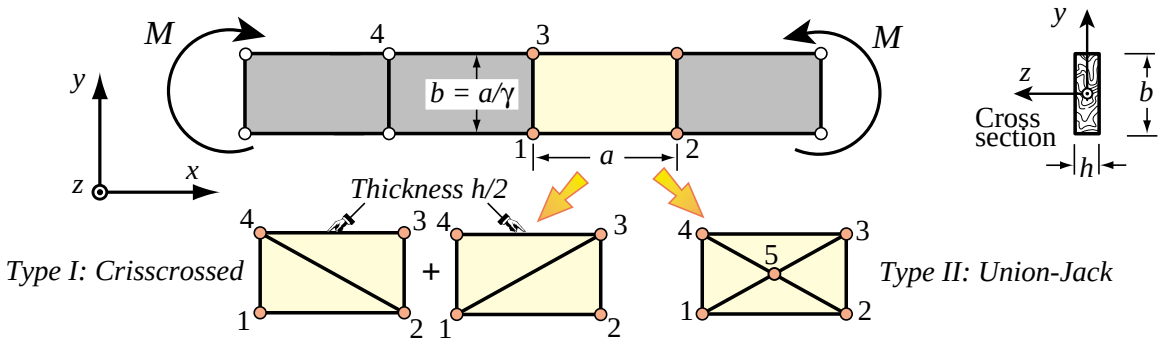

FIGURE 15.15. The bending test with two macroelement types.

What happens in going from 1D to 2D? New effects emerge, notably shear energy and inplane bending. These two can combine to produce *shear locking*: elongated triangles can become extraordinarily stiff under inplane bending because of *spurious shear energy*.[6] The bad news for engineers is that wrong answers caused by locking are *non-conservative*: deflections and stresses can be so grossly underestimated that safety margins are overwhelmed.

To characterize shear locking quantitatively it is convenient to use macroelements in which triangles are combined to form a 4-node rectangle. This simplifies repetition to form regular meshes. The rectangle response under in-plane bending is compared to that of a Bernoulli-Euler beam segment. It is well known that the latter is exact under constant moment. The response ratio of macroelement to beam is a good measure of triangle performance under bending. Such benchmarks are technically called *higher order patch tests*. Test results can be summarized by one number: the *energy ratio*, which gives a scalar measure of relative stiffness.

§15.6.1. *The Inplane Bending Test

The test is defined in Figure 15.15. A Bernoulli-Euler plane beam of thin rectangular cross-section of height b and thickness h is bent under applied end moments M. The beam is fabricated of isotropic material with elastic modulus E and Poisson's ratio ν. Except for possible end effects the exact solution of the beam problem (from both the theory-of-elasticity and beam-theory standpoints) is a constant bending moment $M(x) = M$ along the span. The associated curvature is $\kappa = M/(EI_{zz}) = 12M/(Eb^3h)$. The exact energy taken by a beam segment of length a is $U_{\text{beam}} = \frac{1}{2}M\kappa a = 6M^2\,a/(Eb^3h) = \frac{1}{24}Eb^3h\kappa^2 a = \frac{1}{24}Eb^3h\theta_a^2/a$. In the latter $\theta_a = \kappa a$ is the relative rotation of two cross sections separated by a.

To study the bending performance of triangles the beam is modeled with one layer of identical rectangular macroelements dimensioned $a \times b$ and made up of triangles, as illustrated in Figure 15.15. The rectangle aspect ratio is $\gamma = a/b$. All rectangles undergo the same deformations and thus it is enough to study a individual macroelement 1-2-3-4. Two types are considered here:

Crisscrossed (CC). Formed by overlaying triangles 1-2-4, 3-4-2, 2-3-1 and 4-1-2, each with thickness $h/2$. Using 4 triangles instead of 2 makes the macroelement geometrically and physically symmetric since 2 triangles are attached to each corner.

Union-Jack (UJ). Formed by placing a fifth node at the center and dividing the rectangle into 4 triangles: 1-2-5, 2-3-5, 3-4-5, 4-1-5. By construction this element is also geometrically and physically symmetric.

[6] The deterioration can be even more pronounced for its spatial counterpart: the 4-node tetrahedron element, because shear effects are even more important in three dimensions.

§15.6.2. *Energy Ratios

The assembled macroelement stiffnesses are $\mathbf{K}_{CC}$ and $\mathbf{K}^{+}_{UJ}$, of orders 8×8 and 10×10, respectively. For the latter the internal node 5 is statically condensed producing an 8×8 stiffness $\mathbf{K}_U$. To test performance we apply four alternating corner loads as shown in Figure 15.16. The resultant bending moment is $M = Pb$.

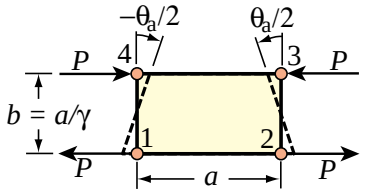

FIGURE 15.16. Bending a macroelement by applying a relative edge rotation.

Although triangles cannot copy curvatures pointwise,[7] macroelement edges can rotate since constituent triangles can expand or contract. Because of symmetries, the rotations of sides 1-2 and 3-4 are $-\theta_a/2$ and $\theta_a/2$, as illustrated in Figure 15.16. The corresponding corner x displacements are $\pm b\theta_a/4$ whereas the y displacements are zero. Assemble these into a node displacement 8-vector $\mathbf{u}_M$.

$$\mathbf{u}_M = \tfrac{1}{4} b\theta_a \, [\, -1 \quad 0 \quad 1 \quad 0 \quad -1 \quad 0 \quad 1 \quad 0 \,]^T \tag{15.48}$$

The internal energy taken by a macroelement of 8×8 stiffness $\mathbf{K}_M$ under (15.48) is $U_M = \frac{1}{2}\mathbf{u}_M^T \mathbf{K}_M \mathbf{u}_M$, which can be expressed as a function of E, ν, a, b, h and θ_a.[8]

```
ClearAll[a,b,Em,h,γ];
b=a/γ; Iz=h*b^3/12; Ubeam=Simplify[(1/2)*Em*Iz*θa^2/a];
Emat=Em*{{1,0,0},{0,1,0},{0,0,1/2}};
nc={{-a,-b},{a,-b},{a,b},{-a,b},{0,0}}/2;
enCC={{1,2,4},{3,4,2},{2,3,1},{4,1,3}};
enUJ={{1,2,5},{2,3,5},{3,4,5},{4,1,5}}; r={0,0};
For [m=1,m<=2,m++, mtype={"CC","UJ"}[[m]];
    nF={8,10}[[m]]; K=Table[0,{nF},{nF}]; f=Table[0,{nF}];
    For [e=1,e<=4,e++,
        If [mtype=="CC", enl=enCC[[e]], enl=enUJ[[e]]];
        {n1,n2,n3}=enl; encoor={nc[[n1]],nc[[n2]],nc[[n3]]};
        ht=h; If [mtype=="CC", ht=h/2];
        Ke=Trig3TurnerMembraneStiffness[encoor,Emat,ht,False];
        eft={2*n1-1,2*n1,2*n2-1,2*n2,2*n3-1,2*n3};
        For [i=1,i<=6,i++, For [j=1,j<=6,j++, ii=eft[[i]];
             jj=eft[[j]]; K[[ii,jj]]+=Ke[[i,j]] ]];
        ]; KM=K=Simplify[K];
        If [mtype=="UJ",
           {K,f}= Simplify[CondenseLastFreedom[K,f]];
           {KM,f}=Simplify[CondenseLastFreedom[K,f]]];
    Print["KM=",KM//MatrixForm];
    uM={1,0,-1,0,1,0,-1,0}*θa*b/4;
    UM=uM.KM.uM/2; rM=Simplify[UM/Ubeam];
    Print["rM=",rM]; r[[m]]=rM;
 ];
 Plot[Evaluate[r],{γ,0,10}];
```

FIGURE 15.17. Script to compute energy ratios for the two macroelements of Figure 15.15.

The ratio $r_M = U_M/U_{beam}$ is called the *energy ratio*. If $r_M > 1$ the macroelement is stiffer than the beam because it take more energy to bend it to conform to the same edge rotations, and the 2D model is said to be *overstiff*. Results for zero Poisson's ratio, computed with the script of Figure 15.17, are

$$r_{CC} = 3 + \frac{3}{2}\gamma^2, \quad r_{UJ} = \frac{3(1+\gamma^2)^2}{2+4\gamma^2}. \tag{15.49}$$

[7] That is the reason why they can be so stiff under bending.

[8] The load P could be recovered via $\mathbf{K}_M\mathbf{u}_M$, but this value is not needed to compute energy ratios.

If for example $\gamma = a/b = 10$, which is an elongated rectangular shape of 10:1 aspect ratio, $r_{CC} = 153$ and the crisscrossed macroelement is 153 times stiffer than the beam. For the Union-Jack configuration $r_{UJ} = 10201/134 = 76.13$; about twice better but still way overstiff. If $\gamma = 1$, $r_{CC} = 4.5$ and $r_{UJ} = 2$: overstiff but not dramatically so. The effect of a nonzero Poisson's ratio is studied in Exercise 15.10.

§15.6.3. *Convergence as Mesh is Refined

Note that if $\gamma = a/b \to 0$, $r_{CC} \to 3$ and $r_{UJ} \to 1.5$. So even if the beam of Figure 15.15 is divided into an infinite number of macroelements along x the solution will not converge. It is necessary to subdivide also along the height. If $2n$ ($n \geq 1$) identical macroelement layers are placed along the beam height while γ is kept fixed, the energy ratio becomes

$$r^{(2n)} = \frac{2^{2n} - 1 + r^{(1)}}{2^{2n}} = 1 + \frac{r^{(1)} - 1}{2^{2n}}, \tag{15.50}$$

where $r^{(1)}$ is the ratio (15.49) for one layer. If $r^{(1)} = 1$, $r^{(2n)} = 1$ for all $n \geq 1$, so bending exactness is maintained as expected. If $n = 1$ (two layers), $r^{(2)} = (3+r^{(1)})/4$ and if $n = 2$ (four layers), $r^{(4)} = (7+r^{(1)})/8$.

If $n \to \infty$, $r^{(2n)} \to 1$, but convergence can be slow. For example, suppose that $\gamma = 1$ (unit aspect ratio $a = b$) and that $r^{(1)} = r_{CC} = 4.5$. To get within 1% of the exact solution, $1 + 3.5/2^{2n} < 1.01$. This is satisfed if $n \geq 5$, meaning 10 layers of elements along y. If the beam span is 10 times the height, 1000 macroelements or 4000 triangles are needed for this simple problem, which is exactly solvable by one beam element.

The stress accuracy of triangles is examined in Chapter 28.

Notes and Bibliography

As a plane stress structural element, the Turner triangle was first developed in the 1956 paper by Turner et. al. [786]. The target application was modeling of delta wing skin panels. Arbitrary quadrilaterals were formed by assembling triangles as macroelements. Because of its geometric flexibility, the element was soon adopted in aircraft structural analysis codes in the late 1950's. It moved to Civil Engineering applications through the research and teaching at Berkeley of Ray Clough, who gave the method its name in [138].

The derivation method of [786] would look unfamiliar to present FEM practicioners used to the displacement method. It was based on assumed stress modes. More precisely: the element, referred to a local Cartesian system $\{x, y\}$, is put under three constant stress states: σ_{xx}, σ_{yy} and σ_{xy}, collected in array $\boldsymbol{\sigma}$. Lumping the stress field to the nodes gives the node forces: $\mathbf{f} = \mathbf{L}\boldsymbol{\sigma}$. The strain field computed from stresses is $\mathbf{e} = \mathbf{E}^{-1}\boldsymbol{\sigma}$. This is integrated to get a deformation-displacement field, to which 3 rigid-body modes are added as integration constants. Evaluating at the nodes produces $\mathbf{e} = \mathbf{A}\mathbf{u}$, and the stiffness matrix follows on eliminating $\boldsymbol{\sigma}$ and $\mathbf{e}$: $\mathbf{K} = \mathbf{L}\mathbf{E}\mathbf{A}$. For constant thickness and material properties it happens that $\mathbf{L} = V\mathbf{A}^T$ and so $\mathbf{K} = V\mathbf{A}^T\mathbf{E}\mathbf{A}$ happily turned out to be symmetric. This $\mathbf{A}$ is the $\mathbf{B}$ of (15.17) times $2A$, so in the end the stiffness matrix (for constant plate thickness) turns out to be the same as (15.21).

The derivation from assumed displacements evolved later. It is not clear who worked it out first, although it is mentioned in [138,830]. The equivalence of the two forms, through energy principles, had been noted by Gallagher [297]. Early displacement derivations typically started from linear polynomials in Cartesian coordinates. For example Przemieniecki [619] begins with

$$u_x = c_1 x + c_2 y + c_3, \quad u_y = c_4 x + c_5 y + c_6. \tag{15.51}$$

Here the c_i play the role of generalized coordinates, which have to be eventually eliminated in favor of node displacements. The same approach is used by Clough in a widely disseminated 1965 article [140]. Even for this simple element the approach is unnecessarily complicated and leads to long hand computations. The elegant derivation in triangular coordinates was popularized by Argyris [28].

The idea of using piecewise linear interpolation over a triangular mesh actually precedes [786] by 13 years. As noted in Chapter 1, it appears in an article by Courant [156], where it is applied to a Poisson's equation modeling St. Venant's torsion. The idea did not influence early work in FEM, however, since as noted above the derivation in [786] was not based on displacement interpolation.

The Veubeke equilibrium triangle appears in [283, p. 170] and is further elaborated in [284, p. 176]. It is constructed there as an *equilibrium element*, that is, the stress field inside the triangle is assumed to be $\sigma_{xx} = \beta_1$, $\sigma_{yy} = \beta_2$ and $\sigma_{xy} = \beta_3$, where $\{\beta_1, \beta_2, \beta_3\}$ are stress parameters. (A field of constant stresses satisfies identically the plane-stress differential equilibrium equations for zero body forces.) Stress parameters can be uniquely expressed in terms of generalized edge loads, which turn out to be virtual-work conjugate to midside displacements.[9] The direct displacement derivation given here as a "Turner triangle mapping" is new. As previously noted, this element is rarely used in structural mechanics because of the danger of spurious kinematic modes discussed in §15.5.4. It has importance, however, in some non-structural applications.

The completeness check worked out in §15.4.2 is a specialization case of a general proof developed by Irons in the mid 1960s (see [411, §3.9] and references therein) for general isoparametric elements. The check works because the Turner triangle *is* isoparametric.

What are here called triangular coordinates were introduced by Möbius in his 1827 book [512].[10] They are often called barycentric coordinates on account on the interpretation discussed in [158]. Other names are listed in Table 15.1. Triangles possess many fascinating geometric properties studied even before Euclid. An exhaustive development can be found, in the form of solved exercises, in [711].

It is unclear when the monomial integration formula (15.26) was first derived. As an expression for integrands expressed in triangular coordinates it was first stated in [211].

The natural strain derivation of §15.4 is patterned after that developed for the so-called ANDES (Assumed Natural Deviatoric Strain) elements [509]. For the Turner triangle it provides nothing new aside of fancy terminology. Energy ratios of the form used in §15.6 were introduced in [89] as a way to tune up the stiffness of Free-Formulation elements.

References

Referenced items have been moved to Appendix R.

[9] The initial step of assuming stresses exactly mimics that of [786] a decade earlier. What is fundamentally different in Fraeijs de Veubeke's derivation is the use of energy theorems (in this case, PVW) to pass from generalized edge loads to mean edge displacements. The approach is characteristic of FEM Generation 2.

[10] He is better remembered for the "Möbius strip" or "Möbius band," the first one-sided 3D surface in mathematics.

Homework Exercises for Chapter 15
The Linear Plane Stress Triangle

EXERCISE 15.1 [A:15] Assume that the 3-node plane stress triangle has *variable* thickness defined over the element by the linear interpolation formula

$$h(\zeta_1, \zeta_2, \zeta_3) = h_1\zeta_1 + h_2\zeta_2 + h_3\zeta_3, \tag{E15.1}$$

where h_1, h_2 and h_3 are the thicknesses at the corner nodes. Show that the element stiffness matrix is still given by (15.21) but with h replaced by the mean thickness $h_m = (h_1 + h_2 + h_3)/3$. *Hint*: use (15.20) and (15.26).

EXERCISE 15.2 [A:20] The exact integrals of triangle-coordinate monomials over a straight-sided triangle are given by the formula (15.26), where A denotes the area of the triangle, and i, j and k are nonnegative integers. Tabulate the right-hand side for combinations of exponents i, j and k such that $i + j + k \le 3$, beginning with $i = j = k = 0$. Remember that $0! = 1$. (*Labor-saving hint*: don't bother repeating exponent permutations; for example $i = 2$, $j = 1$, $k = 0$ and $i = 1$, $j = 2$, $k = 0$ are permutations of the same thing. Hence one needs to tabulate only cases in which $i \ge j \ge k$).

EXERCISE 15.3 [A/C:20] Compute the consistent node force vector $\mathbf{f}^e$ for body loads over a Turner triangle, if the element thickness varies as per (E15.1), $b_x = 0$, and $b_y = b_{y1}\zeta_1 + b_{y2}\zeta_2 + b_{y3}\zeta_3$. Check that for $h_1 = h_2 = h_3 = h$ and $b_{y1} = b_{y2} = b_{y3} = b_y$ you recover (15.25). For area integrals use (15.26). Partial result: $f_{y1} = (A/60)[b_{y1}(6h_1 + 2h_2 + 2h_3) + b_{y2}(2h_1 + 2h_2 + h_3) + b_{y3}(2h_1 + h_2 + 2h_3)]$.

EXERCISE 15.4 [A/C:20] Derive the formula for the consistent force vector $\mathbf{f}^e$ of a Turner triangle of constant thickness $h = 1$, if side 1–2 ($\zeta_3 = 0$, $\zeta_2 = 1 - \zeta_1$), is subject to a linearly varying boundary force $\mathbf{q} = h\hat{\mathbf{t}}$ such that

$$\begin{aligned} q_x &= q_{x1}\zeta_1 + q_{x2}\zeta_2 = q_{x1}(1 - \zeta_2) + q_{x2}\zeta_2, \\ q_y &= q_{y1}\zeta_1 + q_{y2}\zeta_2 = q_{y1}(1 - \zeta_2) + q_{y2}\zeta_2. \end{aligned} \tag{E15.2}$$

This " line boundary force" $\mathbf{q}$ has dimension of force per unit of side length.

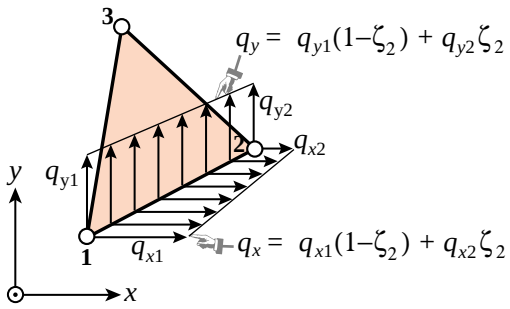

FIGURE E15.1. Line force on triangle side 1–2 for Exercise 15.4.

Procedural Hint. Use the last term of the line integral (14.21), in which $\hat{\mathbf{t}}$ is replaced by $\mathbf{q}/h$, and show that since the contribution of sides 2-3 and 3-1 to the line integral vanish,

$$W^e = (\mathbf{u}^e)^T\,\mathbf{f}^e = \int_{\Gamma^e} \mathbf{u}^T\mathbf{q}\; d\Gamma^e = \int_0^1 \mathbf{u}^T\mathbf{q}\, L_{21}\, d\zeta_2, \tag{E15.3}$$

where L_{21} is the length of side 1–2. Replace $u_x(\zeta_2) = u_{x1}(1-\zeta_2) + u_{x2}\zeta_2$; likewise for u_y, q_x and q_y, integrate and identify with the inner product shown as the second term in (E15.3). Partial result: $f_{x1} = L_{21}(2q_{x1} + q_{x2})/6$, $f_{x3} = f_{y3} = 0$.

Note. The following *Mathematica* script solves this Exercise. If you decide to use it, explain the logic.

```
ClearAll[ux1,uy1,ux2,uy2,ux3,uy3,z2,L12];
ux=ux1*(1-z2)+ux2*z2; uy=uy1*(1-z2)+uy2*z2;
qx=qx1*(1-z2)+qx2*z2; qy=qy1*(1-z2)+qy2*z2;
We=Simplify[L12*Integrate[qx*ux+qy*uy,{z2,0,1}]];
fe=Table[Coefficient[We,{ux1,uy1,ux2,uy2,ux3,uy3}[[i]]],{i,1,6}];
fe=Simplify[fe]; Print["fe=",fe];
```

EXERCISE 15.5 [C+N:15] Compute the entries of $\mathbf{K}^e$ for the following plane stress triangle:

$$x_1 = 0,\ y_1 = 0,\ x_2 = 3,\ y_2 = 1,\ x_3 = 2,\ y_3 = 2,$$
$$\mathbf{E} = \begin{bmatrix} 100 & 25 & 0 \\ 25 & 100 & 0 \\ 0 & 0 & 50 \end{bmatrix}, \qquad h = 1. \tag{E15.4}$$

This may be done by hand (it is a good exercise in matrix multiplication) or (more quickly) using the script of Figure 15.5. Partial result: $K_{11} = 18.75$, $K_{66} = 118.75$.

EXERCISE 15.6 [A+C:15] Show that the sum of the rows (and columns) 1, 3 and 5 of $\mathbf{K}^e$ as well as the sum of rows (and columns) 2, 4 and 6 must vanish, and explain why. Check it with the foregoing script.

EXERCISE 15.7 [A:10]. Consider two triangles T and T^*, both with positive area. The corner coordinates of $T1$ are $\{\{x_1, y_1\}, \{x_2, y_2\}, \{x_3, y_3\}\}$ and those of $T2$ are $\{\{x_1^*, y_1^*\}, \{x_2^*, y_2^*\}, \{x_3^*, y_3^*\}\}$. A point P in T has Cartesian coordinates $\{x, y\}$ and triangular coordinates $\{\zeta_1, \zeta_2, \zeta_3\}$. A point P^* in T^* has Cartesian coordinates $\{x^*, y^*\}$ and the same triangular coordinates. Show that $\{x^*, y^*\}$ and $\{x, y\}$ are connected by the affine transformation

$$\begin{bmatrix} 1 \\ x^* \\ y^* \end{bmatrix} = \begin{bmatrix} 1 & 1 & 1 \\ x_1^* & x_2^* & x_3^* \\ y_1^* & y_2^* & y_3^* \end{bmatrix} \begin{bmatrix} 1 & 1 & 1 \\ x_1 & x_2 & x_3 \\ y_1 & y_2 & y_3 \end{bmatrix}^{-1} \begin{bmatrix} 1 \\ x \\ y \end{bmatrix} \tag{E15.5}$$

(The indicated inverse exists if T has positive area, as assumed.)

EXERCISE 15.8 [A:15]. Let point P have triangular coordinates $\{\zeta_1^P, \zeta_2^P, \zeta_3^P\}$, as shown in Figure E15.2. Find the distances h_{P1}, h_{P2} and h_{P3} of P to the three triangle sides, and the triangular coordinates of points P_1, P_2 and P_3 shown in the Figure (P_i is projection on the side opposite to corner i.) Show that $h_{Pi} = \zeta_{Pi}\, h_i = 2\zeta_{Pi}\, A/L_{kj}$, for $i = 1, 2, 3$, $j = 2, 3, 1$ and $k = 3, 1, 2$, in which L_{ji} denotes the length of the side that joins corners i and j and h_i is the distance from corner i to the opposite side, as illustrated in Figure E15.2. (Note: the distances $\{h_{P1}, h_{P2}, h_{P3}\}$ are called the *trilinear coordinates* of a point P with respect to the vertices of the triangle. They were introduced by Plücker in 1835. They are essentially scaled versions of the triangular coordinates.)

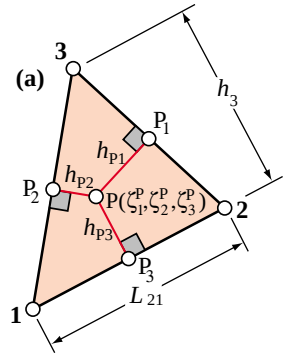

FIGURE E15.2. Distances of arbitrary point P to three triangle sides.

EXERCISE 15.9 [A:10]. Express the distances from the triangle centroid to the 3 sides in term of the triangle area and the side lengths. Answer: $\frac{2}{3}A/L_{21}$, $\frac{2}{3}A/L_{32}$ and $\frac{2}{3}A/L_{13}$, where A is the area of the triangle assumed positive and L_{ji} is the length of side that joins corners i and j, cf. Figure E15.2, Hint: the area of each subtriangle subtended by the centroid and two corners is $\frac{1}{3}A$.

EXERCISE 15.10 [A:20] Find the triangular coordinates of the altitude feet points H_1, H_2 and H_3 pictured in Figure 15.3. Once these are obtained, find the equations of the altitudes in triangular coordinates, and the coordinates of the orthocenter H. Answer for H_3: $\zeta_1 = \frac{1}{2} + (L_{13}^2 - L_{32}^2)/(2L_{21}^2)$, where L_{ji} is the length of side that joins corners i and j; cf. Figure E15.2.

EXERCISE 15.11 [C+D:20] Let $p(\zeta_1, \zeta_2, \zeta_3)$ represent a *polynomial* expression in the natural coordinates. The integral

$$\int_{\Omega^e} p(\zeta_1, \zeta_2, \zeta_3)\, d\Omega \tag{E15.6}$$

over a straight-sided triangle can be computed symbolically by the following *Mathematica* module:

```
IntegrateOverTriangle[expr_,tcoord_,A_,max_]:=Module [{p,i,j,k,z1,z2,z3,c,s=0},
   p=Expand[expr];  {z1,z2,z3}=tcoord;
   For [i=0,i<=max,i++, For [j=0,j<=max,j++, For [k=0,k<=max,k++,
      c=Coefficient[Coefficient[Coefficient[p,z1,i],z2,j],z3,k];
      s+=2*c*(i!*j!*k!)/((i+j+k+2)!);
      ]]];
   Return[Simplify[A*s]] ];
```

This is referenced as `int=IntegrateOverTriangle[p,{z1,z2,z3},A,max]`. Here `p` is the polynomial to be integrated, `z1`, `z2` and `z3` denote the symbols used for the triangular coordinates, `A` is the triangle area and `max` the highest exponent appearing in a triangular coordinate. The module name returns the integral. For example, if `p=16+5*b*z2^2+z1^3+z2*z3*(z2+z3)` the call `int=IntegrateOverTriangle[p,{z1,z2,z3},A,3]` returns `int=A*(97+5*b)/6`. Explain how the module works.

EXERCISE 15.12 [C+D:25] Explain the logic of the script listed in Figure 15.17. Then extend it to account for isotropic material with arbitrary Poisson's ratio ν. Obtain the macroelement energy ratios as functions of γ and ν. Discuss whether the effect of a nonzero ν makes much of a difference if $\gamma >> 1$.

EXERCISE 15.13 [A/C:25] Verify the conclusions of §15.5.4 as regards rank sufficiency or deficiency of the three Veubeke macroelement assemblies pictured in Figure 15.14. Carry out tests with rectangular macroelements dimensioned $a \times b$, constant thickness h, elastic modulus E and Poisson's ratio 0.

EXERCISE 15.14 [C+D:25] To find whether shear is the guilty party in the poor performance of elongated triangles (as alledged in §15.6) run the script of Figure 15.17 with a zero shear modulus. This can be done by setting `Emat=Em*{{1,0,0},{0,1,0},{0,0,0}}` in the third line. Discuss the result. Can `Em` be subsequently reduced to a smaller (fictitious) value so that $r \equiv 1$ for all aspect ratios γ? Is this practical?

```
HomogenizedLinTrigCoorFunction[expr_,{ζ1_,ζ2_,ζ3_}]:=Module[
  {f=expr,repζ0,C0}, repζ0={ζ1->0,ζ2->0,ζ3->0};
   C0=Simplify[f/.repζ0]; f=Simplify[f-C0(1-ζ1-ζ2-ζ3)];
   Return[f]];

HomogenizedQuadTrigCoorFunction[expr_,{ζ1_,ζ2_,ζ3_}]:=Module[
  {f,repζ0,C0,C1,C2,C3}, repζ0={ζ1->0,ζ2->0,ζ3->0};
   f=HomogenizedLinTrigCoorFunction[expr,{ζ1,ζ2,ζ3}];
   C1=Coefficient[f,ζ1]/.repζ0; C2=Coefficient[f,ζ2]/.repζ0;
   C3=Coefficient[f,ζ3]/.repζ0; {C1,C2,C3}=Simplify[{C1,C2,C3}];
   f=Simplify[Expand[f-(C1*ζ1+C2*ζ2+C3*ζ3)(1-ζ1-ζ2-ζ3)]];
   Return[f]];
```

FIGURE E15.3. Two *Mathematica* modules that homogenize linear and quadratic polynomials expressed in triaangular coordinates.

EXERCISE 15.15 [C:15] The two Mathematica modules listed in Figure E15.3 homogenize linear and quadratic polynomials, respectively, expressed in triangular coordinates. Explain their logic.

EXERCISE 15.16 [C+D:25] Access the file `Trig3PlaneStress.nb` from the course Web site by clicking on the appropriate link in Chapter 15 Index. This is a *Mathematica* Notebook that does plane stress FEM analysis using the 3-node Turner triangle.

Download the Notebook into your directory. Load into *Mathematica*. Execute the top 7 input cells (which are actually initialization cells) so the necessary modules are compiled. Each cell is preceded by a short comment cell which outlines the purpose of the modules it holds. Notes: (1) the plot-module cell may take a while to run through its tests; be patient; (2) to get rid of unsightly messages and silly beeps about similar names, initialize each cell twice.

After you are satisfied everything works fine, run the cantilever beam problem, which is defined in the last input cell.

After you get a feel of how this code operate, study the source. Prepare a hierarchical diagram of the modules,[11] beginning with the main program of the last cell. Note which calls what, and briefly explain the purpose of each module. Return this diagram as answer to the homework. You do not need to talk about the actual run and results; those will be discussed in Part III.

Hint: a hierarchical diagram for `Trig3PlaneStress.nb` begins like

```
Main program in Cell 8 - drives the FEM analysis
   GenerateNodes - generates node coordinates of regular mesh
   GenerateTriangles - generate element node lists of regular mesh
   ........
```

EXERCISE 15.17 [A:10] Consider the Veubeke triangle with 3 midside nodes 4, 5 and 6. Show that three possible shape functions are $1-2\zeta_3$, $1-2\zeta_1$ and $1-2\zeta_2$, respectively. Show that these functions satisfy the interpolation and completeness conditions, but fail the compatibility condition.

---

[11] A hierarchical diagram is a list of modules and their purposes, with indentation to show dependence, similar to the table of contents of a book. For example, if module `AAAA` calls `BBBB` and `CCCC`, and `BBBB` calld `DDDD`, the hierarchical diagram may look like:

```
AAAA -  purpose of AAAA
  BBBB  - purpose of BBBB
    DDDD - purpose of DDDD
  CCCC  - purpose of CCCC
```

Hint on Exercise 15.3 (added October 19, 2011)

If doing this Exercise by hand, you should process as follows.

First, multiply $\mathbf{N}^T$ by $\mathbf{b}$:

$$\mathbf{N}^T.\mathbf{b} = \begin{bmatrix} \zeta_1 & 0 \\ 0 & \zeta_1 \\ \zeta_2 & 0 \\ 0 & \zeta_2 \\ \zeta_3 & 0 \\ 0 & \zeta_3 \end{bmatrix} \begin{bmatrix} 0 \\ b_{y1}\zeta_1 + b_{y2}\zeta_2 + b_{y3}\zeta_3 \end{bmatrix}$$

to get a 6-vector. Entries 1,3 and 5 are zero. Entry 2 is $(b_{y1}\zeta_1 + b_{y2}\zeta_2 + b_{y3}\zeta_3)\zeta_1$, and so on for entries 4 and 6. Next, scale this vector by $h = h_1\zeta_1 + h_2\zeta_2 + h_3\zeta_3$. Entries 1,3 and 5 remain zero, whereas entries 2, 4 and 6 become cubic polynomials in the ζ_i. For example, the second entry is

$$(h_1\zeta_1 + h_2\zeta_2 + h_3\zeta_3)\,(b_{y1}\zeta_1 + b_{y2}\zeta_2 + b_{y3}\zeta_3)\zeta_1$$

Expand these in term of cubic monomials. For example, the expanded second entry becomes

$$h_1\, b_{y1}\, \zeta^3 + h_1\, b_{y2}\, \zeta_1^2\, \zeta_2 + 7 \text{ more terms}$$

Next, collect the ζ_i monomials that appear in entries 2, 4 and 6. The 10 possible monomials are ζ_1^3, ζ_2^3, ζ_3^3, $\zeta_1^2\zeta_2$, $\zeta_1^2\zeta_3$, $\zeta_2^2\zeta_1$, $\zeta_2^2\zeta_3$, $\zeta_3^2\zeta_1$, $\zeta_3^2\zeta_2$, and $\zeta_1\zeta_2\zeta_3$. Move all monomial coefficients such as $b_{y1}\,h_1$, etc., outside the area integral, and apply the formula (15.26) to the monomial integrals. Three cases:

$$\int_{\Omega^e} \zeta_1^3\, d\Omega = \int_{\Omega^e} \zeta_2^3\, d\Omega = \int_{\Omega^e} \zeta_3^3\, d\Omega = \frac{A}{10}$$

$$\int_{\Omega^e} \zeta_1^2\zeta_2\, d\Omega = \int_{\Omega^e} \zeta_1^2\zeta_3\, d\Omega = \int_{\Omega^e} \zeta_2^2\zeta_1\, d\Omega = \ldots = \frac{A}{30}$$

$$\int_{\Omega^e} \zeta_1\zeta_2\zeta_3 = \frac{A}{60}$$

Finally, collect the common factor A, collect the h factors of the b_{yi} as in (E15.2) and you are done. Well, not quite. It is instructive to check your results for the special cases $h_1 = h_2 = h_3 = h$ (constant thickness), and $b_{y1} = b_{y2} = b_{y3} = b_y$ (constant body force). If both the thickness h and the body force b_y are constant, the total force on the element, which is then $b_y\, h\, A$, should divide equally in 3 for each node. This would agree with the element-by-element force lumping recipe of Section 7).

If you are good in *Mathematica*, the result can be obtained in milliseconds, but you need to use the module listed under Exercise 15.11.

16

The Isoparametric Representation

TABLE OF CONTENTS

§16.1. Introduction

The procedure used in Chapter 15to formulate the stiffness equations of the linear triangle can be formally extended to quadrilateral elements as well as higher order triangles. But one quickly encounters technical difficulties:

1. The construction of shape functions that satisfy consistency requirements for higher order elements with curved boundaries becomes increasingly complicated.
2. Integrals that appear in the expressions of the element stiffness matrix and consistent nodal force vector can no longer be evaluated in simple closed form.

These two obstacles can be overcome through the concepts of *isoparametric elements* and *numerical quadrature*, respectively. The combination of these two ideas transformed the field of finite element methods in the late 1960s. Together they support a good portion of what is presently used in production finite element programs.

In the present Chapter the concept of isoparametric representation is introduced for two dimensional elements. This representation is illustrated on specific elements. In the next Chapter these techniques, combined with numerical integration, are applied to quadrilateral elements.

§16.2. Isoparametric Representation

§16.2.1. Motivation

The linear triangle presented in Chapter 115*is* an isoparametric element although was not originally derived as such. The two key equations are (15.10), which defines the triangle geometry, and (15.16), which defines the primary variable, in this case the displacement field. These equations are reproduced here for convenience:

$$\begin{bmatrix} 1 \\ x \\ y \end{bmatrix} = \begin{bmatrix} 1 & 1 & 1 \\ x_1 & x_2 & x_3 \\ y_1 & y_2 & y_3 \end{bmatrix} \begin{bmatrix} \zeta_1 \\ \zeta_2 \\ \zeta_3 \end{bmatrix}, \tag{16.1}$$

$$\begin{aligned} u_x &= u_{x1} N_1^e + u_{x2} N_2^e + u_{x3} N_3^e = u_{x1}\zeta_1 + u_{x2}\zeta_2 + u_{x3}\zeta_3, \\ u_y &= u_{y1} N_1^e + u_{y2} N_2^e + u_{y3} N_3^e = u_{y1}\zeta_1 + u_{y2}\zeta_2 + u_{y3}\zeta_3. \end{aligned} \tag{16.2}$$

The interpretation of these equations is as follows. The triangular coordinates define the element geometry via (16.1). The displacement expansion (16.2) is defined by the shape functions, which are in turn expressed in terms of the triangular coordinates. For the linear triangle, shape functions and triangular coordinates coalesce.

These relations are diagrammed in Figure 16.1. Evidently geometry and displacements are not treated equally. If we proceed to higher order triangular elements while keeping straight sides, only the displacement expansion is refined whereas the geometry definition remains the same.

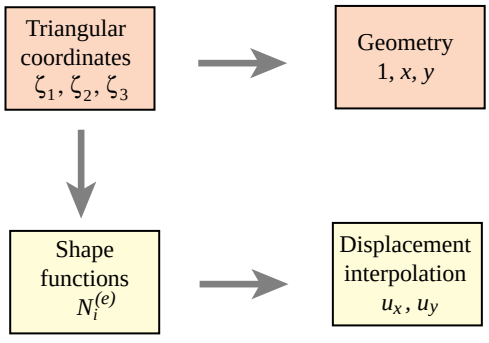

FIGURE 16.1. Superparametric representation of triangular element.

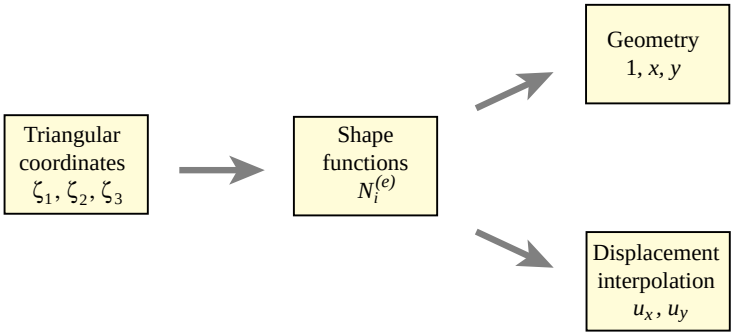

FIGURE 16.2. Isoparametric representation of triangular elements.

Elements built according to the foregoing prescription are called *superparametric*, a term that emphasizes that unequal treatment.

§16.2.2. Equalizing Geometry and Displacements

On first inspection (16.2) and (16.1) do not look alike. Their inherent similarity can be displayed, however, if the second one is rewritten and adjoined to (16.1) to look as follows:

$$\begin{bmatrix} 1 \\ x \\ y \\ u_x \\ u_y \end{bmatrix} = \begin{bmatrix} 1 & 1 & 1 \\ x_1 & x_2 & x_3 \\ y_1 & y_2 & y_3 \\ u_{x1} & u_{x2} & u_{y3} \\ u_{y1} & u_{y2} & u_{y3} \end{bmatrix} \begin{bmatrix} \zeta_1 \\ \zeta_2 \\ \zeta_3 \end{bmatrix} = \begin{bmatrix} 1 & 1 & 1 \\ x_1 & x_2 & x_3 \\ y_1 & y_2 & y_3 \\ u_{x1} & u_{x2} & u_{y3} \\ u_{y1} & u_{y2} & u_{y3} \end{bmatrix} \begin{bmatrix} N_1^e \\ N_2^e \\ N_3^e \end{bmatrix}. \tag{16.3}$$

This form emphasizes that geometry and displacements are given by the *same* parametric representation, as shown in Figure 16.2.

The key idea is to use the shape functions to represent *both the element geometry and the problem unknowns*, which in structural mechanics are displacements. Hence the name *isoparametric element* ("iso" means equal), often abbreviated to *iso-P element*. This property may be generalized to arbitrary elements by replacing the term "triangular coordinates" by the more general one "natural coordinates." This generalization is illustrated in Figure 16.3.

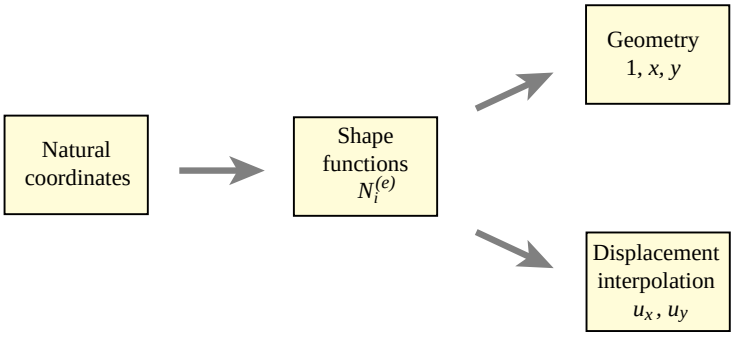

FIGURE 16.3. Isoparametric representation of arbitrary two-dimensional elements: triangles or quadrilaterals. For 3D elements, expand the geometry list to $\{1, x, y, z\}$ and the displacements to $\{u_x, u_y, u_z\}$.

Under this generalization, natural coordinates (triangular coordinates for triangles, quadrilateral coordinates for quadrilaterals) appear as *parameters* that define the shape functions. The shape functions connect the geometry with the displacements.

Remark 16.1. The terms *isoparametric* and *superparametric* were introduced by Irons and coworkers at Swansea in 1966. See **Notes and Bibliography** at the end of this Chapter. There are also *subparametric* elements whose geometry is more refined than the displacement expansion.

§16.3. General Isoparametric Formulation

The generalization of (16.3) to an arbitrary two-dimensional element with n nodes is straightforward. Two set of relations, one for the element geometry and the other for the element displacements, are required. Both sets exhibit the same interpolation in terms of the shape functions.

Geometric relations:

$$\boxed{1 = \sum_{i=1}^{n} N_i^e, \quad x = \sum_{i=1}^{n} x_i N_i^e, \quad y = \sum_{i=1}^{n} y_i N_i^e.} \tag{16.4}$$

Displacement interpolation:

$$\boxed{u_x = \sum_{i=1}^{n} u_{xi} N_i^e, \quad u_y = \sum_{i=1}^{n} u_{yi} N_i^e.} \tag{16.5}$$

These two sets of equations may be combined in matrix form as

$$\begin{bmatrix} 1 \\ x \\ y \\ u_x \\ u_y \end{bmatrix} = \begin{bmatrix} 1 & 1 & \dots & 1 \\ x_1 & x_2 & \dots & x_n \\ y_1 & y_2 & \dots & y_n \\ u_{x1} & u_{x2} & \dots & u_{xn} \\ u_{y1} & u_{y2} & \dots & u_{yn} \end{bmatrix} \begin{bmatrix} N_1^e \\ N_2^e \\ \vdots \\ N_n^e \end{bmatrix}. \tag{16.6}$$

The first three scalar equations in (16.6) express the geometry definition, and the last two the displacement expansion. Note that additional rows may be added to this matrix expression if more variables are interpolated by the same shape functions. For example, suppose that the thickness h and a temperature field T are both interpolated from the n node values:

$$\begin{bmatrix} 1 \\ x \\ y \\ u_x \\ u_y \\ h \\ T \end{bmatrix} = \begin{bmatrix} 1 & 1 & \dots & 1 \\ x_1 & x_2 & \dots & x_n \\ y_1 & y_2 & \dots & y_n \\ u_{x1} & u_{x2} & \dots & u_{xn} \\ u_{y1} & u_{y2} & \dots & u_{yn} \\ h_1 & h_2 & \dots & h_n \\ T_1 & T_2 & \dots & T_n \end{bmatrix} \begin{bmatrix} N_1^e \\ N_2^e \\ \vdots \\ N_n^e \end{bmatrix}. \tag{16.7}$$

Note that the column of shape functions does not change.

To illustrate the use of the isoparametric concept, we take a look at specific 2D isoparametric elements that are commonly used in structural and non-structural applications. These are separated into triangles and quadrilaterals because different natural coordinates are used.

§16.4. Triangular Elements

§16.4.1. The Linear Triangle

The three-noded linear triangle, studied in Chapter 15 and pictured in Figure 16.4, may be presented as an isoparametric element:

$$\begin{bmatrix} 1 \\ x \\ y \\ u_x \\ u_y \end{bmatrix} = \begin{bmatrix} 1 & 1 & 1 \\ x_1 & x_2 & x_3 \\ y_1 & y_2 & y_3 \\ u_{x1} & u_{x2} & u_{x3} \\ u_{y1} & u_{y2} & u_{y3} \end{bmatrix} \begin{bmatrix} N_1^e \\ N_2^e \\ N_3^e \end{bmatrix}. \tag{16.8}$$

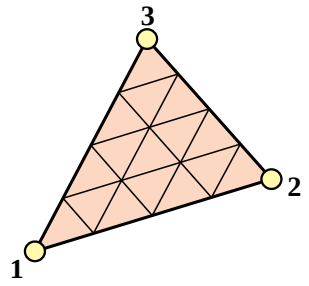

FIGURE 16.4. The 3-node linear triangle.

The shape functions are simply the triangular coordinates:

$$N_1^e = \zeta_1, \qquad N_2^e = \zeta_2, \qquad N_3^e = \zeta_3. \tag{16.9}$$

The linear triangle is the only triangular element that is both superparametric and isoparametric.

§16.4.2. The Quadratic Triangle

The six node triangle shown in Figure 16.5 is the next complete-polynomial member of the isoparametric triangle family. The isoparametric definition is

$$\begin{bmatrix} 1 \\ x \\ y \\ u_x \\ u_y \end{bmatrix} = \begin{bmatrix} 1 & 1 & 1 & 1 & 1 & 1 \\ x_1 & x_2 & x_3 & x_4 & x_5 & x_6 \\ y_1 & y_2 & y_3 & y_4 & y_5 & y_6 \\ u_{x1} & u_{x2} & u_{x3} & u_{x4} & u_{x5} & u_{x6} \\ u_{y1} & u_{y2} & u_{y3} & u_{y4} & u_{y5} & u_{y6} \end{bmatrix} \begin{bmatrix} N_1^e \\ N_2^e \\ N_3^e \\ N_4^e \\ N_5^e \\ N_6^e \end{bmatrix} \tag{16.10}$$

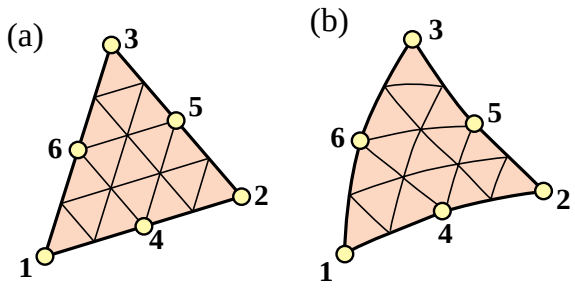

FIGURE 16.5. The 6-node quadratic triangle: (a) the superparametric version, with straight sides and midside nodes at midpoints; (b) the isoparametric version.

The shape functions are

$$\begin{aligned} &N_1^e = \zeta_1(2\zeta_1 - 1), \quad N_2^e = \zeta_2(2\zeta_2 - 1), \quad N_3^e = \zeta_3(2\zeta_3 - 1), \\ &N_4^e = 4\zeta_1\zeta_2, \quad N_5^e = 4\zeta_2\zeta_3, \quad N_6^e = 4\zeta_3\zeta_1. \end{aligned} \tag{16.11}$$

The element may have parabolically curved sides defined by the location of the midnodes 4, 5 and 6. The triangular coordinates for a curved triangle are no longer straight lines, but form a curvilinear system as can be observed in Figure 16.5(b).

§16.4.3. *The Cubic Triangle

The cubic triangle has ten nodes. This shape functions of this element are the subject of an Exercise in Chapter 18. The implementation is studied in Chapter 24.

§16.5. Quadrilateral Elements

§16.5.1. Quadrilateral Coordinates and Iso-P Mappings

Before presenting examples of quadrilateral elements, we must introduce the appropriate *natural coordinate system* for that geometry. The natural coordinates for a triangular element are the triangular coordinates ζ_1, ζ_2 and ζ_3. The natural coordinates for a quadrilateral element are ξ and η, which are illustrated in Figure 16.6 for both straight sided and curved side quadrilaterals. These are called *quadrilateral coordinates*.

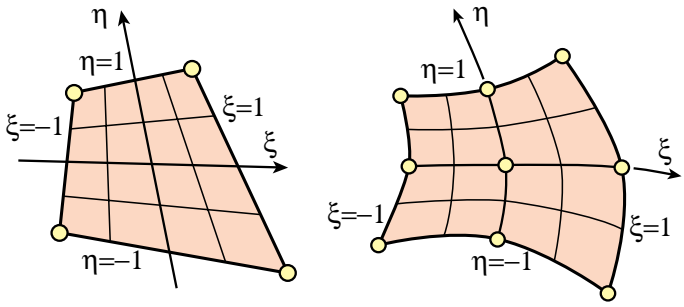

FIGURE 16.6. Quadrilateral coordinates.

These coordinates vary from -1 on one side to $+1$ at the other, taking the value zero over the quadrilateral medians. This particular variation range (instead of taking, say, 0 to 1) was chosen by Irons and coworkers to facilitate use of the standard Gauss integration formulas. Those formulas are discussed in the next Chapter.

Remark 16.2. In some FEM derivations it is convenient to visualize the quadrilateral coordinates plotted as Cartesian coordinates in the $\{\xi, \eta\}$ plane. This is called the *reference plane*. All quadrilateral elements in the reference plane become a square of side 2, called the *reference element*, which extends over $\xi \in [-1, 1]$, $\eta \in [-1, 1]$. The transformation between $\{\xi, \eta\}$ and $\{x, y\}$ dictated by the second and third equations of (16.4), is called the *isoparametric mapping*. A similar version exists for triangles. An important application of this mapping is discussed in §16.6; see Figure 16.9 there.

§16.5.2. The Bilinear Quadrilateral

The four-node quadrilateral shown in Figure 16.7 is the simplest member of the quadrilateral family. It is defined by

$$\begin{bmatrix} 1 \\ x \\ y \\ u_x \\ u_y \end{bmatrix} = \begin{bmatrix} 1 & 1 & 1 & 1 \\ x_1 & x_2 & x_3 & x_4 \\ y_1 & y_2 & y_3 & y_4 \\ u_{x1} & u_{x2} & u_{x3} & u_{x4} \\ u_{y1} & u_{y2} & u_{y3} & u_{y4} \end{bmatrix} \begin{bmatrix} N_1^e \\ N_2^e \\ N_3^e \\ N_4^e \end{bmatrix}. \qquad (16.12)$$

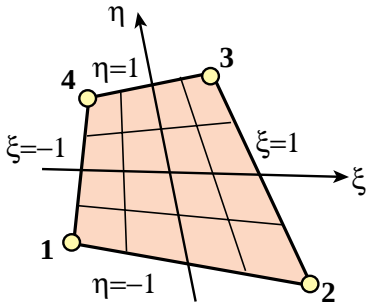

FIGURE 16.7. The 4-node bilinear quadrilateral.

The shape functions are

$$\begin{aligned} N_1^e &= \tfrac{1}{4}(1-\xi)(1-\eta), \qquad & N_2^e &= \tfrac{1}{4}(1+\xi)(1-\eta), \\ N_3^e &= \tfrac{1}{4}(1+\xi)(1+\eta), \qquad & N_4^e &= \tfrac{1}{4}(1-\xi)(1+\eta). \end{aligned} \qquad (16.13)$$

These functions vary *linearly* on quadrilateral coordinate lines $\xi = const$ and $\eta = const$, but are not linear polynomials as in the case of the three-node triangle.

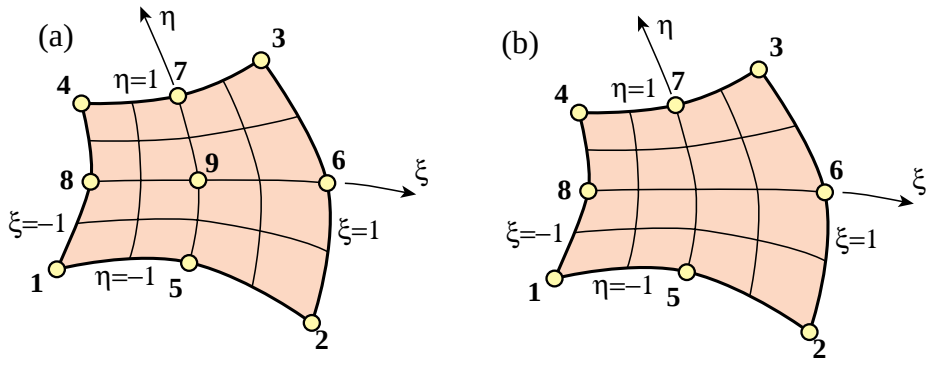

FIGURE 16.8. Two widely used higher order quadrilaterals: (a) the nine-node biquadratic quadrilateral; (b) the eight-node "serendipity" quadrilateral.

§16.5.3. The Biquadratic Quadrilateral

The nine-node quadrilateral shown in Figure 16.8(a) is the next *complete* member of the quadrilateral family. It has eight external nodes and one internal node. It is defined by

$$\begin{bmatrix} 1 \\ x \\ y \\ u_x \\ u_y \end{bmatrix} = \begin{bmatrix} 1 & 1 & 1 & 1 & 1 & 1 & 1 & 1 & 1 \\ x_1 & x_2 & x_3 & x_4 & x_5 & x_6 & x_7 & x_8 & x_9 \\ y_1 & y_2 & y_3 & y_4 & y_5 & y_6 & y_7 & y_8 & y_9 \\ u_{x1} & u_{x2} & u_{x3} & u_{x4} & u_{x5} & u_{x6} & u_{x7} & u_{x8} & u_{x9} \\ u_{y1} & u_{y2} & u_{y3} & u_{y4} & u_{y5} & u_{y6} & u_{y7} & u_{y8} & u_{y9} \end{bmatrix} \begin{bmatrix} N_1^e \\ N_2^e \\ \vdots \\ \\ N_9^e \end{bmatrix}. \tag{16.14}$$

This element is often referred to as the *Lagrangian quadrilateral* in the FEM literature, a term explained in the **Notes and Bibliography**. Its shape functions are

$$\begin{aligned} N_1^e &= \tfrac{1}{4}(1-\xi)(1-\eta)\xi\eta, \quad & N_5^e &= -\tfrac{1}{2}(1-\xi^2)(1-\eta)\eta, \\ N_2^e &= -\tfrac{1}{4}(1+\xi)(1-\eta)\xi\eta, \quad & N_6^e &= \tfrac{1}{2}(1+\xi)(1-\eta^2)\xi, \quad N_9^e = (1-\xi^2)(1-\eta^2) \\ &\cdots & &\cdots \end{aligned} \tag{16.15}$$

These functions vary *quadratically* along the coordinate lines $\xi = const$ and $\eta = const$. The shape function associated with the internal node 9 is called a *bubble function* because of its geometric shape, which is pictured in §18.4.2.

Figure 16.8(a) depicts a widely used eight-node variant called the "serendipity" quadrilateral. (A name that originated from circumstances surrounding the element discovery.) The internal node is eliminated by kinematic constraints as worked out in an Exercise of Chapter 18.

§16.6. Completeness Properties of Iso-P Elements

Some general conclusions as regards the range of applications of isoparametric elements can be obtained from a *completeness analysis*. More specifically, whether the general prescription (16.6) that combines (16.4) and (16.5) satisfies the *completeness* criterion of finite element trial expansions. This is one of the conditions for convergence to the analytical solution. The requirement is treated generally in Chapter 19, and is stated here in recipe form.

§16.6.1. *Completeness Analysis

The plane stress problem has variational index $m = 1$. A set of shape functions is complete for this problem if they can represent exactly any *linear* displacement motions such as

$$u_x = \alpha_0 + \alpha_1 x + \alpha_2 y, \qquad u_y = \beta_0 + \beta_1 x + \beta_2 y. \tag{16.16}$$

To carry out the check, evaluate (16.16) at the nodes

$$u_{xi} = \alpha_0 + \alpha_1 x_i + \alpha_2 y_i \qquad u_{yi} = \beta_0 + \beta_1 x_i + \beta_2 y_i, \qquad i = 1, \ldots n. \tag{16.17}$$

Insert this into the displacement expansion (16.5) to see whether the linear displacement field (16.16) is recovered. Here are the computations for the displacement component u_x:

$$u_x = \sum_{i=1}^{n} (\alpha_0 + \alpha_1 x_i + \alpha_2 y_i)\, N_i^e = \alpha_0 \sum_i N_i^e + \alpha_1 \sum_i x_i N_i^e + \alpha_2 \sum_i y_i N_i^e = \alpha_0 + \alpha_1 x + \alpha_2 y. \tag{16.18}$$

For the last step we have used the geometry definition relations (16.4), reproduced here for convenience:

$$\boxed{1 = \sum_{i=1}^{n} N_i^e, \quad x = \sum_{i=1}^{n} x_i N_i^e, \quad y = \sum_{i=1}^{n} y_i N_i^e.} \tag{16.19}$$

A similar calculation may be made for u_y. It appears that the isoparametric displacement expansion represents (16.18) for *any* element, and consequently meets the completeness requirement for variational order $m = 1$. The derivation carries without essential change to three dimensions.[1]

Can you detect a flaw in this conclusion? The fly in the ointment is the last replacement step of (16.18), which assumes that the geometry relations (16.19) *are identically satisfied*. Indeed they are for all the example elements presented in the previous sections. But if the new shape functions are constructed directly by the methods of Chapter 18, *a posteriori* checks of those identities are necessary.

§16.6.2. Completeness Checks

The first check in (16.19) is easy: *the sum of shape functions must be unity*. This is also called the *unit sum condition*. It can be easily verified by hand for simple elements. Here are two examples.

Example 16.1. Check for the linear triangle: directly from the definition of triangular coordinates,

$$N_1^e + N_2^e + N_3^e = \zeta_1 + \zeta_2 + \zeta_3 = 1. \tag{16.20}$$

[1] This derivation is due to B. M. Irons. See for example [397, p. 75]. The property was known since the mid 1960s and contributed substantially to the rapid acceptance of iso-P elements.

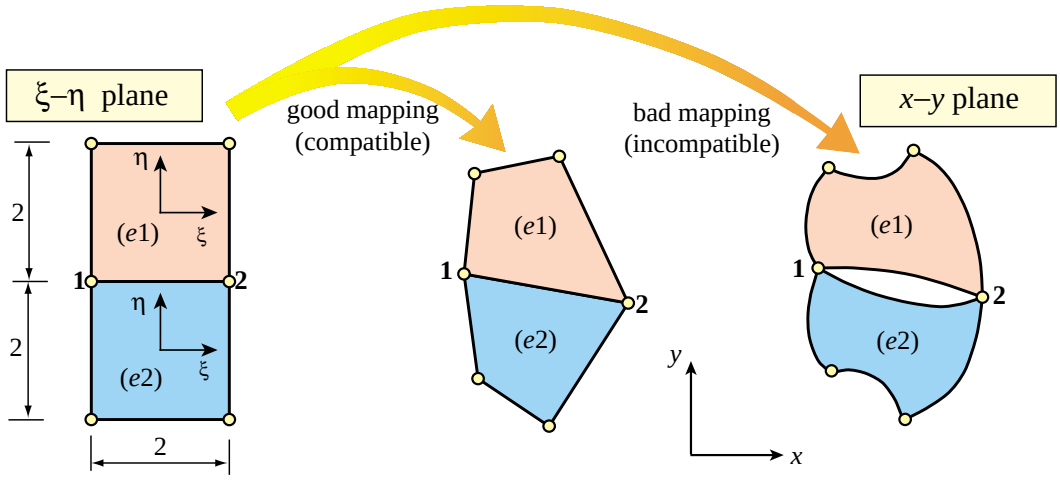

FIGURE 16.9. Good and bad isoparametric mappings of 4-node quadrilateral from the $\{\xi, \eta\}$ reference plane onto the $\{x, y\}$ physical plane.

Example 16.2. Check for the 4-node bilinear quadrilateral:

$$N_1^e + N_2^e + N_3^e + N_4^e = \tfrac{1}{4}(1-\xi-\eta+\xi\eta) + \tfrac{1}{4}(1+\xi-\eta-\xi\eta) + \tfrac{1}{4}(1+\xi+\eta+\xi\eta) + \tfrac{1}{4}(1-\xi+\eta-\xi\eta) = 1 \tag{16.21}$$

For more complicated elements see Exercises 16.2 and 16.3.

The other two checks are less obvious. For specificity consider the 4-node bilinear quadrilateral. The geometry definition equations are

$$x = \sum_{i=1}^{4} x_i N_i^e(\xi, \eta), \quad y = \sum_{i=1}^{4} y_i N_i^e(\xi, \eta). \tag{16.22}$$

Given the corner coordinates, $\{x_i, y_i\}$ and a point $P(x, y)$ one can try to solve for $\{\xi, \eta\}$. This solution requires nontrivial work because it involves two coupled quadratics, but can be done. Reinserting into (16.22) simply gives back x and y, and nothing is gained.[2]

The correct question to pose is: is the correct geometry of the quadrilateral preserved by the mapping from $\{\xi, \eta\}$ to $\{x, y\}$? In particular, are the sides straight lines? Figure 16.9 illustrate these questions. Two side-two squares: $(e1)$ and $(e2)$, contiguous in the $\{\xi, \eta\}$ reference plane, are mapped to quadrilaterals $(e1)$ and $(e2)$ in the $\{x, y\}$ physical plane through (16.22). The common side 1-2 must remain a straight line to preclude interelement gaps or interpenetration.

We are therefore lead to consider *geometric compatibility* upon mapping. But this is equivalent to the question of *interelement displacement compatibility*, which is stipulated as item (C) in §18.1. The statement "the displacement along a side must be uniquely determined by nodal displacements on that side" translates to "the coordinates of a side must be uniquely determined by nodal coordinates on that side." Summarizing:

[2] This tautology is actually a blessing, since finding explicit expressions for the natural coordinates in terms of x and y rapidly becomes impossible for higher order elements. See, for example, the complications that already arise for the bilinear quadrilateral in §23.3.

$$\boxed{\text{Unit-sum condition + interelement compatibility} \rightarrow \text{completeness.}} \tag{16.23}$$

This subdivision of work significantly reduces the labor involved in element testing.

§16.6.3. *Completeness for Higher Variational Index

The completeness conditions for variational index 2 are far more demanding because they involve quadratic motions. No simple isoparametric configurations satisfy those conditions. Consequently isoparametric formulations have limited importance in the finite element analysis of plate and shell bending.

§16.7. Iso-P Elements in One and Three Dimensions

The reader should not think that the concept of isoparametric representation is confined to two-dimensional elements. It applies without conceptual changes to one and three dimensions *as long as the variational index remains one*.[3] Three-dimensional solid elements are covered in an advanced course. The use of the isoparametric formulation to construct a 3-node bar element is the topic of Exercises 16.4 through 16.7.

Notes and Bibliography

A detailed presentation of the isoparametric concept, with annotated references to the original 1960 papers may be found in the textbook [397].

This matrix representation for isoparametric elements used here was introduced in [204].

The term *Lagrangian element* in the mathematical FEM literature identifies quadrilateral and hexahedra (brick) elements that include all polynomial terms $\xi^i \eta^j$ (in 2D) or $\xi^i \eta^j \mu^k$ (in 3D) with $i \le n$, $j \le n$ and $k \le n$, as part of the shape function interpolation. Such elements have $(n+1)^2$ nodes in 2D and $(n+1)^3$ nodes in 3D, and the interpolation is said to be n-bicomplete. For example, if $n = 2$, the biquadratic quadrilateral with $(2+1)^2 = 9$ nodes is Lagrangian and 2-bicomplete. (The qualifier "Lagrangian" in this context refers to Lagrange's interpolation formula, not to Lagrange multipliers.)

References

Referenced items have been moved to Appendix R

[3] A limitation explained in §16.6.3.

Homework Exercises for Chapter 16
The Isoparametric Representation

EXERCISE 16.1 [D:10] What is the physical interpretation of the shape-function unit-sum condition discussed in §16.6? Hint: the element must respond exactly in terms of displacements to rigid-body translations in the x and y directions.

EXERCISE 16.2 [A:15] Check by algebra that the sum of the shape functions for the six-node quadratic triangle (16.11) is exactly one regardless of natural coordinates values. Hint: show that the sum is expressable as $2S_1^2 - S_1$, where $S_1 = \zeta_1 + \zeta_2 + \zeta_3$.

EXERCISE 16.3 [A/C:15] Complete the table of shape functions (16.23) of the nine-node biquadratic quadrilateral. Verify that their sum is exactly one.

EXERCISE 16.4 [A:20] Consider a three-node bar element referred to the natural coordinate ξ. The two end nodes and the midnode are identified as 1, 2 and 3, respectively. The natural coordinates of nodes 1, 2 and 3 are $\xi = -1$, $\xi = 1$ and $\xi = 0$, respectively. The variation of the shape functions $N_1(\xi)$, $N_2(\xi)$ and $N_3(\xi)$ is sketched in Figure E16.1. These functions must be quadratic polynomials in ξ:

$$N_1^e(\xi) = a_0 + a_1\xi + a_2\xi^2, \qquad N_2^e(\xi) = b_0 + b_1\xi + b_2\xi^2, \qquad N_3^e(\xi) = c_0 + c_1\xi + c_2\xi^2. \tag{E16.1}$$

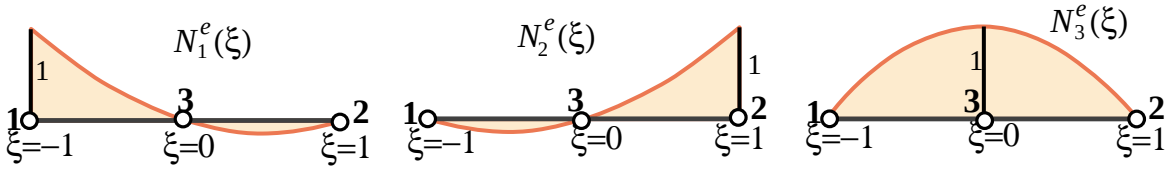

FIGURE E16.1. Isoparametric shape functions for 3-node bar element (sketch). Node 3 has been drawn at the 1–2 midpoint but it may be moved away from it, as in Exercises E16.5 and E16.6.

Determine the coefficients a_0, through c_2 using the node value conditions depicted in Figure E16.1; for example $N_1^e = 1$, 0 and 0 for $\xi = -1$, 0 and 1 at nodes 1, 3 and 2, respectively. Proceeding this way show that

$$N_1^e(\xi) = -\tfrac{1}{2}\xi(1-\xi), \qquad N_2^e(\xi) = \tfrac{1}{2}\xi(1+\xi), \qquad N_3^e(\xi) = 1 - \xi^2. \tag{E16.2}$$

Verify that their sum is identically one.

EXERCISE 16.5

[A/C:15+10+15+5] A 3-node straight bar element is defined by 3 nodes: 1, 2 and 3, with axial coordinates x_1, x_2 and x_3, respectively, as illustrated in Figure E16.2. The element has axial rigidity EA and length $\ell = x_2 - x_1$. The axial displacement is $u(x)$. The 3 degrees of freedom are the axial node displacements u_1, u_2 and u_3. The isoparametric definition of the element is

$$\begin{bmatrix} 1 \\ x \\ u \end{bmatrix} = \begin{bmatrix} 1 & 1 & 1 \\ x_1 & x_2 & x_3 \\ u_1 & u_2 & u_3 \end{bmatrix} \begin{bmatrix} N_1^e \\ N_2^e \\ N_3^e \end{bmatrix}, \tag{E16.3}$$

in which $N_i^e(\xi)$ are the shape functions (E16.2) of the previous Exercise. Node 3 lies between 1 and 2 but is not necessarily at the midpoint $x = \frac{1}{2}\ell$. For convenience define

$$x_1 = 0, \qquad x_2 = \ell, \qquad x_3 = (\tfrac{1}{2} + \alpha)\ell, \tag{E16.4}$$

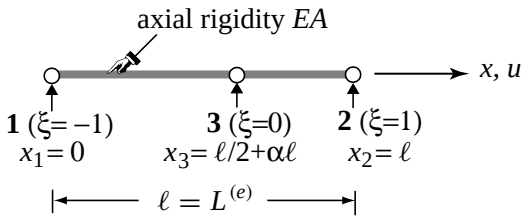

FIGURE E16.2. The 3-node bar element in its local system.

where $-\frac{1}{2} < \alpha < \frac{1}{2}$ characterizes the location of node 3 with respect to the element center. If $\alpha = 0$ node 3 is located at the midpoint between 1 and 2. See Figure E16.2.

(a) From (E16.4) and the second equation of (E16.3) get the Jacobian $J = dx/d\xi$ in terms of ℓ, α and ξ. Show that: (i) if $-\frac{1}{4} < \alpha < \frac{1}{4}$ then $J > 0$ over the whole element $-1 \le \xi \le 1$; (ii) if $\alpha = 0$, $J = \ell/2$ is constant over the element.

(b) Obtain the 1×3 strain-displacement matrix $\mathbf{B}$ relating $e = du/dx = \mathbf{B}\,\mathbf{u}^e$, where $\mathbf{u}^e$ is the column 3-vector of node displacements u_1, u_2 and u_3. The entries of $\mathbf{B}$ are functions of ℓ, α and ξ. Hint: $\mathbf{B} = d\mathbf{N}/dx = J^{-1} d\mathbf{N}/d\xi$, where $\mathbf{N} = [\, N_1 \;\; N_2 \;\; N_3 \,]$ and J comes from item (a).

(c) Show that the element stiffness matrix is given by

$$\mathbf{K}^e = \int_0^\ell E A\, \mathbf{B}^T \mathbf{B}\, dx = \int_{-1}^{1} E A\, \mathbf{B}^T \mathbf{B}\, J\, d\xi. \tag{E16.5}$$

Evaluate the rightmost integral for arbitrary α but constant EA using the 2-point Gauss quadrature rule (E13.7). Specialize the result to $\alpha = 0$, for which you should get $K_{11} = K_{22} = 7EA/(3\ell)$, $K_{33} = 16EA/(3\ell)$, $K_{12} = EA/(3\ell)$ and $K_{13} = K_{23} = -8EA/(3\ell)$, with eigenvalues $\{8EA/\ell, 2EA/\ell, 0\}$. Note: use of a CAS is recommended for this item to save time.

(d) What is the minimum number of Gauss points needed to integrate $\mathbf{K}^e$ exactly if $\alpha = 0$?

EXERCISE 16.6 [A/C:20] This Exercise is a continuation of the foregoing one, and addresses the question of why $\mathbf{K}^e$ was computed by numerical integration in item (c). Why not use exact integration? The answer is that the exact stiffness for arbitrary α is numerically useless. To see why, try the following script in *Mathematica*:

```
ClearAll[EA,L,alpha,xi]; (* Define J and B={{B1,B2,B3}} here *)
Ke=Simplify[Integrate[EA*Transpose[B].B*J,{xi,-1,1},
   Assumptions->alpha>0&&alpha<1/4&&EA>0&&L>0]];
Print["exact Ke=",Ke//MatrixForm];
Print["exact Ke for alpha=0",Simplify[Ke/.alpha->0]//MatrixForm];
Keseries=Normal[Series[Ke,{alpha,0,2}]];
Print["Ke series about alpha=0:",Keseries//MatrixForm];
Print["Ke for alpha=0",Simplify[Keseries/.alpha->0]//MatrixForm];
```

At the start of this script define `J` and `B` with the results of items (a) and (b), respectively. Then run the script. The line `Print["exact Ke for alpha=0",Simplify[Ke/.alpha->0]//MatrixForm]` will trigger error messages. Comment on why the exact stiffness cannot be evaluated directly at $\alpha = 0$ (look at the printed expression before this one). A Taylor series expansion about $\alpha = 0$ circumvents these difficulties but the 2-point Gauss integration rule gives the correct answer without the gyrations.

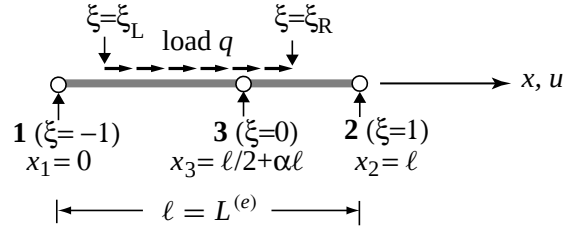

FIGURE E16.3. The 3-node bar element under a "box" axial load q.

EXERCISE 16.7 [A/C:20] Construct the consistent force vector for the 3-node bar element of the foregoing exercise, if the bar is loaded by a uniform axial force q (given per unit of x length) that extends from $\xi = \xi_L$ through $\xi = \xi_R$, and is zero otherwise. Here $-1 \le \xi_L < \xi_R \le 1$. See Figure E16.3. Use

$$\mathbf{f}^e = \int_{-\xi_L}^{\xi_R} q\, \mathbf{N}^T\, J\, d\xi, \tag{E16.6}$$

with the $J = dx/d\xi$ found in Exercise 16.5(a) and analytical integration. The answer is quite complicated and nearly hopeless by hand. Specialize the result to $\alpha = 0$, $\xi_L = -1$ and $\xi_R = 1$.

17

Isoparametric Quadrilaterals

TABLE OF CONTENTS

§17.1. Introduction

In this Chapter the isoparametric representation of element geometry and shape functions discussed in the previous Chapter is used to construct *quadrilateral* elements for the plane stress problem. Formulas given in Chapter 14 for the stiffness matrix and consistent load vector of general plane stress elements are of course applicable to these elements. For a practical implementation, however, we must go through more specific steps:

1. Construction of shape functions.
2. Computations of shape function derivatives to form the strain-displacement matrix.
3. Numerical integration over the element by Gauss quadrature rules.

The first topic was dealt in the previous Chapter in recipe form, and is systematically covered in the next one. Assuming the shape functions have been constructed (or readily found in the FEM literature) the second and third items are combined in an algorithm suitable for programming any isoparametric quadrilateral. The implementation of the algorithm in the form of element modules is partly explained in the Exercises of this Chapter, and covered more systematically in Chapter 23.

We shall not deal with isoparametric triangles here to keep the exposition focused. Triangular coordinates, being linked by a constraint, require "special handling" techniques that would complicate and confuse the exposition. Chapter 24 discusses isoparametric triangular elements in detail.

§17.2. Partial Derivative Computation

Partial derivatives of shape functions with respect to the Cartesian coordinates x and y are required for the strain and stress calculations. Because shape functions are not directly functions of x and y but of the natural coordinates ξ and η, the determination of Cartesian partial derivatives is not trivial. The derivative calculation procedure is presented below for the case of an arbitrary isoparametric quadrilateral element with n nodes.

§17.2.1. The Jacobian

In quadrilateral element derivations we will need the Jacobian of two-dimensional transformations that connect the differentials of $\{x, y\}$ to those of $\{\xi, \eta\}$ and vice-versa. Using the chain rule:

$$\begin{bmatrix} dx \\ dy \end{bmatrix} = \begin{bmatrix} \dfrac{\partial x}{\partial \xi} & \dfrac{\partial x}{\partial \eta} \\ \dfrac{\partial y}{\partial \xi} & \dfrac{\partial y}{\partial \eta} \end{bmatrix} \begin{bmatrix} d\xi \\ d\eta \end{bmatrix} = \mathbf{J}^T \begin{bmatrix} d\xi \\ d\eta \end{bmatrix}, \quad \begin{bmatrix} d\xi \\ d\eta \end{bmatrix} = \begin{bmatrix} \dfrac{\partial \xi}{\partial x} & \dfrac{\partial \xi}{\partial y} \\ \dfrac{\partial \eta}{\partial x} & \dfrac{\partial \eta}{\partial y} \end{bmatrix} \begin{bmatrix} dx \\ dy \end{bmatrix} = \mathbf{J}^{-T} \begin{bmatrix} dx \\ dy \end{bmatrix}. \tag{17.1}$$

Here $\mathbf{J}$ denotes the Jacobian matrix of (x, y) with respect to (ξ, η), whereas $\mathbf{J}^{-1}$ is the Jacobian matrix of (ξ, η) with respect to (x, y):

$$\mathbf{J} = \frac{\partial(x, y)}{\partial(\xi, \eta)} = \begin{bmatrix} \dfrac{\partial x}{\partial \xi} & \dfrac{\partial y}{\partial \xi} \\ \dfrac{\partial x}{\partial \eta} & \dfrac{\partial y}{\partial \eta} \end{bmatrix} = \begin{bmatrix} J_{11} & J_{12} \\ J_{21} & J_{22} \end{bmatrix}, \quad \mathbf{J}^{-1} = \frac{\partial(\xi, \eta)}{\partial(x, y)} = \begin{bmatrix} \dfrac{\partial \xi}{\partial x} & \dfrac{\partial \eta}{\partial x} \\ \dfrac{\partial \xi}{\partial y} & \dfrac{\partial \eta}{\partial y} \end{bmatrix} = \frac{1}{J} \begin{bmatrix} J_{22} & -J_{12} \\ -J_{21} & J_{11} \end{bmatrix}, \tag{17.2}$$

where $J = |\mathbf{J}| = \det(\mathbf{J}) = J_{11} J_{22} - J_{12} J_{21}$. In FEM work $\mathbf{J}$ and $\mathbf{J}^{-1}$ are called simply the *Jacobian* and *inverse Jacobian*, respectively; the fact that it is a matrix being understood. The scalar symbol

J is reserved for the determinant of $\mathbf{J}$. In one dimension $\mathbf{J}$ and J coalesce. Jacobians play a crucial role in differential geometry. For the general definition of Jacobian matrix of a differential transformation, see Appendix D.

Remark 17.1. Observe that the matrices relating the differentials in (17.1) are the *transposes* of what we call $\mathbf{J}$ and $\mathbf{J}^{-1}$. The reason is that coordinate differentials transform as contravariant quantities: $dx = (\partial x/\partial\xi)\,d\xi + (\partial x/\partial\eta)\,d\eta$, etc. But Jacobians are arranged as in (17.2) because of earlier use in covariant transformations: $\partial\phi/\partial x = (\partial\xi/\partial x)(\partial\phi/\partial\xi) + (\partial\eta/\partial x)(\partial\phi/\partial\eta)$, as in (17.5) below.

The reader is cautioned that notations vary among application areas. As quoted in Appendix D, one author puts it this way: "When one does matrix calculus, one quickly finds that there are two kinds of people in this world: those who think the gradient is a row vector, and those who think it is a column vector."

Remark 17.2. To show that $\mathbf{J}$ and $\mathbf{J}^{-1}$ are in fact inverses of each other we form their product:

$$\mathbf{J}^{-1}\mathbf{J} = \begin{bmatrix} \frac{\partial x}{\partial\xi}\frac{\partial\xi}{\partial x} + \frac{\partial x}{\partial\eta}\frac{\partial\eta}{\partial x} & \frac{\partial y}{\partial\xi}\frac{\partial\xi}{\partial x} + \frac{\partial y}{\partial\eta}\frac{\partial\eta}{\partial x} \\ \frac{\partial x}{\partial\xi}\frac{\partial\xi}{\partial y} + \frac{\partial x}{\partial\eta}\frac{\partial\eta}{\partial y} & \frac{\partial y}{\partial\xi}\frac{\partial\xi}{\partial y} + \frac{\partial y}{\partial\eta}\frac{\partial\eta}{\partial y} \end{bmatrix} = \begin{bmatrix} \frac{\partial x}{\partial x} & \frac{\partial y}{\partial x} \\ \frac{\partial x}{\partial y} & \frac{\partial y}{\partial y} \end{bmatrix} = \begin{bmatrix} 1 & 0 \\ 0 & 1 \end{bmatrix}, \tag{17.3}$$

where we have taken into account that $x = x(\xi,\eta)$, $y = y(\xi,\eta)$ and the fact that x and y are independent coordinates. This proof would collapse, however, if instead of $\{\xi,\eta\}$ we had the triangular coordinates $\{\zeta_1,\zeta_2,\zeta_3\}$ because rectangular matrices have no conventional inverses. This case requires special handling and is covered in Chapter 24.

§17.2.2. Shape Function Derivatives

The shape functions of a quadrilateral element are expressed in terms of the quadrilateral coordinates ξ and η introduced in §16.5.1. The derivatives with respect to x and y are given by the chain rule:

$$\frac{\partial N_i^e}{\partial x} = \frac{\partial N_i^e}{\partial\xi}\frac{\partial\xi}{\partial x} + \frac{\partial N_i^e}{\partial\eta}\frac{\partial\eta}{\partial x}, \qquad \frac{\partial N_i^e}{\partial y} = \frac{\partial N_i^e}{\partial\xi}\frac{\partial\xi}{\partial y} + \frac{\partial N_i^e}{\partial\eta}\frac{\partial\eta}{\partial y}. \tag{17.4}$$

This can be put in matrix form as

$$\begin{bmatrix} \frac{\partial N_i^e}{\partial x} \\ \frac{\partial N_i^e}{\partial y} \end{bmatrix} = \begin{bmatrix} \frac{\partial\xi}{\partial x} & \frac{\partial\eta}{\partial x} \\ \frac{\partial\xi}{\partial y} & \frac{\partial\eta}{\partial y} \end{bmatrix} \begin{bmatrix} \frac{\partial N_i^e}{\partial\xi} \\ \frac{\partial N_i^e}{\partial\eta} \end{bmatrix} = \frac{\partial(\xi,\eta)}{\partial(x,y)} \begin{bmatrix} \frac{\partial N_i^e}{\partial\xi} \\ \frac{\partial N_i^e}{\partial\eta} \end{bmatrix} = \mathbf{J}^{-1} \begin{bmatrix} \frac{\partial N_i^e}{\partial\xi} \\ \frac{\partial N_i^e}{\partial\eta} \end{bmatrix}. \tag{17.5}$$

where $\mathbf{J}^{-1}$ is defined in (17.2). The computation of $\mathbf{J}$ is addressed in the next subsection.

§17.2.3. Computing the Jacobian Matrix

To compute the entries of $\mathbf{J}$ at any quadrilateral location we make use of the last two geometric relations in (16.4), which are repeated here for convenience:

$$x = \sum_{i=1}^{n} x_i N_i^e, \qquad y = \sum_{i=1}^{n} y_i N_i^e. \tag{17.6}$$

Differentiating with respect to the quadrilateral coordinates,

$$\frac{\partial x}{\partial \xi} = \sum_{i=1}^{n} x_i \frac{\partial N_i^e}{\partial \xi}, \quad \frac{\partial y}{\partial \xi} = \sum_{i=1}^{n} y_i \frac{\partial N_i^e}{\partial \xi}, \quad \frac{\partial x}{\partial \eta} = \sum_{i=1}^{n} x_i \frac{\partial N_i^e}{\partial \eta}, \quad \frac{\partial y}{\partial \eta} = \sum_{i=1}^{n} y_i \frac{\partial N_i^e}{\partial \eta}. \tag{17.7}$$

because the x_i and y_i do not depend on ξ and η. In matrix form:

$$\mathbf{J} = \begin{bmatrix} J_{11} & J_{12} \\ J_{21} & J_{22} \end{bmatrix} = \begin{bmatrix} \dfrac{\partial x}{\partial \xi} & \dfrac{\partial y}{\partial \xi} \\ \dfrac{\partial x}{\partial \eta} & \dfrac{\partial y}{\partial \eta} \end{bmatrix} = \mathbf{PX} = \begin{bmatrix} \dfrac{\partial N_1^e}{\partial \xi} & \dfrac{\partial N_2^e}{\partial \xi} & \cdots & \dfrac{\partial N_n^e}{\partial \xi} \\ \dfrac{\partial N_1^e}{\partial \eta} & \dfrac{\partial N_2^e}{\partial \eta} & \cdots & \dfrac{\partial N_n^e}{\partial \eta} \end{bmatrix} \begin{bmatrix} x_1 & y_1 \\ x_2 & y_2 \\ \vdots & \vdots \\ x_n & y_n \end{bmatrix}. \tag{17.8}$$

Given a quadrilateral point of coordinates ξ, η we calculate the entries of $\mathbf{J}$ using (17.8). The inverse Jacobian $\mathbf{J}^{-1}$ is then obtained by numerically inverting this 2×2 matrix.

Remark 17.3. The symbolic inversion of $\mathbf{J}$ for arbitrary ξ, η in general leads to extremely complicated expressions unless the element has a particularly simple geometry, (for example rectangles as in Exercises 17.1–17.3). This was one of the difficulties that motivated the use of Gaussian numerical quadrature, as discussed in §17.3 below.

§17.2.4. The Strain-Displacement Matrix

The strain-displacement matrix $\mathbf{B}$ that appears in the computation of the element stiffness matrix is given by the general expression (14.18), which is reproduced here for convenience:

$$\mathbf{e} = \begin{bmatrix} e_{xx} \\ e_{yy} \\ 2e_{xy} \end{bmatrix} = \begin{bmatrix} \dfrac{\partial N_1^e}{\partial x} & 0 & \dfrac{\partial N_2^e}{\partial x} & 0 & \cdots & \dfrac{\partial N_n^e}{\partial x} & 0 \\ 0 & \dfrac{\partial N_1^e}{\partial y} & 0 & \dfrac{\partial N_2^e}{\partial y} & \cdots & 0 & \dfrac{\partial N_n^e}{\partial y} \\ \dfrac{\partial N_1^e}{\partial y} & \dfrac{\partial N_1^e}{\partial x} & \dfrac{\partial N_2^e}{\partial y} & \dfrac{\partial N_2^e}{\partial x} & \cdots & \dfrac{\partial N_n^e}{\partial y} & \dfrac{\partial N_n^e}{\partial x} \end{bmatrix} \mathbf{u}^e = \mathbf{B}\mathbf{u}^e. \tag{17.9}$$

The nonzero entries of $\mathbf{B}$ are partials of the shape functions with respect to x and y. The calculation of those partials is done by computing $\mathbf{J}$ via (17.8), inverting and using the chain rule (17.5).

```
Quad4IsoPShapeFunDer[ncoor_,qcoor_]:= Module[
  {Nf,dNx,dNy,dNξ,dNη,i,J11,J12,J21,J22,Jdet,ξ,η,x,y},
  {ξ,η}=qcoor;
   Nf={(1-ξ)*(1-η),(1+ξ)*(1-η),(1+ξ)*(1+η),(1-ξ)*(1+η)}/4;
   dNξ ={-(1-η), (1-η),(1+η),-(1+η)}/4;
   dNη= {-(1-ξ),-(1+ξ),(1+ξ), (1-ξ)}/4;
   x=Table[ncoor[[i,1]],{i,4}]; y=Table[ncoor[[i,2]],{i,4}];
   J11=dNξ.x; J12=dNξ.y; J21=dNη.x; J22=dNη.y;
   Jdet=Simplify[J11*J22-J12*J21];
   dNx= ( J22*dNξ-J12*dNη)/Jdet;  dNx=Simplify[dNx];
   dNy= (-J21*dNξ+J11*dNη)/Jdet;  dNy=Simplify[dNy];
   Return[{Nf,dNx,dNy,Jdet}]
];
```

FIGURE 17.1. A shape function module for the 4-node bilinear quadrilateral.

§17.2.5. *A Shape Function Implementation

To make the foregoing discussion more specific, Figure 17.1 shows the *shape function module* for the 4-node bilinear quadrilateral. This is a code fragment that returns the value of the shape functions and their $\{x, y\}$ derivatives at a given point of quadrilateral coordinates $\{\xi, \eta\}$. The module is invoked by saying

```
{Nf,Nfx,Nfy,Jdet}=Quad4IsoPShapeFunDer[ncoor,qcoor]
```
(17.10)

where the arguments are

`ncoor`	Quadrilateral node coordinates arranged in two-dimensional list form: `{{x1,y1},{x2,y2},{x3,y3},{x4,y4}}`.
`qcoor`	Quadrilateral coordinates $\{\xi,\ \eta\}$ of the point.

The module returns:

`Nf`	Value of shape functions, arranged as list `{Nf1,Nf2,Nf3,Nf4}`.
`Nfx`	Value of x-derivatives of shape functions, arranged as list `{Nfx1,Nfx2,Nfx3,Nfx4}`.
`Nfy`	Value of y-derivatives of shape functions, arranged as list `{Nfy1,Nfy2,Nfy3,Nfy4}`.
`Jdet`	Jacobian determinant.

Example 17.1. Consider a 4-node bilinear quadrilateral shaped as an axis-aligned 2:1 rectangle, with $2a$ and a as the x and y dimensions, respectively. The node coordinate array is `ncoor={{0,0},{2*a,0},{2*a,a},{0,a}}`. The shape functions and their $\{x, y\}$ derivatives are to be evaluated at the rectangle center $\xi = \eta = 0$. The appropiate call is

```
{Nf,Nfx,Nfy,Jdet}=Quad4IsoPShapeFunDer[ncoor,{0,0}]
```

This returns `Nf={1/8,1/8,3/8,3/8}`, `Nfx={-1/(8*a),1/(8*a),3/(8*a),-3/(8*a)}`, `Nfy={-1/(2*a),-1/(2*a),1/(2*a),1/(2*a)}` and `Jdet=a^2/2`.

§17.3. Numerical Integration by Gauss Rules

Numerical integration is essential for practical evaluation of integrals over isoparametric element domains. The standard practice has been to use *Gauss integration* because such rules use a *minimal number of sample points to achieve a desired level of accuracy*. This economy is important for efficient element calculations, since a *matrix product* is evaluated at each sample point. The fact that the location of the sample points in Gauss rules is usually given by non-rational numbers is of no concern in digital computation.

§17.3.1. One Dimensional Rules

The classical Gauss integration rules are defined by

$$\int_{-1}^{1} F(\xi)\, d\xi \approx \sum_{i=1}^{p} w_i F(\xi_i). \tag{17.11}$$

Here $p \geq 1$ is the number of Gauss integration points (also known as sample points), w_i are the integration weights, and ξ_i are sample-point abcissae in the interval $[-1,1]$. The use of the canonical interval $[-1,1]$ is no restriction, because an integral over another range, say from a to b, can be

Table 17.1 - One-Dimensional Gauss Rules with 1 through 5 Sample Points

Points	Rule
1	$\int_{-1}^{1} F(\xi)\,d\xi \approx 2F(0)$
2	$\int_{-1}^{1} F(\xi)\,d\xi \approx F(-1/\sqrt{3}) + F(1/\sqrt{3})$
3	$\int_{-1}^{1} F(\xi)\,d\xi \approx \frac{5}{9}F(-\sqrt{3/5}) + \frac{8}{9}F(0) + \frac{5}{9}F(\sqrt{3/5})$
4	$\int_{-1}^{1} F(\xi)\,d\xi \approx w_{14}F(\xi_{14}) + w_{24}F(\xi_{24}) + w_{34}F(\xi_{34}) + w_{44}F(\xi_{44})$
5	$\int_{-1}^{1} F(\xi)\,d\xi \approx w_{15}F(\xi_{15}) + w_{25}F(\xi_{25}) + w_{35}F(\xi_{35}) + w_{45}F(\xi_{45}) + w_{55}F(\xi_{55})$

For the 4-point rule, $\xi_{34} = -\xi_{24} = \sqrt{(3-2\sqrt{6/5})/7}$, $\xi_{44} = -\xi_{14} = \sqrt{(3+2\sqrt{6/5})/7}$, $w_{14} = w_{44} = \frac{1}{2} - \frac{1}{6}\sqrt{5/6}$, and $w_{24} = w_{34} = \frac{1}{2} + \frac{1}{6}\sqrt{5/6}$.

For the 5-point rule, $\xi_{55} = -\xi_{15} = \frac{1}{3}\sqrt{5+2\sqrt{10/7}}$, $\xi_{45} = -\xi_{35} = \frac{1}{3}\sqrt{5-2\sqrt{10/7}}$, $\xi_{35} = 0$, $w_{15} = w_{55} = (322 - 13\sqrt{70})/900$, $w_{25} = w_{45} = (322 + 13\sqrt{70})/900$ and $w_{35} = 512/900$.

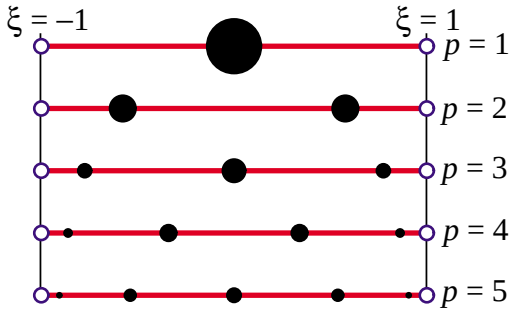

FIGURE 17.2. The first five one-dimensional Gauss rules $p = 1, 2, 3, 4, 5$ depicted over the line segment $\xi \in [-1, +1]$. Sample point locations are marked with black circles. The radii of those circles are proportional to the integration weights.

transformed to $[-1, +1]$ via a simple linear transformation of the independent variable, as shown in the Remark below.

The first five one-dimensional Gauss rules, illustrated in Figure 17.2, are listed in Table 17.1. These integrate exactly polynomials in ξ of orders up to 1, 3, 5, 7 and 9, respectively. In general a one-dimensional Gauss rule with p points integrates exactly polynomials of order up to $2p - 1$. This is called the *degree* of the formula.

Remark 17.4. A more general integral, such as $F(x)$ over $[a, b]$ in which $\ell = b - a > 0$, is transformed to the canonical interval $[-1, 1]$ through the mapping $x = \frac{1}{2}a(1-\xi) + \frac{1}{2}b(1+\xi) = \frac{1}{2}(a+b) + \frac{1}{2}\ell\xi$, or $\xi = (2/\ell)(x - \frac{1}{2}(a+b))$. The Jacobian of this mapping is $J = dx/d\xi = 1/2\ell$. Thus

$$\int_a^b F(x)\,dx = \int_{-1}^{1} F(\xi)\,J\,d\xi = \int_{-1}^{1} F(\xi)\,\tfrac{1}{2}\ell\,d\xi. \tag{17.12}$$

```
LineGaussRuleInfo[{rule_,numer_},point_]:= Module[
  {g2={-1,1}/Sqrt[3],w3={5/9,8/9,5/9},
   g3={-Sqrt[3/5],0,Sqrt[3/5]},
   w4={(1/2)-Sqrt[5/6]/6, (1/2)+Sqrt[5/6]/6,
       (1/2)+Sqrt[5/6]/6, (1/2)-Sqrt[5/6]/6},
   g4={-Sqrt[(3+2*Sqrt[6/5])/7],-Sqrt[(3-2*Sqrt[6/5])/7],
        Sqrt[(3-2*Sqrt[6/5])/7], Sqrt[(3+2*Sqrt[6/5])/7]},
   g5={-Sqrt[5+2*Sqrt[10/7]],-Sqrt[5-2*Sqrt[10/7]],0,
        Sqrt[5-2*Sqrt[10/7]], Sqrt[5+2*Sqrt[10/7]]}/3,
   w5={322-13*Sqrt[70],322+13*Sqrt[70],512,
       322+13*Sqrt[70],322-13*Sqrt[70]}/900,
   i=point,p=rule,info={{Null,Null},0}},
  If [p==1, info={0,2}];
  If [p==2, info={g2[[i]],1}];
  If [p==3, info={g3[[i]],w3[[i]]}];
  If [p==4, info={g4[[i]],w4[[i]]}];
  If [p==5, info={g5[[i]],w5[[i]]}];
  If [numer, Return[N[info]], Return[Simplify[info]]];
];
```

FIGURE 17.3. A *Mathematica* module that returns the first five one-dimensional Gauss rules.

Remark 17.5. Higher order Gauss rules are tabulated in standard manuals for numerical computation. For example, the widely used Handbook of Mathematical Functions [2] lists (in Table 25.4) rules with up to 96 points. For $p > 6$ the abscissas and weights of sample points are not expressible as rational numbers or radicals, and can only be given as floating-point numbers.

§17.3.2. Implementation of 1D Rules

The *Mathematica* module shown in Figure 17.3 returns either exact or floating-point information for the first five unidimensional Gauss rules. To get information for the i^{th} point of the p^{th} rule, in which $1 \le i \le p$ and $p = 1, 2, 3, 4, 5$, call the module as

```
{xii,wi}=LineGaussRuleInfo[{p,numer},i]
```  (17.13)

Logical flag `numer` is `True` to get numerical (floating-point) information, or `False` to get exact information. The module returns the sample point abcissa ξ_i in `xii` and the weight w_i in `wi`. If `p` is not in the implemented range 1 through 5, the module returns `{Null,0}`.

Example 17.2. `{xi,w}=LineGaussRuleInfo[{3,False},2]` returns `xi=0` and `w=8/9`, whereas `{xi,w}=LineGaussRuleInfo[{3,True},2]` returns (to 16 places) `xi=0.` and `w=0.888888888888889`.

§17.3.3. Two Dimensional Rules

The simplest two-dimensional Gauss rules are called *product rules*. They are obtained by applying the one-dimensional rules to each independent variable in turn. To apply these rules we must first reduce the integrand to the canonical form:

$$\int_{-1}^{1}\int_{-1}^{1} F(\xi,\eta)\,d\xi\,d\eta = \int_{-1}^{1} d\eta \int_{-1}^{1} F(\xi,\eta)\,d\xi. \tag{17.14}$$

Once this is done we can process numerically each integral in turn:

$$\int_{-1}^{1}\int_{-1}^{1} F(\xi,\eta)\,d\xi\,d\eta = \int_{-1}^{1} d\eta \int_{-1}^{1} F(\xi,\eta)\,d\xi \approx \sum_{i=1}^{p_1}\sum_{j=1}^{p_2} w_i w_j F(\xi_i,\eta_j). \tag{17.15}$$

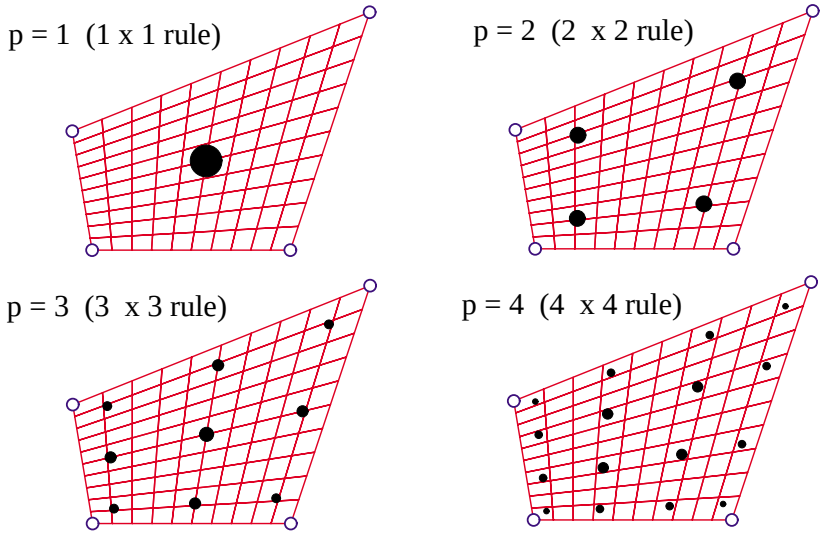

FIGURE 17.4. The first four two-dimensional Gauss product rules $p = 1, 2, 3, 4$ depicted over a straight-sided quadrilateral region. Sample points are marked with black circles. The areas of these circles are proportional to the integration weights.

where p_1 and p_2 are the number of Gauss points in the ξ and η directions, respectively. Usually the same number $p = p_1 = p_2$ is chosen if the shape functions are taken to be the same in the ξ and η directions. This is in fact the case for all quadrilateral elements presented here. The first four two-dimensional Gauss product rules with $p = p_1 = p_2$ are illustrated in Figure 17.4.

§17.3.4. Implementation of 2D Gauss Rules

The *Mathematica* module listed in Figure 17.5 implements two-dimensional product Gauss rules having 1 through 5 points in each direction. The number of points in each direction may be the same or different. If the rule has the same number of points p in both directions the module is called in either of two ways:

```
{{xii,etaj},wij}=QuadGaussRuleInfo[{p, numer}, {i,j}]
{{xii,etaj},wij}=QuadGaussRuleInfo[{p, numer},k ]
```
(17.16)

The first form is used to get information for point $\{i, j\}$ of the $p \times p$ rule, in which $1 \le i \le p$ and $1 \le j \le p$. The second form specifies that point by a "visiting counter" k that runs from 1 through p^2; if so $\{i, j\}$ are internally extracted[1] as `j=Floor[(k-1)/p]+1; i=k-p*(j-1).`

If the integration rule has p_1 points in the ξ direction and p_2 points in the η direction, the module may be called also in two ways:

```
{{xii,etaj},wij}=QuadGaussRuleInfo[{{p1,p2}, numer},{i,j}]
{{xii,etaj},wij}=QuadGaussRuleInfo[{{p1,p2}, numer},k ]
```
(17.17)

The meaning of the second argument is as follows. In the first form i runs from 1 to p_1 and j from 1 to p_2. In the second form k runs from 1 to $p_1 p_2$; if so i and j are extracted by `j=Floor[(k-1)/p1]+1;`

[1] Indices i and j are denoted by `i1` and `i2`, respectively, inside the module.

```
QuadGaussRuleInfo[{rule_,numer_},point_]:= Module[
 {ξ,η,p1,p2,i,j,w1,w2,m,info={{Null,Null},0}},
  If [Length[rule]==2,  {p1,p2}=rule, p1=p2=rule];
  If [p1<0, Return[QuadNonProductGaussRuleInfo[
      {-p1,numer},point]]];
  If [Length[point]==2, {i,j}=point, m=point;
      j=Floor[(m-1)/p1]+1; i=m-p1*(j-1) ];
  {ξ,w1}=  LineGaussRuleInfo[{p1,numer},i];
  {η,w2}=  LineGaussRuleInfo[{p2,numer},j];
  info={{ξ,η},w1*w2};
  If [numer, Return[N[info]], Return[Simplify[info]]];
];
```

FIGURE 17.5. A *Mathematica* module that returns two-dimensional product Gauss rules.

`i=k-p1*(i-1)`. In all four forms, logical flag `numer` is set to `True` if numerical information is desired and to `False` if exact information is desired.

The module returns ξ_i and η_j in `xii` and `etaj`, respectively, and the weight product $w_i w_j$ in `wij`. This code is used in the Exercises at the end of the chapter. If the inputs are not in range, the module returns `{{Null,Null},0}`.

Example 17.3. `{{xi,eta},w}=QuadGaussRuleInfo[{3,False},{2,3}]` returns `xi=0`, `eta=Sqrt[3/5]` and `w=40/81`.

Example 17.4. `{{xi,eta},w}=QuadGaussRuleInfo[{3,True},{2,3}]` returns (to 16-place precision) `xi=0.`, `eta=0.7745966692414834` and `w=0.49382716049382713`.

§17.4. The Stiffness Matrix

The stiffness matrix of a general plane stress element is given by the expression (14.23), which is reproduced here:

$$\mathbf{K}^e = \int_{\Omega^e} h\, \mathbf{B}^T \mathbf{E} \mathbf{B}\, d\Omega^e \tag{17.18}$$

Of the terms that appear in (17.18) the strain-displacement matrix **B** has been discussed previously. The thickness h, if variable, may be interpolated via the shape functions. The stress-strain matrix **E** is usually constant in elastic problems, but we could in principle interpolate it as appropriate should it vary over the element. To integrate (17.18) numerically by a two-dimensional product Gauss rule, we have to reduce it to the canonical form (17.14), that is

$$\mathbf{K}^e = \int_{-1}^{1} \int_{-1}^{1} \mathbf{F}(\xi, \eta)\, d\xi\, d\eta. \tag{17.19}$$

If ξ and η are the quadrilateral coordinates, everything in (17.19) already fits this form, except the element of area $d\Omega^e$.

To complete the reduction we need to express $d\Omega^e$ in terms of the differentials $d\xi$ and $d\eta$. The desired relation is (see Remark below)

$$d\Omega^e = dx\, dy = \det \mathbf{J}\; d\xi\, d\eta = J\, d\xi\, d\eta. \tag{17.20}$$

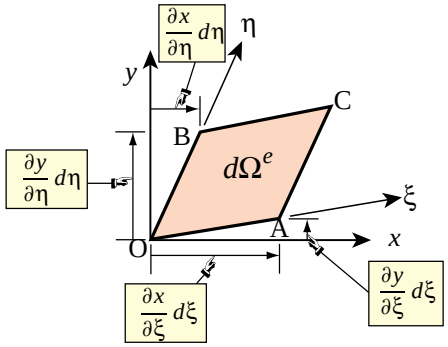

FIGURE 17.6. Geometric interpretation of the Jacobian-determinant formula.

We therefore have

$$\mathbf{F}(\xi,\eta) = h\,\mathbf{B}^T\mathbf{E}\mathbf{B}\,\det\mathbf{J}. \tag{17.21}$$

This matrix function can be numerically integrated over the domain $-1 \le \xi \le +1$, $-1 \le \eta \le +1$ by an appropriate Gauss product rule.

Remark 17.6. To geometrically justify the area transformation formula (17.20), consider the element of area OACB depicted in Figure 17.6. The area of this differential parallelogram can be computed as

$$\begin{aligned} dA = \vec{OB}\times\vec{OA} &= \frac{\partial x}{\partial \xi}d\xi\,\frac{\partial y}{\partial \eta}d\eta - \frac{\partial x}{\partial \eta}d\eta\,\frac{\partial y}{\partial \xi}d\xi \\ &= \begin{vmatrix} \frac{\partial x}{\partial \xi} & \frac{\partial x}{\partial \eta} \\ \frac{\partial y}{\partial \xi} & \frac{\partial y}{\partial \eta} \end{vmatrix} d\xi\,d\eta = |\mathbf{J}|\,d\xi\,d\eta = \det\mathbf{J}\,d\xi\,d\eta. \end{aligned} \tag{17.22}$$

This formula can be extended to any number of dimensions, as shown in textbooks on differential geometry; for example [265,319,708].

§17.5. *Integration Variants

Several deviations from the standard integration schemes described in the foregoing sections are found in the FEM literature. Two variations are described below and supplemented with motivation Exercises.

§17.5.1. *Weighted Integration

It is sometimes useful to form the element stiffness as a linear combination of stiffnesses produced by two different integration rules Such schemes are known as *weighted integration* methods. They are distinguished from the selective-integration schemes described in the next subsection in that the constitutive properties are not modified.

For the 4-node bilinear element weighted integration is done by combining the stiffnesses $\mathbf{K}^e_{1\times1}$ and $\mathbf{K}^e_{2\times2}$ produced by 1×1 and 2×2 Gauss product rules, respectively:

$$\mathbf{K}^e_\beta = (1-\beta)\mathbf{K}^e_{1\times1} + \beta\mathbf{K}^e_{2\times2}. \tag{17.23}$$

Here β is a scalar in the range $[0,1]$. If $\beta = 0$ or $\beta = 1$ one recovers the element integrated by the 1×1 or 2×2 rule, respectively.[2]

[2] For programming the combination (17.23) may be regarded as a 5-point integration rule with weights $w_1 = 4(1-\beta)$ at the sample point at $\xi = \eta = 0$ and $w_i = \beta$ $(i = 2,3,4,5)$ at the four sample points at $\xi = \pm1/\sqrt{3}$, $\eta = \pm1/\sqrt{3}$.

The idea behind (17.23) is that $\mathbf{K}^e_{1\times 1}$ is rank-deficient and too soft whereas $\mathbf{K}^e_{2\times 2}$ is rank-sufficient but too stiff. A combination of too-soft and too-stiff hopefully "balances" the stiffness. An application of this idea to the mitigation of *shear locking* for modeling in-plane bending is the subject of Exercise E17.4.

§17.5.2. *Selective Integration

In the FEM literature the term *selective integration* is used to described a scheme for forming $\mathbf{K}^e$ as the sum of two or more matrices computed with different integration rules *and* different constitutive properties.[3] We consider here the case of a two-way decomposition. Split the plane stress constitutive matrix $\mathbf{E}$ into two:

$$\mathbf{E} = \mathbf{E}_{\rm I} + \mathbf{E}_{\rm II} \tag{17.24}$$

This is called a *stress-strain splitting*. Inserting (17.24) into (17.13) the expression of the stiffness matrix becomes

$$\mathbf{K}^e = \int_{\Omega^e} h\,\mathbf{B}^T\mathbf{E}_{\rm I}\mathbf{B}\,d\Omega^e + \int_{\Omega^e} h\,\mathbf{B}^T\mathbf{E}_{\rm II}\mathbf{B}\,d\Omega^e = \mathbf{K}^e_{\rm I} + \mathbf{K}^e_{\rm II}. \tag{17.25}$$

If these two integrals were done through the same integration rule, the stiffness would be identical to that obtained by integrating $h\,\mathbf{B}^T\mathbf{E}\,\mathbf{B}\,d\Omega^e$. The trick is to use two different rules: rule (I) for the first integral and rule (II) for the second.

In practice selective integration is mostly useful for the 4-node bilinear quadrilateral. For this element rules (I) and (II) are the 1×1 and 2×2 Gauss product rules, respectively. Exercises E17.5–7 investigate stress-strain splittings (17.24) that improve the in-plane bending performance of rectangular elements.

Notes and Bibliography

The 4-node quadrilateral has a checkered history. It was first derived as a rectangular panel with edge reinforcements (not included here) by Argyris in his 1954 *Aircraft Engineering* series [22, p. 49 in the Butterworths reprint]. Argyris used bilinear displacement interpolation in Cartesian coordinates.[4]

After much flailing, a conforming generalization to arbitrary geometry was published in 1964 by Taig and Kerr [719] using quadrilateral-fitted coordinates already denoted as $\{\xi, \eta\}$ but running from 0 to 1. (Reference [719] cites an 1961 English Electric Aircraft internal report as original source but [397, p. 520] remarks that the work goes back to 1957.) Bruce Irons, who was aware of Taig's work while at Rolls Royce, changed the $\{\xi, \eta\}$ range to $[-1, 1]$ to fit Gauss quadrature tables. He proceeded to create the seminal isoparametric family as a far-reaching extension upon moving to Swansea [64,197,394,397].

Gauss integration is also called Gauss-Legendre quadrature. Gauss presented these rules, derived from first principles, in 1814; cf. Sec 4.11 of [310]. Legendre's name is often adjoined because the abcissas of the 1D sample points turned out to be the zeros of Legendre polynomials. A systematic description is given in [706]. For references in multidimensional numerical integration, see **Notes and Bibliography** in Chapter 24.

Selective and reduced integration in FEM developed in the early 1970s, and by now there is a huge literature. An excellent textbook source is [385].

References

Referenced items have been moved to Appendix R.

---

[3] This technique is also called "selective reduced integration" to reflect the fact that one of the rules (the "reduced rule") underintegrates the element.

[4] This work is probably the first derivation of a continuum-based finite element by assumed displacements. As noted in §1.7.1, Argyris was aware of the ongoing work in stiffness methods at Turner's group in Boeing, but the plane stress models presented in [758] were derived by interelement flux assumptions. Argyris used the unit displacement theorem, displacing each DOF in turn by one. The resulting displacement pattern is now called a shape function.

Homework Exercises for Chapter 17

Isoparametric Quadrilaterals

The *Mathematica* module `Quad4IsoPMembraneStiffness` listed in Figure E17.1 computes the element stiffness matrix of the 4-node bilinear quadrilateral. This module is useful as a tool for the Exercises that follow.

```
Quad4IsoPMembraneStiffness[ncoor_,Emat_,th_,options_]:=
  Module[{i,k,p=2,numer=False,h=th,qcoor,c,w,Nf,
    dNx,dNy,Jdet,Be,Ke=Table[0,{8},{8}]},
  If [Length[options]==2, {numer,p}=options,{numer}=options];
  If [p<1||p>4, Print["p out of range"]; Return[Null]];
  For [k=1, k<=p*p, k++,
       {qcoor,w}= QuadGaussRuleInfo[{p,numer},k];
       {Nf,dNx,dNy,Jdet}=Quad4IsoPShapeFunDer[ncoor,qcoor];
        If [Length[th]==4, h=th.Nf]; c=w*Jdet*h;
        Be={Flatten[Table[{dNx[[i]],       0},{i,4}]],
            Flatten[Table[{0,       dNy[[i]]},{i,4}]],
            Flatten[Table[{dNy[[i]],dNx[[i]]},{i,4}]]};
        Ke+=Simplify[c*Transpose[Be].(Emat.Be)];
      ]; Return[Simplify[Ke]]
   ];
```

FIGURE E17.1. Mathematica module to compute the stiffness matrix of a 4-node bilinear quadrilateral in plane stress.

The module makes use of the shape function module `Quad4IsoPShapeFunDer` listed in Figure 17.1, and of the Gauss integration modules `QuadGaussRuleInfo` and (indirectly) `LineGaussRuleInfo`, listed in Figures 17.5 and are included in the web-posted Notebook `Quad4Stiffness.nb`.[5] The module is invoked as

```
Ke=Quad4IsoPMembraneStiffness[ncoor,Emat,thick,options]
```
(E17.1)

The arguments are:

`ncoor` Quadrilateral node coordinates arranged in two-dimensional list form: `{{x1,y1},{x2,y2},{x3,y3},{x4,y4}}`.

`Emat` A two-dimensional list storing the 3×3 plane stress matrix of elastic moduli:

$$\mathbf{E} = \begin{bmatrix} E_{11} & E_{12} & E_{13} \\ E_{12} & E_{22} & E_{23} \\ E_{13} & E_{23} & E_{33} \end{bmatrix} \tag{E17.2}$$

arranged as `{{E11,E12,E33},{E12,E22,E23},{E13,E23,E33}}`. Must be symmetric. If the material is isotropic with elastic modulus E and Poisson's ratio ν, this matrix becomes

$$\mathbf{E} = \frac{E}{1-\nu^2}\begin{bmatrix} 1 & \nu & 0 \\ \nu & 1 & 0 \\ 0 & 0 & \frac{1}{2}(1-\nu) \end{bmatrix} \tag{E17.3}$$

`thick` The plate thickness specified either as a four-entry list: `{h1,h2,h3,h4}` or as a scalar: `h`.

[5] This Notebook does not include scripts for doing the Exercises below, although it has some text statements at the bottom of the cell. You will need to enter the Exercise scripts yourself.

The first form is used to specify an element of variable thickness, in which case the entries are the four corner thicknesses and h is interpolated bilinearly. The second form specifies uniform thickness.

`options` Processing options. This list may contain two items: {`numer,p`} or one: {`numer`}.

`numer` is a logical flag with value `True` or `False`. If `True`, the computations are done in floating point arithmetic. For symbolic or exact arithmetic work set `numer` to `False`.[6]

`p` specifies the Gauss product rule to have `p` points in each direction. `p` may be 1 through 4. For rank sufficiency, `p` must be 2 or higher. If `p` is 1 the element will be rank deficient by two.[7] If omitted `p` = 2 is assumed.

The module returns `Ke` as an 8×8 symmetric matrix pertaining to the following arrangement of nodal displacements:

$$\mathbf{u}^e = [\, u_{x1} \quad u_{y1} \quad u_{x2} \quad u_{y2} \quad u_{x3} \quad u_{y3} \quad u_{x4} \quad u_{y4} \,]^T . \tag{E17.4}$$

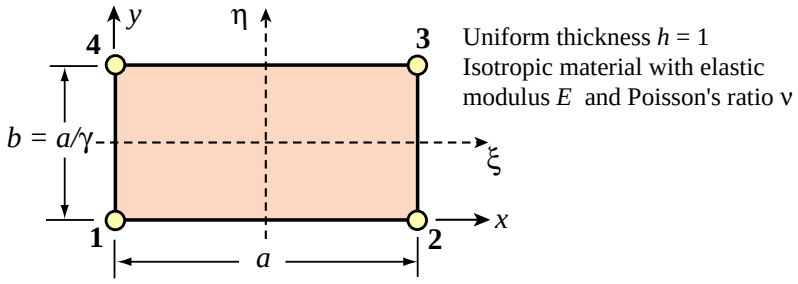

FIGURE E17.2. Element for Exercises 17.1 to 17.3.

For the following three exercises we consider the specialization of the general 4-node bilinear quadrilateral to a *rectangular* element dimensioned a and b in the x and y directions, respectively, as depicted in Figure E17.2. The element has uniform unit thickness h. The material is isotropic with elastic modulus E and Poisson's ratio ν and consequently $\mathbf{E}$ reduces to (E17.3). The stiffness matrix of this element can be expressed in closed form.[8] For convenience define $\gamma = a/b$ (rectangle aspect ratio), $\psi_1 = (1+\nu)\gamma$, $\psi_2 = (1-3\nu)\gamma$, $\psi_3 = 2 + (1-\nu)\gamma^2$, $\psi_4 = 2\gamma^2 + (1-\nu)$, $\psi_5 = (1-\nu)\gamma^2 - 4$, $\psi_6 = (1-\nu)\gamma^2 - 1$, $\psi_7 = 4\gamma^2 - (1-\nu)$ and $\psi_8 = \gamma^2 - (1-\nu)$. Then the stiffness matrix in closed form is

$$\mathbf{K}^e = \frac{Eh}{24\gamma(1-\nu^2)} \begin{bmatrix} 4\psi_3 & 3\psi_1 & 2\psi_5 & -3\psi_2 & -2\psi_3 & -3\psi_1 & -4\psi_6 & 3\psi_2 \\ & 4\psi_4 & 3\psi_2 & 4\psi_8 & -3\psi_1 & -2\psi_4 & -3\psi_2 & -2\psi_7 \\ & & 4\psi_3 & -3\psi_1 & -4\psi_6 & -3\psi_2 & -2\psi_3 & 3\psi_1 \\ & & & 4\psi_4 & 3\psi_2 & -2\psi_7 & 3\psi_1 & -2\psi_4 \\ & & & & 4\psi_3 & 3\psi_1 & 2\psi_5 & -3\psi_2 \\ & & & & & 4\psi_4 & 3\psi_2 & 4\psi_8 \\ & & & & & & 4\psi_3 & -3\psi_1 \\ \text{symm} & & & & & & & 4\psi_4 \end{bmatrix} . \tag{E17.5}$$

[6] The reason for this option is speed. A symbolic or exact computation can take orders of magnitude more time than a floating-point evaluation. This becomes more pronounced as elements get more complicated.

[7] The rank of an element stiffness is discussed in Chapter 19.

[8] This closed form can be obtained by either exact integration, or numerical integration with a 2×2 or higher Gauss rule.

EXERCISE 17.1 [C:20] Exercise the *Mathematica* module of Figure E17.1 with the following script:

```
ClearAll[Em,nu,a,b,h];  Em=48; h=1; a=4; b=2; nu=0;
ncoor={{0,0},{a,0},{a,b},{0,b}};
Emat=Em/(1-nu^2)*{{1,nu,0},{nu,1,0},{0,0,(1-nu)/2}};
For [p=1, p<=4, p++,
     Ke= Quad4IsoPMembraneStiffness[ncoor,Emat,h,{True,p}];
     Print["Gauss integration rule: ",p," x ",p];
     Print["Ke=",Chop[Ke]//MatrixForm];
     Print["Eigenvalues of Ke=",Chop[Eigenvalues[N[Ke]]]]
];
```

Verify that for integration rules `p=2,3,4` the stiffness matrix does not change and has three zero eigenvalues, which correspond to the three two-dimensional rigid body modes. On the other hand, for `p` = 1 the stiffness matrix is different and displays five zero eigenvalues, which is physically incorrect. (This phenomenon is analyzed further in Chapter 19.) Question: why does the stiffness matrix stays exactly the same for $p \geq 2$? Hint: take a look at the entries of the integrand $h\,\mathbf{B}^T\mathbf{E}\mathbf{B}\,J$;for a *rectangular geometry* are those polynomials in ξ and η, or rational functions? If the former, of what polynomial order in ξ and η are the entries?

EXERCISE 17.2 [C:20] Check the rectangular element stiffness closed form given in (E17.5). This may be done by hand (takes a while) or (quicker) running the script of Figure E17.3, which calls the *Mathematica* module of Figure E17.1.

```
ClearAll[Em,ν,a,b,h,γ];  b=a/γ;
ncoor={{0,0},{a,0},{a,b},{0,b}};
Emat=Em/(1-ν^2)*{{1,ν,0},{ν,1,0},{0,0,(1-ν)/2}};
Ke= Quad4IsoPMembraneStiffness[ncoor,Emat,h,{False,2}];
scaledKe=Simplify[Ke*(24*(1-ν^2)*γ/(Em*h))];
Print["Ke=",Em*h/(24*γ*(1-ν^2)),"*\n",scaledKe//MatrixForm];
```

FIGURE E17.3. Script suggested for Exercise E17.2.

The scaling introduced in the last two lines is for matrix visualization convenience. Verify (E17.5) by printout inspection and report any typos to instructor.

EXERCISE 17.3 [A/C:25=5+10+10] A Bernoulli-Euler plane beam of thin rectangular cross-section with span L, height b and thickness h (normal to the plane of the figure) is bent under end moments M as illustrated in Figure E17.4. The beam is fabricated of isotropic material with elastic modulus E and Poisson's ratio ν. The *exact* solution of the beam problem (from both the theory-of-elasticity and beam-theory standpoints) is a constant bending moment M along the span. Consequently the beam deforms with uniform curvature $\kappa = M/(E\,I_z)$, in which $I_z = \frac{1}{12}hb^3$ is the cross-section second moment of inertia about z.

The beam is modeled with *one layer* of identical 4-node iso-P bilinear quadrilaterals through its height. These are rectangles with horizontal dimension a; in the Figure $a = L/4$. The aspect ratio b/a is denoted by γ. By analogy with the exact solution, all rectangles in the finite element model will undergo the same deformation. We can therefore isolate a typical element as illustrated in Figure E17.4.

The exact displacement field for the beam segment referred to the $\{x, y\}$ axes placed at the element center as shown in the bottom of Figure E17.4, are

$$u_x = -\kappa xy, \quad u_y = \tfrac{1}{2}\kappa(x^2 + \nu y^2), \tag{E17.6}$$

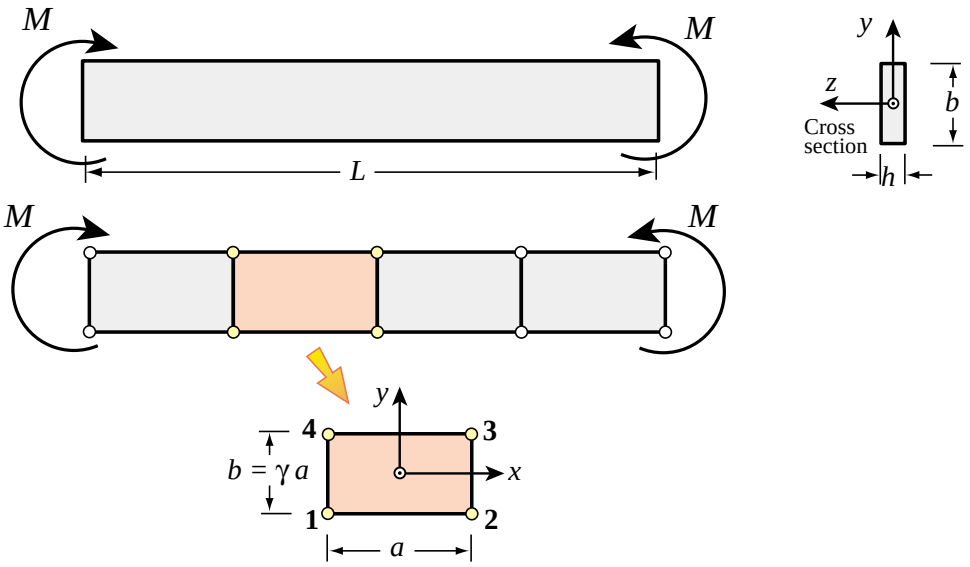

FIGURE E17.4. Pure bending of Bernoulli-Euler plane beam of thin rectangular cross section, for Exercises 17.3–7. The beam is modeled by one layer of 4-node iso-P bilinear quadrilaterals through its height.

where κ is the deformed beam curvature M/EI. The stiffness equations of the typical rectangular element are given by the close form expression (E17.5).

The purpose of this Exercise is to compare the in-plane bending response of the 4-node iso-P bilinear rectangle to that of a Bernoulli-Euler beam element (which would be exact for this configuration). The quadrilateral element will be called *x-bending exact* if it reproduces the beam solution for all $\{\gamma, \nu\}$. This comparison is distributed into three items.

(a) Check that (E17.6), as a plane stress 2D elasticity solution, is in full agreement with Bernoulli-Euler beam theory. This can be done by computing the strains $e_{xx} = \partial u_x/\partial x$, $e_{yy} = \partial u_y/\partial y$ and $2e_{xy} = \partial u_y/\partial x + \partial u_x/\partial y$. Then get the stresses σ_{xx}, σ_{yy} and σ_{xy} through the plane stress constitutive matrix (E17.3) of an isotropic material. Verify that both σ_{yy} and σ_{xy} vanish for any ν, and that $\sigma_{xx} = -E\,\kappa y = -My/I_z$, which agrees with equation (13.4) in Chapter 13.

(b) Compute the strain energy $U_{\text{quad}} = \frac{1}{2}(\mathbf{u}_{\text{beam}})^T\mathbf{K}^e\mathbf{u}_{\text{beam}}$ absorbed by the 4-node element under nodal displacements $\mathbf{u}_{\text{beam}}$ constructed by evaluating (E17.6) at the nodes 1,2,3,4. To simplify this calculation, it is convenient to decompose that vector as follows:

$$\begin{aligned}\mathbf{u}_{\text{beam}} = \mathbf{u}^x_{\text{beam}} + \mathbf{u}^y_{\text{beam}} &= \tfrac{1}{4}\kappa ab\,[-1\ \ 0\ \ 1\ \ 0\ \ -1\ \ 0\ \ 1\ \ 0\,]^T \\ &\quad + \tfrac{1}{8}\kappa(a^2+\nu b^2)\,[\,0\ \ 1\ \ 0\ \ 1\ \ 0\ \ 1\ \ 0\ \ 1\,]^T\end{aligned} \tag{E17.7}$$

Explain why $\mathbf{K}^e\mathbf{u}^y_{\text{beam}}$ must vanish and consequently

$$U_{\text{quad}} = \tfrac{1}{2}(\mathbf{u}^x_{\text{beam}})^T\mathbf{K}^e\mathbf{u}^x_{\text{beam}}. \tag{E17.8}$$

This energy can be easily computed by *Mathematica* by using the first 4 lines of the script of the previous Exercise, except that here `ncoor={{-a,-b},{a,-b},{a,b},{-a,b}}/2`. If vector $\mathbf{u}^x_{\text{beam}}$ is formed in `u` as a one-dimensional list, `Uquad=Simplify[u.Ke.u/2]`. This should come out as a function of M, E, ν, h, a and γ because $\kappa = M/(EI_z) = 12M/(Eha^3\gamma^3)$.

(c) From Mechanics of Materials, or equation (13.7) of Chapter 13, the strain energy absorbed by the beam segment of length a under a constant bending moment M is $U_{beam} = \frac{1}{2}M\kappa a = M^2a/(2EI_z) =$

$6M^2/(Eha^2\gamma^3)$. Form the *energy ratio* $r = U_{quad}/U_{beam}$ and show that it is a function of the rectangle aspect ratio $\gamma = b/a$ and of Poisson's ratio ν only:

$$r = r(\gamma, \nu) = \frac{1 + 2/\gamma^2 - \nu}{(2/\gamma^2)(1 - \nu^2)}. \tag{E17.9}$$

This happens to be the ratio of the 2D model solution to the exact (beam) solution. Hence $r = 1$ means that we get the exact answer, that is the 2D model is x-bending exact. If $r > 1$ the 2D model is overstiff, and if $r < 1$ the 2D model is overflexible. Evidently $r > 1$ for all γ if $0 \le \nu \le \frac{1}{2}$. Moreover if $b << a$, $r >> 1$; for example if $a = 10b$ and $\nu = 0$, $r \approx 50$ and the 2D model gives only about 2% of the correct solution. This phenomenon is referred to in the FEM literature as *shear locking*, because overstiffness is due to the bending motion triggering spurious shear energy in the element. Remedies to shear locking at the element level are studied in advanced FEM courses. Draw conclusions as to the adequacy or inadequacy of the 2D model to capture inplane bending effects, and comment on how you might improve results by modifying the discretization of Figure E17.4.[9]

EXERCISE 17.4 [A+C:20] A naive remedy to shear locking can be attempted with the weighted integration methodology outlined in §17.6.1. Let $\mathbf{K}^e_{1\times1}$ and $\mathbf{K}^e_{2\times2}$ denote the element stiffnesses produced by 1×1 and 2×2 Gauss product rules, respectively. Take

$$\mathbf{K}^e_\beta = (1 - \beta)\mathbf{K}^e_{1\times1} + \beta\mathbf{K}^e_{2\times2} \tag{E17.10}$$

where β is adjusted so that shear locking is reduced or eliminated. It is not difficult to find β if the element is rectangular and isotropic. For the definition of *x-bending exact* please read the previous Exercise. Inserting $\mathbf{K}^e_\beta$ into the test introduced there verify that

$$r = \frac{\beta(1 + 2\gamma^2 - \nu)}{(2/\gamma^2)(1 - \nu^2)}. \tag{E17.11}$$

Whence show that if

$$\beta = \frac{2/\gamma^2(1 - \nu^2)}{1 + 2/\gamma^2 - \nu}, \tag{E17.12}$$

then $r \equiv 1$ for all $\{\gamma, \nu\}$ and the element is x-bending exact. A problem with this idea is that it does not make it y-bending exact because $r(\gamma) \ne r(1/\gamma)$ if $\gamma \ne 1$. Moreover the device is not easily extended to non-rectangular geometries or non-isotropic material.

EXERCISE 17.5 [A+C:35] (Advanced) To understand this Exercise please begin by reading Exercise 17.3, and the concept of shear locking. The material is again assumed isotropic with elastic modules E and Poisson's ratio ν. The 4-node rectangular element will be said to be *bending exact* if $r = 1$ for any $\{\gamma, \nu\}$ if the bending test described in Exercise 17.3 is done in both x and y directions. A bending-exact element is completely shear-lock-free.

The selective integration scheme outlined in §17.6.2 is more effective than weighted integration (covered in the previous exercise) to fully eliminate shear locking. Let the integration rules (I) and (II) be the 1×1 and 2×2 product rules, respectively. However the latter is generalized so the sample points are located at $\{-\chi, \chi\}$, $\{\chi, -\chi\}$, $\{\chi, \chi\}$ and $\{-\chi, \chi\}$, with weight 1.[10] Consider the stress-strain splitting

$$\mathbf{E} = \frac{E}{1-\nu^2}\begin{bmatrix} 1 & \nu & 0 \\ \nu & 1 & 0 \\ 0 & 0 & \frac{1-\nu}{2} \end{bmatrix} = \frac{E}{1-\nu^2}\begin{bmatrix} \alpha & \beta & 0 \\ \beta & \alpha & 0 \\ 0 & 0 & \frac{1-\nu}{2} \end{bmatrix} + \frac{E}{1-\nu^2}\begin{bmatrix} 1-\alpha & \nu-\beta & 0 \\ \nu-\beta & 1-\alpha & 0 \\ 0 & 0 & 0 \end{bmatrix} = \mathbf{E}_{\rm I} + \mathbf{E}_{\rm II}, \tag{E17.13}$$

[9] Note that even if we make $a \to 0$ and $\gamma = b/a \to \infty$ by taking an infinite number of rectangular elements along x, the energy ratio r remains greater than one if $\nu > 0$ since $r \to 1/(1 - \nu^2)$. Thus the 2D model would not generally converge to the correct solution if we keep one layer through the height.

[10] For a rectangular geometry these sample points lie on the diagonals. In the case of the standard 2-point Gauss product rule $\chi = 1/\sqrt{3}$.

where α and β are scalars. Show that if

$$\chi = \sqrt{\frac{1-\nu^2}{3(1-\alpha)}} \tag{E17.14}$$

the resulting element stiffness $\mathbf{K}^e_{\rm I} + \mathbf{K}^e_{\rm II}$ is bending exact for any $\{\alpha, \beta\}$. As a corollary show that that if $\alpha = \nu^2$, which corresponds to the splitting

$$\mathbf{E} = \frac{E}{1-\nu^2}\begin{bmatrix} 1 & \nu & 0 \\ \nu & 1 & 0 \\ 0 & 0 & \frac{1-\nu}{2} \end{bmatrix} = \frac{E}{1-\nu^2}\begin{bmatrix} \nu^2 & \beta & 0 \\ \beta & \nu^2 & 0 \\ 0 & 0 & \frac{1-\nu}{2} \end{bmatrix} + \frac{E}{1-\nu^2}\begin{bmatrix} 1-\nu^2 & \nu-\beta & 0 \\ \nu-\beta & 1-\nu^2 & 0 \\ 0 & 0 & 0 \end{bmatrix} = \mathbf{E}_{\rm I} + \mathbf{E}_{\rm II}, \tag{E17.15}$$

then $\chi = 1/\sqrt{3}$ and rule (II) becomes the standard 2×2 Gauss product rule. What are two computationally convenient settings for β?

EXERCISE 17.6 [A+C:35] (Advanced) A variation on the previous exercise on selective integration to make the isotropic rectangular 4-node element bending exact. Integration rule (I) is not changed. However rule (II) has four sample points located at $\{0, -\chi\}$, $\{\chi, 0\}$, $\{0, \chi\}$ and $\{-\chi, 0\}$ each with weight 1.[11] Show that if one selects the stress-strain splitting (E17.13) and

$$\chi = \sqrt{\frac{2(1-\nu^2)}{3(1-\alpha)}} \tag{E17.16}$$

the resulting element stiffness $\mathbf{K}^e_{\rm I} + \mathbf{K}^e_{\rm II}$ is bending exact for any $\{\alpha, \beta\}$. Discuss which choices of α reduce χ to $1/\sqrt{3}$ and $\sqrt{2/3}$, respectively.

EXERCISE 17.7 [A+C:40] (Advanced, research paper level, requires a CAS to be tractable) Extend Exercise 17.5 to consider the case of general anisotropic material:

$$\mathbf{E} = \begin{bmatrix} E_{11} & E_{12} & E_{13} \\ E_{12} & E_{22} & E_{23} \\ E_{13} & E_{23} & E_{33} \end{bmatrix} \tag{E17.17}$$

The rules for the selective integration scheme are as described in Exercise 17.5. The appropriate stress-strain splitting is

$$\mathbf{E} = \mathbf{E}_{\rm I} + \mathbf{E}_{\rm II} = \begin{bmatrix} E_{11}\,\alpha_1 & E_{12}\beta & E_{13} \\ E_{12}\,\beta & E_{22}\,\alpha_2 & E_{23} \\ E_{13} & E_{23} & E_{33} \end{bmatrix} + \begin{bmatrix} E_{11}(1-\alpha_1) & E_{12}(1-\beta) & 0 \\ E_{12}(1-\beta) & E_{22}(1-\alpha_2) & 0 \\ 0 & 0 & 0 \end{bmatrix} \tag{E17.18}$$

in which β is arbitrary and

$$\begin{aligned} 1-\alpha_1 &= \frac{|\mathbf{E}|}{3\chi^2 E_{11}(E_{22}E_{33}-E_{23}^2)} = \frac{1}{3\chi^2 C_{11}}, \quad 1-\alpha_2 = \frac{|\mathbf{E}|}{3\chi^2 E_{22}(E_{11}E_{33}-E_{13}^2)} = \frac{1}{3\chi^2 C_{22}}, \\ |\mathbf{E}| &= \det(\mathbf{E}) = E_{11}E_{22}E_{33} + 2E_{12}E_{13}E_{23} - E_{11}E_{23}^2 - E_{22}E_{13}^2 - E_{33}E_{12}^2, \\ C_{11} &= E_{11}(E_{22}E_{33}-E_{13}^2)/|\mathbf{E}|, \quad C_{22} = E_{22}(E_{11}E_{33}-E_{13}^2)/|\mathbf{E}|. \end{aligned} \tag{E17.19}$$

Show that the resulting rectangular element is bending exact for any $\mathbf{E}$ and $\chi \neq 0$. (In practice one would select $\chi = 1/\sqrt{3}$.)

[11] This is called a 4-point median rule, since the four points are located on the quadrilateral medians.

18

Shape Function Magic

TABLE OF CONTENTS

§18.1. Requirements

This Chapter explains, through a series of examples, how isoparametric shape functions can be directly constructed by geometric considerations. For a problem of variational index 1, the isoparametric shape function N_i^e associated with node i of element e must satisfy the following conditions:

(A) *Interpolation condition*. Takes a unit value at node i, and is zero at all other nodes.

(B) *Local support condition*. Vanishes over any element boundary (a side in 2D, a face in 3D) that does not include node i.

(C) *Interelement compatibility condition.* Satisfies C^0 continuity between adjacent elements over any element boundary that includes node i.

(D) *Completeness condition*. The interpolation is able to represent exactly any displacement field which is a linear polynomial in x and y; in particular, a constant value.

Requirement (A) follows directly by interpolation from node values. Conditions (B), (C) and (D) are consequences of the *convergence* requirements discussed further in the next Chapter.[1] For the moment these three conditions may be viewed as recipes.

One can readily verify that all isoparametric shape function sets listed in Chapter 16 satisfy the first two conditions from construction. Direct verification of condition (C) is also straightforward for those examples. A statement equivalent to (C) is that the value of the shape function over a side (in 2D) or face (in 3D) common to two elements must uniquely depend only on its nodal values on that side or face.

Completeness is a property of *all* element isoparametric shape functions taken together, rather than of an individual one. If the element satisfies (B) and (C), in view of the discussion in §16.6 it is sufficient to check that the *sum of shape functions is identically one*.

§18.2. Direct Fabrication of Shape Functions

Contrary to the what the title of this Chapter implies, the isoparametric shape functions listed in Chapter 16 did not come out of a magician's hat. They can be derived systematically by a judicious inspection process. By "inspection" it is meant that the *geometric* visualization of shape functions plays a crucial role.

The method is based on the following observation. In all examples given so far the isoparametric shape functions are given as *products* of fairly simple polynomial expressions in the natural coordinates. This is no accident but a direct consequence of the definition of natural coordinates. All shape functions of Chapter 16 can be expressed as the product of m factors:

$$N_i^e = c_i \, L_1 \, L_2 \, \ldots \, L_m, \tag{18.1}$$

where

$$L_j = 0, \qquad j = 1, \ldots \, m. \tag{18.2}$$

are the homogeneous equation of lines or curves expressed as *linear* functions in the natural coordinates, and c_i is a normalization coefficient.

[1] Convergence means that the discrete FEM solution approaches the exact analytical solution as the mesh is refined.

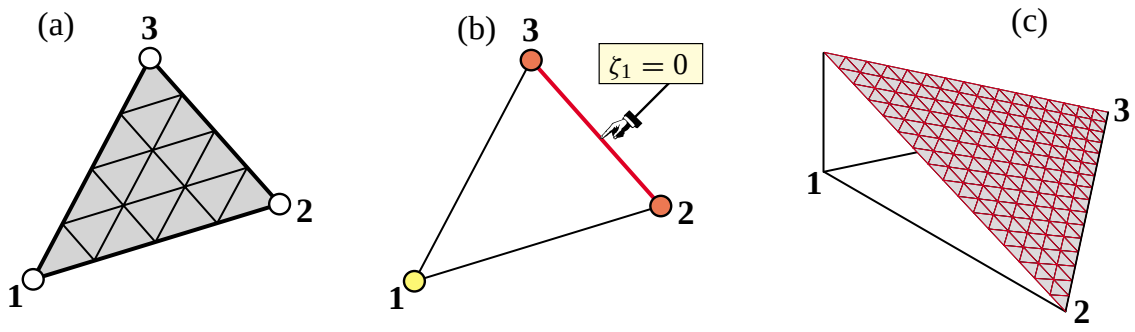

FIGURE 18.1. The three-node linear triangle: (a) element geometry; (b) equation of side opposite corner 1; (c) perspective view of the shape function $N_1 = \zeta_1$.

For two-dimensional isoparametric elements, the ingredients in (18.1) are chosen according to the following five rules.

R1 Select the L_j as the minimal number of lines or curves linear in the natural coordinates that cross all nodes except the i^{th} node. (A *sui generis* "cross the dots" game.) Primary choices in 2D are the element sides and medians.

R2 Set coefficient c_i so that N_i^e has the value 1 at the i^{th} node.

R3 Check that N_i^e vanishes over all element sides that do not contain node i.

R4 Check the polynomial order over each side that contains node i. If the order is n, there must be exactly $n + 1$ nodes on the side for compatibility to hold.

R5 If local support (R3) and interelement compatibility (R4) are satisfied, check that the sum of shape functions is identically one.

The examples that follow show these rules in action for two-dimensional elements. Essentially the same technique is applicable to one- and three-dimensional elements.

§18.3. Triangular Element Shape Functions

This section illustrates the use of (18.1) in the construction of shape functions for the linear and the quadratic triangle. The cubic triangle is dealt with in Exercise 18.1.

§18.3.1. The Three-Node Linear Triangle

Figure 18.1 shows the three-node linear triangle that was studied in detail in Chapter 15. The three shape functions are simply the triangular coordinates: $N_i = \zeta_i$, for $i = 1, 2, 3$. Although this result follows directly from the linear interpolation formula of §15.2.4, it can be also quickly derived from the present methodology as follows.

The equation of the triangle side opposite to node i is $L_{j\text{-}k} = \zeta_i = 0$, where j and k are the cyclic permutations of i. Here symbol $L_{j\text{-}k}$ denotes the left hand side of the homogeneous equation of the natural coordinate line that passes through node points j and k. See Figure 18.1(b) for $i = 1$, $j = 2$ and $k = 3$. Hence the obvious guess is

$$N_i^e \stackrel{\text{guess}}{=} c_i L_i . \tag{18.3}$$

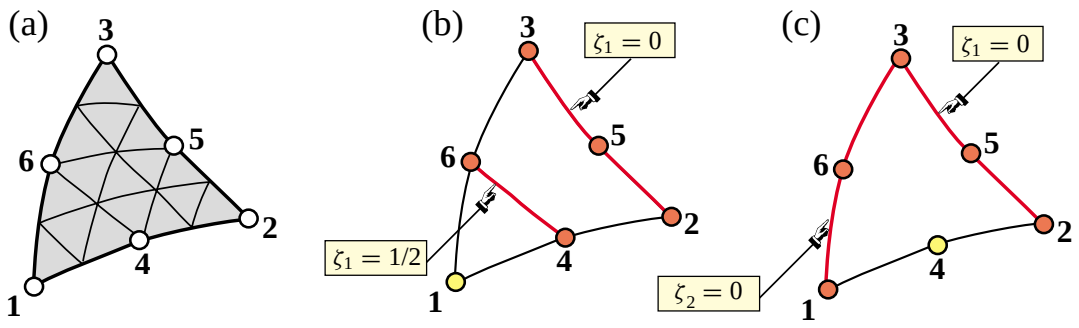

FIGURE 18.2. The six-node quadratic triangle: (a) element geometry; (b) lines (in red) whose product yields N_1^e; (c) lines (in red) whose product yields N_4^e.

This satisfies conditions (A) and (B) except the unit value at node i; this holds if $c_i = 1$. The local support condition (B) follows from construction: the value of ζ_i is zero over side j–k. Interelement compatibility follows from R4: the variation of ζ_i along the 2 sides meeting at node i is linear and that there are two nodes on each side; cf. §15.4.2. Completeness follows since $N_1^e + N_2^e + N_3^e = \zeta_1 + \zeta_2 + \zeta_3 = 1$. Figure 18.1(c) depicts $N_1^e = \zeta_1$, drawn normal to the element in perspective view.

§18.3.2. The Six-Node Quadratic Triangle

The geometry of the six-node quadratic triangle is shown in Figure 18.2(a). Inspection reveals two types of nodes: corners (1, 2 and 3) and midside nodes (4, 5 and 6). Consequently we can expect two types of associated shape functions. We select nodes 1 and 4 as representative cases.

For both cases we try the product of *two* linear functions in the triangular coordinates because we expect the shape functions to be quadratic. These functions are illustrated in Figures 18.2(b,c) for corner node 1 and midside node 4, respectively.

For corner node 1, inspection of Figure 18.2(b) suggests trying

$$N_1^e \stackrel{\text{guess}}{=} c_1 \, L_{2\text{-}3} \, L_{4\text{-}6}, \tag{18.4}$$

Why is (18.4) expected to work? Clearly N_1^e will vanish over 2-5-3 and 4-6. This makes the function zero at nodes 2 through 6, as is obvious upon inspection of Figure 18.2(b), while being nonzero at node 1. This value can be adjusted to be unity if c_1 is appropriately chosen. The equations of the lines that appear in (18.4) are

$$L_{2\text{-}3}\text{:} \quad \zeta_1 = 0, \qquad\qquad L_{4\text{-}6}\text{:} \quad \zeta_1 - \tfrac{1}{2} = 0. \tag{18.5}$$

Replacing into (18.3) we get

$$N_1^e = c_1 \, \zeta_1(\zeta_1 - \tfrac{1}{2}), \tag{18.6}$$

To find c_1, evaluate $N_1^e(\zeta_1, \zeta_2, \zeta_3)$ at node 1. The triangular coordinates of this node are $\zeta_1 = 1$, $\zeta_2 = \zeta_3 = 0$. We require that it takes a unit value there: $N_1^e(1, 0, 0) = c_1 \times 1 \times \frac{1}{2} = 1$ whence $c_1 = 2$ and finally

$$N_1^e = 2\zeta_1(\zeta_1 - \tfrac{1}{2}) = \zeta_1(2\zeta_1 - 1), \tag{18.7}$$

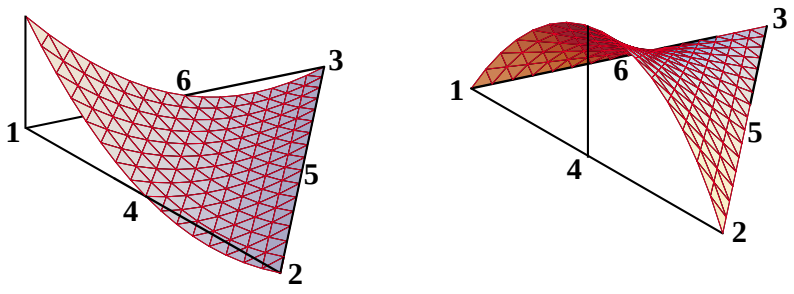

$N_1^e = \zeta_1(2\zeta_1 - 1)$ $\qquad$ $N_4^e = 4\zeta_1\zeta_2$

FIGURE 18.3. Perspective view of shape functions N_1^e and N_4^e for the quadratic triangle. The plot is done over a straight side triangle for programming simplicity.

as listed in §16.5.2. Figure 18.3 shows a perspective view. The other two corner shape functions follow by cyclic permutations of the corner index.

For midside node 4, inspection of Figure 18.2(c) suggests trying

$$N_4^e \stackrel{\text{guess}}{=} c_4\, L_{2\text{-}3}\, L_{1\text{-}3} \tag{18.8}$$

Evidently (18.8) satisfies requirements (A) and (B) if c_4 is appropriately normalized. The equation of sides $L_{2\text{-}3}$ and $L_{1\text{-}3}$ are $\zeta_1 = 0$ and $\zeta_2 = 0$, respectively. Therefore $N_4^e(\zeta_1, \zeta_2, \zeta_3) = c_4\,\zeta_1\zeta_2$. To find c_4, evaluate this function at node 4, the triangular coordinates of which are $\zeta_1 = \zeta_2 = \frac{1}{2}$, $\zeta_3 = 0$. We require that it takes a unit value there: $N_4^e(\frac{1}{2}, \frac{1}{2}, 0) = c_4 \times \frac{1}{2} \times \frac{1}{2} = 1$. Hence $c_4 = 4$, which gives

$$N_4^e = 4\zeta_1\zeta_2 \tag{18.9}$$

as listed in §16.5.2. Figure 18.3 shows a perspective view of this shape function. The other two midside shape functions follow by cyclic permutations of the node indices.

It remains to carry out the interelement continuity check. Consider node 1. The boundaries containing node 1 and common to adjacent elements are 1–2 and 1–3. Over each one the variation of N_1^e is quadratic in ζ_1. Therefore the polynomial order over each side is 2. Because there are three nodes on each boundary, the compatibility condition (C) of §18.1 is verified. A similar check can be carried out for midside node shape functions. Exercise 16.1 verified that the sum of the N_i is unity. Therefore the element is complete.

§18.4. Quadrilateral Element Shape Functions

Three quadrilateral elements, with 4, 9 and 8 nodes, respectively, which are commonly used in computational mechanics serve as examples to illustrate the construction of shape functions. Elements with more nodes, such as the bicubic quadrilateral, are not treated as they are rarely used.

§18.4.1. The Four-Node Bilinear Quadrilateral

The element geometry and natural coordinates are shown in Figure 18.4(a). Only one type of node (corner) and associated shape function is present. Consider node 1 as typical. Inspection of

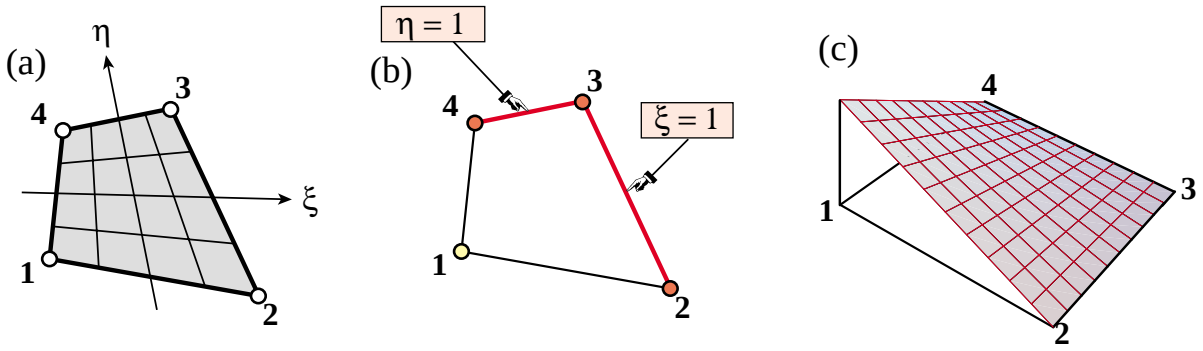

FIGURE 18.4. The four-node bilinear quadrilateral: (a) element geometry; (b) sides (in red) that do not contain corner 1; (c) perspective view of the shape function N_1^e.

Figure 18.4(b) suggests trying

$$N_1^e \stackrel{\text{guess}}{=} c_1 \, L_{2\text{-}3} \, L_{3\text{-}4} \tag{18.10}$$

This plainly vanishes over nodes 2, 3 and 4, and can be normalized to unity at node 1 by adjusting c_1. By construction it vanishes over the sides 2–3 and 3–4 that do not belong to 1. The equation of side 2-3 is $\xi = 1$, or $\xi - 1 = 0$. The equation of side 3-4 is $\eta = 1$, or $\eta - 1 = 0$. Replacing in (18.10) yields

$$N_1^e(\xi, \eta) = c_1(\xi - 1)(\eta - 1) = c_1(1 - \xi)(1 - \eta). \tag{18.11}$$

To find c_1, evaluate at node 1, the natural coordinates of which are $\xi = \eta = -1$:

$$N_1^e(-1, -1) = c_1 \times 2 \times 2 = 4c_1 = 1. \tag{18.12}$$

Hence $c_1 = \frac{1}{4}$ and the shape function is

$$N_1^e = \tfrac{1}{4}(1 - \xi)(1 - \eta), \tag{18.13}$$

as listed in §16.6.2. Figure 18.4(c) shows a perspective view.

For the other three nodes the procedure is the same, traversing the element cyclically. It can be verified that the general expression of the shape functions for this element is

$$N_i^e = \tfrac{1}{4}(1 + \xi_i \, \xi)(1 + \eta_i \, \eta). \tag{18.14}$$

The continuity check proceeds as follows, using N_1^e as example. Node 1 belongs to interelement boundaries 1–2 and 1–3. Over side 1–2, $\eta = -1$ is constant and N_1^e is a *linear* function of ξ. To see this, replace $\eta = -1$ in (18.13). Over side 1–3, $\xi = -1$ is constant and N_1^e is a *linear* function of η. Consequently the polynomial variation order is 1 over both sides. Because there are two nodes on each side the compatibility condition is satisfied. The sum of the shape functions is one, as shown in (16.21); thus the element is complete.

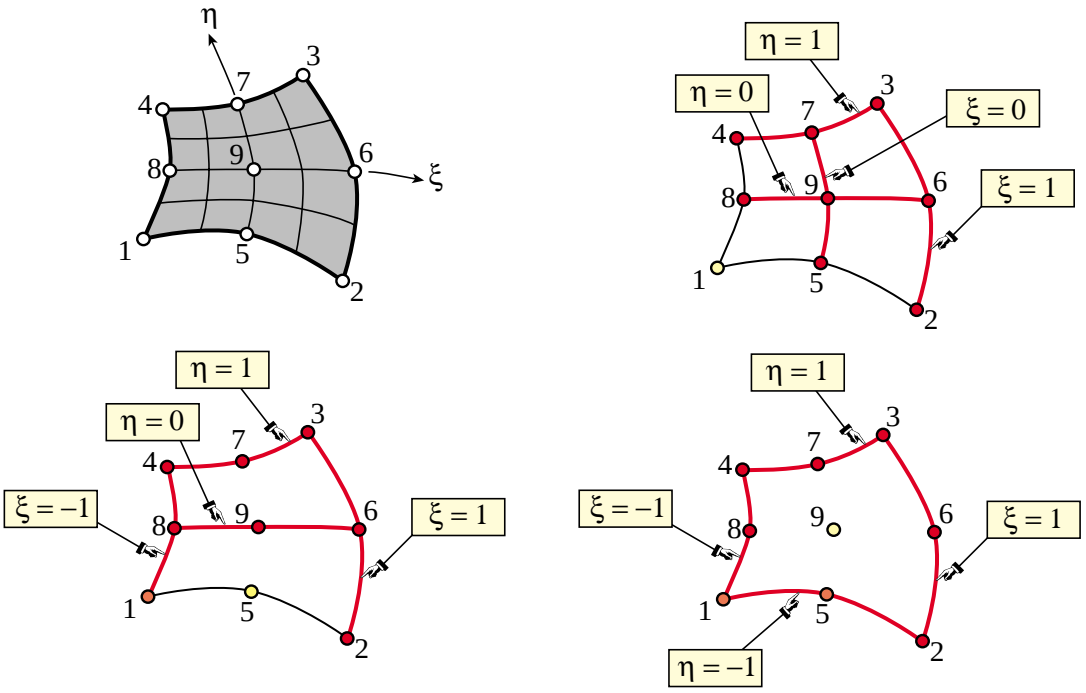

FIGURE 18.5. The nine-node biquadratic quadrilateral: (a) element geometry; (b,c,d): lines (in red) whose product makes up the shape functions N_1^e, N_5^e and N_9^e, respectively.

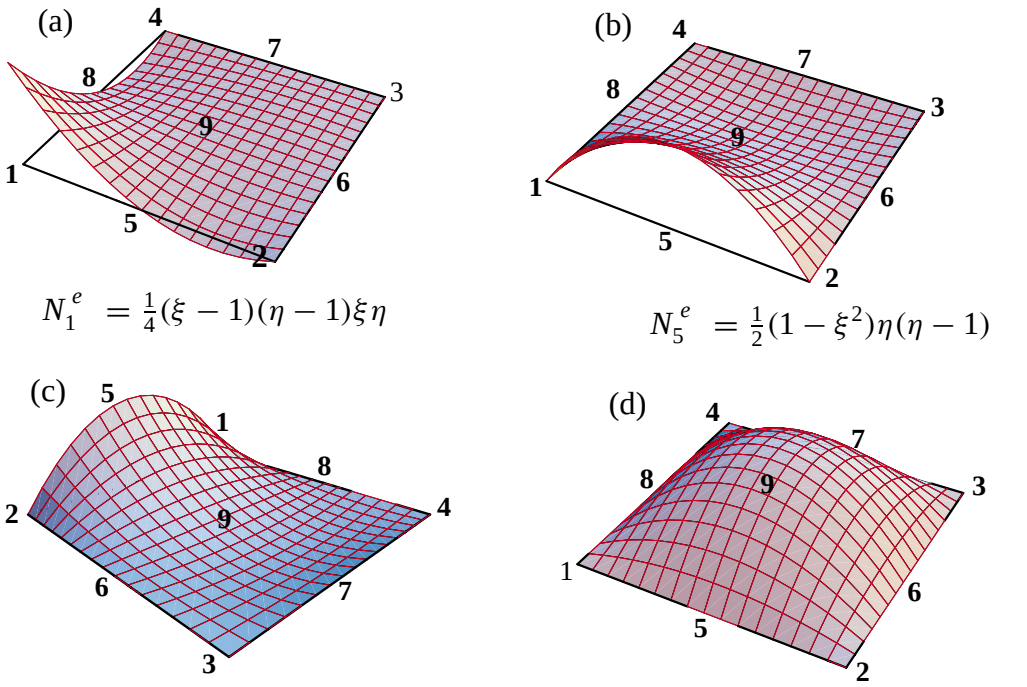

$N_1^e = \frac{1}{4}(\xi-1)(\eta-1)\xi\eta$

$N_5^e = \frac{1}{2}(1-\xi^2)\eta(\eta-1)$

$N_5^e = \frac{1}{2}(1-\xi^2)\eta(\eta-1)$ (back view)

$N_9^e = (1-\xi^2)(1-\eta^2)$

FIGURE 18.6. Perspective view of the shape functions for nodes 1, 5 and 9 of the nine-node biquadratic quadrilateral.

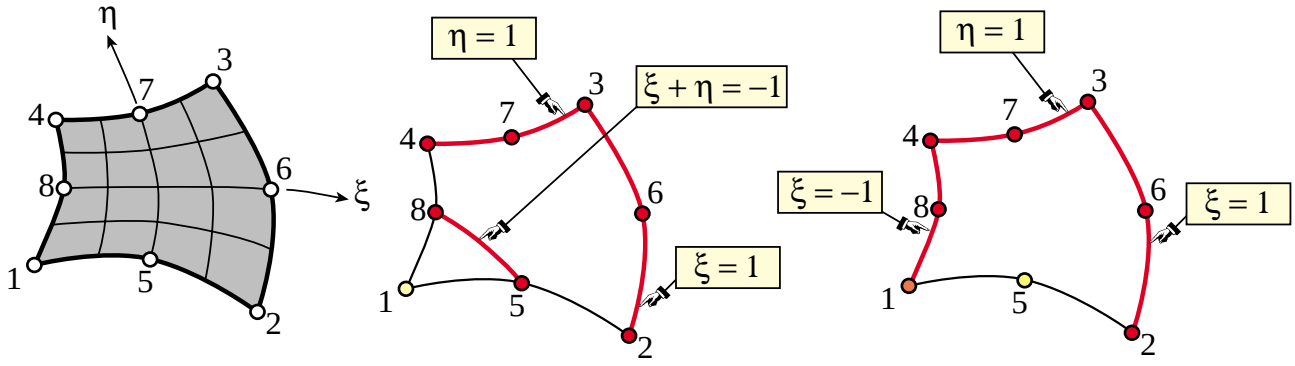

FIGURE 18.7. The eight-node serendipity quadrilateral: (a) element geometry; (b,c): lines (in red) whose product make up the shape functions N_1^e and N_5^e, respectively.

§18.4.2. The Nine-Node Biquadratic Quadrilateral

The element geometry is shown in Figure 18.5(a). This element has three types of shape functions, which are associated with corner nodes, midside nodes and center node, respectively.

The lines whose product is used to construct three types of shape functions are illustrated in Figure 18.5(b,c,d) for nodes 1, 5 and 9, respectively. The technique has been sufficiently illustrated in previous examples. Here we summarize the calculations for nodes 1, 5 and 9, which are taken as representatives of the three types:

$$N_1^e = c_1 L_{2\text{-}3} L_{3\text{-}4} L_{5\text{-}7} L_{6\text{-}8} = c_1(\xi-1)(\eta-1)\xi\eta. \tag{18.15}$$

$$N_5^e = c_5 L_{2\text{-}3} L_{1\text{-}4} L_{6\text{-}8} L_{3\text{-}4} = c_5\,(\xi-1)(\xi+1)\eta(\eta-1) = c_5\,(1-\xi^2)\eta(1-\eta). \tag{18.16}$$

$$N_9^e = c_9\, L_{1\text{-}2} L_{2\text{-}3} L_{3\text{-}4} L_{4\text{-}1} = c_9\,(\xi-1)(\eta-1)(\xi+1)(\eta+1) = c_9\,(1-\xi^2)(1-\eta^2) \tag{18.17}$$

Imposing the normalization conditions we find

$$c_1 = \tfrac{1}{4}, \qquad c_5 = -\tfrac{1}{2}, \qquad c_9 = 1, \tag{18.18}$$

and we obtain the shape functions listed in §16.6.3. Perspective views are shown in Figure 18.6. The remaining N_i's are constructed through a similar procedure.

Verification of the interelement continuity condition is immediate: the polynomial variation order of N_i^e over any side that belongs to node i is two and there are three nodes on each side. Exercise 16.2 checks that the sum of shape function is unity. Thus the element is complete.

§18.4.3. The Eight-Node "Serendipity" Quadrilateral

This is an eight-node quadrilateral element that results when the center node 9 of the biquadratic quadrilateral is eliminated by kinematic constraints. The geometry and node configuration is shown in Figure 18.7(a). This element has been widely used in commercial codes since the 70s for static problems. It is gradually being phased out in favor of the 9-node quadrilateral for dynamic problems.

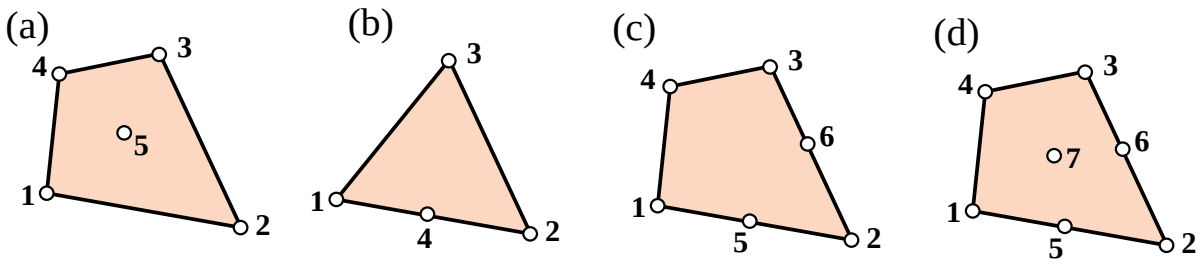

FIGURE 18.8. Node configurations for which the magic recipe does not work.

The 8-node quadrilateral has two types of shape functions, which are associated with corner nodes and midside nodes. Lines whose products yields the shape functions for nodes 1 and 5 are shown in Figure 18.7(b,c).

Here are the calculations for shape functions of nodes 1 and 5, which are taken again as representative cases.

$$N_1^e = c_1 L_{2\text{-}3} L_{3\text{-}4} L_{5\text{-}8} = c_1(\xi-1)(\eta-1)(1+\xi+\eta) = c_1(1-\xi)(1-\eta)(1+\xi+\eta), \quad (18.19)$$

$$N_5^e = c_5 L_{2\text{-}3} L_{3\text{-}4} L_{4\text{-}1} = c_5\,(\xi-1)(\xi+1)(\eta-1) = c_5\,(1-\xi^2)(1-\eta). \quad (18.20)$$

Imposing the normalization conditions we find

$$c_1 = -\tfrac{1}{4}, \qquad c_5 = \tfrac{1}{2} \quad (18.21)$$

The other shape functions follow by appropriate permutation of nodal indices. The interelement continuity and completeness verification are similar to that carried out for the nine-node element, and are relegated to exercises.

§18.5. Does the Magic Wand Always Work?

The "cross the dots" recipe (18.1)–(18.2) is not foolproof. It fails for certain node configurations although it is a reasonable way to start. It runs into difficulties, for instance, in the problem posed in Exercise 18.6, which deals with the 5-node quadrilateral depicted in Figure 18.8(a). If for node 1 one tries the product of side 2–3, side 3–4, and the diagonal 2–5–4, the shape function is easily worked out to be $N_1^e = -\frac{1}{8}(1-\xi)(1-\eta)(\xi+\eta)$. This satisfies conditions (A) and (B). However, it violates (C) along sides 1–2 and 4–1, because it varies quadratically over them with only two nodes per side.

§18.5.1. Hierarchical Corrections

A more robust technique relies on a *correction approach*, which employs a combination of terms such as (18.1). For example, a combination of two patterns, one with m factors and one with n factors, is

$$N_i^e = c_i\, L_1^c\, L_2^c\, \ldots\, L_m^c + d_i\, L_1^d\, L_2^d\, \ldots\, L_n^d, \quad (18.22)$$

Here two normalization coefficients: c_i and d_i, appear. In practice trying forms such as (18.22) from scratch becomes cumbersome. The development is best done *hierarchically*. The first term is

taken to be that of a lower order element, called the *parent element*, for which the one-shot approach works. The second term is then a corrective shape function that vanishes at the nodes of the parent element. If this is insufficient one more corrective term is added, and so on.

The technique is best explained through examples. Exercise 18.6 illustrates the procedure for the element of Figure 18.8(a). The next subsection works out the element of Figure 18.8(b).

§18.5.2. Transition Element Example

The hierarchical correction technique is useful for *transition elements*, which have corner nodes but midnodes only over certain sides. Three examples are pictured in Figure 18.8(b,c,d). Shape functions that work can be derived with one, two and three hierarchical corrections, respectively.

As an example, let us construct the shape function N_1^e for the 4-node transition triangle shown in Figure 18.8(b). Candidate lines for the recipe (18.1) are obviously the side 2–3: $\zeta_1 = 0$, and the median 3–4: $\zeta_1 = \zeta_2$. Accordingly we try

$$N_1^e \stackrel{\text{guess}}{=} c_1\zeta_1(\zeta_1 - \zeta_2), \qquad N_1(1, 0, 0) = 1 = c_1. \tag{18.23}$$

This function $N_1^e = \zeta_1(\zeta_1 - \zeta_2)$ satisfies conditions (A) and (B) but fails compatibility: over side 1–3 of equation $\zeta_2 = 0$, because $N_1^e(\zeta_1, 0, \zeta_3) = \zeta_1^2$. This varies quadratically but there are only 2 nodes on that side. Thus (18.23) is no good.

To proceed hierarchically we start from the shape function for the 3-node linear triangle: $N_1^e = \zeta_1$. This will not vanish at node 4, so apply a correction that vanishes at all nodes but 4. From knowledge of the quadratic triangle midpoint functions, that is obviously $\zeta_1\zeta_2$ times a coefficient to be determined. The new guess is

$$N_1^e \stackrel{\text{guess}}{=} \zeta_1 + c_1\zeta_1\zeta_2. \tag{18.24}$$

Coefficient c_1 is determined by requiring that N_1^e vanish at 4: $N_1^e(\frac{1}{2}, \frac{1}{2}, 0) = \frac{1}{2} + c_1\frac{1}{4} = 0$, whence $c_1 = -2$ and the shape function is

$$N_1^e = \zeta_1 - 2\zeta_1\zeta_2. \tag{18.25}$$

This is easily checked to satisfy compatibility on all sides. The verification of completeness is left to Exercise 18.8.

Note that since $N_1^e = \zeta_1(1 - 2\zeta_2)$, (18.25) can be constructed as the normalized product of lines $\zeta_1 = 0$ and $\zeta_2 = 1/2$. The latter passes through 4 and is parallel to 1–3. As part of the opening moves in the shape function game this would be a lucky guess indeed. If one goes to a more complicated element no obvious factorization is possible.

Cell 18.1 *Mathematica* **Module to Draw a Function over a Triangle Region**

```
PlotTriangleShapeFunction[xytrig_,f_,Nsub_,aspect_]:=Module[
  {Ni,line3D={},poly3D={},zc1,zc2,zc3,xyf1,xyf2,xyf3,
   xc,yc, x1,x2,x3,y1,y2,y3,z1,z2,z3,iz1,iz2,iz3,d},
  {{x1,y1,z1},{x2,y2,z2},{x3,y3,z3}}=Take[xytrig,3];
   xc={x1,x2,x3}; yc={y1,y2,y3}; Ni=Nsub*3;
   Do [ Do [iz3=Ni-iz1-iz2; If [iz3<=0, Continue[]]; d=0;
      If [Mod[iz1+2,3]==0&&Mod[iz2-1,3]==0, d= 1];
      If [Mod[iz1-2,3]==0&&Mod[iz2+1,3]==0, d=-1];
      If [d==0, Continue[]];
      zc1=N[{iz1+d+d,iz2-d,iz3-d}/Ni];
      zc2=N[{iz1-d,iz2+d+d,iz3-d}/Ni];
      zc3=N[{iz1-d,iz2-d,iz3+d+d}/Ni];
      xyf1={xc.zc1,yc.zc1,f[zc1[[1]],zc1[[2]],zc1[[3]]]};
      xyf2={xc.zc2,yc.zc2,f[zc2[[1]],zc2[[2]],zc2[[3]]]};
      xyf3={xc.zc3,yc.zc3,f[zc3[[1]],zc3[[2]],zc3[[3]]]};
      AppendTo[poly3D,Polygon[{xyf1,xyf2,xyf3}]];
      AppendTo[line3D,Line[{xyf1,xyf2,xyf3,xyf1}]],
   {iz2,1,Ni-iz1}],{iz1,1,Ni}];
    Show[ Graphics3D[RGBColor[1,0,0]],Graphics3D[poly3D],
      Graphics3D[Thickness[.002]],Graphics3D[line3D],
      Graphics3D[RGBColor[0,0,0]],Graphics3D[Thickness[.005]],
      Graphics3D[Line[xytrig]],PlotRange->All,
      BoxRatios->{1,1,aspect},Boxed->False]
];
ClearAll[f1,f4];
xyc1={0,0,0}; xyc2={3,0,0}; xyc3={Sqrt[3],3/2,0};
xytrig=N[{xyc1,xyc2,xyc3,xyc1}]; Nsub=16;
f1[zeta1_,zeta2_,zeta3_]:=zeta1*(2*zeta1-1);
f4[zeta1_,zeta2_,zeta3_]:=4*zeta1*zeta2;
PlotTriangleShapeFunction[xytrig,f1,Nsub,1/2];
PlotTriangleShapeFunction[xytrig,f4,Nsub,1/2.5];
```

§18.6. *Mathematica Modules to Plot Shape Functions

A *Mathematica* module called `PlotTriangleShape Functions`, listed in Cell 18.1, has been developed to draw perspective plots of shape functions $N_i(\zeta_1, \zeta_2, \zeta_3)$ over a triangular region. The region is assumed to have straight sides to simplify the logic. The test statements that follow the module produce the shape function plots shown in Figure 18.3 for the 6-node quadratic triangle. Argument `Nsub` controls the plot resolution while `aspect` controls the xyz box aspect ratio. The remaining arguments are self explanatory.

Another *Mathematica* module called `PlotQuadrilateralShape Functions`, listed in Cell 18.2, has been developed to produce perspective plots of shape functions $N_i(\xi, \eta)$ over a quadrilateral region. The region is assumed to have straight sides to simplify the logic. The test statements that follow the module produce the shape function plots shown in Figure 18.6(a,b,d) for the 9-node biquadratic quadrilateral. Argument `Nsub`

Cell 18.2 *Mathematica* **Module to Draw a Function over a Quadrilateral Region**

```
PlotQuadrilateralShapeFunction[xyquad_,f_,Nsub_,aspect_]:=Module[
  {Ne,Nev,line3D={},poly3D={},xyf1,xyf2,xyf3,i,j,n,ixi,ieta,
  xi,eta,x1,x2,x3,x4,y1,y2,y3,y4,z1,z2,z3,z4,xc,yc},
  {{x1,y1,z1},{x2,y2,z2},{x3,y3,z3},{x4,y4,z4}}=Take[xyquad,4];
   xc={x1,x2,x3,x4}; yc={y1,y2,y3,y4};
   Ne[xi_,eta_]:=N[{(1-xi)*(1-eta),(1+xi)*(1-eta),
                    (1+xi)*(1+eta),(1-xi)*(1+eta)}/4]; n=Nsub;
   Do [ Do [ ixi=(2*i-n-1)/n; ieta=(2*j-n-1)/n;
        {xi,eta}=N[{ixi-1/n,ieta-1/n}]; Nev=Ne[xi,eta];
         xyf1={xc.Nev,yc.Nev,f[xi,eta]};
        {xi,eta}=N[{ixi+1/n,ieta-1/n}]; Nev=Ne[xi,eta];
         xyf2={xc.Nev,yc.Nev,f[xi,eta]};
        {xi,eta}=N[{ixi+1/n,ieta+1/n}]; Nev=Ne[xi,eta];
         xyf3={xc.Nev,yc.Nev,f[xi,eta]};
        {xi,eta}=N[{ixi-1/n,ieta+1/n}]; Nev=Ne[xi,eta];
         xyf4={xc.Nev,yc.Nev,f[xi,eta]};
         AppendTo[poly3D,Polygon[{xyf1,xyf2,xyf3,xyf4}]];
         AppendTo[line3D,Line[{xyf1,xyf2,xyf3,xyf4,xyf1}]],
   {i,1,Nsub}],{j,1,Nsub}];
    Show[ Graphics3D[RGBColor[1,0,0]],Graphics3D[poly3D],
         Graphics3D[Thickness[.002]],Graphics3D[line3D],
         Graphics3D[RGBColor[0,0,0]],Graphics3D[Thickness[.005]],
         Graphics3D[Line[xyquad]], PlotRange->All,
         BoxRatios->{1,1,aspect},Boxed->False]
];
ClearAll[f1,f5,f9];
xyc1={0,0,0}; xyc2={3,0,0}; xyc3={3,3,0}; xyc4={0,3,0};
xyquad=N[{xyc1,xyc2,xyc3,xyc4,xyc1}]; Nsub=16;
f1[xi_,eta_]:=(1/2)*(xi-1)*(eta-1)*xi*eta;
f5[xi_,eta_]:=(1/2)*(1-xi^2)*eta*(eta-1);
f9[xi_,eta_]:=(1-xi^2)*(1-eta^2);
PlotQuadrilateralShapeFunction[xyquad,f1,Nsub,1/2];
PlotQuadrilateralShapeFunction[xyquad,f5,Nsub,1/2.5];
PlotQuadrilateralShapeFunction[xyquad,f9,Nsub,1/3];
```

controls the plot resolution while `aspect` controls the xyz box aspect ratio. The remaining arguments are self explanatory.

Notes and Bibliography

The name "shape functions" for interpolation functions directly expressed in terms of physical coordinates (the node displacements in the case of isoparametric elements) was coined by Irons. The earliest published reference seems to be the paper [64]. This was presented in 1965 at the first Wright-Patterson conference, the first all-FEM meeting that strongly influenced the development of computational mechanics in Generation 2. The key connection to numerical integration was presented in [394], although it is mentioned in prior internal reports. A comprehensive exposition is given in the textbook by Irons and Ahmad [397].

The quick way of developing shape functions presented here was used in the writer's 1966 thesis [203] for triangular elements. The qualifier "magic" arose from the timing for covering this Chapter in a Fall Semester course: the lecture falls near Halloween.

References

Referenced items have been moved to Appendix R.

Homework Exercises for Chapter 18
Shape Function Magic

EXERCISE 18.1 [A/C:10+10] The complete cubic triangle for plane stress has 10 nodes located as shown in Figure E18.1, with their triangular coordinates listed in parentheses.

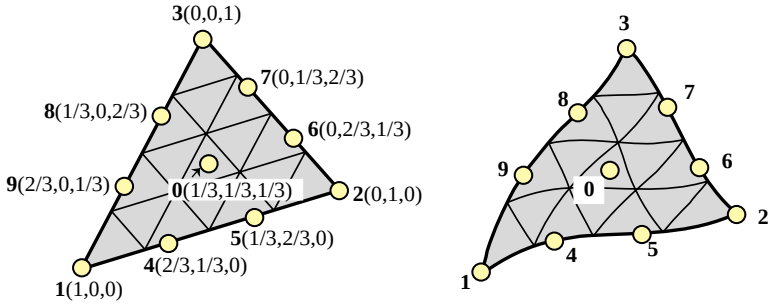

FIGURE E18.1. Ten-node cubic triangle for Exercise 18.1. The left picture shows the superparametric element whereas the right one shows the isoparametric version with curved sides.

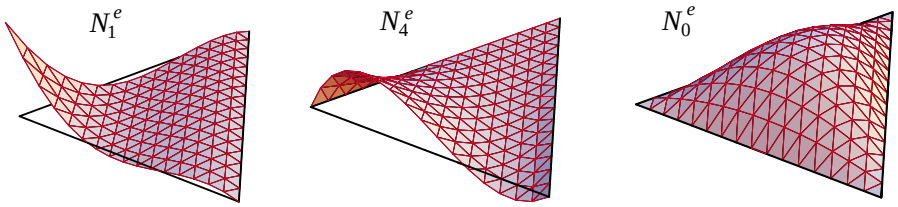

FIGURE E18.2. Perspective plots of the shape functions N_1^e, N_4^e and N_0^e for the 10-node cubic triangle.

(a) Construct the cubic shape functions N_1^e, N_4^e and N_0^e for nodes 1, 4, and 0 (the interior node is labeled as zero, not 10) using the line-product technique. [Hint: each shape function is the product of 3 and only 3 lines.] Perspective plots of those 3 functions are shown in Figure E18.2.

(b) Construct the missing 7 shape functions by appropriate node number permutations, and verify that the sum of the 10 functions is identically one. For the unit sum check use the fact that $\zeta_1 + \zeta_2 + \zeta_3 = 1$.

EXERCISE 18.2 [A:15] Find an alternative shape function N_1^e for corner node 1 of the 9-node quadrilateral of Figure 18.5(a) by using the diagonal lines 5–8 and 2–9–4 in addition to the sides 2–3 and 3–4. Show that the resulting shape function violates the compatibility condition (C) stated in §18.1.

EXERCISE 18.3 [A/C:15] Complete the above exercise for all nine nodes. Add the shape functions (use a CAS and simplify) and verify whether their sum is unity.

EXERCISE 18.4 [A/C:20] Verify that the shape functions N_1^e and N_5^e of the eight-node serendipity quadrilateral discussed in §18.4.3 satisfy the interelement compatibility condition (C) stated in §18.1. Obtain all 8 shape functions and verify that their sum is unity.

EXERCISE 18.5 [C:15] Plot the shape functions N_1^e and N_5^e of the eight-node serendipity quadrilateral studied in §18.4.3 using the module `PlotQuadrilateralShapeFunction` listed in Cell 18.2.

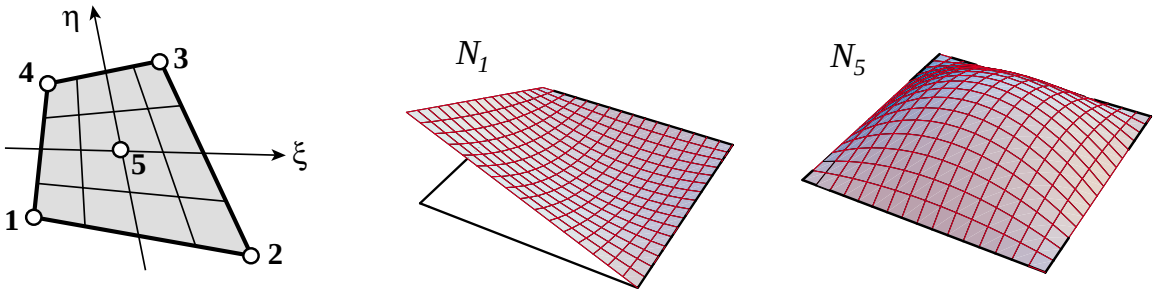

FIGURE E18.3. Five node quadrilateral element for Exercise 18.6.

EXERCISE 18.6 [A:15]. A five node quadrilateral element has the nodal configuration shown in Figure E18.3. Perspective views of N_1^e and N_5^e are shown in that Figure.[2] Find five shape functions N_i^e, $i = 1, 2, 3, 4, 5$ that satisfy compatibility, and also verify that their sum is unity.

Hint: develop $N_5(\xi, \eta)$ first for the 5-node quad using the line-product method; then the corner shape functions $\bar{N}_i(\xi, \eta)$ ($i = 1, 2, 3, 4$) for the 4-node quad (already given in the Notes); finally combine $N_i = \bar{N}_i + \alpha N_5$, determining α so that all N_i vanish at node 5. Check that $N_1 + N_2 + N_3 + N_4 + N_5 = 1$ identically.

EXERCISE 18.7 [A:15]. An eight-node "brick" finite element for three dimensional analysis has three isoparametric natural coordinates called ξ, η and μ. These coordinates vary from -1 at one face to $+1$ at the opposite face, as sketched in Figure E18.4.

Construct the (trilinear) shape function for node 1 (follow the node numbering of the figure). The equations of the brick faces are:

1485 : $\xi = -1$	2376 : $\xi = +1$
1265 : $\eta = -1$	4378 : $\eta = +1$
1234 : $\mu = -1$	5678 : $\mu = +1$

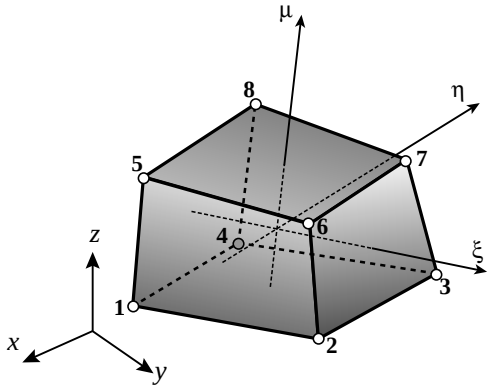

FIGURE E18.4. Eight-node isoparametric "brick" element for Exercise 18.7.

EXERCISE 18.8 [A:15]. Consider the 4-node transition triangular element of Figure 18.8(b). The shape function for node 1, $N_1 = \zeta_1 - 2\zeta_1\zeta_2$ was derived in §18.5.2 by the correction method. Show that the others are $N_2 = \zeta_2 - 2\zeta_1\zeta_2$, $N_3 = \zeta_3$ and $N_4 = 4\zeta_1\zeta_2$. Check that compatibility and completeness are verified.

EXERCISE 18.9 [A:15]. Construct the six shape functions for the 6-node transition quadrilateral element of Figure 18.8(c). Hint: for the corner nodes, use two corrections to the shape functions of the 4-node bilinear quadrilateral. Check compatibility and completeness. Partial result: $N_1 = \frac{1}{4}(1-\xi)(1-\eta) - \frac{1}{4}(1-\xi^2)(1-\eta)$.

EXERCISE 18.10 [A:20]. Consider a 5-node transition triangle in which midnode 6 on side 1–3 is missing. Show that $N_1^e = \zeta_1 - 2\zeta_1\zeta_2 - 2\zeta_2\zeta_3$. Can this be expressed as a line product like (18.1)?

[2] Although this N_1^e resembles the N_1^e of the 4-node quadrilateral depicted in Figure 18.4, they are not the same. That in Figure E18.3 must vanish at node 5 ($\xi = \eta = 0$). On the other hand, the N_1^e of Figure 18.4 takes the value $\frac{1}{4}$ there.

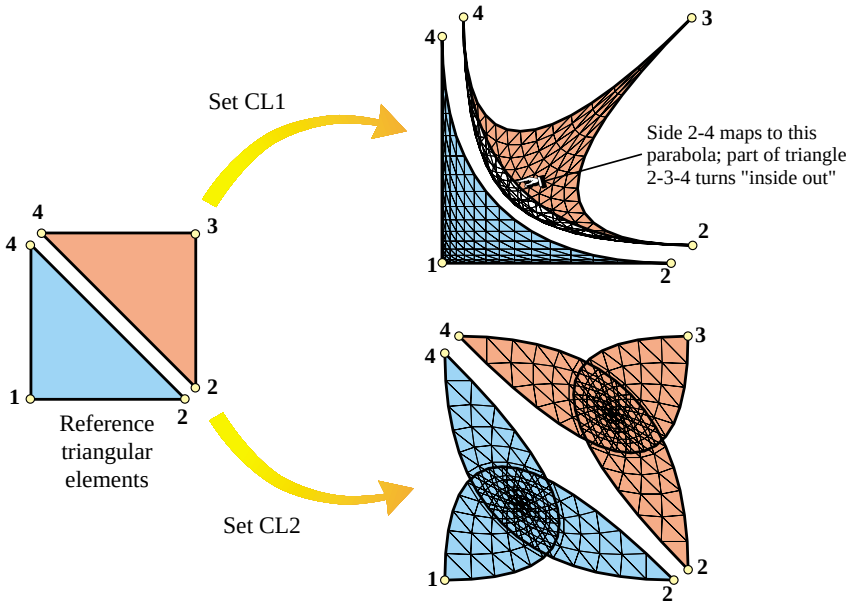

FIGURE E18.5. Mapping of reference triangles under sets (E18.1) and (E18.2). Triangles are slightly separated at the diagonal 2–4 for visualization convenience.

EXERCISE 18.11 [A:30]. The three-node linear triangle is known to be a poor performer for stress analysis. In an effort to improve it, Dr. I. M. Clueless proposes two sets of quadratic shape functions:

$$\text{CL1:} \qquad N_1 = \zeta_1^2, \quad N_2 = \zeta_2^2, \quad N_3 = \zeta_3^2. \tag{E18.1}$$

$$\text{CL2:} \qquad N_1 = \zeta_1^2 + 2\zeta_2\zeta_3, \quad N_2 = \zeta_2^2 + 2\zeta_3\zeta_1, \quad N_3 = \zeta_3^2 + 2\zeta_1\zeta_2. \tag{E18.2}$$

Dr. C. writes a learned paper claiming that both sets satisfy the interpolation condition, that set CL1 will work because it is conforming and that set CL2 will work because $N_1 + N_2 + N_3 = 1$. He provides no numerical examples. You get the paper for review. Show that the claims are false, and both sets are worthless. Hint: study §16.6 and Figure E18.5.

EXERCISE 18.12 [A:25]. Another way of constructing shape functions for "incomplete" elements is through kinematic multifreedom constraints (MFCs) applied to a "parent" element that contains the one to be derived. Suppose that the 9-node biquadratic quadrilateral is chosen as parent, with shape functions called N_i^P, $i = 1, \ldots 9$ given in §18.4.2. To construct the shape functions of the 8-node serentipity quadrilateral, the motions of node 9 are expressed in terms of the motions of the corner and midside nodes by the interpolation formulas

$$\begin{aligned} u_{x9} &= \alpha(u_{x1} + u_{x2} + u_{x3} + u_{x4}) + \beta(u_{x5} + u_{x6} + u_{x7} + u_{x8}), \\ u_{y9} &= \alpha(u_{y1} + u_{y2} + u_{y3} + u_{y4}) + \beta(u_{y5} + u_{y6} + u_{y7} + u_{y8}), \end{aligned} \tag{E18.3}$$

where α and β are scalars to be determined. (In the terminology of Chapter 9, u_{x9} and u_{y9} are slaves while boundary DOFs are masters.) Show that the shape functions of the 8-node quadrilateral are then $N_i = N_i^P + \alpha N_9^P$ for $i = 1, \ldots 4$ and $N_i = N_i^P + \beta N_9^P$ for $i = 5, \ldots 8$. Furthermore, show that α and β can be determined by two conditions:

1. The unit sum condition: $\sum_{i=1}^{8} N_i = 1$, leads to $4\alpha + 4\beta = 1$.
2. Exactness of displacement interpolation for ξ^2 and η^2 leads to $2\alpha + \beta = 0$.

Solve these two equations for α and β, and verify that the serendipity shape functions given in §18.4.3 result.

EXERCISE 18.13 [A:25] Construct the 16 shape functions of the bicubic quadrilateral.

19

FEM Convergence Requirements

TABLE OF CONTENTS

§19.1. Overview

Chapters 11 through 18 have discussed, in piecemeal fashion, requirements for shape functions of isoparametric elements. These are motivated by *convergence*: as the mesh is refined, the FEM solution should approach the analytical solution of the mathematical model.[1] This attribute is obviously necessary to instill confidence in FEM results from the standpoint of mathematics.

This Chapter provides unified information on convergence requirements. These requirements can be grouped into three:

Completeness. The elements must have enough *approximation power* to capture the analytical solution in the limit of a mesh refinement process. This intuitive statement is rendered more precise below.

Compatibility. The shape functions should provide *displacement continuity* between elements. Physically these insure that no material gaps appear as the elements deform. As the mesh is refined, such gaps would multiply and may absorb or release spurious energy.

Stability. The system of finite element equations must satify certain *well posedness* conditions that preclude nonphysical zero-energy modes in elements, as well as the absence of excessive element distortion.

Completeness and compatibility are two aspects of the so-called **consistency** condition between the discrete and mathematical models. A finite element model that passes both completeness and continuity requirements is called *consistent*. This is the FEM analog of the famous Lax-Wendroff theorem,[2] which says that consistency and stability imply convergence.

Remark 19.1. A deeper mathematical analysis done in more advanced courses shows that completeness is *necessary* for convergence whereas failure of the other requirements does not necessarily precludes it. There are, for example, FEM models in common use that do not satisfy compatibility. Furthermore, numerically unstable models may be used (with caution) in situations where that property is advantageous, as in the modeling of local singularities. Nonetheless, the satisfaction of the three criteria guarantees convergence and may therefore be regarded as a safe choice for the beginner user.

§19.2. The Variational Index

For the mathematical statement of the completeness and continuity conditions, the variational index alluded to in previous sections plays a fundamental role.

The FEM is based on the direct discretization of an energy functional $\Pi[u]$, where u (displacements for the elements considered in this book) is the primary variable, or (equivalently) the function to be varied. Let m be the highest spatial derivative order of u that appears in Π. This m is called the *variational index*.

---

[1] Of course FEM convergence does not guarantee the correctness of the mathematical model in capturing the physics. As discussed in Chapter 1, *model verification* against experiments is a different and far more difficult problem.

[2] Proven originally for classical finite difference discretizations in fluid mechanics. More precisely, it states that a numerical scheme for the scalar conservation law, $du/dt + df/dx = 0$ converges to a unique (weak) solution, if it is consistent, stable and conservative. There is no equivalent theorem for systems of conservation laws.

Example 19.1. In the bar problem discussed in Chapter 11,

$$\Pi[u] = \int_0^L \left(\tfrac{1}{2}\, u' E A u' - q u \right)\, dx. \tag{19.1}$$

The highest derivative of the displacement $u(x)$ is $u' = du/dx$, which is first order in the space coordinate x. Consequently $m = 1$. This is also the case on the plane stress problem studied in Chapter 14, because the strains are expressed in terms of first order derivatives of the displacements.

Example 19.2. In the plane beam problem discussed in Chapter 12,

$$\Pi[v] = \int_0^L \left(\tfrac{1}{2}\, v'' E I v'' - q v \right)\, dx. \tag{19.2}$$

The highest derivative of the transverse displacement is the curvature $\kappa = v'' = d^2v/dx^2$, which is of second order in the space coordinate x. Consequently $m = 2$.

§19.3. Consistency Requirements

Using the foregoing definition of variational index, we can proceed to state the two key requirements for finite element shape functions.

§19.3.1. Completeness

> The element shape functions must represent exactly all polynomial terms of order $\leq m$ in the Cartesian coordinates. A set of shape functions that satisfies this condition is called m-complete.

Note that this requirement applies *at the element level* and involves *all* shape functions of the element.

Example 19.3. Suppose a displacement-based element is for a plane stress problem, in which $m = 1$. Then 1-completeness requires that the linear displacement field

$$u_x = \alpha_0 + \alpha_1 x + \alpha_2 y, \qquad u_y = \alpha_0 + \alpha_1 x + \alpha_2 y \tag{19.3}$$

be exactly represented for any value of the α coefficients. This is done by evaluating (19.3) at the nodes to form a displacement vector $\mathbf{u}^e$ and then checking that $\mathbf{u} = \mathbf{N}^e \mathbf{u}^e$ recovers exactly (19.3). Section 16.6 presents the details of this calculation for an arbitrary isoparametric plane stress element. That analysis shows that completeness is satisfied if the *sum of the shape functions is unity* and *the element is compatible*.

Example 19.4. For the plane beam problem, in which $m = 2$, the quadratic transverse displacement

$$v = \alpha_0 + \alpha_1 x + \alpha_2 x^2 \tag{19.4}$$

must be exactly represented over the element. This is easily verified in for the 2-node beam element developed in Chapter 13, because the assumed transverse displacement is a complete cubic polynomial in x. A complete cubic contains the quadratic (19.4) as special case.

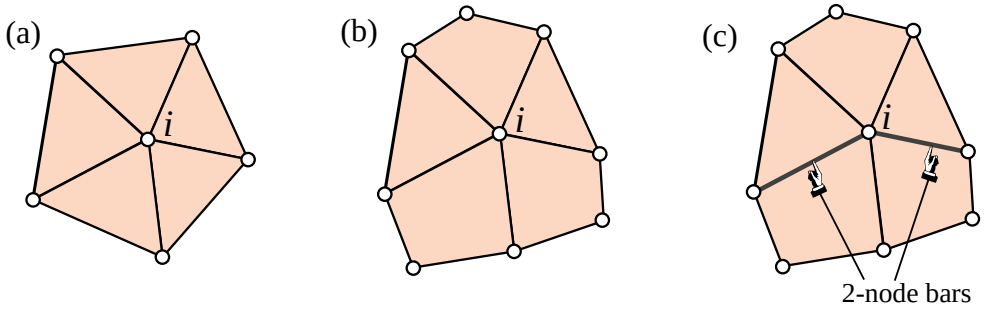

FIGURE 19.1. An element patch is the set of all elements attached to a patch node, labeled i. (a) illustrates a patch of triangles; (b) a mixture of triangles and quadrilaterals; (c) a mixture of triangles, quadrilaterals, and bars.

§19.3.2. Compatibility

To state this requirement succintly, it is convenient to introduce the concept of *element patch*, or simply *patch*. This is the set of all elements attached to a given node, called the *patch node*. The definition is illustrated in Figure 19.1, which shows three different kind of patches attached to patch node i in a plane stress problem. The patch of Figure 19.1(a) contains only one type of element: 3-node linear triangles. The patch of Figure 19.1(b) mixes two plane stress element types: 3-node linear triangles and 4-node bilinear quadrilaterals. The patch of Figure 19.1(c) combines three element types: 3-node linear triangles, 4-node bilinear quadrilaterals, and 2-node bars.

We define a finite element *patch trial function* as the union of shape functions activated by setting a degree of freedom at the patch node to unity, while all other freedoms are zero.

A patch trial function "propagates" only over the patch, and is zero beyond it. This property follows from the local-support requirement stated in §18.1: a shape function for node i should vanish on all sides or faces that do not include i.

With the help of these definitions we can enunciate the compatibility requirement as follows.

> Patch trial functions must be $C^{(m-1)}$ continuous between interconnected elements, and C^m piecewise differentiable inside each element.

If the variational index is $m = 1$, the patch trial functions must be C^0 continuous between elements, and C^1 inside elements.

A set of shape functions that satisfies the first requirement is called *conforming*. A conforming expansion that satisfies the second requirement is said to be of *finite energy*. Note that this condition applies at two levels: individual element, and element patch. An element endowed with conforming shape functions is said to be *conforming*. A conforming element that satisfies the finite energy requirement is said to be *compatible*.[3]

[3] The FEM literature is a bit fuzzy as regards these terms. It seems better to leave the qualifier "conforming" to denote interelement compatibility; informally "an element that gets along with its neighbors." The qualifier "compatible" is used in the stricter sense of conforming while possessing sufficient internal smoothness.

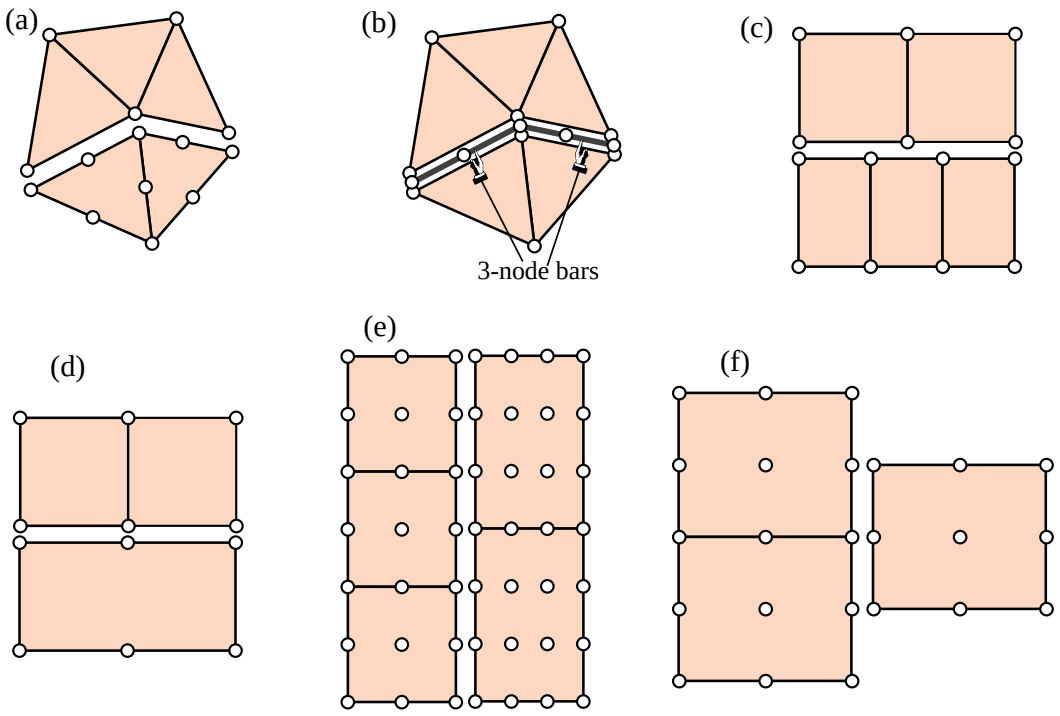

FIGURE 19.2. Examples of 2D non-matching meshes. Interelement boundaries that fail matching conditions are shown offset for visualization convenience. In (a,b,c) some nodes do not match. In (d,e,f) nodes and DOFs match but some sides do not, leading to violations of C^0 continuity.

Figures 19.1(b,c) illustrates the fact that one needs to check the possible connection of *matching elements* of different types and possibly different dimensionality.

§19.3.3. Matching and Non-Matching Meshes

As stated, compatibility refers to the *complete finite element mesh* because mesh trial functions are a combination of patch trial functions, which in turn are the union of element shape functions. This generality poses some logistical difficulties because the condition is necessarily mesh dependent. Compatibility can be checked at the *element level* by restricting attention to *matching meshes*. A matching mesh is one in which adjacent elements share sides, nodes and degrees of freedom, as in the patches shown in Figure 19.1.

For a matching mesh it is sufficient to restrict consideration first to a pair of adjacent elements, and then to the side shared by these elements. Suppose that the variation of a shape function *along that side* is controlled by k nodal values. Then a polynomial variation of order up to $k-1$ in the natural coordinate(s) can be specified uniquely over the side. This is sufficient to verify interelement compatibility for $m = 1$, implying C^0 continuity, if the shape functions are polynomials.

This simplified criterion is the one used in previous Chapters. Specific 2D examples were given in Chapters 15 through 18.

Remark 19.2. If the variational index is $m = 2$ and the problem is multidimensional, as in the case of plates and shells, the check is far more involved and trickier because continuity of *normal derivatives along a side* is involved. This practically important scenario is examined in advanced FEM treatments. The case of non-polynomial shape functions is, on the other hand, of little practical interest.

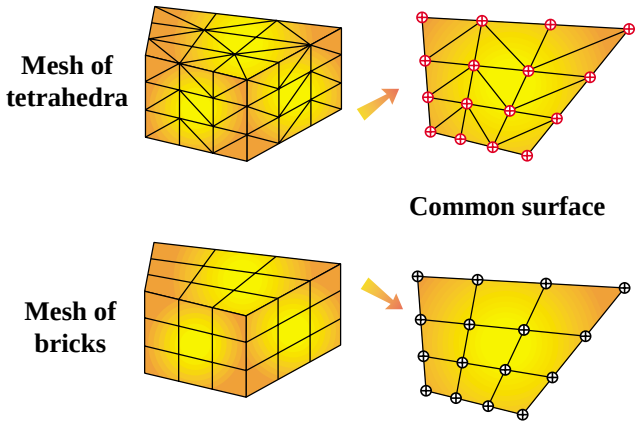

FIGURE 19.3. Example of a 3D non-matching mesh. Top portion discretized with tetrahedra, lower portion with bricks. Nodes and boundary-quad edges and DOFs match, but element types are different, leading to violation of C^0 continuity.

A mesh that does not satisfy the matching criteria stated above is called a *nonmatching mesh*. Several two-dimensional examples are shown in Figure 19.2. As can be seen there is a wide range of possibilities: nonmatching nodes, matching nodes but different element types, etc. Figure 19.3 depicts a three-dimensional example, in which case even more variety can be expected.

Nonmatching meshes are the rule rather than the exception in contact and impact problems (which, being geometrically nonlinear, are outside the scope of this book). See Figure 19.4 illustrates what happens in a problem of slipping contact.

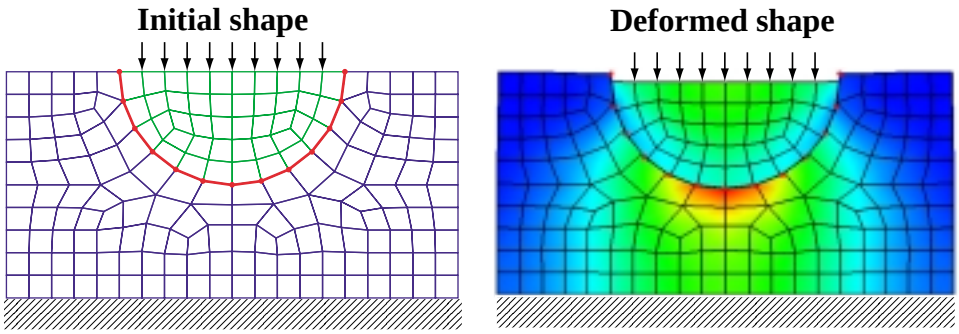

FIGURE 19.4. In contact and impact problems, matching meshes are the exception rather than the rule. Even if the meshes match at initial contact, slipping may produce a nonmatching mesh in the deformed configuration, as illustrated in the figure.

In multiphysics simulations nonmatching meshes are common, since they are often prepared separately for the different physical components, as illustrated in Figure 19.5.

§19.4. Stability

Stability may be informally characterized as ensuring that the finite element model enjoys the same solution uniqueness properties of the analytical solution of the mathematical model. For example, if the only motions that produce zero internal energy in the mathematical model are rigid body motions,

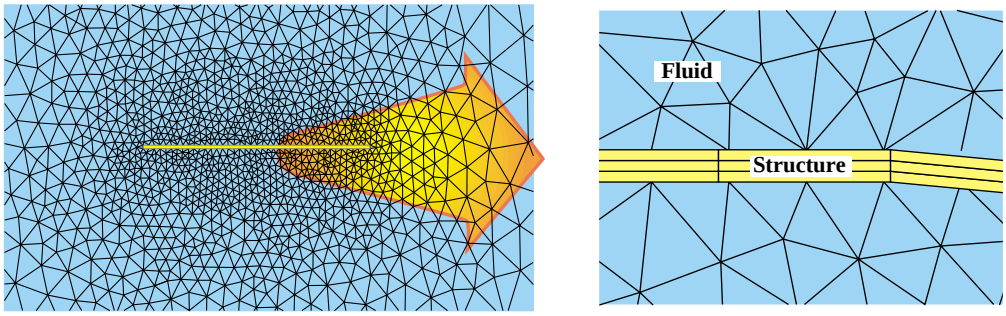

FIGURE 19.5. Nonmatching meshes are common in multiphysics problems, as in this example of fluid-structure interaction (FSI). Two-dimensional model to simulate flow around a thin plate. If the meshes are independenly prepared node locations will not generally match.

the finite element model must inherit that property. Since FEM can handle arbitrary assemblies of elements, including individual elements, this property is required to hold at the element level.

In the present outline we are concerned with stability at the element level. Stability is not a property of shape functions *per se* but of the implementation of the element as well as its geometrical definition. It involves two subordinate requirements: rank sufficiency, and Jacobian positiveness. Of these, rank sufficiency is the most important one.

§19.4.1. Rank Sufficiency

The element stiffness matrix must not possess any zero-energy kinematic mode other than rigid body modes.

This can be mathematically expressed as follows. Let n_F be the number of element degrees of freedom, and n_R be the number of independent rigid body modes. Let r denote the rank of $\mathbf{K}^e$. The element is called *rank sufficient* if $r = n_F - n_R$ and *rank deficient* if $r < n_F - n_R$. In the latter case, the *rank deficiency* is defined by

$$d = (n_F - n_R) - r \tag{19.5}$$

If an isoparametric element is numerically integrated, let n_G be the number of Gauss points, while n_E denotes the order of the stress-strain matrix $\mathbf{E}$. Two additional assumptions are made:

(i) The element shape functions satisfy completeness in the sense that the rigid body modes are exactly captured by them.

(ii) Matrix $\mathbf{E}$ is of full rank.

Then each Gauss point adds n_E to the rank of $\mathbf{K}^e$, up to a maximum of $n_F - n_R$. Hence the rank of $\mathbf{K}^e$ will be

$$r = \min(n_F - n_R, n_E\, n_G) \tag{19.6}$$

To attain rank sufficiency, $n_E n_G$ must equal or exceed $n_F - n_R$:

$$\boxed{n_E\, n_G \geq n_F - n_R} \tag{19.7}$$

from which the appropriate Gauss integration rule can be selected.

In the plane stress problem, $n_E = 3$ because $\mathbf{E}$ is a 3×3 matrix of elastic moduli; see equation $(14.5)_2$. Also $n_R = 3$. Consequently $r = \min(n_F - 3, 3n_G)$ and $3n_G \geq n_F - 3$.

Table 19.1 Rank-sufficient Gauss Rules for Some Plane Stress Elements

Element	n	n_F	$n_F - 3$	Min n_G	Recommended rule
3-node triangle	3	6	3	1	centroid*
6-node triangle	6	12	9	3	3-point rules*
10-node triangle	10	20	17	6	6-point rule*
4-node quadrilateral	4	8	5	2	2 x 2
8-node quadrilateral	8	16	13	5	3 x 3
9-node quadrilateral	9	18	15	5	3 x 3
16-node quadrilateral	16	32	29	10	4 x 4

* These triangle integration rules are introduced in §24.2.

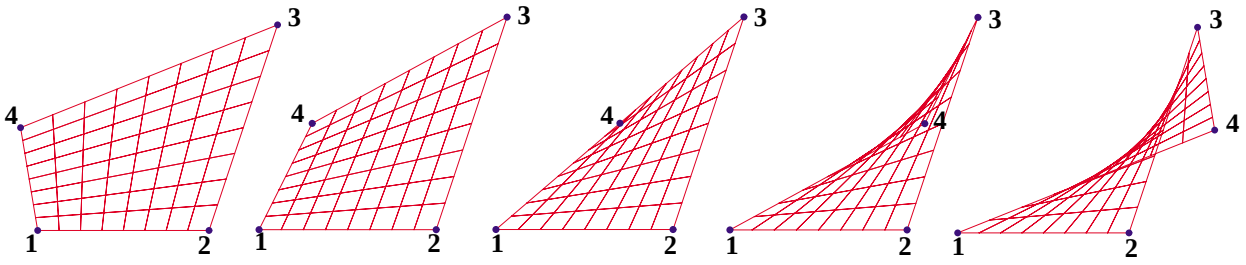

FIGURE 19.6. Effect of displacing node 4 of the four-node bilinear quadrilateral shown on the leftmost picture, to the right.

Remark 19.3. The fact that each Gauss point adds $n_E n_G$ to the rank can be proven considering the following property. Let $\mathbf{B}$ be a $n_E \times n_F$ rectangular real matrix with rank $r_B \le n_E$, and $\mathbf{E}$ an $n_E \times n_E$ positive-definite (p.d.) symmetric matrix. Then the rank of $\mathbf{B}^T\,\mathbf{E}\,\mathbf{B}$ is r_B. Proof: let $\mathbf{u} \neq \mathbf{0}$ be a non-null n_F-vector. If $\mathbf{B}^T\,\mathbf{E}\,\mathbf{B}\,\mathbf{u} = \mathbf{0}$ then $0 = \mathbf{u}^T\mathbf{B}^T\,\mathbf{E}\,\mathbf{B}\,\mathbf{u} = ||\mathbf{E}^{1/2}\,\mathbf{B}\,\mathbf{u}||$. Therefore $\mathbf{B}\,\mathbf{u} = \mathbf{0}$. Identify now $\mathbf{B}$ and $\mathbf{E}$ with the strain-displacement and stress-strain (constitutive) matrix, respectively. In the plane stress case $n_E = 3$, $n_F = 2n > 3$ is the number of element freedoms. Thus $\mathbf{B}$ has rank 3 and *a fortiori* $\mathbf{B}^T\mathbf{E}\,\mathbf{B}$ must also have rank 3 since $\mathbf{E}$ is p.d. At each Gauss point i a contribution of $w_i\mathbf{B}^T\,\mathbf{E}\,\mathbf{B}$, which has rank 3 if $w_i > 0$, is added to $\mathbf{K}^e$. By a theorem of linear algebra, the rank of $\mathbf{K}^e$ increases by 3 until it reaches $n_F - n_R$.

Example 19.5. Consider a plane stress 6-node quadratic triangle. Then $n_F = 2 \times 6 = 12$. To attain the proper rank of $12 - n_R = 12 - 3 = 9$, $n_G \ge 3$. A 3-point Gauss rule, such as the midpoint rule defined in §24.2, makes the element rank sufficient.

Example 19.6. Consider a plane stress 9-node biquadratic quadrilateral. Then $n_F = 2 \times 9 = 18$. To attain the proper rank of $18 - n_R = 18 - 3 = 15$, $n_G \ge 5$. The 2×2 product Gauss rule is insufficient because $n_G = 4$. Hence a 3×3 rule, which yields $n_G = 9$, is required to attain rank sufficiency.

Table 19.1 collects rank-sufficient Gauss integration rules for some widely used plane stress elements with n nodes and $n_F = 2n$ freedoms.

§19.4.2. Jacobian Positiveness

The geometry of the element should be such that the determinant $J = \det \mathbf{J}$ of the Jacobian matrix defined[4] in §17.2, is positive everywhere. As illustrated in Equation (17.20), J characterizes the local metric of the element natural coordinates.

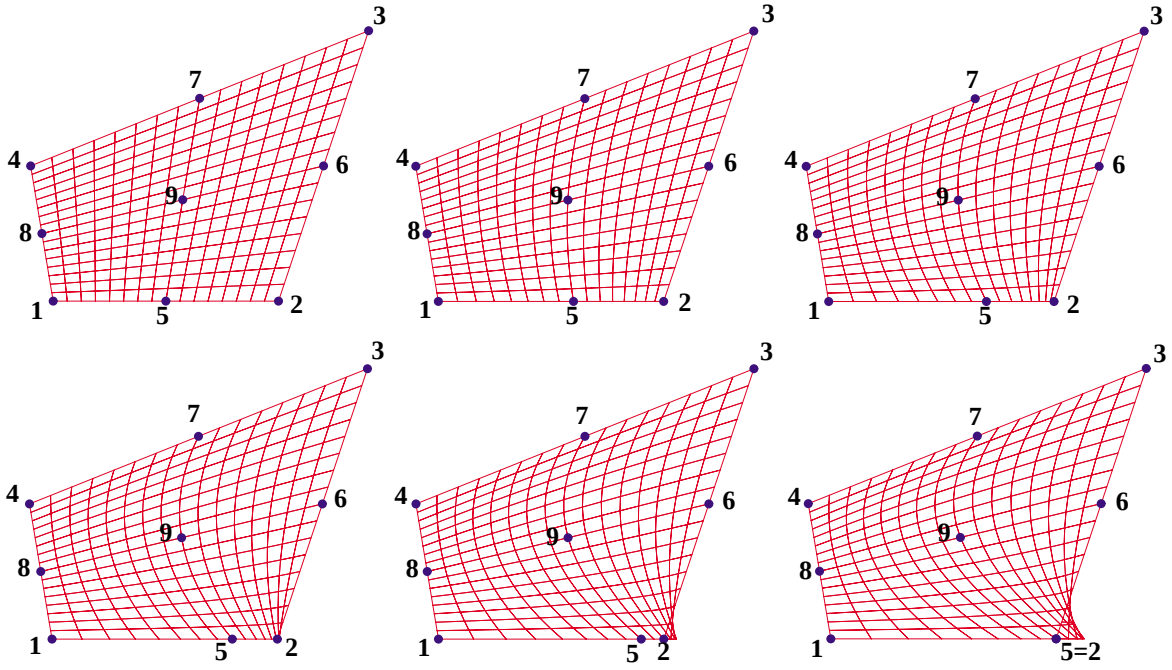

FIGURE 19.7. Effect of moving midpoint 5 of a 9-node biquadratic quadrilateral tangentially toward corner 2.

For a three-node triangle J is constant and in fact equal to $2A$. The requirement $J > 0$ is equivalent to saying that corner nodes must be positioned and numbered so that a positive area $A > 0$ results. This is called a *convexity condition*. It is easily checked by a finite element program.

But for 2D elements with more than 3 nodes distortions may render *portions* of the element metric negative. This is illustrated in Figure 19.6 for a 4-node quadrilateral in which node 4 is gradually moved to the right. The quadrilateral gradually morphs from a convex figure into a nonconvex one. The center figure is a triangle; note that the metric near node 4 is badly distorted (in fact $J = 0$ there) rendering the element unacceptable. This clearly contradicts the erroneous advice of some FE books, which state that quadrilaterals can be reduced to triangles as special cases, thereby rendering triangular elements unnecessary.

For higher order elements proper location of corner nodes is not enough. The non-corner nodes (midside, interior, etc.) must be placed sufficiently close to their natural locations (midpoints,

[4] This definition applies to quadrilateral elements. The Jacobian determinant of an arbitrary triangular element is defined in §24.2.

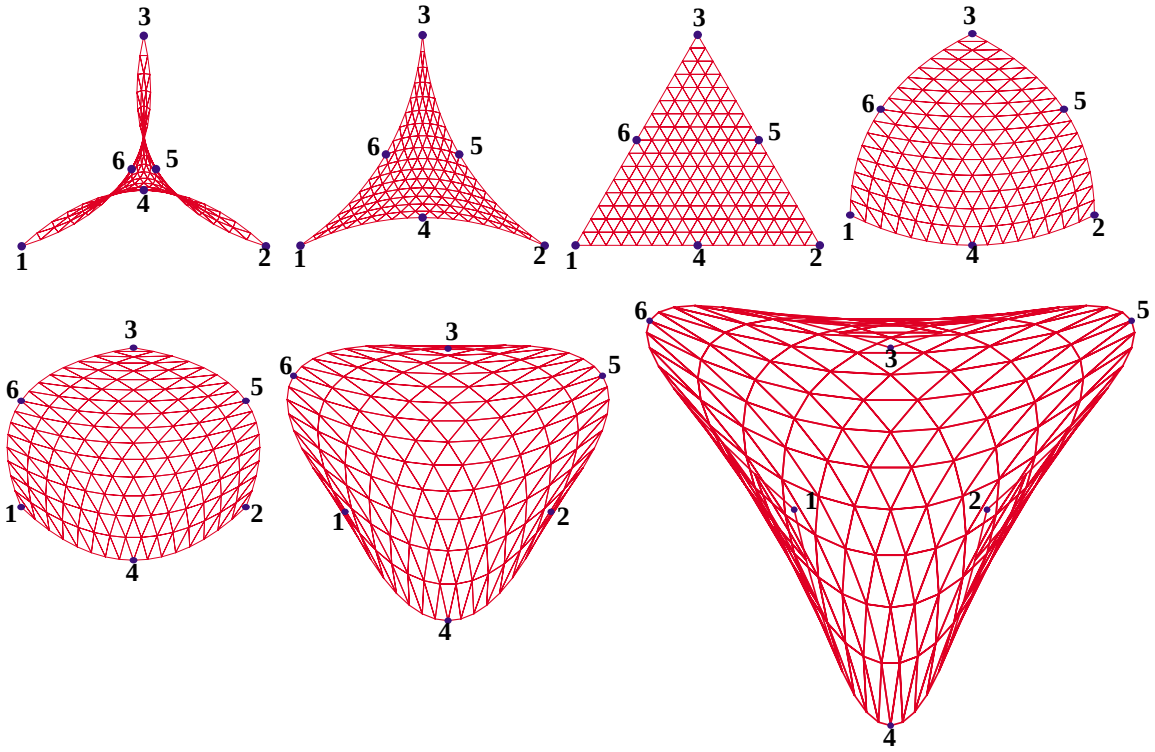

FIGURE 19.8. Effect of displacing midpoints 4, 5 and 6 of an equilateral 6-node triangle along the midpoint normals. Motion is inwards in first two top frames, outwards in the last four. In the lower leftmost picture nodes 1 through 6 lie on a circle.

centroids, etc.) to avoid violent local distortions. The effect of midpoint motions in quadratic elements is illustrated in Figures 19.7 and 19.8.

Figure 19.7 depicts the effect of moving midside node 5 tangentially in a 9-node quadrilateral element while keeping all other 8 nodes fixed. When the location of 5 reaches the quarter-point of side 1-2, the metric at corner 2 becomes singular in the sense that $J = 0$ there. Although this is disastrous in ordinary FE work, it has applications in the construction of special "crack" elements for linear fracture mechanics.

Displacing midside nodes normally to the sides is comparatively more forgiving, as illustrated in Figure 19.8. This depicts a 6-node equilateral triangle in which midside nodes 4, 5 and 6 are moved inwards and outwards along the normals to the midpoint location. As shown in the lower left picture, the element may be even morphed into a "parabolic circle" (meaning that nodes 1 through 6 lie on a circle) without the metric breaking down.

Notes and Bibliography

The literature on the mathematics of finite element methods has grown exponentially since the monograph of Strang and Fix [705]. This is very readable but out of print. A more up-to-date exposition is the textbook by Szabo and Babuska [721]. The subjects collected in this Chapter tend to be dispersed in recent monographs and obscured by overuse of functional analysis.

References

Referenced items have been moved to Appendix R.

Homework Exercises for Chapter 19
FEM Convergence Requirements

EXERCISE 19.1 [D:20] Explain why the two-dimensional meshes pictured in Figure 19.2(d,e,f) fail interelement compatibility although nodes and DOFs match.

EXERCISE 19.2 [A:20] The isoparametric definition of the straight 3-node bar element in its local system $\bar{x}$ is

$$\begin{bmatrix} 1 \\ \bar{x} \\ \bar{v} \end{bmatrix} = \begin{bmatrix} 1 & 1 & 1 \\ \bar{x}_1 & \bar{x}_2 & \bar{x}_3 \\ \bar{u}_1 & \bar{u}_2 & \bar{u}_3 \end{bmatrix} \begin{bmatrix} N_1^e(\xi) \\ N_2^e(\xi) \\ N_3^e(\xi) \end{bmatrix}. \tag{E19.1}$$

Here ξ is the isoparametric coordinate that takes the values -1, 1 and 0 at nodes 1, 2 and 3, respectively, while N_1^e, N_2^e and N_3^e are the shape functions found in Exercise 16.3 and listed in (E16.2).

For simplicity, take $\bar{x}_1 = 0$, $\bar{x}_2 = L$, $\bar{x}_3 = \frac{1}{2}L + \alpha L$. Here L is the bar length and α a parameter that characterizes how far node 3 is away from the midpoint location $\bar{x} = \frac{1}{2}L$. Show that the minimum α's (minimal in absolute value sense) for which $J = d\bar{x}/d\xi$ vanishes at a point in the element are $\pm 1/4$ (the quarter-points). Interpret this result as a singularity by showing that the axial strain becomes infinite at a an end point. (This result has application in fracture mechanics modeling.)

EXERCISE 19.3 [A:15] Consider one dimensional bar-like elements with n nodes and 1 degree of freedom per node so $n_F = n$. The correct number of rigid body modes is 1. Each Gauss integration point adds 1 to the rank; that is $N_E = 1$. By applying (19.7), find the minimal rank-preserving Gauss integration rules with p points in the longitudinal direction if the number of node points is $n = 2$, 3 or 4.

EXERCISE 19.4 [A:20] Consider three dimensional solid "brick" elements with n nodes and 3 degrees of freedom per node so $n_F = 3n$. The correct number of rigid body modes is 6. Each Gauss integration point adds 6 to the rank; that is, $N_E = 6$. By applying (19.7), find the minimal rank-preserving Gauss integration rules with p points in each direction (that is, $1\times1\times1$, $2\times2\times2$, etc) if the number of node points is $n = 8$, 20, 27, or 64. Partial answer: for $n = 27$ the minimal rank preserving rule is $3 \times 3 \times 3$.

EXERCISE 19.5 [A/C:35] (Requires use of a CAS help to be tractable). Repeat Exercise 19.2 for a 9-node plane stress element. The element is initially a perfect square, nodes 5,6,7,8 are at the midpoint of the sides 1–2, 2–3, 3–4 and 4–1, respectively, and 9 at the center of the square. Displace 5 tangentially towards 2 until the Jacobian determinant at 2 vanishes. This result is important in the construction of "singular elements" for fracture mechanics.

EXERCISE 19.6 [A/C:35] Repeat Exercise 19.5 but moving node 5 along the normal to the side. Discuss the range of motion for which $\det \mathbf{J} > 0$ within the element.

EXERCISE 19.7 [A:20] Discuss whether the deVeubeke triangle presented in Chapter 15 satisfies completeness and interelement-compatbility requirements.